Tribological Studies of Polymer-matrix-composites

Larsen, Thomas Ricco Ølholm

Publication date:
2007

Document Version
Publisher's PDF, also known as Version of record

Tribological studies of polymer-matrix-composites

Thomas Ølholm Larsen

16th January 2007

Danish Polymer Centre
Department of Chemical Engineering
Technical University of Denmark
DK-2800 Kongens Lyngby, Denmark

ISBN 978-87-91435-62-5
Printed by Frydenberg a/s, Copenhagen, Denmark

Preface

The work presented in this Ph.D. thesis has been carried out at the Danish Polymer Centre, Department of Chemical Engineering, Technical University of Denmark (DTU) in the period from January 2004 to January 2007. The project was supervised by Martin E. Vigild (DTU) and Tom L. Andersen from Risø National Laboratory (Risø), and was conducted in collaboration with Elektro-Isola A/S and the Materials Research Department at Risø.

The work was financially supported by a grant given in equal parts by the Technical University of Denmark, The Danish Research Training Council and Civilingeniør Frederik Leth Christensens ALMENNYTTIGE FOND. The latter is furthermore gratefully acknowledged by the author for financing the Pin-On-Disk apparatus which was built as a part of this project.

I would like to thank Elektro-Isola A/S for their outstanding support and interest in this project, especially Bent Thorning with whom I had some fruitful e-mail correspondence throughout this project. I would also like to thank my supervisors Martin and Tom for encouraging inspiration and good discussions during this project. Additionally, I would like to thank the following persons for technical support or guidance: Christian H. Madsen, Henning Olsen, Jakob I. Bech, Jørgen Bilde-Sørensen from Risø, and Andy Horsewell, Lejla Leth, Jan L. Andreasen, Rene Sobiecki, Kim C. Szabo, Erik M. Kjær from DTU, and Birgitte M. Hansen from Elektro-Isola A/S.

Finally, many thanks to family and friends for moral support, and a special thanks to Natanya for valuable help, understanding and support especially during the last months of this project.

Lyngby, December 2006

Thomas Ricco Ølholm Larsen

Contents

Appendices

Synopsis

This thesis reports the outcome of a Ph.D. study on tribological properties of polymer-matrix-composites (PMCs). These materials are used increasingly in applications where friction and wear are important parameters. In a large fraction of these applications the PMCs are rubbing against steel counterfaces e.g. when acting as seals, hip implants or rotary vanes in vacuum pumps. One of the benefits of using polymers for sliding applications against steel counterfaces is their typically low coefficient of friction, which in some cases may be attributed to self-lubricating properties. These properties make it possible to apply PMCs for dry-sliding applications i.e. without using lubricants such as oil or grease. To enhance the mechanical properties as well as the wear resistance of polymers, reinforcement by different fibers or particles is frequently utilized.

This work is conducted in collaboration with the company Elektro-Isola A/S, which is specialized in producing PMCs using thermoset resins reinforced by different kinds of fabrics. This collaborative work is intented to establish a overview of the current status of this field by studying the existing literature. Based on this, materials are selected for production of PMCs, which are expected to exhibit good tribological properties when dry-sliding against smooth steel counterfaces. It is furthermore a selection criteria that the applied materials are interesting from a scientific point of view by representing new material combinations. The PMCs examined in this study are produced using an epoxy resin as matrix, which is reinforced by either a glass fiber weave or a carbon/aramid fiber hybrid weave. Furthermore, the effect of incorporating CuO nanoparticles and PTFE microparticles is examined. The influence of the mentioned components are examined both individually and in combination.

The micro-structures of the produced PMCs are studied by electron microscopy, which indicate good composite qualities in terms of low porosities and well-dispersed particles. In order to evaluate the tribological properties of the materials, a tribo-tester of the Pin-On-Disk (POD) type is designed and built as a part of this project. This apparatus is successfully applied to collect coefficients of friction, wear rates and counterface temperatures.

The following main conclusions are drawn for PMCs without fibrous reinforcement. When CuO nanoparticles are added to the neat epoxy resin in the range of 0 to 10 vol%, it is found that friction is roughly independent of the CuO content. Wear increases at all concentrations of CuO relative to the neat epoxy resin, which is correlated with the appearance of large-scale cracks on the worn surfaces. This leads to the conclusion that addition of nano-CuO possibly reduces the fracture strength of the

resin. When PTFE microparticles are added to the neat epoxy resin (7.5 vol%) a decrease in friction of about 35% is obtained, which also results in a reduction in counterface temperature due to diminished frictional heating. The influence on wear by adding PTFE depends on the applied pv condition, i.e. the product of contact pressure p and sliding velocity v. When sliding occurs at a low p - high v condition, wear increases relative to the neat epoxy, which is probably due to deteriorated mechanical properties caused by the presence of the weak PTFE phase. Measurements performed at a high p - low v condition show that PTFE addition leads to a superior performance caused by the friction reducing effect, which counteracts wear enhancements due to thermally induced degradation of the resin. Composites without PTFE generally show high wear rates, decomposition and a fluctuating frictional behavior at the same condition. When a low content of CuO nanoparticles is added to epoxy along with PTFE, a positive synergistic effect is indicated by minor improvements of friction and wear. However, the good frictional properties due to PTFE deteriorate at a high CuO content, which consequently results in higher values of both friction and wear.

The performance of the two types of reinforcing weave are compared at nine different pv conditions. The purpose is to systematically compare these differently reinforced materials while going from mild to severe sliding conditions. It is found that the coefficient of friction on average is reduced by 35% by substituting the glass fiber weave with the carbon/aramid weave. The latter shows superior wear behavior at the six mildest pv conditions with wear rates an average factor of 22 lower than the rates for glass fiber reinforcement. At the three most severe pv conditions all tested composites show signs of decomposition. Despite this, glass fiber reinforcement has a relatively steady behavior, while carbon/aramid reinforcement gives rise to a gradually increasing frictional force as a function of time, which ultimately results in failure of the test-specimen. No changes in friction and wear are seen for the carbon/aramid reinforced epoxy by additionally incorporating either PTFE microparticles or CuO nanoparticles. The latter indicates that the tribological properties are largely controlled by the fibers.

In summary, despite promising particle dispersions, no clear positive effects of adding inorganic nano-scale particles to epoxy are found in this study. PTFE particles prove to be effective in reducing the coefficient of friction and hence frictional heating when added to an epoxy resin. This makes the PMC material useful at more severe sliding conditions since thermal enhancement of wear rates is suppressed. Carbon/aramid reinforcement also shows good friction and wear properties. However, this reinforcement fails at sliding conditions leading to high counterface temperatures. An attempt to counteract this by incorporating PTFE particles together with carbon/aramid did not show the intended effect.

Dansk Resumé

Denne afhandling rapporter resultatet af et Ph.d. studie vedrørende polymer-matrix-kompositter (PMCs) tribologiske egenskaber. Disse materialer bliver i stigende grad anvendt i applikationer hvor friktion og slid er vigtige parametre. I en stor del af disse applikationer gnider PMCs mod ståloverflader f.eks. i tætninger, hofteimplantater eller vakuumpumper. En af fordelene ved at bruge polymerer til sådanne applikationer er deres typisk lave friktionskoefficient, som i nogle tilfælde kan tilskrives selvsmørende egenskaber. Disse egenskaber gør det muligt at anvende PMCs til tør-glidningsapplikationer dvs. uden brug af smøringsmidler såsom olie eller fedt. Med henblik på at øge både de mekaniske og tribologiske egenskaber, er forstærkningsmaterialer i form af fibre og partikler ofte anvendt.

Dette arbejde er udført i samarbejde med virksomheden Elektro-Isola A/S, som er specialiseret i produktion af PMCs ved brug af hærdeplast forstærket med væv af forskellige typer. Det er hensigten med dette samarbejde at danne et overblik over det pågældende forskningsområde ved at studere den eksisterende litteratur. Baseret på dette, er materialer valgt til produktion af PMCs, som forventes at udvise gode tribologiske egenskaber når de tør-glider mod glatte ståloverflader. Det er ydermere et krav til materialevalget, at det er interessant fra en forskningsmæssig synsvinkel ved at repræsentere nye materialekombinationer. De PMCs, der er undersøgt i dette Ph.d. studie, er produceret ved brug af epoxy harpiks, der er forstærket med enten et glasfiber væv eller et carbon/aramid fiber hybrid væv. Effekten af at inkorporere CuO nanopartikler og PTFE mikropartikler er ydermere undersøgt. Indflydelsen af de nævnte komponenter er undersøgt både enkeltvis og i kombination.

Mikrostrukturen af de fremstillede kompositter er undersøgt via elektronmikroskopi, som indiker gode kompositegenskaber mht. lav porøsitet og en god partikelfordeling. En tribo-tester af Pin-On-Disk (POD) typen, er designet og fremstillet som en del at dette projekt med henblik på at evaluere de tribologiske egenskaber af de fremstillede PMCs. Dette apparat er med succes anvendt til måling af friktionskoefficienter, slidrater og modflade-temperaturer.

Hovedkonklusionerne for PMCs uden brug af forstærkningsvæv er som følger. Tilsætning af CuO nanopartikler (0.1 til 10 vol%) til den ufyldte epoxy harpiks giver ikke anledning til væsentlige ændringer i friktion. Slidraten øges for alle koncentrationer af CuO relativ til ufyldt epoxy, hvilket er korreleret med dannelsen af relativt store revner på de slidte overflader. Dette fører til konklusionen, at tilsætning af nano-CuO sandsynligvis nedsætter brudstyrken af harpiksen. Tilsætning at PTFE mikropartikler (7,5 vol%) til den ufyldte epoxy resulter i en reduktion af friktionen

med ca. 35%, hvilket samtidig mindsker modflade-temperaturen pga. nedsat friktionsvarme. Effekten på slid ved tilsætning af PTFE afhænger af den anvendte *pv* betingelse, dvs. produktet af kontakttrykket p og gnidningshastigheden v. Sliddet øges relativ til ufyldt epoxy, når glidning forgår ved en lav p - høj v betingelse, hvilket sandsynligvis skyldes en forringelse af de mekaniske egenskaber pga. den svage PTFE fase. Målinger udført ved en høj p - lav v betingelse viser, at PTFE giver anledning til overlegne egenskaber pga. af den friktionreducerende effekt, der modvirker termisk nedbrydning af harpiksen. Test af kompositter uden PTFE ved samme betingelser udviser dekomponering, høje slidrater og en fluktuerende friktion. En positiv synergieffekt ses, når et lavt indhold af CuO nanopartikler tilsættes harpiksen sammen med PTFE, hvilket giver udslag i moderate forbedringer af friktions- og slidegenskaberne. De gode friktionsegenskaber pga. PTFE bliver imidlertid forringet ved et højt indhold af CuO, hvilket resulter i øgede værdier af både friktion og slid.

Effektiviteten af de to typer forstærkningvæv er sammenlignet ved ni forskellige *pv* betingelser. Dette er med henblik på systematisk at sammenligne disse forskelligt forstærkede materialer under slidbetingelser varierende fra milde til hårde. Det er fundet, at friktionen i gennemsnit reduceres med 35% ved at substituere glasvævet med carbon/aramid vævet. Sidstnævnte udviser desuden overlegen slidmodstand ved de seks mildeste *pv* betingelser med en gennemsnitlig slidrate, der er en faktor 22 lavere end raterne for glasvævet. Alle testede PMCs udviser tegn på dekomponering ved de tre hårdeste *pv* betingelser. På trods af dette har glasvævet en relativ stabil opførsel, hvorimod carbon/aramid vævet giver anledning til en friktion der gradvist stiger som funktion af tiden, hvilket i sidste instans fører til sammenbrud af prøveemnet. Ingen ændringer i friktion og slid ses for carbon/aramid forstærket epoxy når der yderligere tilsættes PTFE mikropartikler eller CuO nanopartikler. Sidstnævnte indikerer at de tribologiske egenskaber i høj grad er styret af fibrene.

Kort sagt, på trods af lovende partikeldispersioner i epoxy harpiksen, er der i dette studie ikke fundet klare positive effekter ved tilsætning af uorganiske nanopartikler til epoxy. PTFE partikler viste sig effektive til at reducere friktionskoefficienten og dermed friktionsvarmen når de blev tilsat en epoxy harpiks. Dette gør PMC materialet brugbart ved hårdere slidbetingelser, da en termisk betinget forøgelse af sliddet bliver undertrykt. Carbon/aramid vævet udviser generelt også gode friktions- og slidegenskaber. Dette væv har imidlertid nogle utilsigtede egenskaber ved slidbetingelser, der resulterer i høje modflade-temperaturer. Et forsøg på at modvirke dette ved inkorporering af PTFE partikler sammen med carbon/aramid vævet viser ikke den tilsigtede effekt.

List of Abbreviations

Table 1. Symbols

Symbol	Description
A_a	Apparent area of contact
A_p	Area of an asperity projected in the sliding direction
A_r	Real area of contact
E	Elastic modulus
F_f	Frictional force
H	Indentation hardness
HV	Vickers hardness
Δh	Height reduction
k	Wear coefficient
k_{ab}	Abrasive wear coefficient
k_{ad}	Adhesive wear coefficient
k^*	Wear factor
Δm	Mass loss
p	Contact pressure over the apparent contact area
p_J	Contact pressure at the junctions
P	Probability
$\dot{Q}_d$	Specific rate of energy dissipation
r	Radius
R_a	Average roughness parameter
t	Time
T_a	Average temperature over the apparent contact area
T_e	Environmental temperature
ΔT_f	Flash temperature
T_g	Glass transition temperature
T_p	Average peak temperature at the asperities
v	Sliding velocity
V_{ab}	Abrasive wear volume
V_{ad}	Adhesive wear volume
$\dot{w}$	Wear rate

Table 2. Symbols - continued

Symbol	Description
$\dot{w}_s$	Specific wear rate
$\dot{w}_t$	Depth wear rate
W_N	Load normal to the surfaces
x	Sliding distance
ϵ	Ultimate elongation
θ	Roughness angle of asperities
μ	Coefficient of friction
μ_a	The adhesive contribution to the coefficient of friction
μ_d	The deformation contribution to the coefficient of friction
ρ	Density
σ_s	Tensile strength
σ_y	Compressive yield strength
σ^*	Standard deviation of the asperity height distribution
τ_{av}	Average shear stress over the real area of contact
τ_s	Shear strength

Table 3. Abbreviations

Abbreviations	**Description**
AF	Aramid fibers
CA	Carbon/aramid weave
CF	Carbon fibers
EP	Epoxy
EDS	Energy-dispersive analysis
G	Glass fiber weave
GF	Glass fibers
HDPE	High density polyethylene
PA	Polyamide
PA6	Polyamide 6
PA4,6	Polyamide 4,6
PA6,6	Polyamide 6,6
PA11	Polyamide 11
PA12	Polyamide 12
PAEKs	Polyaryletherketones
PE	Polyethylene
PEEK	Polyetheretherketone
PEI	Polyetheramide
PES	polyethersulfone
PET	Polyethylene terephthalate
PI	Polyimide
PMCs	Polymer-matrix-composites
PMMA	Polymethylmethacrylate
POD	Pin-on-disk
PPA	Polyphthalamide
PPS	Polyphenylenesulphide
PTFE	Polytetrafluoroethylene
SEM	Scanning electron microscopy
TEM	Transmission electron microscopy
UHMWPE	Ultra high molecular weight polyethylene
XPS	Electron spectroscopy for chemical analysis

1

Introduction

1.1 Tribology of polymer-matrix-composites

Friction and wear are well known phenomena which occur in basically all forms of machines and instruments containing moving parts. These phenomena result in energy losses and machine break downs, and are of significant economical importance [1, 2]. It is estimated that approximately one third of the world's energy resources in present use are consumed in overcoming different kinds of friction and wear. However, consistent research in this field is relatively recent [3].

Polymer-matrix-composites (PMCs) is a class of materials which is used increasingly in applications where tribology control is essential [4] e.g. in vacuum pumps, seals, bearings, brakes and implants. PMCs generally have the benefits of easy processability, high strength-to-density ratio, chemical resistance and low coefficients of friction. Furthermore, some polymers have self-lubricating properties e.g. polytetrafluoroethylene (PTFE) and polyethylene (PE). This ability makes PMCs applicable for dry-sliding applications against steel counterfaces and obvious candidates for tribological systems where addition of lubricants such as oil or grease can not be tolerated. Additionally, these self-lubricating properties decreases the need for maintenance and the risk of emergency sliding conditions, which is seen for metals if these are insufficiently lubricated.

In many applications the combination of both good mechanical and tribological properties is required. Neat polymers are generally limited by inferior thermal and mechanical properties relative to metals and ceramics. These properties are in turn often correlated with tribological parameters. Mechanical energy is dissipated as heat during sliding. This may lead to decomposition and deterioration of mechanical properties, which often decrease the friction and wear performance. The latter limits the life time and application range of components made from PMCs. This is especially a problem in applications involving high contact pressures (p) and/or sliding velocities (v) since this gives rise to a high rate of energy dissipation. Thus, optimization of PMCs for dry-sliding applications can roughly be divided into two main objectives: a) Reduction of friction, and hence heating, by applying lubricating polymers or fillers and b) Improving mechanical properties by incorporating different types of reinforcements, which simultaneously decrease wear and possibly also friction.

Relatively extensive research has been conducted on the effect of solid lubricants [5–11], reinforcing fibers [12–21] and inorganic particles [22–27] for tribological optimization of PMCs. However, published data frequently seems to be conflicting and general guidelines are difficult to extract. This is due to the fact that friction and wear are complicated phenomena, which are not merely material properties but rather system properties. Hence, many parameters influence friction and wear and these may all have significant impact on the observed behavior. This causes design and optimization of tribological systems to be largely controlled by trial and error. Thus, there is a need for more knowledge and understanding, which may lay the foundation for predictive guidelines for structuring self-lubricating PMCs toward enhanced friction and wear control.

1.2 The scope of the Ph.D. project

This Ph.D. work is conducted in collaboration with the company Elektro-Isola A/S. The latter specializes in production of PMCs using thermoset resins, e.g. epoxy, phenol and polyimide, which are reinforced by different fabrics e.g. polyester, cotton and glass weaves. The PMCs are produced by prepreg technology where the fibers in the weave are impregnated with the resin formulation and after a heat treatment becomes a prepreg. Individual layers of prepreg are subsequently stacked and bonded together into a rigid material upon curing under high temperature and pressure. Elektro-Isola A/S produces PMCs for various applications some of which tribological properties are of significant importance. The overall aim of this collaborative work is to examine new material combinations, which are expected to exhibit good tribological properties when tested under well-defined conditions. It has been decided to limit the choice of materials to thermoset resins and reinforcements, which can be produced by prepreg technology. Friction and wear of produced PMCs are examined by dry-sliding against smooth steel counterfaces at ambient temperature and humidity.

Tribological studies of PMCs have not previously been conducted on the Danish Polymer Centre. Consequently, this work started from the foundation in the sense that neither tribological test-equipment or knowledge of this field existed. To obtain knowledge a literature study has been conducted, which constitutes the basis for choice of components for production of PMCs. In order to examine the produced PMCs, tribological test-equipment has been designed and built as a part of this project.

1.3 Research content

In this Ph.D. work, PMCs are produced using an epoxy resin (EP) as matrix. Epoxy typically exhibits relatively high wear rates and coefficients

of friction when dry-sliding against steel counterfaces. This is basically due to the cross-linked molecular structure, which inhibits formation of an efficient transfer film on the steel counterface and results in a relatively high degree of brittleness. However, EP has other favorable properties such as strong adhesion to many materials, good mechanical and electrical properties, relatively high chemical and thermal resistance [28], and a low price compared to advanced polymers such as polyetheretherketone (PEEK) and polyimide (PI). From this perspective, it is an attractive goal to obtain a well functioning EP-based composite for dry-sliding by incorporating the right kind of components e.g. fibers or particles.

Two types of fibrous reinforcement are examined and compared in this study: a plain glass fiber weave (G) and a carbon/aramid hybrid weave (CA), which in both cases give rise to bidirectional fiber orientations in the composite. Others have for unidirectional oriented fiber composites demonstrated the general superiority of continuous carbon and aramid fibers compared to glass fibers when dry-sliding against smooth steel [29, 30]. Furthermore, a positive synergistic effect of combining aramid and carbon fibers has been reported [31]. Thus, application of a carbon/aramid hybrid weave seems interesting to explore further. Tribological comparison between different PMCs are often made at one or a few combinations of contact pressure p and sliding velocity v (pv conditions). However, the tribological properties of PMCs are frequently highly sensitive to the applied pv condition. In this study, the two types of weave are therefore compared at nine different pv conditions in order to systematically examine and compare the performance of these differently reinforced materials as they are exposed to increasingly severe sliding conditions.

Additionally, experiments with incorporation of micro-scale PTFE particles and nano-scale CuO particles into either the neat EP resin or into the resin along with the carbon/aramid weave is conducted. Furthermore, possible synergistic effects of adding different amounts of nano-CuO together with PTFE microparticles into the neat EP is examined. PTFE is widely used as a solid lubricant due its chemical resistance, thermal stability, low surface energy and generally excellent frictional properties. Thus, it is anticipated that the lubricating effect of the PTFE particles might reduce frictional heating and thereby make the composite useful at more severe pv conditions.

Presently, the use of inorganic nano-scale particles receives a lot of attention [32–41]. Utilization of these nanoparticles seems to be a promising way to improve friction and wear properties. Generally, an optimum concentration of nanoparticles is found in the range of 2-5 vol% [42], which is approximately a factor of 10 lower than typically found for microparticles. Such a low particle content makes it possible to use nanoparticles to improve the properties of resins used for continuous fiber reinforced composites with a high fiber content. The mechanisms behind optimization by nanoparticles are not entirely understood and can not be explained by

models for larger-scale reinforcement. However, based on existing publications, the overall reasons for tribological improvements can roughly be divided into two categories: a) Improvements are due to better mechanical and thermal properties of the PMC, and b) Improvements are due to an enhanced ability of the PMC to form a thin, homogeneous and tenacious transfer film on the steel counterface. With respect to mechanical properties, it is reported that nanoparticles frequently increase strength and stiffness while simultaneously increasing strain-to-failure and toughness [43–48]. This is opposite the trend typically found for microparticles where improvement in one property often is obtained at the expense of another [49]. The stabilization of transfer films is typically attributed to tribo-chemical reactions, which increase the adhesion of the film to the counterface, or to an ability of the particles to smoothen the counterface in a manner, which favors adhesion. Furthermore, it has been suggested that the cohesive strength of transfer films possibly increases, because the nanoparticles are capable of blending well with the wear debris [42, 50].

The effect of different microparticles, e.g. TiO_2, CuO, CuS, ZnF_2 and CaF_2, have been reported by others [51]. The effect on wear depends on the type of particles applied and seems to be linked to the ability of the particles to engage in tribo-chemical reactions during sliding. Since CuO is reported to yield good results on micro-scale [52, 53] it seems like a logical choice also to test this compound on nano-scale.

As mentioned above, the positive effect of particles is often through stabilization of transfer films. However, EP resins do generally not form effective transfer films due to the cross-linked molecular structure. Therefore, the combined effect of adding PTFE as a solid lubricant as well as nano-CuO is investigated. The underlying hypothesis is that the nanoparticles might stabilize a transfer film created by the incorporated PTFE and thereby decrease friction and wear. Furthermore, a possible toughening of EP by nanoparticles, which counteracts the inherent brittleness, is also expected to increase the wear resistance.

In order to evaluate the tribological properties of the produced PMCs, a tribotester is designed and built as a part of this Ph.D. work. It is chosen to build a tribotester of the Pin-On-Disk (POD) type, which is capable of measuring coefficients of friction, wear rates and disk temperatures.

1.4 Thesis outline

In chapter 2 basic concepts and theories of friction and wear are introduced with special emphasis on polymer tribology. The chapter is meant as an introduction to tribology for readers, who are not familiar with this field. Chapter 3 reviews some of the published literature, which has inspired the work presented here. This chapter is intended to be a more thorough introduction to the research field in question, which may inspire to further reading. It is, however, not a prerequisite for reading the remainder of

this report. In chapter 4 various experimental details are given. The latter includes information on applied materials, methods for production of PMCs, measuring procedures and a description of the produced POD apparatus. Chapter 5 presents the main results obtained during the work on this Ph.D. These results are mainly a summary of the findings given in the three papers located in appendices A, B and C with the titles:

- *Comparison of friction and wear for an epoxy resin reinforced by a glass or a carbon/aramid hybrid weave*. Current status: published in the journal *Wear* March 2007.
- *The effect of particle addition and fibrous reinforcement on epoxy-matrix composites for severe sliding conditions*. Current status: accepted for publication in the journal *Wear* and is available on-line.
- *Changes in the tribological behavior of an epoxy resin by incorporating CuO nanoparticles and PTFE microparticles*. Current status: accepted for publication in the journal *Wear*.

Finally, conclusions are given in chapter 6 followed by a list of references.

2

Background

In this chapter basic concepts and theories of friction and wear are introduced. Despite being overly simplified, these theories give a basic understanding and are useful for interpretation of tribological data. The described models are not in all cases equally applicable to metals and polymers. Specific tribological behaviors for polymers which cause significant deviations from the more classical theory will be mentioned. This introduction is mainly based on the books by J. K. Lancaster [54], A. D. Sarkar [55], E. Rabinowicz [1], I. M. Hutchings [2] and J. A. Williams [56]. These books are recommended for further reading.

2.1 Real area of contact

Surfaces which appear smooth to the eye are in most cases rough when studied in a microscope. When two such surfaces are pressed together the real area of contact (A_r) will differ from the geometrical (apparent) area of contact (A_a), as the surfaces are in contact only in small regions referred to as junctions, cf. figure 2.1.

Interactions between surfaces occur at the junctions as these are close enough for short-range intermolecular forces to be significant. These forces cause adhesion between the surfaces. The magnitude of the adhesional force, which restricts relative movement, is proportional to A_r. Thus, A_r is an important parameter in tribology and it is therefore relevant to know which parameters controls the magnitude of this parameter.

Imagine two surfaces, with asperities of a given height distribution, pressed together by a load normal to the surfaces (W_N). These asperities, i.e the peaks of the surface roughness, form junctions, which will deform elastically or plastically depending mainly on the surface topographies and on the material properties. When the load increases, both the number and size of junctions increase. Hence, it might be expected that A_r is a function of W_N and material properties such as the elastic modulus (E) and the compressive yield stress (σ_y).

For the idealized case of a single deformable asperity pressed against a rigid plane, the following simple relationships apply, cf. equation (2.1) for plastic deformation and (2.2) for elastic deformation.

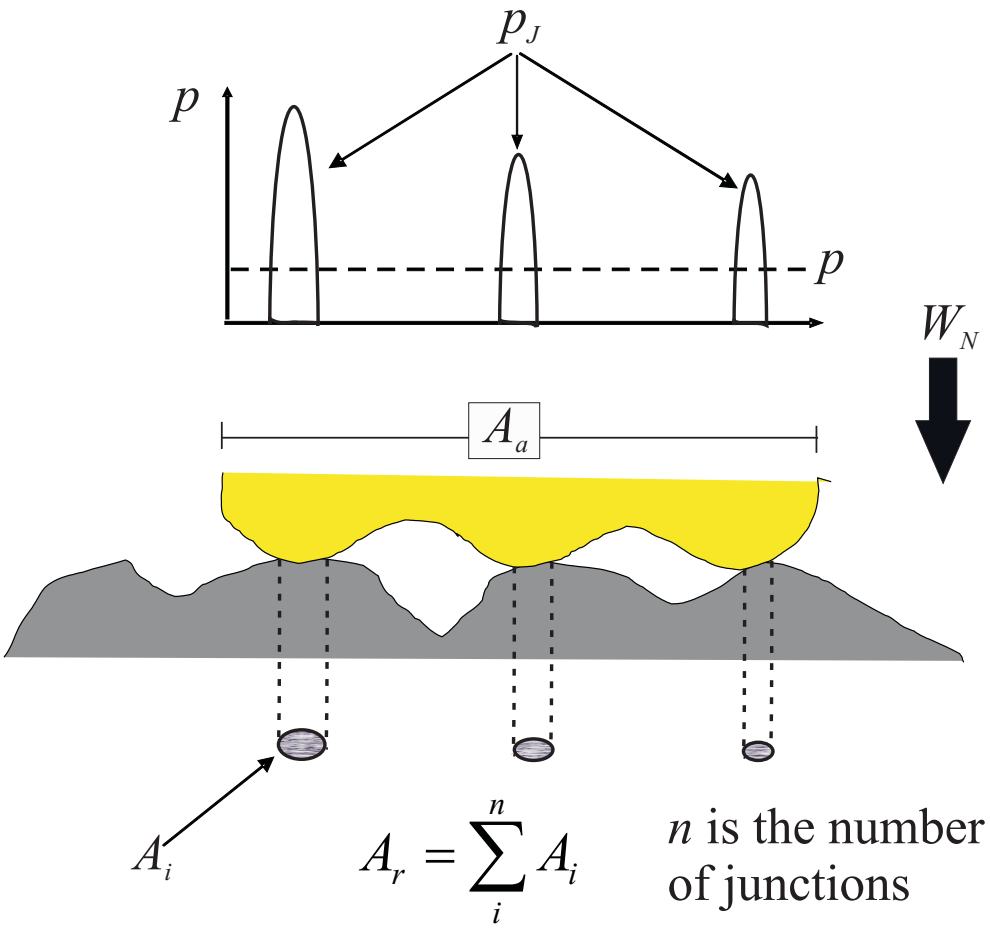

Figure 2.1. An illustration of the distinction between the apparent (A_a) and the real area of contact (A_r) between two surfaces pressed together by a force W_N. Furthermore, the difference between the apparent contact pressure (p) and the actual contact pressure at the junctions (p_J) is exemplified.

$$A_r = C_p \cdot \frac{W_N}{\sigma_y} \approx \frac{W_N}{H} \tag{2.1}$$

$$A_r = C_e \cdot \left(\frac{W_N}{E}\right)^{2/3} \tag{2.2}$$

Here
C_p is a constant which typically has a value of $\frac{1}{3}$
H is indentation hardness of the softer material
σ_y is compressive yield stress of the softer material
C_e is a constant which depends on asperity size and contact geometry
E is the elastic modulus of the deformable material

The relationship given in equation (2.1) is the basis for the indentation hardness test and is often found to agree with experimental determinations of A_r. Prediction of A_r in the elastic case is complicated by the fact that it requires knowledge about asperity size and contact geometry. However, the important point seen by these equations is that A_r ideally is directly proportional to W_N for plastic deformation and to $W_N^{2/3}$ for elastic deformation.

Asperities of real surfaces typically have a distribution of sizes and shapes. Whether asperity deformation is mainly elastic or plastic can be estimated by the plasticity index (ψ) introduced by Greenwood and Williamson [57]:

$$\psi = \frac{E}{H}\left(\frac{\sigma^*}{r}\right)^{1/2} \tag{2.3}$$

Here
σ^* is the standard deviation of the asperity height distribution
r is the average radius of curvature of the asperities

It is seen that the deformation mode is controlled by material properties and surface topographies. A value of ψ less than 0.6 indicates predominately elastic deformation, whereas values larger than 1 implies plastic deformation. According to equation (2.3), an increase in surface roughness will increase the tendency to deform plastically. Furthermore, the ratio E/H is typically significantly lower for polymers than for metals, which implies that polymers typically deform elastically contrary to metals.

Greenwood and Williamson also carried out statistical analysis of multiple asperity contacts. It was found that for real surfaces with a statistical distribution of asperity heights, A_r is directly proportional to W_N even though the asperities are mainly elastically deformed. Thus, for real surfaces A_r typically increases linearly with load and is independent of the apparent contact area A_a. However, if a polymeric material is loaded to an extent where there no longer exists a statistical distribution of asperity

heights, the relation between A_r and W_N given by equation (2.2) is likely to give a better approximation.

2.2 Friction

Consider two bodies in contact which slide across each other. This relative movement will be restricted by a force known as friction. During this process mechanical energy is transformed into other forms of energy but mainly into heat. This energy dissipation is caused by different mechanisms occurring on micro-scale e.g. brittle fracture, plastic deformation, shearing of interfacial adhesive bonds, elastic hysteresis and chemical reactions (tribo-chemistry). The relative importance of these contributions depends on the sliding partners, operating conditions and use of lubricants. For instance, if the surfaces are smooth, non-lubricated and have affinity for each other, the adhesion contribution is likely to be important, whereas elastic hysteresis, brittle fracture and plastic deformation are likely to be important in the case of rubbers, thermosetting polymers and thermoplastics, respectively. The basic empirical law of dry-sliding friction often attributed to Amontons is given in equation (2.4).

$$\begin{aligned} F_f &= \mu \cdot W_N \\ \Downarrow & \\ \mu &= \frac{F_f}{W_N} \end{aligned} \tag{2.4}$$

Here
F_f is frictional force
μ is the kinetic coefficient of friction

According to Amontons law, F_f is proportional to W_N and independent of A_a. This is often found experimentally to be the case and is a consequence of the direct proportionality between A_r and W_N. However, many exceptions exist especially for heavily loaded polymers due to their tendency to deform elastically [58], cf. section 2.1.

2.2.1 The two-term model of friction

It has become conventional to divide the origin of μ into two main contributions namely an adhesion term and a deformation (or ploughing) term [56]. The components of friction are not easily separated as these are correlated. However, an attempt to do this is made with the two-term non-interacting model of friction. In this model it is assumed that the

frictional work is dissipated in two discrete zones, which are a thin interfacial zone and a much larger cohesive bulk zone, respectively, cf. figure 2.2.

The interfacial zone is characterized by localized interfacial shear, which is restricted by adhesion forces only. The cohesive zone is characterized by larger-scale deformations, which presumably do not depend on adhesion but on the geometry of the rigid counterface asperities. A value for the deformation term can in principle be achieved experimentally by efficient lubrication and hence suppression of adhesion forces [59]. Which of the two terms is most important depends especially on the counterface roughness, relative hardness and affinity of the sliding partners. The two terms will shortly be described in the following starting with the adhesion component.

When two relatively smooth surfaces in contact slide relative to each other, junctions will be formed in the interface due to adhesion and these will subsequently be broken due to interfacial shear stress. Assuming that the average shear stress over A_r has a value of τ_{av}, then F_f can be written as in equation (2.5).

$$F_f = \tau_{av} \cdot A_r \tag{2.5}$$

Here
τ_{av} is average shear stress over A_r

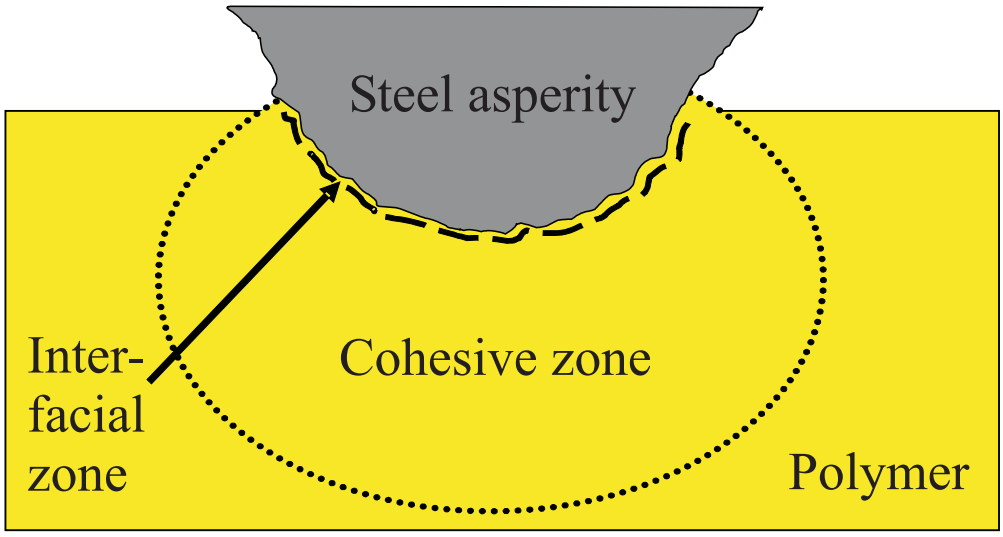

Figure 2.2. Illustration of the two-term model of friction. A steel asperity of the counterface partially penetrates and slides on a polymer surface and gives rise to dissipation of energy in two presumably separate processes. These process are associated with two distinct zones i.e. an interfacial zone and a much larger cohesive zone. Sliding direction is normal to the plane of the paper.

By using the relations given by equation (2.1), (2.4) and (2.5), the following equation for the adhesive term (μ_a) can be obtained:

$$\mu_a = \frac{F_f}{W_N} = \frac{\tau_{av} A_r}{H A_r} = \frac{\tau_{av}}{H} \tag{2.6}$$

It may be argued that τ_{av} can not exceed the shear strength (τ_s) of the weaker material. Thus, if the adhesion force between junctions is larger than the cohesive force, then shear will take place in the weaker material and particles will be formed adhering to the stronger surface. Based on these arguments the coefficient of friction may be written as in equation (2.7).

$$\mu_a = \frac{\tau_s}{H} \tag{2.7}$$

Here
τ_s is the shear strength of the weaker material

Hence, equation (2.7) gives an estimate for μ_a solely based on properties of the weaker material. Even though this equation agrees relatively well with measurements of μ for some polymers, it can not be expected to give a quantitatively reliable estimate [54]. However, important qualitative trends can be deduced from this equation. It explains why materials with very different material properties show relatively little variation in μ. Since H and τ_s are properties related to the bond strength of the material, these are correlated such that a high value of H corresponds to a high value of τ_s and vise versa. The theory given above indicates that a low friction material can be obtained, if it is designed with a thin surface layer with low shear and/or adhesive strength, which is supported by a bulk with a high compressive yield strength. These criteria can be satisfied by for example using a hard material combined with solid or fluid lubricants.

The deformation component of friction plays a significant role when a hard and rough surface slides across a softer surface. In this situation the sharp asperities of the hard material penetrate the softer material and produce grooves during sliding, cf. figure 2.3.

The energy needed for deformation when producing a groove gives an additional contribution to μ, which is not taken into account in equations (2.6) and (2.7). As discussed previously the adhesion component of the frictional force is directly proportional to A_r. This is not the case for the deformation component of the frictional force, which presumably is proportional to the area of the penetrating asperity projected in the sliding direction (A_p) given by equation (2.8).

$$A_p = r^2 tan\theta \tag{2.8}$$

Here
θ is the roughness angle of the asperity defined in figure 2.3

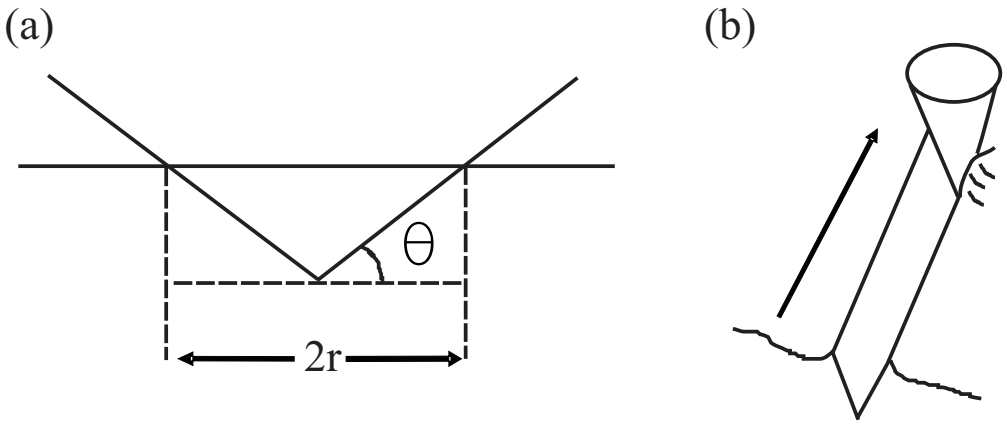

Figure 2.3. (a) Illustration of a conical steel asperity pressed into a polymer surface, where θ is roughness angle and r is radius. (b) Illustration of a conical steel asperity producing a groove in a polymer surface during sliding.

r is radius of the indentation made by the asperity

Assuming the contribution to the frictional force originating from creating a grove during sliding is given by $F_f = A_p \cdot H$ and the load supported by the asperity is given by $W_N = \pi r^2 \cdot H$, then the deformation term (μ_d) can be written as in equation (2.9).

$$\mu_d = \frac{F_f}{W_N} = \frac{r^2 tan\theta \cdot H}{\pi r^2 \cdot H} = \frac{tan\theta}{\pi} \tag{2.9}$$

Since the hardness is used as a measure for both the resistance against groove formation and indentation, this parameter cancels out and μ_D is solely controlled by θ. Finally, μ consisting of the two described terms is given in equation (2.10).

$$\mu = \mu_a + \mu_d = \frac{\tau_s}{H} + \frac{tan\theta}{\pi} \tag{2.10}$$

The counterface roughness to a large extent determines the relative contributions of these two terms. Experimental determinations of μ as a function of counterface roughness frequently show a minimum at a certain intermediate roughness. At the extremes, high friction may be seen either due to a dominating deformation term or due to strong interfacial adhesion. A high deformation term is not necessarily caused by a rough counterface, it may also be significant due to the presence of abrasive particles between the sliding surfaces.

An important tribological property of polymers (especially thermoplastics) is their ability to form transfer films when sliding against steel counterfaces [60], which is illustrated in figure 2.4. When such a film is present, shear no longer occurs between the bulk polymer and the steel but instead between the polymer and the transfer film or within the transfer

film. Thus, the transfer film acts as a protective spacer between the surfaces and the film properties become the controlling factor for friction and wear. PTFE and HDPE are known for their ability to from thin, oriented transfer films under certain conditions, which give rise to very low values of μ. Also in relation to transfer film formation and stability an optimum intermediate counterface roughness is often found [61]. A very smooth counterface might result in poor film stability due to the absence of mechanical interlocking (i.e. polymeric material which is locked between asperities and in crevices in the steel surface), while a very rough counterface might be difficult to cover and thereby give rise to an inhomogeneous film.

2.3 Wear

Wear can be defined as removal of material from interacting surfaces in relative motion. Whereas friction induces energy losses, wear causes material losses [62]. Wear, like friction, is a complex matter, because different often correlated forms of wear may exist simultaneously. Attempts have been made to divide wear into different main groups e.g. adhesive wear, abrasive wear, fatigue wear and tribo-chemical wear. These wear types are briefly described below.

- **Adhesive wear** occurs when junctions with a relatively high adhesive strength are formed during sliding. In this situation a fragment typically from the material with the lowest cohesive strength is removed by adhering to the stronger surface. Thus, the breakage of

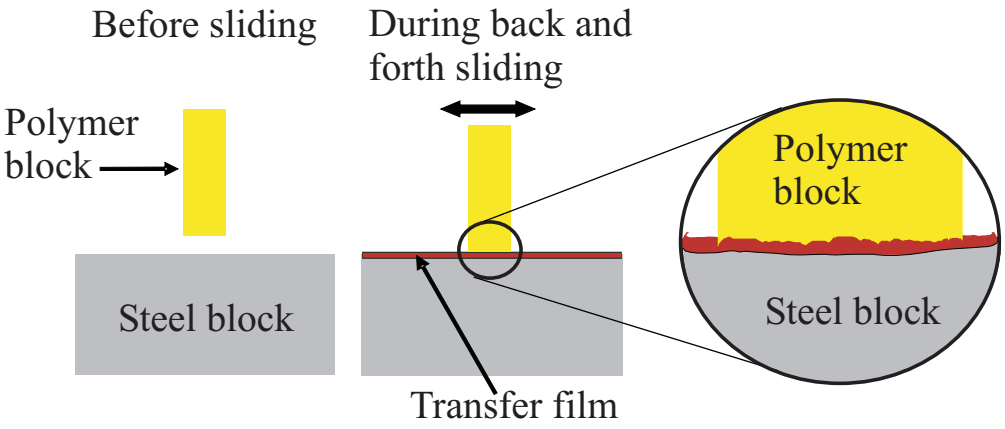

Figure 2.4. A polymer block is loaded against a steel block and is forced to slide back and forth. In this process energy is dissipated and the polymer is worn. The produced polymeric wear debris is compressed between the surfaces and form a transfer film on the counterface.

the junction occurs in the weaker material and not in the stronger bonded interface. This type of wear is likely to be significant in the case of sliding between smooth surfaces with a high affinity for each other.

- **Abrasive wear** occurs when a hard rough surface slides on a significantly softer surface. In this case hard asperities partially penetrate the softer surface and produces a groove during sliding, which results in loss of material. Abrasive wear can also occur between two soft surfaces, if hard particles (abrasives) are caught between them.

- **Tribo-chemical wear** occurs when chemical reactions between the materials and the environment governs the wear process. An example of this is when oxygen from the environment is the chemical species involved in thermal degradation and hence high wear of a thermoset polymer.

- **Fatigue wear** may occur when asperities are exposed to cyclic stress variations during sliding. These fluctuating stresses can result in surface or subsurface cracks, which can grow, intersect and eventually lead to the release of relatively large wear particles from the surface.

The following will mainly focus on adhesive and abrasive wear, since a understanding of these is considered to be most relevant in relation to this thesis. In analog to friction, different wear mechanisms can be related to either interfacial or cohesive dissipation processes, cf. figure 2.2. Adhesive wear is related to the interfacial zone while both abrasive and fatigue wear are related to dissipation of frictional work in the larger cohesive zone.

2.3.1 Adhesive wear

Consider two bodies in close enough contact for adhesional bonding to occur. If these bodies are pulled apart, the adhesional forces will attempt to pull material from one body to the other. If material actually is pulled from one surface, while adhering to the other, then the material loss is characterized as adhesive wear. The principle of this is shown in figure 2.5.

Quantitatively, the adhesive wear volume (V_{ad}) can be estimated by the Archard wear equation, cf. equation (2.11). The Archard equation is based on the assumption that every time a junction is sheared, there is a constant probability (P) that an adhesive wear particle will be formed, which has a hemispherical shape with a radius equal to the radius of the junctions.

$$V_{ad} = P \cdot \frac{W_N \cdot x}{3H} = k_{ad} \cdot \frac{W_N \cdot x}{H} \tag{2.11}$$

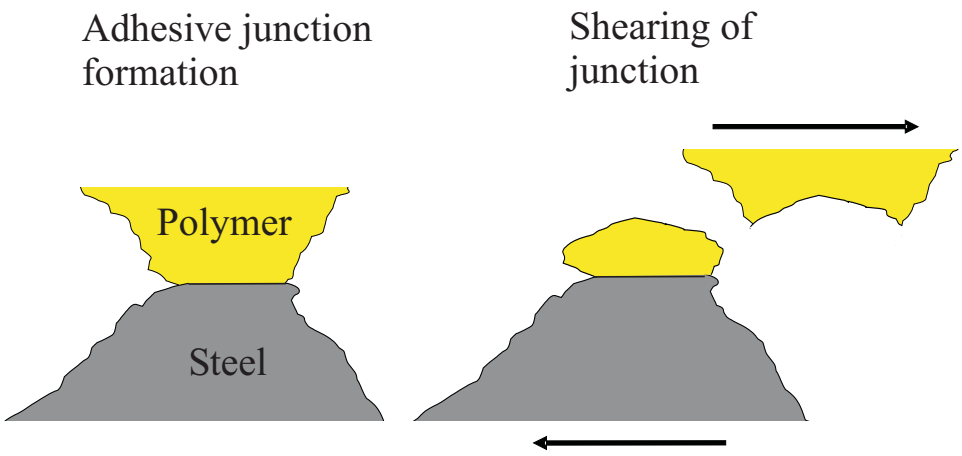

Figure 2.5. Illustration of an adhesive junction formed between a polymer and a steel surface. Since, the interfacial adhesive strength is larger than the cohesive strength of the polymer, fracture occurs in the latter when exposed to shear stress. This results in formation of an adhesive wear particle which adhere to the steel surface.

Here
x is sliding distance
k_{ad} is the adhesive wear coefficient

According to equation (2.11) the amount of wear is directly proportional to both the sliding distance and the load, and inversely proportional to H of the softer material. Thus, wear can presumably be reduced by using hard materials as sliding partners in order to limit A_r. Furthermore, the surfaces should have a low tendency to adhere to each other (i.e. a low work of adhesion) in order to reduce the probability of cohesive junction fracture, P, and hence limit wear. The proportionality between wear and load is found experimentally to apply for both polymers [63] and metals [64] when tested in a load range where other parameters are fairly constant. Also the direct proportionality between wear and sliding distance is normally valid after a certain running-in period, where the sliding surfaces are modified or transfer films are formed. Hence, a transition from an initial wear rate to a steady state wear rate is often observed.

For polymers, matters are in general significantly more complicated than indicated by equation (2.11). This is especially due to their tendency to form transfer films when sliding against relatively smooth counterfaces, cf. figure 2.4. Transfer film formation is also regarded as adhesive wear, which may be divided into the following three steps: 1) Adhesion of the polymer to the counterface, 2) Build-up of a transfer film after repeated sliding and 3) Gradual detachment and reestablishment of the transfer film. In such cases, the rate determining step seems to be detachment of the transfer film. Hence, measures which improve adhesion of the transfer

film to the counterface often results in a significant wear reduction. This means that strong adhesion between the polymer and counterface might result in a high initial wear rate (in agreement with equation 2.11), while also giving rise to a low steady state wear rate due to a stable protective transfer film. Since the role of transfer films is so important in relation to tribology of polymers, it is found difficult to correlate adhesive wear with mechanical properties such as hardness.

2.3.2 Abrasive wear

Abrasive wear can be divided into two-body and three-body abrasion, respectively. Two-body abrasion occurs when a hard and rough body slides across a significantly softer body and produces grooves and scratches in the process. The lost material is typically removed in the form of loose particles or left as mounds along the grooves. Three-body abrasion occurs when particles, which are harder than the sliding partners, are present between the surfaces. Such particles can dig into or adhere to one surface while producing a groove in the other. These third body particles may come from the environment or it might be wear debris produced during sliding.

A simple expression for two-body abrasive wear, cf. equation (2.12) can be obtained by considering a conical steel asperity, which penetrates a softer surface and producing a groove during sliding, cf. figure 2.3. It is assumed that all material which was formerly in the groove is removed as debris.

$$V_{ab} = \frac{W_N \cdot tan\theta \cdot x}{\pi H} = k_{ab}\frac{W_N \cdot x}{H} \tag{2.12}$$

Here
V_{ab} is the abrasive wear volume
k_{ab} is the abrasive wear coefficient

It is seen that the equation for abrasive wear is of the same form as the one for adhesive wear. However, the meaning of the wear coefficient is different. In the case of adhesive wear, k_{ad} depends on the probability of forming a wear particle when a junction is broken, whereas k_{ab} depends on the average roughness angle θ. Hence, rougher counterfaces with larger values of θ will produce more abrasive wear. It should be noted that equation (2.12) is overly simplified and does not take any distribution of roughness angle or shape of asperities into consideration. Furthermore, material from produced grooves tend to pile up in front of the asperities or be plastically relocated instead of being removed as loose debris. Additionally, repeated sliding on the same wear track will cause wear particles to clog the space between the hard asperities. These phenomena will typically result in lower wear than predicted by equation (2.12) [56].

Despite the shortcomings of equation (2.12), it has been verified experimentally for both polymers and metals that the proportionality between W_N and V_{ab} is valid [54, 65]. The inverse relationship between V_{ab} and H seems to apply to metals but generally not to polymers. The latter, is due to the tendency of polymers to deform elastically instead of plastically. When the deformation mode is mostly elastic, the wear mechanism is dominated by fatigue wear rather than abrasion. This is typically the case for low E-modulus polymers, while high modulus polymers such as thermosets are mainly worn by abrasion. Polymers with an intermediate modulus are expected to be worn by a combination of the two mechanisms. Instead of hardness, a better correlation is found between V_{ab} and $1/\sigma_s\epsilon$, where σ_s is tensile strength and ϵ is ultimate elongation. This is known as the Ratner-Lancaster correlation and implies that toughness is an important anti-wear property of polymers when exposed to abrasive conditions. Rubbers for example often perform very well in abrasive environments despite a low H, which is due to their large ultimate elongation ϵ.

2.3.3 Wear rate equations

When publishing wear data, these are typically expressed as wear rates instead of wear volume. In the following some frequently applied wear rate equations are given which are also applied for presentation of wear data in this report, cf. chapter 5. A specific wear rate ($\dot{w}_s$) can be obtained by differentiation of the Archard equation (2.11) and normalizing it to W_N, cf. equation (2.13). The subscripts for V and k are omitted in the treatment given below since no specific wear mechanism is assumed.

$$\begin{aligned} \dot{w} &= \frac{dV}{dx} = k \cdot \frac{W_N}{H} \; [mm^3/m] \\ \Downarrow & \\ \dot{w}_s &= \frac{\dot{w}}{W_N} = \frac{k}{H} = k^* \; [mm^3/Nm] \end{aligned} \tag{2.13}$$

Here
$\dot{w}$ is wear rate
V is wear volume given by the Archard equation
k is an unspecified wear coefficient
$\dot{w}_s$ is specific wear rate
k^* is the wear factor

Thus, $\dot{w}_s$ is equal to the wear factor k^*, which can be calculated from measured quantities by using equation (2.14).

$$k^* = \frac{\Delta m}{x \rho W_N} \; [mm^3/Nm] \tag{2.14}$$

Here
Δm is mass loss during sliding
ρ is density of the worn material

Since, $\dot{w}_s$ from a simplified point is independent of W_N and x, it is a convenient parameter to apply when comparing data obtained in different wear studies. By utilizing that $x = v \cdot t$, where t is time and v is sliding velocity, and $p \cdot A_a = W_N$, the following rearrangements of equation (2.14) can be performed:

$$\begin{aligned} k^* &= \frac{\Delta m}{\rho A_a t \cdot pv} = \frac{\Delta h}{t \cdot pv} \\ \Downarrow & \\ \dot{w}_t &= \frac{\Delta h}{t} = k^* \cdot pv \; [\mu m/h] \end{aligned} \tag{2.15}$$

Here
t is time
p is apparent contact pressure
Δh is height reduction of the test specimen
$\dot{w}_t$ is the depth wear rate

The depth wear rate $\dot{w}_t$ can be regarded as height reduction of the test-specimen as a function of time t during experiments. Note, that $\dot{w}_t$ is directly proportional to the pv factor (i.e. the product of apparent contact pressure and sliding velocity) as long as k^* is a constant. The latter depends on both material properties and system properties. Thus, if the system properties are fixed, k^* can to some extent be regarded as a material property. Generally, equation (2.15) applies inside a certain range of moderate pv factors. However, if either v or p exceeds a certain level, a change in wear mechanism might occur due to e.g. thermal softening and decomposition of the material. The pv condition where equation (2.15) breaks down and excessive wear may be observed is referred to as the limiting pv factor (pv_{lim}), which can be regarded as a performance parameter for a given PMC at specified sliding conditions. Generally, performance improvement aims at decreasing k^* and increasing pv_{lim}.

2.4 Frictional heat and contact temperature

Frictional heat is generated during sliding which may lead to melting, decomposition and deterioration of mechanical properties. As described

previously, mechanical properties such as H, E and σ_s play an important role in relation to tribology and all decrease as a function of temperature. Equation (2.16) gives an estimate for the specific rate of energy dissipation ($\dot{Q}_d$) i.e. the rate of dissipated energy per unit apparent contact area A_a during sliding:

$$\dot{Q}_d = \mu \cdot pv \ [J/m^2 s] \tag{2.16}$$

It is seen that $\dot{Q}_d$ is directly proportional to μ and to the pv factor (or pv condition). The relationship for the estimation of $\dot{w}_t$ given by equation (2.15) does not take temperature increases in the interfacial zone into consideration. However, equation (2.16) shows that the dissipated energy, and hence the temperature in the interfacial zone will rise with increasing pv factors and possibly induce changes in mechanical properties.

Equation (2.16) predicts how much heat is generated per unit A_a and time, but it tells nothing about how the heat is distributed in the interfacial zone. As illustrated in figure 2.1, the load is not carried by A_a but by a number of junctions, which collectively give A_r. These junctions absorb significant amounts of energy associated with a high temperature increase referred to as flash temperatures (ΔT_f) or hot spots. Since junctions are constantly formed and broken, these hot spots have a short life time (hence the term flash) and continuously change position. Flash temperatures are difficult to measure and may have a large impact on the tribological behavior. When sliding initiates, both the average temperature over A_a (T_a) and the higher average peak temperature at the junctions will rise and eventually reach a steady state.

The magnitude of T_a is the sum of the environmental temperature (T_e), i.e. the temperature of the surroundings, and the temperature rise caused by friction:

$$T_a = T_e + C \cdot \mu \cdot W_N \cdot v \tag{2.17}$$

Here
C is a constant

In mathematical models for the flash temperature ΔT_f, this parameter is not treated as an absolute temperature but as a temperature difference. More precisely, ΔT_f is the average temperature increase at the junctions above that of T_a. Thus, the mean peak temperature encountered at the polymeric asperities may be written as in equation (2.18).

$$T_p = T_a + \Delta T_f \tag{2.18}$$

Based on the work by Jaeger [66], the flash temperature can be estimated by equation (2.19) for low sliding velocities or by equation (2.20) for high sliding velocities. These equations are based on the assumption that the load is carried by one large asperity and that the magnitude of

A_r is determined by equation (2.1) i.e. by plastic deformation. If sliding is between a polymeric material and a steel counterface, it may also be assumed that practically all heat flows into the steel body since the thermal conductivity of the polymer specimen is insignificant relative to the steel counterface.

$$\Delta T_f = 10^{-4} \cdot \mu \cdot H^{1/2} \cdot W_N^{1/2} \cdot v \tag{2.19}$$

$$\Delta T_f = 5.7 \cdot 10^{-5} \cdot \mu \cdot H^{3/4} \cdot W_N^{1/4} \cdot v^{1/2} \tag{2.20}$$

As may be expected from equation (2.16), ΔT_f increases with W_N, v and μ. Additionally, ΔT_f also increases with H since a high resistance against deformation will cause a decrease in A_r. Thus, energy absorption will occur over a smaller area, which will elevate ΔT_f if all other parameters are unchanged. For simplicity the magnitude of A_r is expressed in terms of H even though it probably is more correct to express it in terms of E for polymers, cf. section 2.1. Another limitation of equations (2.19) and (2.20) is the assumption that H is a constant. Actually, H decreases approximately exponentially with temperature for polymers, which may result in an overestimation of ΔT_f. The flash temperature calculated by equation (2.20) may be corrected for the temperature sensitivity of H by using equation (2.21).

$$\Delta T_f = \Delta T_{f0} + exp\left(-\frac{3}{4} a \cdot \Delta T_f\right) \tag{2.21}$$

Here
ΔT_{f0} is calculated flash temperature assuming H is a constant
a is a constant with a typical value of 0.005

3

Literature review

The possibilities for designing PMCs for tribolocial applications are numerous. However, a common overall approach to design of a low friction PMC with a high wear resistance is illustrated in figure 3.1. Thus, mechanical properties are typically improved by different types of reinforcements, which in turn often result in a simultaneous increase in wear resistance. Solid lubricants may be added to the polymer matrix to decrease adhesion and/or to obtain a transfer film with a low shear strength, which reduces friction and possibly also wear. An additional benefit of solid lubricants is a decrease in frictional heating, which may contribute to a reduced wear rate. It can also be beneficial to add components with good thermal conductivities e.g. metal particles or graphite fibers. Such components may reduce flash temperatures (ΔT_f), cf. section 2.4, by enhancing heat conduction away from the interface.

Extensive research has been conducted on the effect of different fillers on

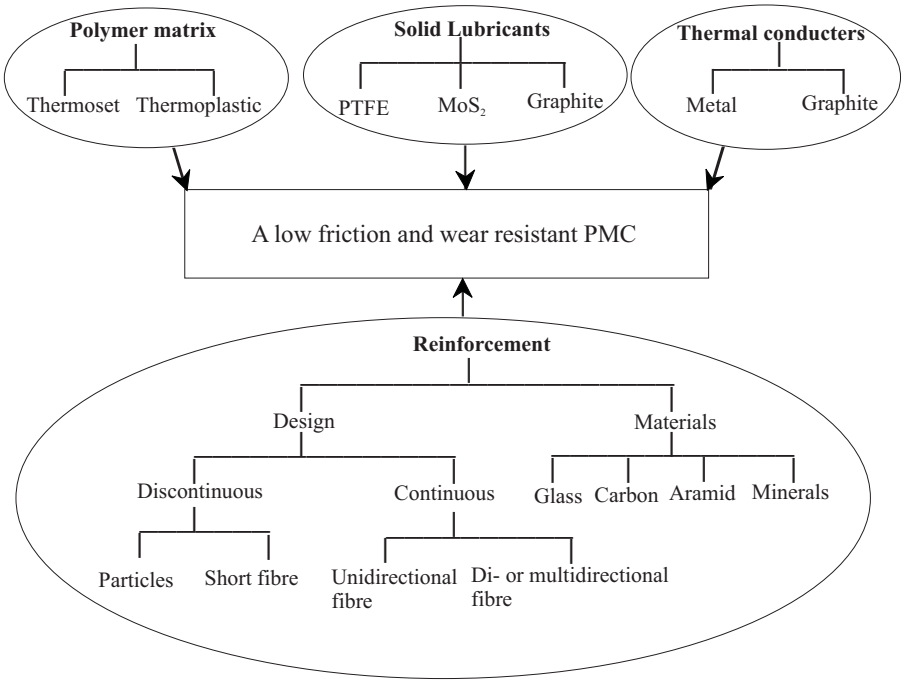

Figure 3.1. Illustration of the typical main components used when designing PMCs for tribological applications.

the tribological properties of PMCs. In this chapter some of the literature, which has inspired this Ph.D. work is reviewed. It is not the intention to give a complete review of the existing literature but merely to summarize some published results, which are related to the work presented in this report. Unless stated otherwise, the mentioned results are obtained by dry-sliding against relatively smooth steel counterfaces at ambient conditions.

3.1 Solid lubricants

The improvements of tribological performance by means of solid lubricants are often attributed to the formation of a transfer film [67], which to some extent is capable of protecting the polymer matrix from the hard steel asperities. Some of the most frequently used solid lubricants are PTFE, graphite and MoS_2. These are weak and soft materials relative to many polymeric matrices used for PMCs. Consequently, addition of solid lubricants often deteriorate mechanical properties. Thus, when adding solid lubricants an optimum concentration typically exists, where there is a useful balance between a positive lubricating effect and a negative weakening of the PMC. This will typically be the case when sliding against relatively smooth counterfaces. However, under very abrasive conditions, addition of solid lubricants is likely to have a detrimental effect since a homogeneous transfer film can not be formed on the rough counterface. Hence, the only effect is a deterioration of mechanical properties and thereby an increase in wear.

Graphite and MoS_2 are lamellar solids in the sense that their molecular structure consists of sheets, which are located parallel to and relatively far from each other. It is suggested that the relatively large space and weak intermolecular forces between the sheets are the reason for the low shear strength. Thus, as shear forces are applied the sheets will be able to slide across each other. When a transfer film is produced on the counterface, sliding and shearing will in principle occur inside the film produced by the solid lubricant [68].

PTFE is one of the most frequently used solid lubricants because of excellent film forming abilities, chemical resistance and a high melting point. Other polymers also form transfer films but these are typically thicker, more lumpy, less homogeneous and hence less efficient. The efficiency of PTFE has been attributed to the "smooth" molecular structure, and low surface and cohesive energy. PTFE consists of long non-branched chains ($-CF_2-CF_2-$), which become oriented in the sliding direction and thereby less entangled than in the bulk zone. The combination of low cohesive strength and oriented polymer chains, is presumably what makes interchain sliding easy during exposure to shear stress [42]. The hypothesis about the role of the smooth molecular profile is supported by the observation that high density polyethylene (HDPE) and ultra high molecular

weight polyethylene (UHMWPE) also have good film forming abilities. Polyethylene, like PTFE, has a smooth molecular profile (-CH_2-CH_2-), which presumably contributes to the formation of a thin homogeneous transfer film, which is not seen in the case of more bulky polymers [69].

Palabiyik et al. [70] examined blends of polyamide 6 (PA6) and HDPE in different proportions. It was found that hardness (H) and tensile strength (σ_s) both increased when elevating the content of PA6. Friction was low for all blends compared to the neat polymers especially compared to PA6. Lowest wear was measured for a blend with 60 wt% PA6 and 40 wt% HDPE. In cases of low wear, a transfer film was seen on the steel disk, which was absent in cases of high wear.

In another study Liu et al. [71] examined polyamide (PA), UHMWPE and a 80/20 wt% blend of the two. Both the neat UHMWPE and the blend showed low friction relative to the neat PA, which was attributed to the self-lubricating properties of UHMWPE. The neat PA and the blend were worn with similar rates, while the neat UHMWPE showed sligthy enhanced wear relative to these.

Bijwe et al. [72] tested blends of polyetheretherketone (PEEK) and PTFE in the range of 0-30 wt% PTFE in oscillating and abrasive wear mode. PTFE addition led to deterioration of all measured mechanical properties. In oscillating movement (against a smooth steel counterface) the PEEK-PTFE blend with the ratio 70/30 wt% showed superior performance with friction and wear reductions of 5 and 30 times, respectively, relative to the neat PEEK. Furthermore, PEEK with 30 wt% PTFE incorporated also showed the highest limiting pv factor. A completely different result was seen in abrasive wear mode. In that case, wear increased for all PTFE concentrations, which was correlated with reductions in H and σ_s.

McCook et al. [73] prepared expanded PTFE films where the porosities were filled with epoxy (EP) resin. By using this procedure EP-PTFE composites were made with a PTFE content of either 50 wt% or 70 wt%. The presence of EP improved the mechanical properties relative to neat PTFE. The frictional properties of the composites were significantly better than for neat EP and even better than for neat PTFE. Also a marked improvement in wear resistance was seen relative to both neat EP and PTFE. Compared to neat PTFE the wear rate was reduced with as much as a factor of 100. The beneficial properties were explained by a sliding process where PTFE in the surface was being drawn out and formed a film over the EP regions.

3.2 Inorganic microparticles

It is known that inorganic particles can enhance both mechanical and tribological properties of polymers. Various inorganic microparticles have been applied in this context, especially different metal oxides and sulphides. The impact on friction and wear of such particles have been stud-

ied extensively by S. Bahadur and co-workers. Application of inorganic particles are often found to decrease the wear rate significantly, however, often at the expense of a slight increase in friction. This increase in friction may be due to: a) Enhanced shear strength of the composite, b) Stronger interfacial adhesion due to affinity between the particles and the counterface, c) An increase in the ploughing contribution to the frictional force due to abrasive action of the particles and d) Increase in the real area of contact (A_r) due to transfer film formation.

It is not completely understood why some particles decrease wear while others do the opposite. Based on published data, it seems like the applicability of inorganic particles depends on whether or not these decompose during sliding and/or take part in tribo-chemical reactions. Such reactions may modify the sliding surfaces in a way that facilitates adhesion between the transfer film and the steel counterface. This will result in a more homogeneous, coherent and stable transfer film, which in turn decreases wear.

It has been reported that a composite consisting of PA11 and CuS was capable of forming an efficient transfer film when sliding on a steel disk. Electron spectroscopy for chemical analysis (XPS) showed the presence of the species Cu and $FeSO_4$, which were not found in the sample prior to sliding. It was hypothesized that tribo-induced formations of anions from decomposition of CuS led to the formation of $FeSO_4$, which in turn was capable of enhancing the bond strength between PA11 and the steel surface by facilitating hydrogen bonds [60].

Zhao et al. [52] studied addition of CuS and CuO to PTFE, CuS, CuF_2, CaO, PbS and AgS to PA11, CuO, CuS and CuF_2 to PEEK. In all cases, decreased wear rates were measured. Furthermore, it was found that addition of BaF_2, CaF_2, ZnF_2, SnF_2, ZnS, SnS, ZnO and SnO to some polymers had a tendency to increase wear. In the cases of wear reduction, XPS analysis showed decomposition of the filler, which was not detected for the particles which increased wear. This led to the conclusion that the wear depressing ability of inorganic particles depends on whether these decompose during sliding, and thereby form products, which enhance adhesion between the transfer film and the counterface. However, this conclusion was questioned by the lack of correlation between the decomposition temperatures of the fillers and the actual detected decompositions. Instead, it was proposed that it is not decomposition of the filler but a tribo-chemical reaction between the filler and metal counterface, which is required for wear reduction. As a criterion for particle selection, it was proposed to use Gibbs free energy change to predict possible reactions between particles and the steel counterface.

Zhao et al. [23] also investigated the effect of adding Ag_2S and PbFe particles, respectively, to a polyphenylene sulphide (PPS) matrix. In the case of Ag_2S, wear was reduced significantly when an optimum filler concentration of 20-30 vol% was applied. This favorable effect was attributed to

the formation of a thin homogeneous transfer film when Ag_2S was present, which according to XPS analysis could be partly explained by a chemical reaction between the filler and the counterface metal. On the other hand, when PbFe was added the wear rate increased, the transfer film was absent and no chemical reactions were detected. However, the coefficient of friction (μ) decreased in the case of both fillers.

Bahadur et al. [74] examined friction and wear of thermosetting polyester with added CuO, ZnO, ZnF_2 and $Zn(C_{18}H_{35}O_2)_2$, respectively. The particle concentration was in all cases in the range of 30-35 vol%. Addition of CuO and $Zn(C_{18}H_{35}O_2)_2$ resulted in a reduced wear rate combined with formation of a thin homogeneous transfer film associated with filler decomposition according to XPS analysis. Addition of ZnO and ZnF_2 resulted in an increased wear rate relative to the unfilled polymer, and in a lumpy and patchy transfer film. The use of fillers resulted in an increase in μ in all cases.

Yu et al. [75] examined the effect of adding CuS, CuO, CaF_2 and ZnF_2 particles, respectively, to PPS (35 vol%). CuS increased the wear resistance significantly while CuO only increased it moderately. On the other hand, particles consisting of CaF_2 and ZnF_2 caused a significant decrease in wear resistance. The determined wear rates were found to correlate with the morphology of formed transfer films. The best wear performance was seen for CuS, which also gave rise to the smoothest transfer film. The reason for this was shown by Energy-Dispersive Analysis (EDS) to be due to tribo-chemical reactions, which presumably enhanced adhesion to the counterface.

Schwartz et al. [22] examined how the deformability of particles and the interfacial strength between particles and a PPS matrix were correlated with the cohesional properties of the transfer film. The particle concentrations were in the range of 20-30 wt%. It was found that particles consisting of Ag_2S or CuS deformed plastically and obtained a smooth surface topography when compressed in a die, while the fillers ZnF_2 and SnS showed multiple cracks when compressed. PPS composites containing Ag_2S or CuS had a higher flexural strength than composites containing ZnF_2 or SnS, indicating that the former fillers adhered better to the polymer matrix. Composites containing Ag_2S or CuS showed very low wear rates relative to unfilled PPS, while composites containing ZnF_2 or SnS increased the wear rate relative to unfilled PPS. In the cases of wear reduction, a homogeneous transfer film with good asperity coverage was observed. All particles resulted in a decrease in μ, but to a lesser extent for the non-deformable fillers.

In another study Yu et al. [76] tested the effect on friction and wear of adding Fe and Cu particles, respectively, to PEEK (35 vol%). Both kinds of particles resulted in a decrease in wear and an increase in friction. The favorable effect on wear was mainly attributed to improved shear strength of the composites. Furthermore, it was argued that pure metal particles

is more reluctant to react chemically with steel counterfaces than metal oxides or sulphides. Therefore, positive effects of pure metal particles are more likely to be due to increases in shear strength (relative to the neat polymer), instead of transfer film improvements caused by tribochemical reactions. The increase in friction was attributed to the higher shear strength and abrasive action of the particles, which may increase the deformation contribution to friction.

Voort et al. [77] studied the effect of adding PTFE and CuS to a PEEK matrix. Wear was significantly reduced at an optimum CuS concentration of 35 vol%. An increase in friction was observed when CuS was added, which was explained by an increase in the ploughing contribution to the frictional force due to the presence of hard CuS particles in the interface. When PTFE was added (5 vol%) along with CuS, the increase in friction was less pronounced and the wear reduction was even higher. As in the previously cited studies, the wear reduction was correlated with the establishment of a continuous and adherent transfer film.

Bhabani et al. [78] tested the abrasive wear resistance of a phenolic matrix containing different amounts of Al_2O_3 microparticles. The counterface was silicon carbide abrasive paper of grade 1200. It was concluded that the lowest wear rate, in the examined range 0-20 w% Al_2O_3, was obtained with a filler concentration of 15 w%. This minimum in wear rate was correlated with a maximum in both H and σ_s.

3.3 Fibrous reinforcement

Various mechanical, tribological and directional properties can be obtained by incorporating fibers of different types, which may be oriented using different architectures or designs. Commonly used fiber materials are glass (GF), carbon (CF) and aramid (AF), which are typically applied as either short fibers or as continuous fibers in unidirectional, bidirectional or multidirectional orientations. Fiber reinforced composites are often highly anisotropic materials, which means that the sliding direction relative to the fiber orientation frequently is an important parameter.

3.3.1 Short fiber reinforcement

Short fibers are typically applied in order to increase parameters such as creep resistance, hardness, compressive strength, impact resistance and thermal conductivity of the polymer matrix. Improvements of these parameters can be especially beneficial at elevated temperatures to counteract thermal softening [79]. Besides improving the mechanical properties, short fibers generally also improve the wear resistance. However, the ability of short fibers to reduce wear has shown to be highly dependent on whether the test conditions are of an adhesive (smooth counterface) or abrasive (rough counterface) nature. In the case of adhesive wear, the use

of short fibers generally leads to reduction of wear while addition of short fibers may be detrimental in the abrasive wear mode.

K. Friedrich and co-workers have studied the influence of short fiber reinforcement extensively. Results for different polymers containing short GF and CF, respectively, indicate that the optimum wear resistance typically is obtained at a fiber concentration in the range of 20-30 vol%. It is generally found that for weak polymers with low wear resistance, the mechanical properties and wear resistance can be enhanced by almost any type of reinforcing fiber, whereas the tribological properties of stronger polymers can be improved only by using certain fibers [80]. CF have often shown to be superior relative to GF, which is explained by the lower abrasiveness of CF relative to GF. Thus, hard particulate wear debris originating from crushing of GF might lead to third body abrasive wear, which opposes the beneficial effect GF may otherwise have on the wear rate. A small degree of abrasiveness, e.g. shown by high strength CF, is suggested to be beneficial since it may smoothen the counterface. Additional benefits of CF relative to GF are a higher thermal conductivity and a lubricating ability [81].

Bijwe et al. [82] reported the tribological performance of polyimide (PI) added GF and different solid lubricants. According to the authors, the performance of a short fiber reinforced thermoplastic is mainly determined by the type of fiber, length of fiber, volume fraction, orientation and fiber/matrix adhesion. The best performance was obtained in the case of PI filled with 25 % GF, 15 % PTFE and a 15 % graphite + MoS_2 mixture. For this composite it was found that μ versus time showed a peak before reaching steady state. It was suggested that the initial increase in μ was due to abrasive action of GF, while the drop in μ and eventual steady state was due to establishment of an effective transfer film. The wear rate increased with normal load (W_N) and time, which was explained by a heat induced deterioration of fiber/matrix adhesion at high pv factors leading to cracking and pull-out of fibers. This wear mechanism was supported by SEM images of worn composite surfaces showing micro-cracking, pulverization, wear thinning of fibers and matrix damage in the form of cracks and melt flow.

Reinicke et al. [83] conducted a study on four relatively heat resistant thermoplastic polymers i.e. PA4,6, polyphthalamide (PPA), polyetherimide (PEI) and PPS which were added short GF (30 wt%) as reinforcement and PTFE (15 wt%) as solid lubricant. Friction measured in fretting (oscillating) mode was reduced for all four fiber reinforced polymers when PTFE was added, and was largely independent of whether the measurements were performed at room temperature or at 150°C. Furthermore, the composites had a significantly higher fretting wear rate without PTFE at both temperatures. It was proposed that the wear rates of the four reinforced polymers were largely controlled by the breakdown and abrasive action of the glass fibers. During fretting mode relatively large fiber parts

were broken off and stayed in the interfacial zone long enough to cause abrasive wear. This effect was less pronounced when the composites instead were tested in sliding mode as the produced glass particles in that case were smaller and appeared to escape more easily from the interfacial zone thereby contributing less to third body abrasive wear.

Bolvari et al. [84] examined the possibilities of optimizing the tribological properties of PA6,6 by using aramid fibers and PTFE. Without PTFE, it was found that the optimum wear performance was obtained at an aramid concentration in the range of 5 to 15 wt%. At aramid concentrations in the range of 25 to 30 wt% the mechanical properties were improved further but the wear rate was higher than for the unfilled polymer, which was suggested to be caused by the presence of large amounts of fibrous debris in the interface causing transfer film disruption. However, when PTFE was added together with aramid, the effect of loose fibers in the interface was diminished. Thus, by using PTFE combined with 25 wt% aramid fibers, a composite with good mechanical properties as well as low friction and wear could be obtained.

Jacobs et al. [85] reported the effect of adding MoS_2 (20 vol%), graphite (20 vol%) , PTFE (20 vol%), GF (15 vol%), CF (15 vol%) and CF (15 vol%) + PTFE (10 vol%), respectively to an EP resin. The only two composites showing significant wear reductions relative to neat EP was the one with only PTFE added and to a lesser extent the one with CF + PTFE. The authors argued that CF at higher concentrations tended to mask the positive effect of PTFE. Furthermore, it was hypothesized that the reason why no effect of fibers was seen could be due to the low value of the applied pv factor.

Harsa et al. [86] studied the correlation between the content of GF, CF, graphite and PTFE, and the abrasive wear rate for different polyaryletherketones (PAEKs). As generally observed for thermoplastics, addition of GF and CF increased the mechanical strength, while decreasing the tensile elongation at break (ϵ). Addition of short fibers and solid lubricants both had a negative effect on the abrasive wear rate. Some of the tested compositions are used as bearing materials and have excellent properties when sliding against smooth steel, but these failed against the rough counterfaces applied in the study in question. This underlines the importance of knowing the governing wear mode when optimizing a PMC. The negative effect on the abrasive wear rate was partly explained in terms of the Ratner-Lancaster correlation. Thus, the fibers cause a decrease in the product $\sigma_s\epsilon$, and therefore also a decrease in wear resistance. Furthermore, it was found that wear increased as a function of W_N and abrasive grit size in the range of 20 to 200 μm (SiC abrasive paper).

Rajesh et al. [87] studied the effect of GF, PTFE, Cu and bronze particles on the tribological behavior of PA6 under abrasive conditions. GF reduced the wear resistance relative to the neat polymer. Addition of fibers combined with PTFE and metal particles led to an even worse wear

behavior. The wear performance was most closely correlated with the product $H\sigma_s\epsilon$. Thus, PTFE had a reducing effect on H and the fibers had a reducing effect on ϵ, which in combination led to a poor abrasive wear resistance.

Bijwe et al. [6] examined the performance of three PEI based materials in four different wear modes. The three materials had the following compositions: a) Neat PEI, b) PEI filled with 20% short GF and c) PEI filled with 25 % short GF, 15% PTFE and a 15% mixture of MoS_2 and graphite. In the adhesive wear mode i.e. sliding against smooth steel, the wear resistance showed the following order c $>>$ b $>>$ a, and μ showed the order c $<<$ a $<$ b. Hence, the use of GF resulted in a low wear rate but in a significant increase in μ. This problem was, however, solved by also adding solid lubricants, which resulted in a composite with a very good tribological performance. In the abrasive wear mode i.e. sliding against SiC paper, the wear resistance followed the order a $>$ b $>>$ c. Hence, in this wear mode the trend was interestingly the exact opposite of what was found for the adhesive wear mode. In the fretting wear mode against a mild steel surface, the wear resistance followed the order c $>>$ b $>$ a, and μ showed the order c $<<$ a $\leq$ b. This trend was similar to what was found for adhesive wear. However, the effect of adding solid lubricants and GF was more pronounced in fretting mode. Furthermore, it was shown that wear debris had an increased tendency to get trapped in the interface in fretting wear mode, thereby increasing the role of a third body interface, which could be of both an abrasive or lubricating nature. In the erosive wear mode, which was tested by using a sand blasting machine, the wear resistance followed the order a $>$ b $>>$ c. This trend was identical to what was found for abrasive wear, namely that solid lubricants and fibers deteriorated the erosive wear resistance. Thus, this study showed in agreement with others that the wear mechanisms and material requirements in adhesive and abrasive wear mode are entirely different.

In another study Bijwe et al. [88] examined the influence of CF (up to 30 vol%) combined with PTFE (up to 20 vol%) on the performance of PA12 in adhesive, fretting and abrasive wear mode. Mechanical properties were improved by CF and reduced by PTFE. The wear rate was found to be a decreasing function of the CF content in adhesive and fretting mode. Further reductions in friction and wear were obtained when adding PTFE together with 30 vol% CF. The best performance was seen for a composite containing 30 vol% CF and 20 vol% PTFE. In the abrasive wear mode the exact opposite was seen i.e. both PTFE and CF had a detrimental effect on the wear properties.

3.3.2 Continuous fiber reinforcement

Continuous fibers applied as reinforcement in a uni-, di- or multi-directional architecture have shown to be a promising way of obtaining high perfor-

mance PMCs for tribological applications. This type of reinforcement often results in excellent mechanical properties and a high load bearing capacity. Furthermore, the anisotropic nature increases the possibilities for tailoring a PMC for a given application. Additionally, continuous fibers do not seem to be as sensitive to the wear mode as short fibers and do often perform well in both adhesive and abrasive wear mode. When fiber orientations are mentioned in the text below it may be helpful to look at figure 4.5, which illustrates the different fiber orientations.

The wear performance of different unidirectional reinforced polymers (mainly EP) with a fiber content of about 70 vol% has been reported. The general conclusions were the following: the wear properties were in all cases good in the parallel (P) direction and poor in the anti-parallel (AP) direction. The best tribological performances were found for EP reinforced with high strength CF or high modulus CF, while EP reinforced with GF or stainless steel fibers showed the poorest performances. Epoxy reinforced with AF, in parallel and antiparallel orientations, had an intermediate performance. The success of the CF containing composites was attributed to good mechanical properties combined with self-lubricating abilities [30].

The effect of wear mode, fiber type and fiber orientation have been examined for the thermoplastics polyethylene teraphthalate (PET), PA6, polyethersulfone (PES), PPS, PTFE and for an EP resin at different *pv* conditions. For short fiber reinforced thermoplastics, it was shown that short fibers decreased the wear rate when sliding against a relatively smooth steel surface, whereas the use of short fibers increased the wear rate when sliding against a very abrasive 70 μm Al_2O_3 paper. This observation is in general agreement with other results cited in this chapter. In the case of EP, it was found that different continuous unidirectional fibers (GF, CF and AF) reduced the wear rate in both adhesive and abrasive wear mode. Good results were especially obtained with AF in normal orientation. When AF were applied, brittle cracking mechanisms were eliminated and substituted by rupture and fibril formation, which apparently made material removal more difficult especially when AF were mostly in the normal orientation. The reason why continuous fibers increase the abrasive wear resistance and short fibers do not was explained as follows. The increased brittleness of the composite due to short GF or CF fibers leads to an increased degree of multiple microcracking events, where broken fibers are relatively easily swept away together with the polymer matrix resulting in a high wear rate. When continuous fibers are applied, the brittleness might still be high, but because the fibers are long and arranged in large bundles, the asperities which are smaller than the bundles can only cause local damage. Thus, despite local damage to the bundles, these will still be capable of supporting the load and contributing to the wear resistance [89].

Composites with very low wear rates have been reported for bidirectional and tridirectional continuous fiber reinforced polymers. In the case

of PEEK it has been shown that a CF woven fabric resulted in lower wear rates than unidirectional fibers, which was suggested to be caused by fiber interlocking in the interface when applying a woven structure. A composite based on laminates of PA impregnated CF and AF strands with CF in parallel and AF in normal orientation showed a positive synergistic effect on the wear rate compared to just using one type of fiber [79]. Furthermore, results have indicated excellent wear resistances of high temperature tridirectional reinforced composites using GF or CF and PI as matrix [80, 90]. Further improvements in wear resistance by using a tridirectional architecture compared to a unidirectional one is also reported by Zheng et al. [91] for CF reinforced PA composites, and by Wan et al. [92] for polyethylene (PE) fiber reinforced poly(methyl methacrylate) (PMMA).

Suresha et al. [93] compared two types of reinforcing weaves (bidirectional reinforcement) consisting of either GF (45 vol%) or CF (60 vol%). The matrix was in both cases EP. Increasing W_N and v elevated the wear rate for both composites. Furthermore, CF were superior relative to GF at all sliding conditions, which was partly attributed to the self-lubricating properties of CF.

Bahadur et al. [53] studied the possibilities of optimizing the tribological properties of a PA matrix by using glass fabric (bidirectional reinforcement), CuO particles and PTFE. When only glass fabric was applied, it was found that the wear rate decreased with an optimum glass fabric concentration of 20 vol%. Additional use of CuO was intented to strengthen the formation of a transfer film and thereby decrease the wear rate further. This was, however, not obtained partly because GF disrupted the transfer film, and partly because of increased brittleness of the composite due to the relative large volume fraction of GF + CuO. When PTFE was added together with GF and CuO a transfer film was formed and both friction and wear decreased. In conclusion, the best performance was obtained for a composite with the composition 11.3 vol% GF fabric, 25 vol% CuO and 10 vol% PTFE. The GF fabric layers were perpendicular to the steel counterface and parallel to the sliding direction.

Bijwe et al. [94] conducted a study with the purpose of exploring the applicability of different fabric reinforcements (bidirectional) to reduce abrasive wear of a PEI matrix. The three different types of examined fabrics consisted of GF, CF and AF, respectively. AF fabrics were superior relative to GF fabrics, CF fabrics and the unfilled PEI. The largest wear improvement was obtained with the AF fabric perpendicular to the counterface, i.e. with half the fibers in normal orientation, which agrees well with other results cited in this chapter. As mentioned previously a high $\sigma_s\epsilon$ factor should correspond to a high abrasive wear resistance. Such a correlation was not found in this study. However, the composites with AF fabrics had a significantly higher impact strength than the other composites. The counterface consisted of SiC 80 grade paper with a grit size

of 176 μm.

In another study Bijwe et al. [95] investigated the effect of an aramid fabric on the abrasive wear behavior of PES. Abrasive wear rates were reduced with factors of 3 to 8 (relative to neat PES) in the aramid range of 62 to 83 wt%. Futhermore, the abrasive wear rate followed the Ratner-Lancaster correlation. The fiber orientation during sliding were N-P, cf. figure 4.5. Bijwe et al. reported the influence of fiber orientation in another paper [14]. At light loads the wear rates were in the order P-AP $>>$ N-AP $>$ N-P. At high loads the order was the same except that N-P and N-AP had changed places. Thus, in agreement with other studies, continuous AF are especially effective when oriented in the normal direction.

Tripathy et al. [96] examined the effect of fiber orientation and thermal conductivity on interfacial temperature for an unidirectional graphite fiber reinforced EP matrix. The thermal conductivity of the composite in normal orientation was a factor of 50 higher than in parallel and anti parallel orientation. Despite this, it was shown both theoretically and experimentally that the interfacial temperature was only weakly dependent on the fiber orientation and hence on the thermal conductivity of the composite. The explanation for this phenomenon was as follows. When sliding occurs between a PMC with a relatively low conductivity and a counterface with a much higher conductivity, then the heat transfer is completely dominated by the latter. Thus, the conducting counterface dissipates almost all the frictionally generated heat, while the thermal conductivity of the PMC has little influence on the interfacial temperature. Measurements were performed on a pin-on-disk apparatus equipped with a sapphire (Al_2O_3) disk and a infrared microscope for temperature measurements.

Su et al. [97] studied the effect of solid lubricants on Nomex fabric composites using a phenolic resin as matrix. Nomax is an especially thermo-resistant type of Kevlar fibers. When 15 vol% irradiated PTFE was incorporated, both friction and wear improved, while negative effects were observed by incorporating 10 vol% MoS_2 or 10 vol% graphite. Also the limiting *pv* factor was significantly enhanced by incorporating PTFE. The different effects of the tested solid lubricants were accounted for by two contributions: a) The bond strength between the fabric and the resin seemed to deteriorate when MoS_2 and graphite were mixed in the resin and b) The transfer film formed on the counterface when PTFE was applied appeared to be more thin, smooth and coherent.

3.4 Inorganic nanoparticles

Inorganic nanoparticles have shown promising results with respect to improvements of mechanical, thermal and tribological properties of PMCs. The optimum nanoparticle concentration is typically in the range of 2-5 vol%, which is a factor of 10 lower than often found for microparticles. This low particle content results in a minimal density gain relative to the

neat polymers and increases the possibilities for combining nanoparticles with other fillers e.g. fibers, microparticles and solid lubricants. Furthermore, nanoparticles are often found to toughen polymers, which is expected to be especially beneficial for thermoset polymers due to their brittleness. A decrease in wear by nanoparticle addition is frequently attributed to improved adhesion of a transfer film to the counterface, which is similar to the behavior of microparticles. However, hard microparticles sometime cause problems due to their abrasiveness. This problem is expected to be reduced significantly by going to nano-size. Thus, it might be imagined that while larger particles roughen the counterface, nanoscale particles merely polish the counterface. Utilization of nanoparticles is associated with some difficulties though. Firstly, a good particle dispersion is typically required for property improvements and may be difficult to obtain. Secondly, the predictability and robustness of applying nanoparticles is hampered by a lack of understanding of the underlying mechanisms.

Rong et al. [47] examined three different ways of producing TiO_2 nanocomposites based on an EP resin. The study showed that the friction and wear properties depended significantly on the way the composites were compounded. Only one of the three production methods showed significant wear improvements. This improvement was arguably associated with a good particle dispersion caused by the applied mixing procedure. Thus, when the particles were insufficiently mixed no property improvements were evident.

Bahadur et al. [27] examined the effect of TiO_2, ZnO, CuO and SiC nanoparticles on the tribological behavior of PPS. It was found that wear was reduced for CuO and TiO_2 with an optimum at 2 vol% in both cases. ZnO and SiC, on the other hand, led to a deterioration of the wear resistance at all examined concentrations. The flexural strength decreased (relative to neat PPS) for all type of particles, with a typical minimum in strength at 1 or 2 vol%. The low wear measured for CuO and TiO_2 was associated with a thin and uniform transfer film, which bonded strongly to the counterface.

García et al. [98] investigated the effect of SiO_2 nanoparticles on the friction and wear behavior of PA6 at two concentrations i.e. 2 wt% and 14 wt%. Significant improvements of friction and wear were obtained with 2 wt%, while only moderat improvements were optained with 14 wt% SiO_2. The improvements were attributed to enhanced adhesion of a polymeric transfer film to the steel counterface.

Shi et al. [46] studied an EP resin filled with nano-sized Si_3N_4 particles. It was found that addition of Si_3N_4 increased the flexural strength, the flexural modulus and the impact strength in the examined range of 0 - 2 vol%. Regarding friction and wear, a significant reduction was found for both parameters at a filler concentration of about 1 vol%. No obvious correlation was found between the optimum particle concentration and mechanical and tribological properties, respectively. The decrease in fric-

tion, due to the presence of Si_3N_4, was partly explained by an observed decrease in thermally induced deformations of the composite. Furthermore, XPS analysis indicated that tribo-chemical reactions had occurred during sliding, which contributed to the improved tribological performance.

Li et al. [99] examined the effect of adding nanoscale ZnO particles to PTFE. The frictional properties was unchanged, while the wear rate decreased significantly with the best result obtained at a particle concentration of 15 vol%. The improved wear resistance was attributed to the development of a more uniform and thin transfer film when ZnO was present.

In another study Sawyer et al. [42] tested PTFE filled with nanoscale Al_2O_3 particles. A slight increase in μ was observed, while the fretting wear rate (oscillating mode) decreased monotonically in the range of 0-20 wt%. At a filler concentration of 20 wt%, wear was reduced by a factor of 600 relative to the neat PTFE. Contrary to most other studies an optimum particle concentration was not found.

Rong et al. [100] examined the possibilities for obtaining further improvements by coating nanoparticles prior to mixing them with the resin. It was argued that in order for inorganic particle fillers to have the intended effect, a good dispersion in the matrix and a high interfacial filler/polymer strength are required. The latter is especially true for nanoparticles since the interfacial area, for a given volume fraction, increases as the particles become smaller. A good dispersion is difficult to obtain, since the nanoparticles are typically strongly aggregated. Thus, the composite is likely to contain agglomerated nanoparticles, which might crumble under tribological action and thereby have a negative effect on the wear resistance. In order to overcome these difficulties, the effect of graft polymerization onto nanoparticles was investigated. This was done by chemically modifying Al_2O_3, SiC and Si_3N_4 nanoparticles, respectively, by attaching polyacrylamide (PAAM) to the surface prior to mixing with the EP matrix. The hypothesis was that acrylamide monomers were capable of penetrating the agglomerated nanoparticles and thereby cause grafting, not only on the surface of the agglomerates, but in the interstitial volume as well. Thus, the increased hydrophobicity of the particles, due to grafting, was expected to facilitate deagglomeration and increased epoxy/particle adhesion. The conclusions of this study were the following: a) Nanoparticles without surface modification were capable of reducing friction and wear at particle concentrations in the range of 1-2 vol%. b) The improvements in tribological performance were significantly more pronounced when the grafting process was applied. c) Wear rates were more closely correlated with the increased thermal diffusivity than with the micro-hardness of the composites.

In a similar study Shi et al. [45] examined the effect of Al_2O_3 nanoparticles (0 to 2 vol%) with or without pretreatments when added to an EP resin. The tested pretreatments were graft polymerization using PAAM

and the use of an siliane coupling agent, respectively. The former pretreatment proved to be most effective. Improvements in friction and wear were clearly seen and the best result was found for PAAM treated Al_2O_3 at 0.24 vol%. Nanoparticle addition enhanced the flexural strength, but this parameter was not clearly correlated with measured wear rates. The best positive correlation was found between impact strength and wear resistance.

The applicability of PAAM coating was also demonstrated in a study by Zhang et al [101], which showed that friction and wear of an EP resin was reduced by adding about 2 vol% SiO_2 nanoparticles. This improvement was more pronounced when the particles were coated with PAAM prior to mixing with the resin. Yet another study by Ji et al. [102] examined the effect of PAAM coating of SiC nanoparticles incorporated into an EP resin. Also in this case, the best performance was found for the PAAM coated particles at a very low particle content (0.2 vol%).

Wang et al. [103] studied the effect of particle size of ZrO_2 (in the range of 10 to 100 nm) on the tribological behavior of PEEK. Only the smallest particles (10 and 15 nm) gave rise to significant improvements in wear resistance. The optimum concentration was 7.5 wt% ZrO_2, and the positive effect was attributed to formation of a thin, uniform and tenacious transfer film. A particle size of 86 nm, on the other hand, reduced the wear resistance relative to neat PEEK, which was associated with a thick and discontinuous transfer film.

Schwartz et al. [50] examined the effect on the tribological behavior of PPS by adding alumina (Al) nanoparticles in the range of 0 to 10 vol%. Flexural strength measured for PPS with Al particles in the range of 0 to 5 vol% showed a decrease in strength for all composites (relative to neat PPS) with a minimun at 2 vol%. When applying counterface roughnesses of 0.060 and 0.100 μm R_a, reduced wear was seen for particle contents of 1 and 2 vol% while higher concentrations increased wear. At a counterface roughness of 0.027 μm R_a, addition of Al nanoparticles led to a decrease of the wear resistance at all examined concentrations. The improvements found in this study were not correlated with the flexural strength but with the bond strength between the formed transfer film and the steel counterface, which was the probable cause for wear reduction. It was hypothesized that higher particle concentrations reduced the counterface - transfer film bond strength due to abrasive action.

3.4.1 Nanoparticles combined with other fillers

Recently, the combined effect of adding nanoparticles together with other fillers have been reported especially by K. Friedrich and co-workers. Wetzel et al. [49] studied the effect of adding TiO_2 nanoparticles (200 - 400 nm) into an EP resin in the concentration range of 0 to 10 vol%. Addition of these particles generally improved the impact strength (optimum at 4

vol%) and the wear resistance (optimum at 5 vol%). Furthermore, possible synergistic effects of adding $CaSiO_3$ microparticles (in the range of 3 to 15 vol%) together with 4 vol% TiO_2 were examined. This led to a decrease in impact strength but an increase in stiffness and wear resistance. The best overall result was considered to be obtained by a composite containing 4 vol% TiO_2 and 3 vol% $CaSiO_3$. The combination of toughening by nanoparticles and stiffening by microparticles was suggested to play a dominant role in relation to this result. In addition to this, the reduction in wear also seemed to be related to formation of a protective transfer layer.

In a related study Xian et al. [104] added graphite powder (7.2 vol%) and aramid particles (in the range of 2-14 vol%) to an EP resin containing 4 vol% TiO_2 nanoparticles. Wear testing was conducted in both sliding mode and fretting mode. In sliding mode the incorporated TiO_2 nanoparticles had a positive effect on the tribological behavior relative to neat EP. When graphite and aramid were added together with the nanoparticles, these improvements were even more pronounced. In fretting mode, the incorporated TiO_2 nanoparticles had a detrimental effect on the wear rate (relative to neat EP). However, addition of graphite and aramid together with TiO_2 had a major positive impact on the fretting wear rate, which at an aramid content of 10 vol% was about a factor of 10 lower than the rate for neat EP. The negative effect of TiO_2 in fretting mode was suggested to be due to abrasive action of these hard particles. This study underlines, in agreement with others, that friction and wear are system properties and not merely material properties.

Chang et al. [105] examined the effect of adding TiO_2 nanoparticles (5 vol%), graphite (5 vol%) and short CF (15 vol%) to an PEI resin. Both the combination of adding CF + graphite and CF + graphite + TiO_2 resulted in a marked reduction in wear. However, the latter combination (i.e. with nanoparticles) also caused a pronounced reduction in friction and hence in frictional heating. Consequently, the nanoparticles made the composite applicable at more severe *pv* conditions.

Zhang et al. [106] examined both the individual and combined effect of adding TiO_2 nanoparticles, graphite, PTFE and short CF to an EP resin. It was generally found that each type of filler improved the wear rate relative to neat EP. However, it was demonstrated that composites with very low wear rates could be obtained by combining these fillers. The lowest wear rate was measured for a composite with 15 vol% graphite + 5 vol% TiO_2 + 15 vol% CF. It was suggested that the nanoparticles give rise to a rolling effect in the interface, which reduces interfacial shear stress and frictional heating, and thereby also limits the severity of the wear process. This proposed rolling effect was discussed further in a paper by Chang et al. [33] for the same kind of composite materials.

Cho et al. [8] studied the individual and combined effect of incorporating CuO nanoparticles, CF and AF into PPS. Each filler improved the wear

resistance relative to neat PPS, but only CF caused a significant reduction in friction. AF proved to be the most effective for wear reduction. By combining CuO and CF or CuO and AF a further reduction in wear was obtained. The best wear performance was measured for a composite consisting of PPS + 15 vol% AF + 2 vol% CuO, while the best frictional performances were seen for the composites PPS + 15 vol% CF and PPS + 15 vol% + 2 vol% CuO. Wear improvements were explained in terms of transfer film morphology. It was concluded that a thin, uniform and coherent transfer film seemed to be a prerequisite for wear reduction.

Su et al. [107] examined the effect of adding different nanoparticles (5 vol%) to a carbon fabric reinforced (bidirectional) phenolic resin. It was found that SiO_2, TiO_2, and $CaCO_3$ nanoparticles improved the tensile strength of the composite. This was attributed to an enhanced resin-fiber adhesion when the particles were present. The friction and wear properties were also improved to some extent by incorporation of nanoparticles. These improvements were mainly explained in terms of differences in the apperance of transfer film.

3.5 Concluding remarks

By reading this chapter it may be realized that friction and wear of PMCs are very complex phenomena, which depend significantly on the type of materials, compositions, directionality, sliding mode, environmental conditions, contact pressures and sliding velocities. However, by studying the existing literature some overall guidelines for design of PMCs for certain applications may be extracted. Furthermore, based on the studies cited above, it is obvious that transfer films play a significant role in relation to tribology of PMCs. In the literature a number of clearly important parameters for transfer film formation and stability can be identified i.e. molecular structure of the polymer, the steel counterface roughness, sliding velocity, contact pressure and environmental conditions. However, the present knowledge lacks predictive qualities, which certainly are desirable from the perspective of designing tribological systems using PMCs.

In this Ph.D. work, it is attempted to produce a PMC with excellent tribological properties when dry-sliding against smooth steel counterfaces. It is chosen to use an EP resin for other reasons than its tribological properties, which normally are relatively poor. The challenge is to incorporate the right kind of reinforcements and fillers, which jointly give rise to low friction and wear. Based on the above, continuous fiber reinforcement using AF and CF seems like a good starting point. In an attempt to minimize friction and thereby frictional heating, PTFE is added as a solid lubricant. However, examples are found in this chapter which show that lubricating and protective transfer films may be disrupted by fibers. To counteract this, CuO particles are added which may stabilize formed transfer films through tribo-chemical reactions as reported above. Fur-

thermore, the applied CuO is added in the form of nanoparticles, which may have additional benefits such as a low abrasiveness and an ability to counteract the inherent brittleness of the EP resin. The low optimum concentration typically found for nanoparticles makes these ideal components to apply in relation to continues fiber reinforced polymers with a high fiber content. However, not much have been reported previously in this respect.

4

Experimental

In this chapter experimental details are given. This includes information about applied materials, production of composites and Pin-On-Disk (POD) measurements. Furthermore, the POD apparatus built as a part of this Ph.D. work is described.

4.1 Materials

Composites are produced using the following components: epoxy resin (EP), glass fiber weave (G), carbon/aramid hybrid weave (CA), PTFE particles and nano-scale CuO particles. An overview of all produced and examined composites are given in table 4.1 for non-fiber reinforced EP and in table 4.2 for fiber reinforced EP.

The applied resin is in all cases a polyfunctional EP of the novolac type obtained from Hexion Specialty Chemicals as a 70 wt% solution in methyl ethyl ketone (Epikote 1153-B-70). Incorporated PTFE particles (TF 9207) are purchased as micropowder from Dyneon^{TM}. CuO nanoparticles (NanoArc^{TM} U1102DBE) are delivered by Nanophase Technologies Corporation. The particles are received as coated particles dispersed in a diester solvent mixture (Dimethyl Adipate, Dimethyl Glutarate and Dimethyl Succinate). The coating accounts for approximately 20 wt% of the dry-weight of the nano-CuO and enabels a relatively stable solvent dispersion. In one case, a test-specimen is prepared using non-coated CuO nanoparticles (NanoArc^{TM} Copper Oxide), which are delivered as powder by Nanophase Technologies as well.

The examined glass fiber composite (G/EP) is produced by Elektro-Isola A/S and is commercially available (G-Etronax EP 11). This material is not intended for use in dry-sliding applications but is used as a reference material in this context. The composites which are reinforced with the carbon/aramid hybrid weave are produced for the purpose of this study. All fiber reinforced materials are produced using the same production method and the same type of resin. The glass fiber weave (Plain, international style 7637) is delivered by P-D Interglas Technologies AG and the carbon/aramid hybrid weave (twill 2x2, style 73210) is obtained from Hexcel Fabrics S.A. and has carbon and aramid fibers both oriented in warp as well as weft with the same ratio (61 vol% aramid/39 vol% carbon) in both directions.

Table 4.1. Nomenclature, composition and density for EP, with or without 7.5 vol% PTFE, containing different amounts of CuO nanoparticles.

Nomenclature without PTFE	Nomenclature with 7.5 vol% PTFE	CuO content [vol%]	Density [g/cm^3] ÷ PTFE / + PTFE
EP	EP/PTFE	0	1.2 / 1.3
EP/0.1	EP/PTFE/0.1	0.1	1.2 / 1.3
EP/0.2	EP/PTFE/0.2	0.2	1.2 / 1.3
EP/0.4	EP/PTFE/0.4	0.4	1.2 / 1.3
EP/1.0	EP/PTFE/1.0	1.0	1.2 / 1.3
EP/3.0	EP/PTFE/3.0	3.0	1.3 / 1.4
EP/6.0	EP/PTFE/6.0	6.0	1.5 / 1.6
EP/10	-	10	1.7 / -

Table 4.2. Nomenclature, composition and density for fiber reinforced EP

Nomenclature	Fiber type / vol%	Particle type / vol%	Density [g/cm^3]
G/EP	glass / 44	-	1.8
CA/EP	carbon/aramid / 44	-	1.3
CA/EP/PTFE	carbon/aramid / 47	PTFE / 5	1.4
CA/EP/CuO	carbon/aramid / 45	nano-CuO / 1	1.4

4.2 Production of composites

4.2.1 Composites without fibrous reinforcement

PTFE and nano-CuO particles are mixed with the EP pre-polymer solution in the following way. A PTFE dispersion is prepared by swelling PTFE micro-powder in xylene (ratio 1:3) while stirring. The PTFE dispersion is subsequently added quantitatively to the epoxy solution and stirred mechanically. The as received nano-CuO dispersion is sonicated for 2 hours before mixing it quantitatively with the EP solution using mechanical stirring for 5 min. Epoxy dispersions with different particle content are transfered to a custom-made mold, cf. figure 4.1(a), and cured by heating: 2 days at 45°C, 1 h at 100°C, 30 min at 130°C, 1.5 h at 150°C and finally 30 h at 170°C. This slow and prolonged heating procedure is applied partly to avoid porosity caused by uncontrolled solvent evaporation and partly to make sure that all residual solvent is removed. The latter is checked by examining the weight loss of the PMCs as a function of time. After curing for 30 h at 170°C, no more weight loss and hence solvent evaporation can be detected.

The dimensions of the composites after curing are 70 mm x 70 mm x 1 mm. These are subsequently divided into smaller slabs with a thickness of 1 mm and a cross section of 7.7 mm x 5.0 mm. In order to perform pin-on-disk measurements, these small slabs are glued on top of a G/EP test-pin with the same cross sectional area and a height of 15 mm. Thus, friction and wear tests are performed on composite slabs with an apparent area

of contact of 38.5 mm^2 and a initial thickness of 1 mm, cf. figure 4.1(b).

4.2.2 Fiber reinforced composites

By using prepreg technology, composite plates are produced in the following way. A certain amount of resin solution, with or without particles, is added quantitatively to a square of weave and distributed by applying a roller. The impregnated weaves are subsequently placed in an oven with air circulation (typically 15 min at 120°C) in order to evaporate the solvent and partially cure the resin. A number of partially cured sheets are then stacked, in order to obtain a laminate thickness of at least 5 mm, and pressed for three hours applying a pressure of 35 bar and a temperature of 160°C. Finally, the plates are post-cured for 2 h in an oven at 170°C. The composite test-pins for tribological evaluation are obtained by reducing the plate thickness to 5.0 mm by milling, and then using a diamond saw to obtain the final dimensions of height 15 mm and cross section 7.7 mm x 5.0 mm. In this case, the weave is parallel to the hight direction of the test-pin. Other test-pins are prepared where the weave is perpendicular to the height direction. These are made by sawing a rectangle (7.7 mm x 5.0 mm x 5.0 mm) from a composite plate and gluing it on top of a G/EP test-pin, cf. figure 4.3(a). After machining, the test-pins are dried in an oven for 20 h at 50°C and subsequently stored in a sealed bag at room temperature.

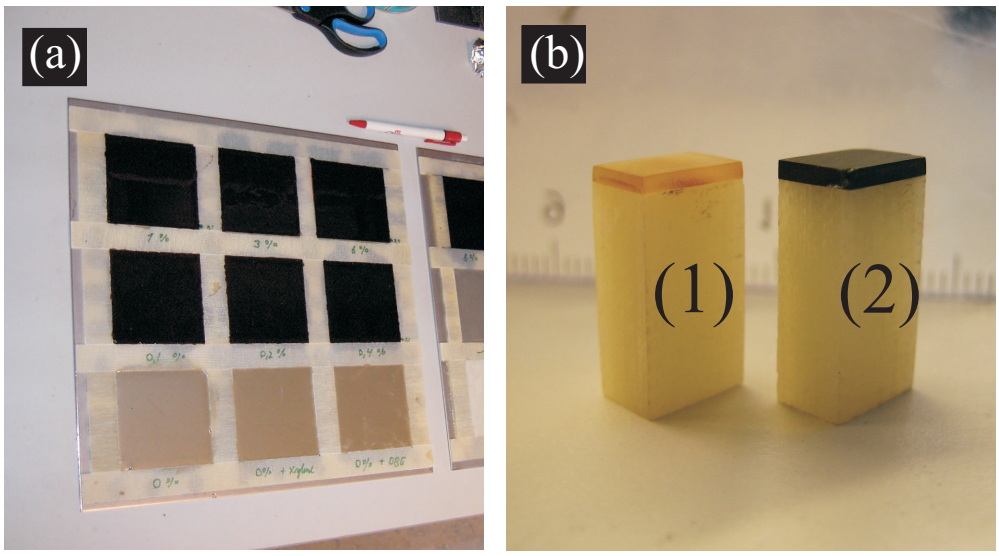

Figure 4.1. (a) Photo of the custom-made mold containing EP dispersions with different particle content. (b) Photo of two G/EP test-pins with 1 mm thick composite slabs glued on top. (1) corresponds to a composite slab consisting of neat EP while (2) corresponds to EP/10.

4.3 Pin-On-Disk apparatus

The principle of the applied Pin-On-Disk method is as follows. A test specimen in the form of a pin is fixed in a lever-arm and loaded perpendicular against a rotating steel disk, cf. figure 4.2. The normal load (W_N) is adjusted simply by placing different dead weights on top of the lever-arm. The latter, which can move freely both in the vertical and horizontal direction, will swing in the same direction as the disk revolves due to friction between the surfaces. However, it is kept in a fixed position by a load cell, which measures the frictional force (F_f). The wear rate is obtained simply by measuring the weight loss of the pin after being worn a certain amount of time in the steady state regime.

4.3.1 Servo drive and steel disk

Rotation of the steel disk is controlled by a servo system consisting of a motor (Parker SMH 60) and a control unit (Parker Compax 3). The motor is mounted underneath a 20 mm thick aluminum plate with a hole drilled for the motor axis. This system is capable of rotating the steel disk at a constant speed (±1%) regardless of the frictional torque in the range of 0 to 1.4 Nm, which for the given system corresponds to F_f in the range of 0 to 40 N. The sliding velocity and contact pressure can be adjusted in the range of 0 to 10 m/s and 0 to 1.2 MPa, respectively. Thus, the product of contact pressure p and sliding velocity v (pv condition) can be adjusted in the range of 0 to 12 MPa m/s.

The disk is made of hardened chrome steel (100 Cr6), and has a diameter of 100 mm and a thickness of 10 mm, cf. figure 4.2(b,7). The steel disk is attached to the motor axis through an adapter and a spacer. The former is made of steel and makes mounting of the steel disk possible, while the spacer is made of glass fiber reinforced polyimide and acts as a thermal isolator. The latter is beneficial, since frictional heating of the disk potentially can cause excessive heating of the motor drive due to heat conduction though the motor axis. To reduce unnecessary heating further, the motor is encapsulated in a steel box with a rotating fan at the bottom which cools the motor by rapid air circulation.

4.3.2 Lever-arm and pin-holder

The lever-arm is made of aluminum and is attached to an aluminum housing containing a set of ball bearings which facilitates free rotation and sliding on a steel axis with a low frictional resistance, cf. figure 4.2(b,5,8). The pin-holder is constructed in such a way that a test-pin can be inserted into the free space of the holder (10 mm x 7.7 mm x 5.0 mm) and tightened by applying two incorporated screws, cf. figure 4.3(b). The pin-holder is designed so it only fits into the lever-arm when inserted in one specific way. This has the benefit that the holder can be removed, for

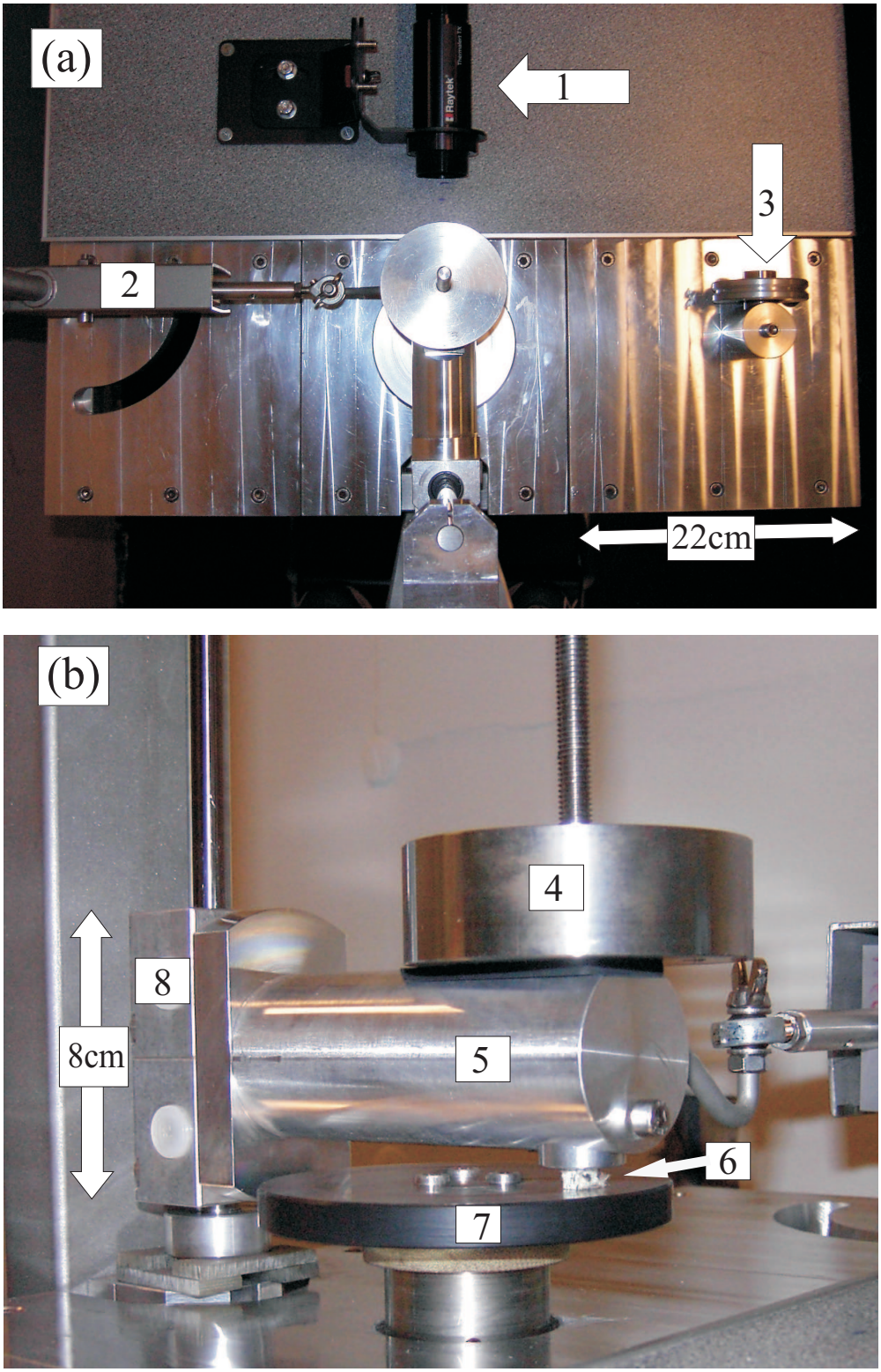

Figure 4.2. Photos of the custom-built Pin-On-Disk apparatus. (a) Top-view of the mechanical parts: 1. Infrared temperature sensor, 2. Load cell and 3. Pulley for calibration of the load cell. (b) Side-view of a composite pin loaded against the rotating steel disk: 4. Weight, 5. Lever-arm, 6. Test-pin, 7. Steel disk and 8. Aluminum housing containing a set of ball bearings.

instance for inspection or weighing, and then reinserted in the exact same position, which is important in order to maintain alignment between the sliding surfaces.

4.3.3 Measurement of frictional force

The load cell keeps the pin and lever-arm in a fixed position and measures F_f. The coefficient of friction (μ) is obtained by using Amontons first law of friction, cf. equation (2.4). The frictional force is measured continuously during the experiment. μ is reported as a time-averaged value based on data points in the steady state regime. The applied load cell (S BEAM MODEL 6110) is capable of measuring F_f in the range of 0 - 49 N. The voltage signal from the load cell is first filtered and amplified by using an analog amplifier (LAU 73.1), and then collected by a computer though an A/D converter (PMD-1208LS). Calibration of the load cell is obtained by attaching a wire to the transducer and then using a pulley, cf. figure 4.2(a,3), and a number of known weights to generate a calibration curve.

4.3.4 Measurement of temperature

The temperature of the steel disk is used as an estimate for the interfacial temperature. It must be emphasized that the disk temperature probably

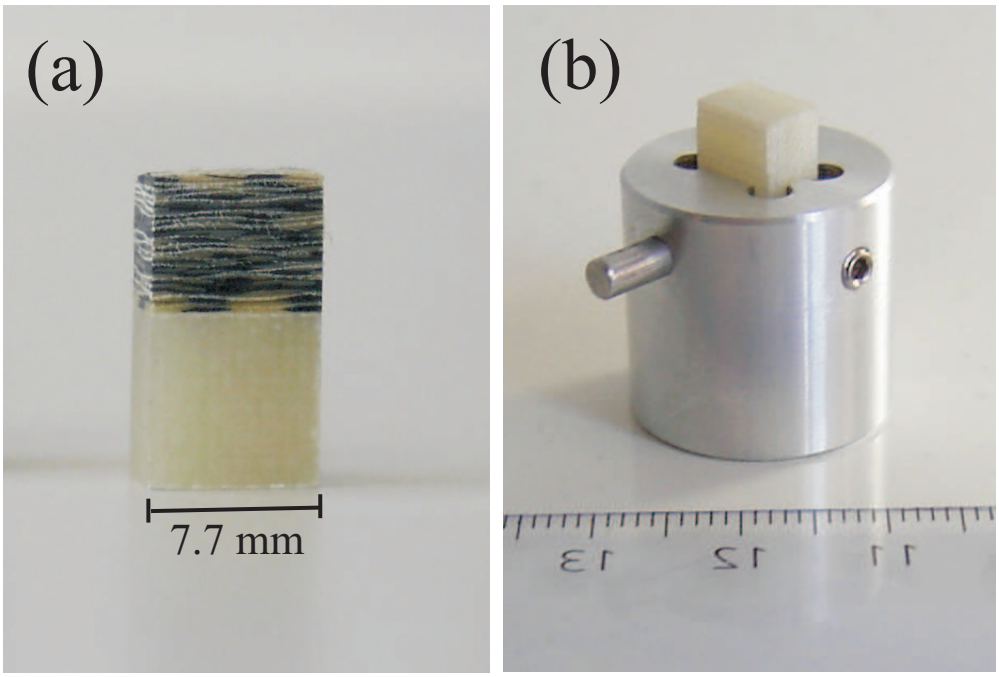

Figure 4.3. (a) Photo of a CA/EP test-pin with the weave perpendicular to the height direction. (b) Photo of the pin-holder with a G/EP test-pin mounted.

will be significantly lower than the actual flash temperatures (ΔT_f) at the contacting asperities. The disk temperature is likely to be closer to T_a given by equation (2.17) i.e. the mean temperature over the apparent contact area (A_a). Measurement of temperature is performed on-line during testing by using an infrared non-contact thermometer (Raytek Thermalert TXSLTCF1). The thermal data is collected by a computer using a HART protocol/RS232 adapter. The sensor is located in a position, which collects radiation from a circular spot of diameter 2.5 mm on the side of the disk, cf. figure 4.2(a,1). In order to obtain a surface suitable for non-contact temperature measurements, i.e. with a high and non-changing factor of emissivity, the side of the disk is painted with black paint capable of withstanding temperatures up to 500°C. In order to verify the accuracy of the temperature measurements, it has been confirmed that these agree with contact thermometer measurements when compared in the relevant temperature range.

4.3.5 Surface finish of the disk

The roughness of the steel counterface is an important parameter, which influences the mechanisms as well as levels of both friction and wear, cf. section 2.2 and 2.3. It is therefore important to limit variation in the initial counterface topography to make measurements comparable. The steel counterface is abraded with an emery cloth of grade P400 before each measurement. Surface finish is obtained by using a hand-held grinding block, which is pressed against the disk while is rotates. This procedure results in the following initial roughness parameters (given in μm) and associated standard deviations based on 5 to 7 determinations performed on 10 different disks: $R_a = 0.26$ (± 0.03), $R_z = 2.3$ (± 0.3), $R_p = 0.96$ (± 0.2) and $R_v = 1.3$ (± 0.2). These values are obtained using a profilometer (Taylor-Hobson, Surtronic3+) with the stylus moving perpendicular to the direction of the grinding marks from abrading (short wavelength filter: 2.5 μm, long wavelength filter: 800 μm, evaluation length 3200 μm). The abrasion procedure gives rise to an anisotropic counterface which is illustrated in figure 4.4. Tests are also performed using a smoother counterface. In these cases the disk is abraded using an emery cloth of grade P800, which give rise to an R_a parameter of 0.074 (± 0.003) μm.

4.4 Pin-On-Disk measurements

The employed test-procedure is given below.

- The steel counterface is abraded using a piece of emery cloth.
- While mounted in the POD lever-arm, the composite pin is abraded against a piece of emery cloth located on the steel disk in order to obtain conformity between the pin and the counterface.

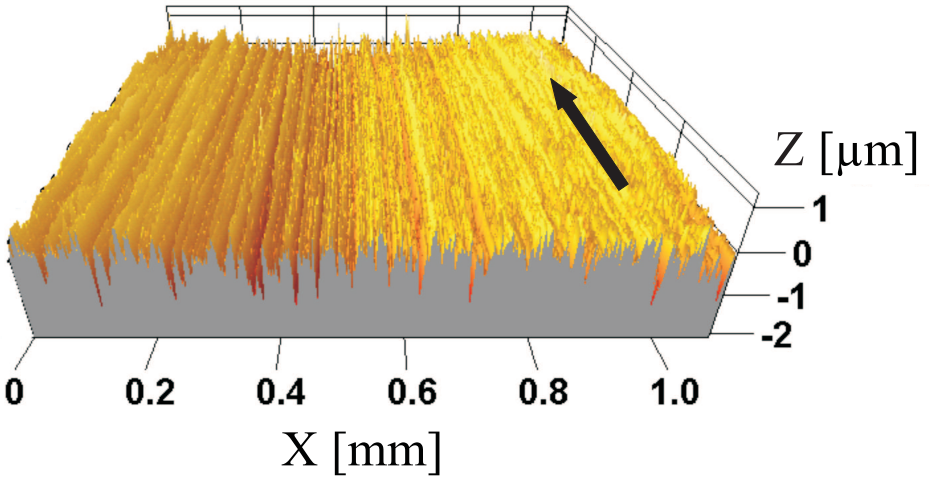

Figure 4.4. Three-dimensional picture of a 1x1 mm square of the steel counterface (aspect ratio 1:1:80). The arrow indicates the sliding direction during Pin-On-Disk tests. The picture is based on 200 traverses perpendicular to the grinding marks using a Taylor-Hobson profilometer (Form TalySurf Serie 2 50i).

- Loose debris is removed from the pin and the counterface by blowing with compressed air.
- The surfaces of the two sliding partners are cleaned by wiping with tissue paper soaked in acetone followed by blowing with compressed air to evaporate any excess of solvent.
- The weight of the pin plus the sample holder is noted to the nearest 0.1 mg.
- During testing the frictional force and the temperature of the steel disk is recorded by a computer.
- After testing the pin and sample holder is cleaned as previously described and weighed again.

It is possible to reinsert the pin and sample holder in the lever-arm and continue the test-run in order to determine how the accumulated weight loss evolves as a function of time. This can reveal, whether the accumulated weight loss is simply a linear function of time or exhibiting a more complicated behavior. Wear curves frequently show a running-in period with an initial high wear rate followed by a lower steady state wear rate. This transition from high to lower wear is typically due to modification of the sliding surfaces and development of transfer films.

Since the tribological behavior depends significantly on both the materials and the applied *pv* conditions some adjustments in measurement procedure are made accordingly. For G/EP, a linear relationship is found between accumulated weight loss and time without any detectable running-in period. In these cases, the experiments span over 2 h to 24 h depending on the *pv* condition. The steady state wear rate is determined based on the initial and final weight of the test specimen. The other tested materials do, at some conditions, show a running-in phenomenon with an initial wear rate, which decreases and ultimately reaches a steady level. In these cases, the accumulated weight loss is measured as a function of time for periods of 3 h to 200 h. The slope of the approximately linear part of the curve is then used for calculation of the steady state wear rate by using the relations given in section 2.3.3. Examples of such curves are given in section 5.1. Interruption of test-runs for weighing is kept brief and it is verified that this does not have any significant influence on the measured parameters. Tribological measurements are as a minimum repeated twice for fiber reinforced PMCs and three times for non-fiber reinforced PMCs at each parameter combination. Any deviations from the procedure described above will be mentioned explicitly in the text.

4.4.1 Fiber orientation

The fiber reinforced test-specimens are placed in such a way that the weaves in the composites are either normal or parallel to the counterface during sliding, cf. figure 4.5. In the normal direction, the fibers in the weave are oriented normal and parallel (N-P) with respect to sliding direction, whereas the fibers are parallel and anti-parallel (P-AP) with the sliding direction when the weave is oriented parallel to the counterface. An example of a test-pin for examination of the P-AP direction is shown in figure 4.3(a). The measured orientation is N-P unless stated otherwise.

4.5 Additional methods

4.5.1 Electron microscopy

Scanning electron microscopy (SEM, type JEOL JSM 5900) is applied to study the structure of produced composites as well as wear scars on the worn surfaces and wear tracks on the counterface. When studying composite structures, the surfaces are polished, cleaned and finally coated with a conducting carbon layer. When studying wear scars, the worn surfaces are cleaned and subsequently coated with a conducting gold layer. Cleaning is in both cases done by removing loose debris by compressed air followed by gently wiping with tissue paper soaked in acetone. Loose debris is removed from the steel disk by blowing with compressed air prior to studying the wear track. However, cleaning with acetone on the

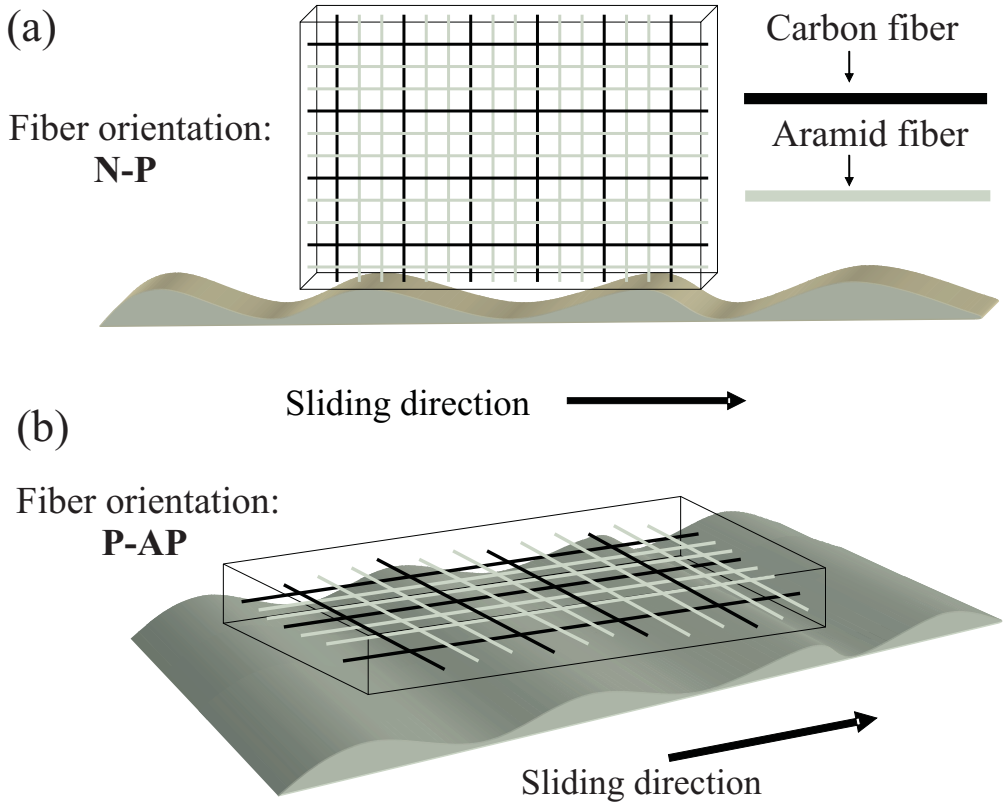

Figure 4.5. Illustration of the two orientations of the reinforcing weaves during POD measurements shown here for the carbon/aramid weave. (a) The weave in the resin is normal to the counterface and the fibers are normal and parallel to the sliding direction (N-P). (b) The weave in the resin is parallel with the counterface and the fibers are parallel and anti-parallel to the sliding direction (P-AP).

wear track is omitted in order to avoid removing possible transfer layers. Transmission electron microscopy (TEM, type JIOL 2000 FX) is applied to study the dispersion state of nanoparticles in the EP resin. This is done by preparing thin foils with a thickness of approximately 50 nm using a ultramicrotome (LEICA EMFCS) equipped with a cryo-chamber.

4.5.2 Vickers micro-hardness

Vickers micro-hardness (HV) are measured on some of the produced composites (LEITZ-Kleinhärtsprüfer). A pyramid-shaped diamond indenter is pressed against polished composite surfaces for 30 s using a load of 200 g. Indentation is repeated at least three times for each composite. The standard error is in all cases below 8%.

4.5.3 Differential scanning calorimetry

Glass transition temperatures (T_g) are measured using differential scanning calorimetry (DSC, type TA instruments Q1000) with a heating/cooling rate of 10°C per min. Measurements are performed one time for each sample.

5

Results and discussion

In this chapter the main results of this Ph.D. work are presented. Most of the results given here are a summary of the three papers located in appendices A, B and C, respectively.

5.1 The Pin-On-Disk method

The purpose of this section is not to discuss the tribological behavior of the tested composites but merely to show typical examples of how friction, wear and disk temperatures evolve as a function of time during Pin-On-Disk (POD) measurements. Examples of measured frictional forces (F_f) and disk temperatures as a function of time are given in figure 5.1. Curve (c) is an example of a smooth frictional behavior where a steady state level is reached for both friction and temperature. The curves (a) and (b) are examples of a test-specimen, which is worn at conditions where thermally induced decomposition leads to fluctuations in F_f. However, F_f fluctuates around a relatively steady average level. Furthermore, measured temperatures and F_f mirror one another as should be expected. The latter is observed in all experiments on the POD apparatus. Additional examples of F_f plotted versus time are given in figure 2 in appendix A.

In figure 5.2, steady state temperatures measured at different pv conditions are plotted as a function of $\dot{Q}_d$ given by equation (2.16). A linear relationship between the rate of energy dissipation, caused by the frictional process, and the disk temperature is seen. Furthermore, the linear trend line extrapolates to a value close to the ambient temperature at $\dot{Q}_d = 0$ as expected. The magnitude of the slope ($\beta_f = 59\ \frac{^\circ C m^2 s}{J}$) is specific for the applied test system and depends on the thermal properties of the applied tribotester. The latter is controlled by e.g. geometry and design of components, thermal conductivities of applied materials and application of cooling devices. This linear relationship between the counterface temperature and the specific rate of energy dissipation (or specific rate of frictional work) is also found by Chang et al. [32]. The magnitude of the slope found on the POD used in that study is approximately a factor of 2 lower than the one presented here. Consequently, the counterface temperatures measured under a certain set of sliding conditions are also a factor of 2 lower than the ones found in this study. Such a temperature difference can potentially result in a significantly different outcome of friction and

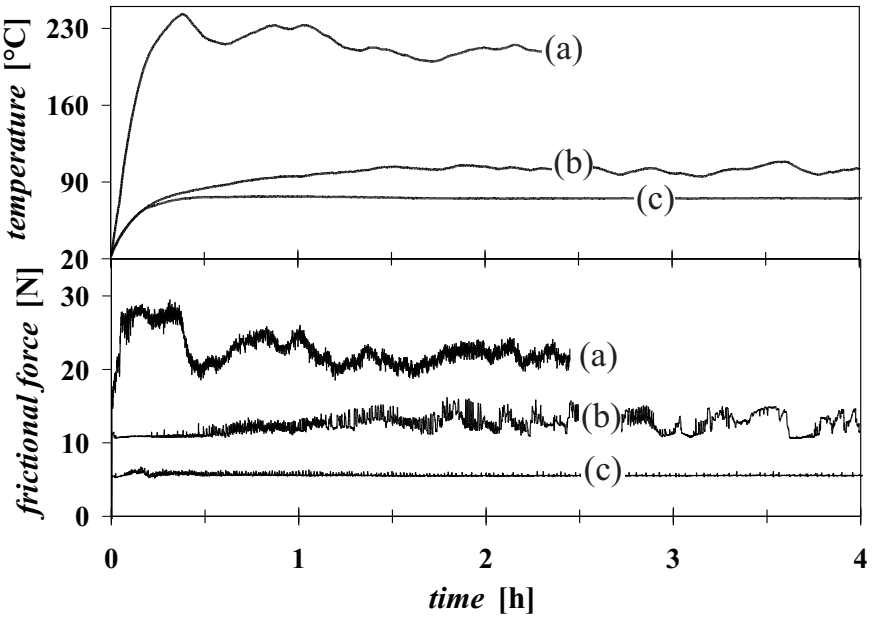

Figure 5.1. Three examples of measured temperatures and frictional forces, respectively, as a function of time. (a) G/EP worn at the *pv* condition 1.0 MPa, 6.0 m/s, (b) EP worn at the *pv* condition 0.5 MPa, 3.0 m/s and (c) EP worn at the *pv* condition 0.25 MPa, 6.0 m/s.

wear tests and is therefore relevant to consider together with the applied *pv* condition.

Figures 5.3 and 5.4 show typical examples of accumulated weight loss measured as a function of time for different composites. EP/PTFE/0.2 and EP (see table 4.1 for nomenclature) in figure 5.3 exhibit a relatively short running-in period after which the curves become linear, whereas the curve for G/EP is linear from the outset. Running-in periods are generally not observed in this study for easily worn materials or at severe sliding conditions. EP reinforced with the carbon/aramid weave (CA/EP) generally shows a low wear rate and a relatively long running-in period before steady state is reached, cf. figure 5.4. This long running-in period is probably due to slow establishment of a transfer layer on the counterface, which eventually reaches steady state in terms of counterface coverage and thickness.

5.2 Structures of produced composites

Electron microscopy images are given in the following to document the micro-structures of some of the tested composites. It is chosen to show composites containing particles as examples, since a good particle distribution is important for the properties and can be difficult to achieve. Figure

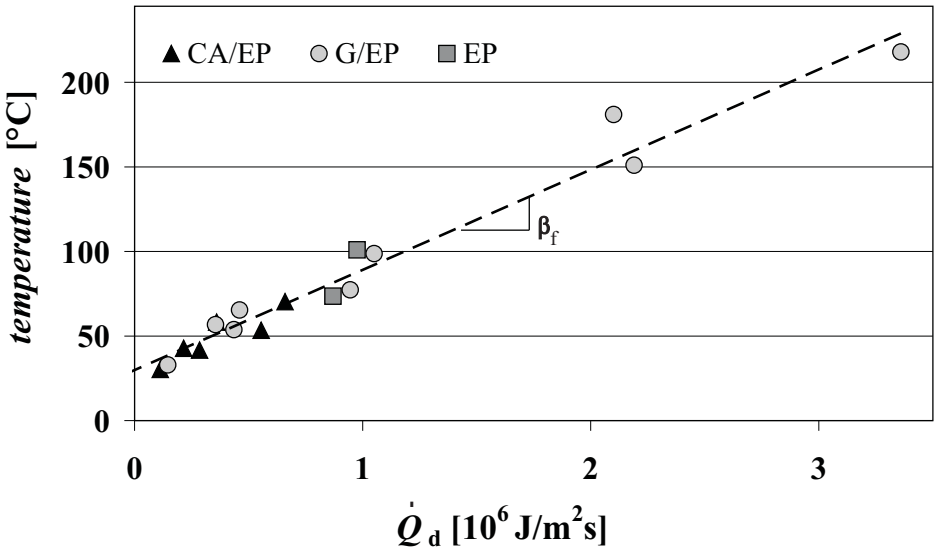

Figure 5.2. Measured steady state temperatures at different pv conditions plotted versus the specific rate of energy dissipation $\dot{Q}_d$. β_f is the slope of the linear trend line.

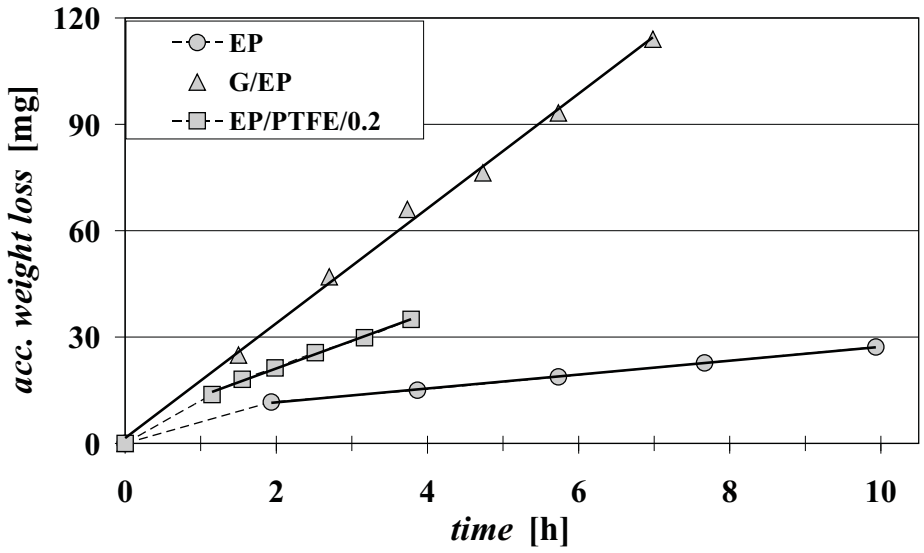

Figure 5.3. Accumulated weight loss as a function of time measured for different composites. The pv condition is in all cases: $p = 0.25$ MPa, $v = 6.0$ m/s. The solid lines are linear trend lines.

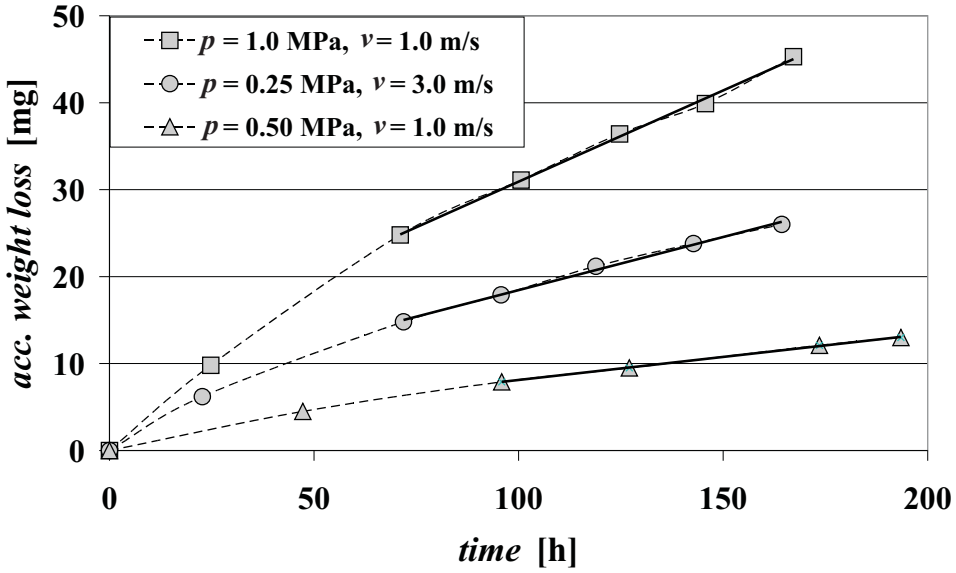

Figure 5.4. Accumulated weight loss as a function of time for CA/EP measured at three different *pv* conditions. The solid lines are linear trend lines.

5.5 shows the micro-structures of (a) EP/PTFE and (b) CA/EP/PTFE. In the case of EP/PTFE, it is seen that the micro-particles are relatively well-distributed in the resin. The image of CA/EP/PTFE shows a zone of resin, marked by the dashed line, containing the PTFE particles. Within this resin zone, the particles are relatively well-distributed. However, it is generally seen that the PTFE particles are only located in the resin between, and not within, fiber bundles. Thus, the particles are too large to enter the fiber bundles, which thereby act as filters preventing a more homogeneous particle distribution. This filtering effect is a common problem with micro-scale particles especially in relation to injection techniques such as Resin Transfer Molding (RTM) [48].

Figure 5.6 shows the micro-structures of (a) EP/1.0 and (b) CA/EP/CuO. The CuO particles seem to be relatively well-dispersed in the EP resin. It is not possible to clearly see, whether the nanoparticles are present as primary particles or as small clusters based on these SEM images. However, all particles or clusters appear to be sub-micron in size. Image 5.6(b) shows nanoparticles distributed in the resin both between and within fiber bundles. Thus, the problem with particle filtering seen for the micro-scale PTFE particles are avoided by going to nano-scale. Additional SEM images showing EP added nano-CuO in the range of 0.1 to 10 vol% are found in figure 1 in appendix C.

In order to get a more clear view of the actual size of the particles, TEM images are produced. Figure 5.7 shows the dispersion state at a nano-CuO content of 1 vol% and 6 vol%, respectively. A distribution of

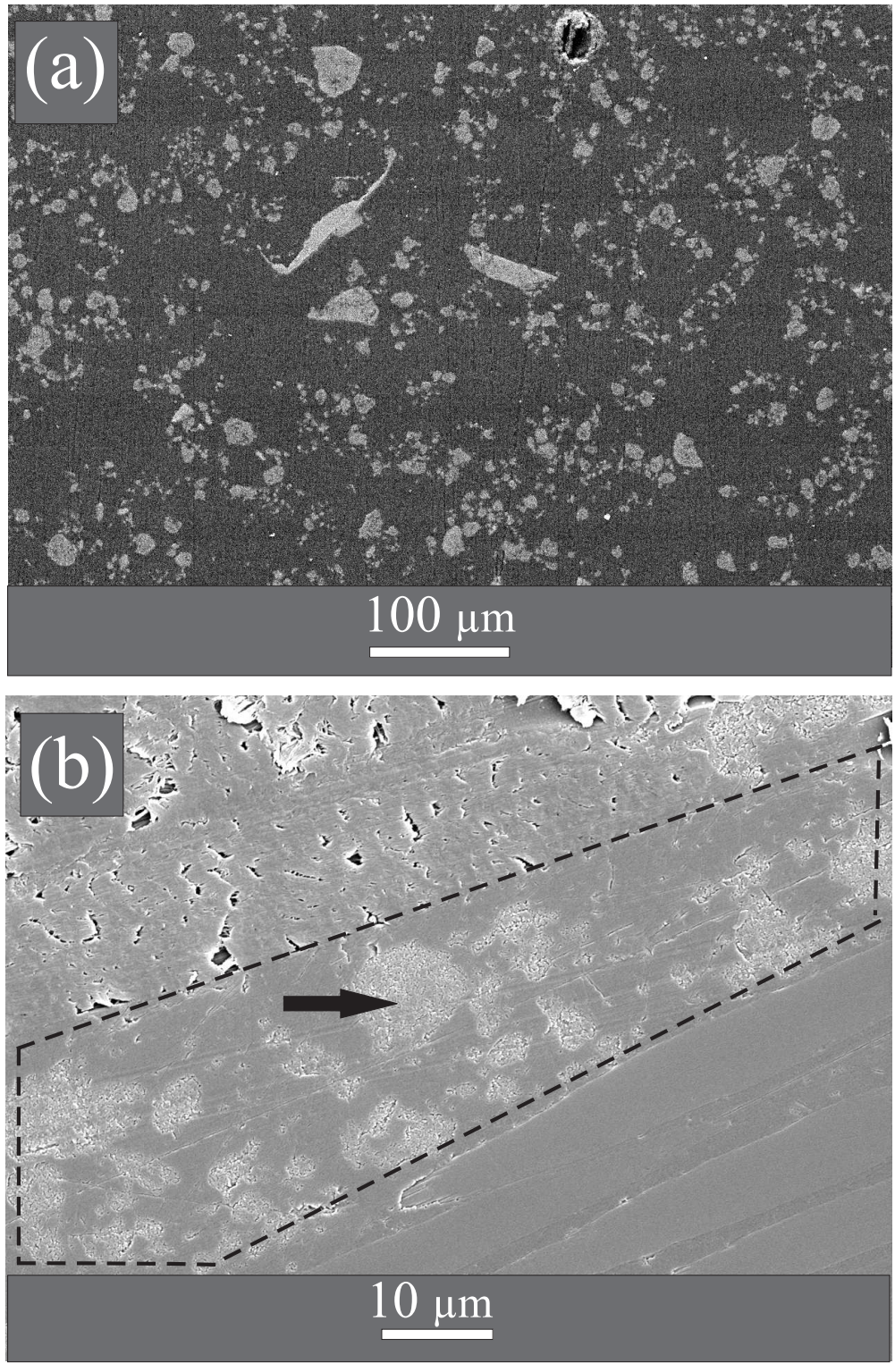

Figure 5.5. SEM images showing the composite structures of (a) EP/PTFE and (b) CA/EP/PTFE. The light gray phase is PTFE and a single particle is marked by an arrow. The area enclosed by the dashed line is a zone of resin where the PTFE particles are located. The lower right corner and the upper left corner of (b) show carbon fibers and aramid fibers, respectively, parallel to the surface.

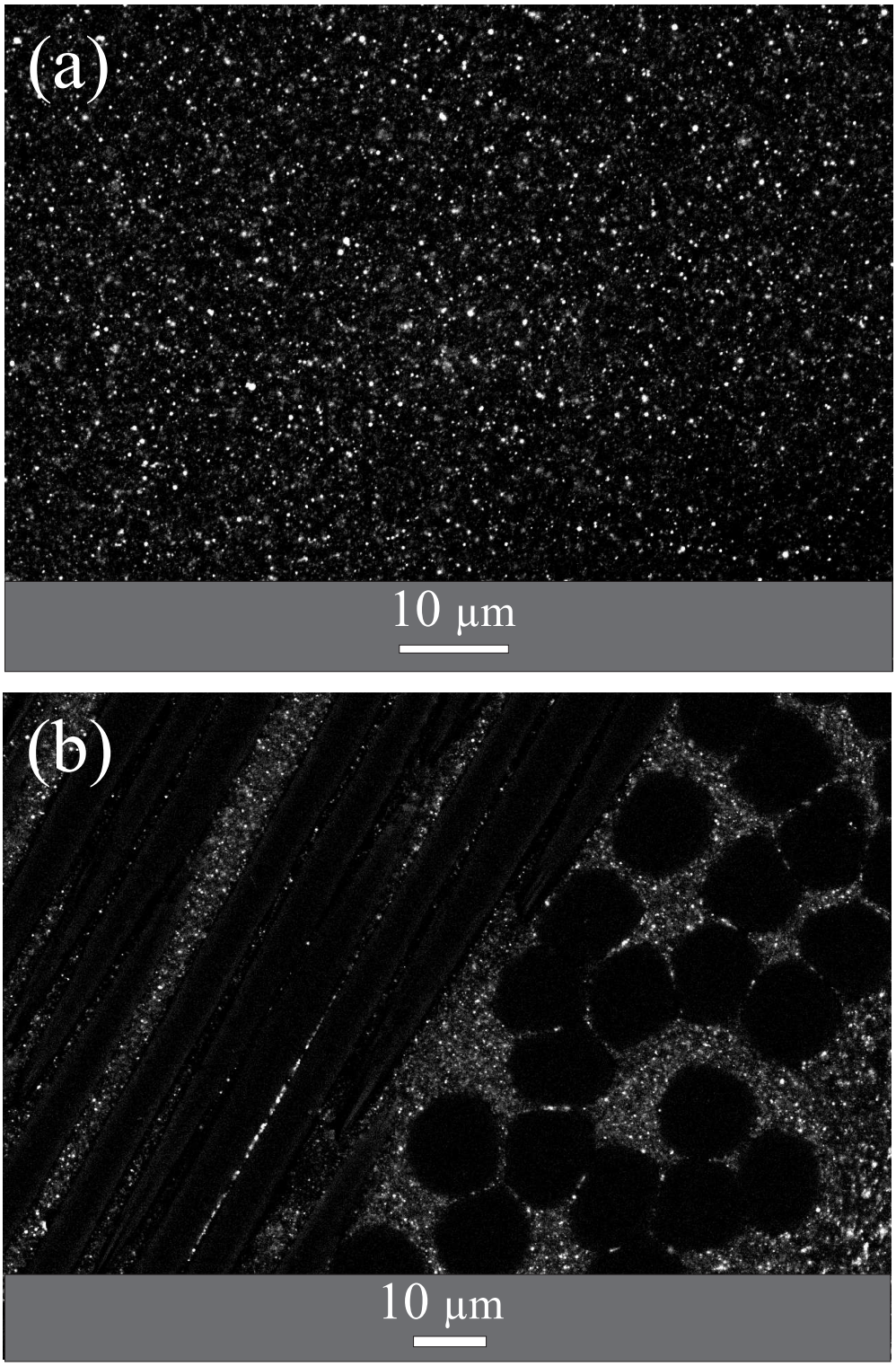

Figure 5.6. SEM images showing the composite structures of (a) EP/1.0 and (b) CA/EP/CuO. Nano-CuO particles are seen as bright stars. In (b) carbon fibers and aramid fibers, respectively, are seen oriented parallel and normal to the surface.

sizes is seen, which ranges from about 30 nm to 250 nm in diameter. The smallest particles are the primary particles which size-wise agrees with the values given by the manufacture of the particles. An increased tendency to form agglomerates is evident at 6 vol%. Furthermore, some of the larger particles do not appear to be agglomerates but rather large particles formed unintentionally during production. These will probably be very difficult to shear into smaller particles. Compared to other publications, e.g. [36, 43, 102], the obtained particle distribution seems satisfactory. The images also show that it is possible to obtain a fairly good dispersion by using a simple laboratory mixer when coated nanoparticles are added in a solvent dispersed form.

Fig. 5.8 shows the micro-structures of (a) EP/PTFE/3.0 and (b)+(c) EP/PTFE/0.2. Image (a) shows PTFE and nano-CuO particles which appear to be relatively well-distributed. Images (b) and (c) show PTFE incorporated together with a low concentration of nano-CuO particles. Examples are indicated by small circles for nanoparticles and large circles for PTFE particles. The images furthermore show that the nanoparticles apparently have a tendency to locate themselves in the interface between PTFE and EP, which is especially evident for EP/PTFE/0.2.

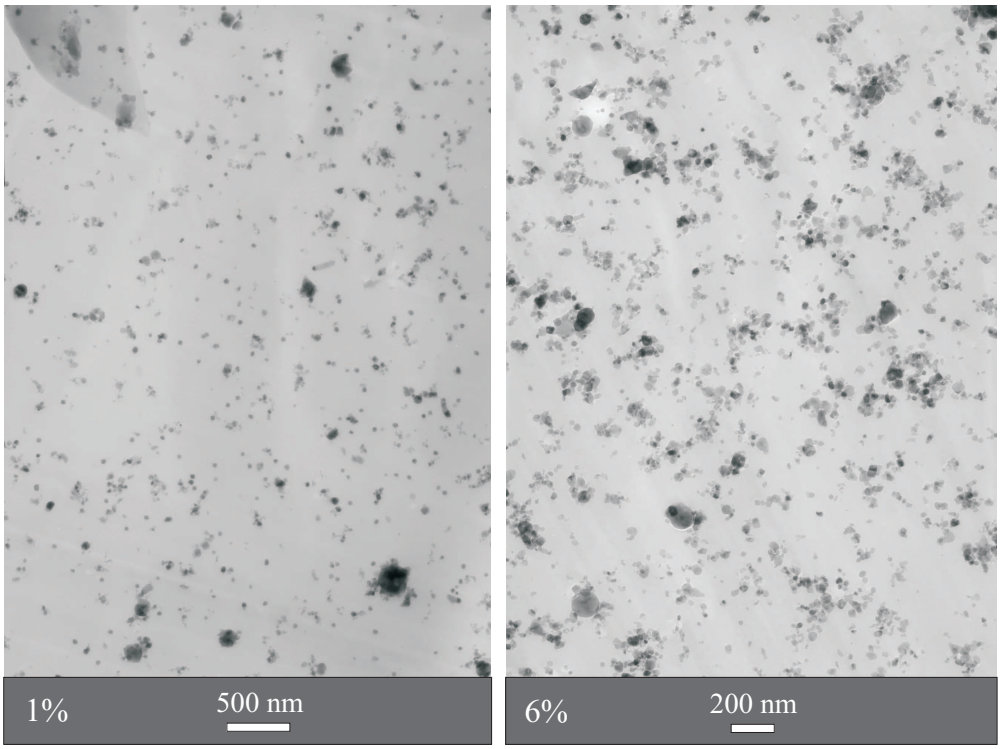

Figure 5.7. TEM images of EP containing 1 vol% and 6 vol% nano-CuO, respectively.

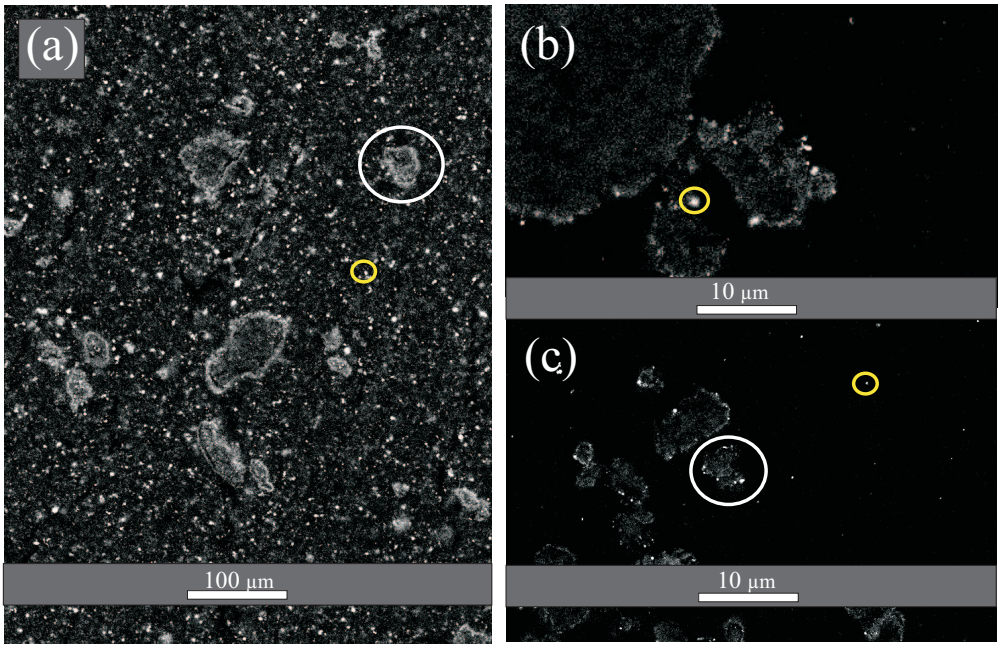

Figure 5.8. SEM images showing the structures of (a) EP/PTFE/3.0 and (b)+(c) EP/PTFE/0.2. Examples of PTFE particles and nanoparticles are indicated by large and small circles, respectively.

5.3 PMCs without fibrous reinforcement

Different amounts of CuO nanoparticles are incorporated into both the neat EP resin and into the resin containing PTFE microparticles. The content of CuO is varied in the range of 0 to 10 vol% while the PTFE content is fixed at 7.5 vol%. The effect of adding these particles is presented in this section.

5.3.1 Hardness and glass transition temperatures

Figure 5.9 shows glass transition temperatures (T_g) and Vickers microhardness (HV) values measured for EP with different particle content. The T_g values do not show any clear trend as a function of the nano-CuO content. It is expected that a strong interaction over the large interfacial area between nanoparticles and resin might restrict mobility to some extent and thereby cause an increase in T_g. For the PTFE containing composites, the T_g values are generally lower, which may be due to an increased mobility caused by a weak interfacial strength between PTFE and EP. Vickers hardness does not show any clear trend as a function of the nano-CuO content either. However, the hardness is on average reduced by 19% when PTFE is incorpored. Since the hardness of neat PTFE is significantly lower than for EP, a decrease would also be expected based on a rule-of-mixtures estimate.

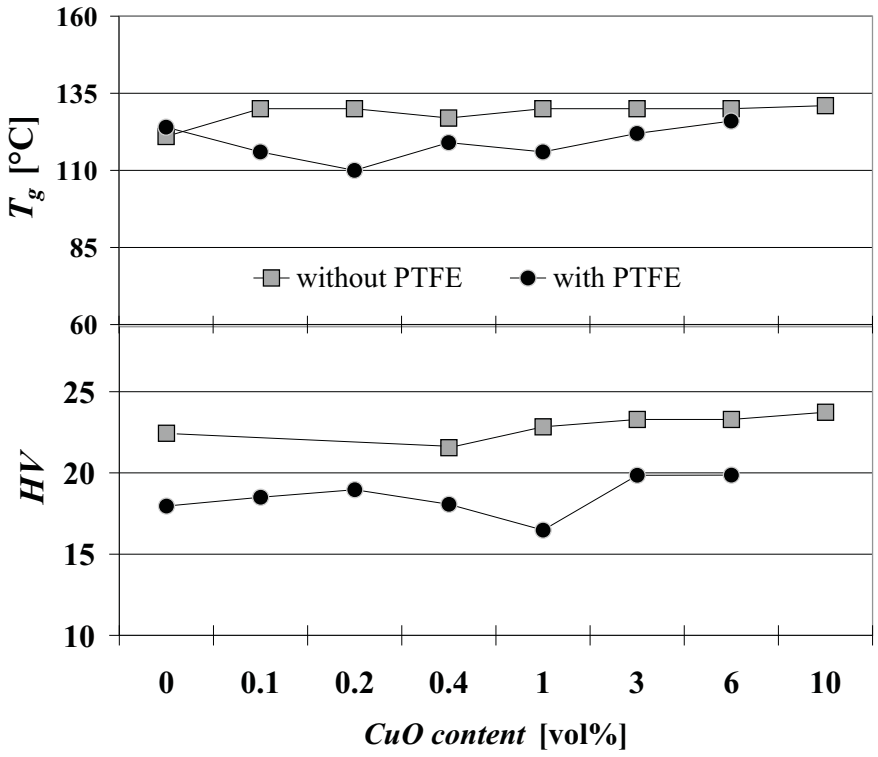

Figure 5.9. Glass transition temperature (T_g) and Vickers hardness (HV) measured for EP with and without PTFE, containing different concentrations of nano-CuO. The lines are guides to the eye.

5.3.2 Sliding at low pressure and high velocity

The tribological data presented in this section is obtained at a *pv* condition of 0.25 MPa, 6.0 m/s and a counterface roughness of 0.26 μm R_a. Note, that the sliding velocity applied here is high relative to similar studies, which typically use velocities of 1 m/s or less. However, PMCs are also used in high velocity applications, which makes laboratory testing at such conditions interesting. Figure 5.10 shows measured coefficients of friction μ and corresponding disk temperatures. General agreement is seen between friction and temperature as should be expected. Without PTFE, μ is roughly independent of the nano-CuO content even though a maximum at EP/1.0 is indicated. When PTFE is added, an average reduction in μ of 35% is found in the CuO range of 0 to 0.4 vol%. At higher concentrations of nano-CuO the curves for composites with and without PTFE begin to coincide. This indicates that the friction lowering effect of PTFE deteriorates at a higher CuO content. Furthermore, note that the error bars for composites with PTFE are significantly smaller, which is due to a much more smooth and stable frictional behavior. The latter is also seen by the frictional profiles shown in figure 5.11. Thus, composites containing PTFE together with low concentrations of nano-CuO (0 to 1.0 vol%) show a smooth frictional behavior. At higher concentrations of nano-CuO (i.e. 6.0 vol%) the frictional force shows significantly more fluctuation in agreement with the results seen in figure 5.10.

Figure 5.12 shows specific wear rates ($\dot{w}_s$) for EP, with and without PTFE, containing different concentrations of nano-CuO. The frictional behavior is to some extent reflected in these wear data. For composites without PTFE an increase in $\dot{w}_s$ is seen, relative to EP, at all concentrations of nano-CuO. The wear rate increases as a function of the CuO content up to EP/1.0, after which it declines. Furthermore, note that the deteriorating effect on the wear resistance due to nano-CuO is seen at a very low content and does not show major changes by increasing the concentration. When PTFE is added to the neat EP, the wear rate increases by a factor of 2.5, which probably is due to weakening of the matrix material caused by PTFE. When CuO is added together with PTFE, the wear rate decreases slightly up to a CuO content of 0.4 vol%, after which it increases significantly.

SEM images of the worn surfaces are produced in order to obtain a better understanding of the wear behavior. Figure 5.13 shows images of worn surfaces for (a) The neat EP and (b) EP/3.0. In the case of EP, compressed wear debris and abrasive wear tracks are seen. The more bright regions, e.g. the upper part of the image, contain many small cracks with a length of about 20-30 μm. Image (b) shows the typical behavior found for EP with a CuO content in the range of 0.1 to 3.0 vol%. Large cracks of about 100 - 200 μm are seen perpendicular to the sliding direction. Furthermore, the number and severity of these cracks follow the measured wear rates i.e. they are mostly observed for EP/1.0 and EP/3.0

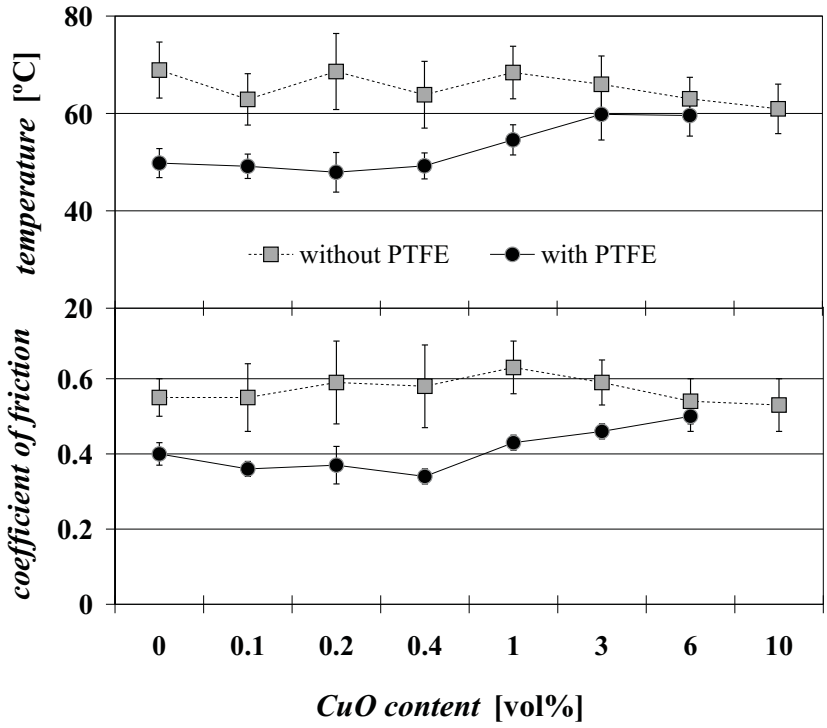

Figure 5.10. Coefficients of friction and corresponding disk temperatures measured for EP with and without PTFE, containing different concentrations of nano-CuO. The applied *pv* condition is 0.25 MPa, 6.0 m/s. The lines are guides to the eye.

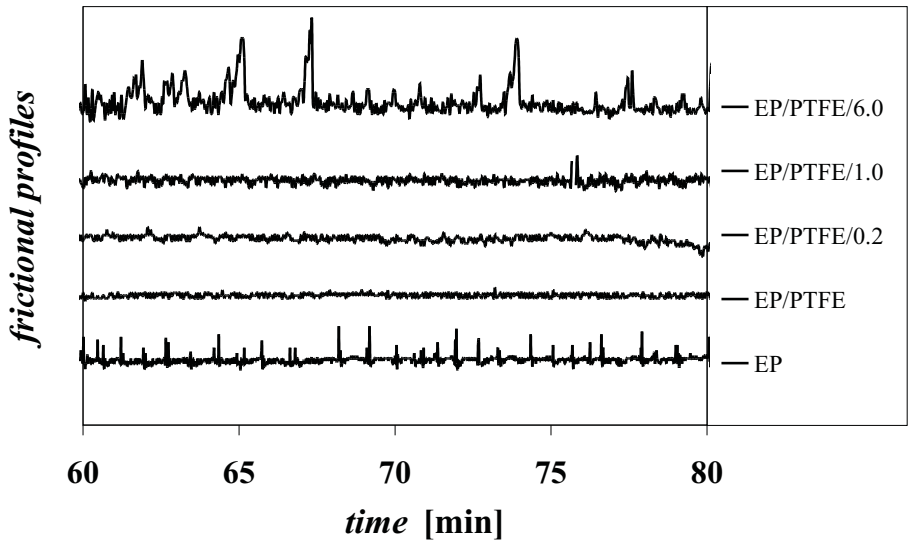

Figure 5.11. Examples of frictional profiles, i.e F_f recorded as a function of time, which show varying degrees of fluctuation for different composites.

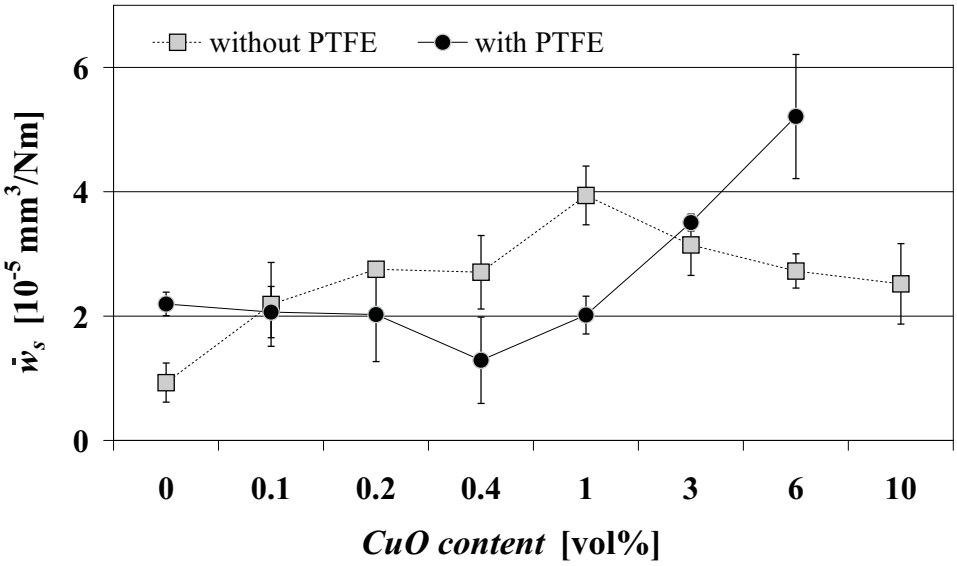

Figure 5.12. Specific wear rates ($\dot{w}_s$) measured for EP with and without PTFE, containing different concentrations of nano-CuO. The applied pv condition is 0.25 MPa, 6.0 m/s. The lines are guides to the eye.

with the highest wear rates.

Since hardness (HV), friction (F_f) and counterface temperature are largely unaffected by the CuO content, cf. figures 5.9 and 5.10, it seems likely that the real area of contact (A_r) is also at the same level at the given load (W_N) assuming equation (2.1) applies. The interfacial shear stress (τ_{av}) during sliding is also likely to be at the same level according to the adhesive model of friction, cf. equation (2.6). Thus, the appearance of the large cracks in figure 5.13(b) is probably caused by a weakening of the matrix material due to incorporation of nano-CuO. This weakening can potentially be caused by poor properties of the as-supplied coating on the incorporated nanoparticles. In order to examine this, the composite with the highest wear rate i.e. EP/1.0 is also produced using non-coated CuO particles from the same manufacturer. The measured values are: $\dot{w}_s$ = 3.2 ($\pm$0.6) 10^{-5} mm^3/Nm and μ = 0.55 ($\pm$0.06) for non-coated particles compared to $\dot{w}_s$ = 3.9 ($\pm$0.5) 10^{-5} mm^3/Nm and μ = 0.63 ($\pm$0.07) for coated particles. Friction and wear are roughly on the same level, which indicates that the coating is not the main reason for the poor wear properties. Bahadur et al. also reported the effect of nano-CuO when added in the range of 0 to 10 vol%. The wear rate of the applied polymer (PPS) decreased, because nano-CuO improved transfer film formation. However, the flexural strength was deteriorated in the entire concentration range with a minimun in strength at 2 vol% CuO [27]. Thus, the strength decreased at a low CuO content and then started to increase at higher

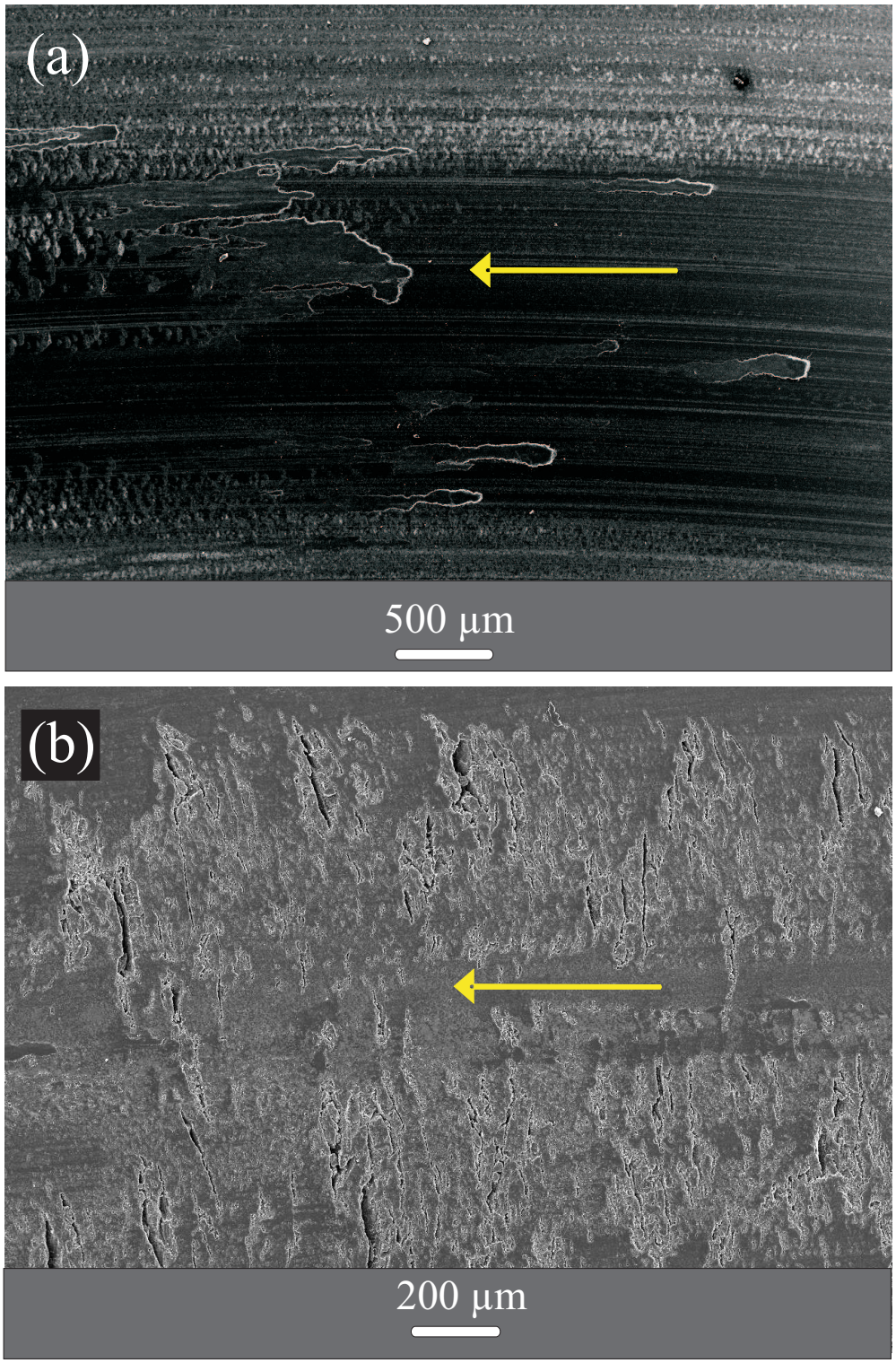

Figure 5.13. SEM images showing worn surfaces of (a) The neat EP and (b) EP/3.0. Arrows indicate sliding direction. The applied *pv* condition is in both cases 0.25 MPa, 6.0 m/s.

concentrations, which is similar to the effect of nano-CuO on the wear resistance presented here. In this study, no significant transfer films are observed visually during the measurements presented in figures 5.10 and 5.12. Generally, only loose debris is formed with no tendency to adhere to the counterface. In short, the high wear rates are believed to be due to weakening of the matrix material by nano-CuO combined with a lack of transfer film formation.

Figure 5.14(a) shows a worn surface of EP/6.0. No large cracks are seen on the surface (the same applies for EP/10), which agrees with the lower wear rate relative to EP/1.0 and EP/3.0. Another phenomenon mostly seen at a high CuO content is the accumulation of CuO on the composite surface, which is seen as a light gray track on the lower part of figure 5.14(a). This accumulation is generally seen as isolated tracks or as spots on the worn composite surface. It is confirmed by EDS that these tracks or spots contain a large fraction of copper and also in some cases iron. The latter indicates that CuO accumulates to an extent where it becomes capable of causing wear of the steel counterface. This patchy accumulation of copper on the surface could possibly act as a protective coating which decreases wear. On the other hand, accumulation of these hard particles could also increase wear due to abrasive action.

Figure 5.14(b) shows the worn surface of EP/6.0 at a higher magnification. The surface appears smooth and only small-scale cracks are seen. Furthermore, it is possible to see nanoparticles distributed in the surface. It is unclear, why the wear rate begins to decrease at a high CuO content, but it may indicate a competition between mechanisms, which depend differently on the nano-CuO content. It is not uncommon that incorporation of rigid particles into a polymeric matrix reduces strength and increases toughness. However, the problem with strength reduction is typically diminished by reducing the particle size [108]. Imagine that the strength decreases rapidly at a low particle content and then levels off at higher concentrations. If the toughness simultaneously increases as a function of the particle content, e.g. due to enhanced crack deflection, it may explain the observed behavior. Thus, incorporation of particles may increase the number of crack initiation sites due to a weak interface while simultaneously increasing toughness by hampering propagation of initiated cracks. Such a behavior has been shown by Spanoudakis et al. for 4.5 μm spherical glass particles in an EP resin [109]. However, a different behavior is typically seen when going to nano-size.

The worn surface of EP/PTFE shown in Fig. 5.15(a) appears to be smooth, free from cracks and also shows individual PTFE particles. Similar surfaces are seen for all PTFE containing composites with a nano-CuO content up to 1 vol%. The surface for EP/PTFE/6.0 (not shown) appears slightly more rough and the PTFE phase is not easily identified, which agrees with the higher wear rate and coefficient of friction. Figure 5.15(b) shows the wear track on the steel counterface after sliding against

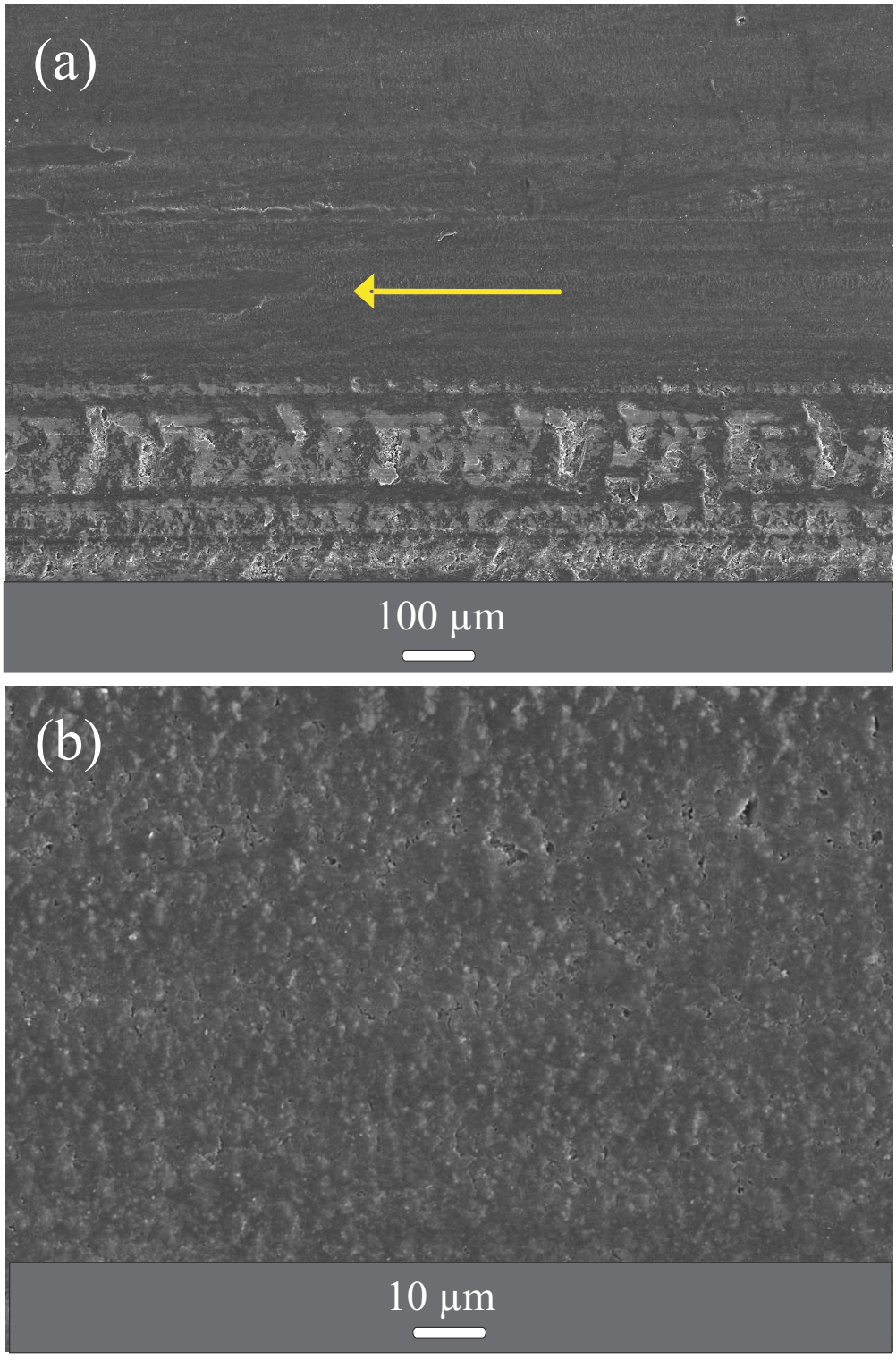

Figure 5.14. SEM images showing the worn surface of EP/6.0 at two different magnifications (a) and (b). The arrow indicates sliding direction. The applied *pv* condition is 0.25 MPa, 6.0 m/s.

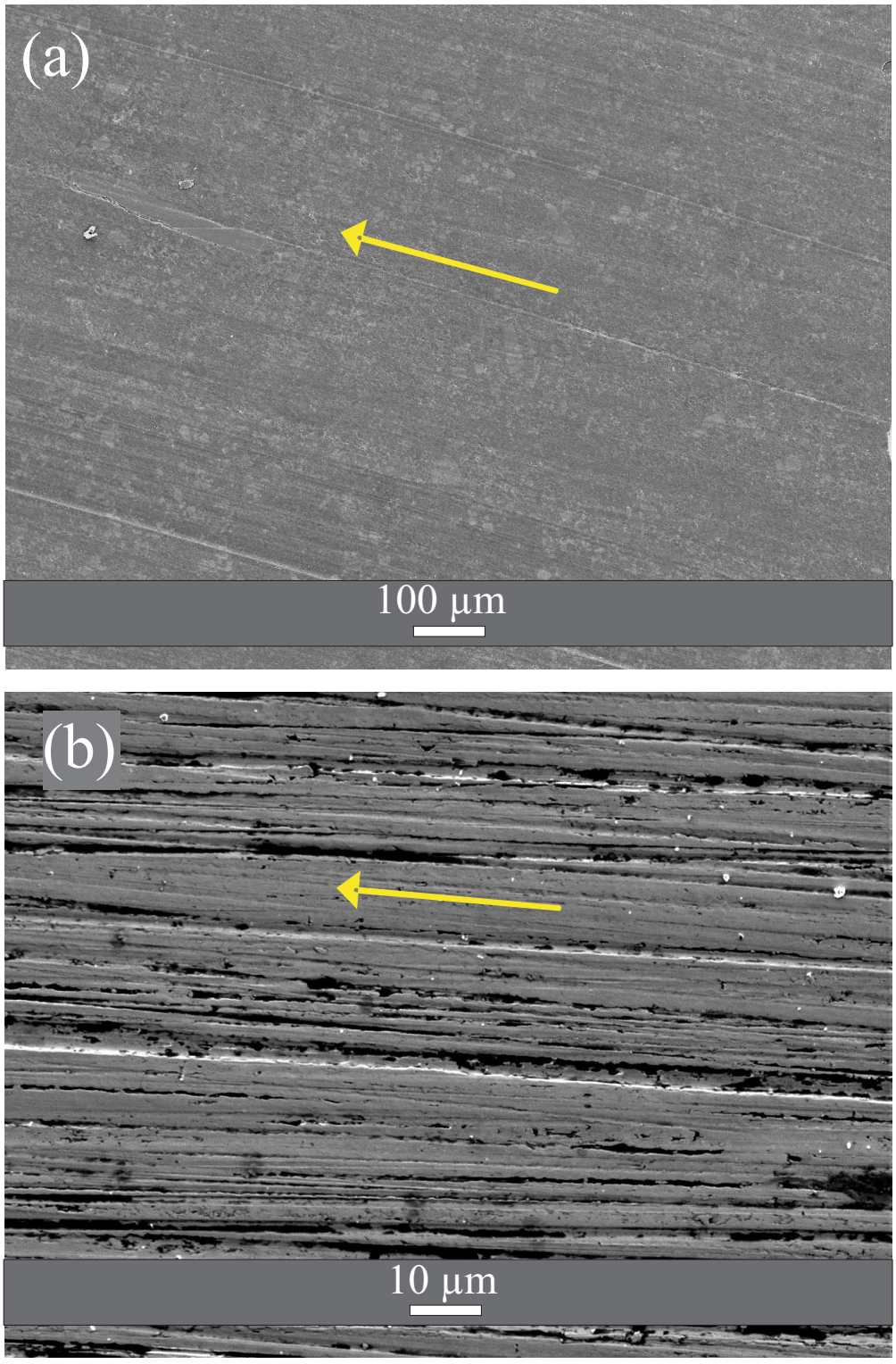

Figure 5.15. SEM images of (a) The worn surface of EP/PTFE and (b) The wear track on the steel counterface after sliding against EP/PTFE/0.2. The arrows indicate sliding direction. The applied *pv* condition is 0.25 MPa, 6.0 m/s.

EP/PTFE/0.2. The appearance of the counterface is similar for all the PTFE containing composites. The dark regions seen in the image are deposits from the composite, which are stuck in grooves on the counterface. However, it is not possible to see any indications of an continuous transfer film.

Note, that the PTFE particles in figure 5.15(a) seem to be stuck in the surface instead of being pulled out during sliding. Thus, the particles are gradually worn while staying in the surface. It is hypothesized that the formed PTFE containing debris is smeared over the composite surface and thereby decreasing the interfacial shear stress, which lowers μ and results in a more gentle wear mechanism.

Friction and wear begin to increase as a function of the CuO content at EP/PTFE/1.0, which probably is due to the aforementioned interfacial accumulation of hard nanoparticles. This may disrupt the interfacial PTFE containing layer and thereby decrease the lubricating effect. The latter will in turn increase the interfacial shear force and frictional heating, which cause the wear rate to increase simultaneously.

5.3.3 Sliding against a smoother counterface

It is known that the counterface roughness can have a large impact on the formation and stability of polymeric transfer films [60, 61]. Schwartz et al. found that addition of alumina nanoparticles to PPS increased wear when sliding against a counterface with a roughness of 0.27 μm R_a, while improvements were obtained at other counterface roughnesses. The improvements were attributed to enhanced transfer film coverage [50].

To examine the effect of counterface roughness, some of the tribological tests presented in section 5.3.2 are repeated using a smoother counterface with a roughness of 0.074 μm R_a. In figure 5.16 friction and wear data obtained at the two different counterface roughnesses are compared. A slight increase in μ is seen when applying the smoothest counterface except for EP/PTFE/0.2. Furthermore, a significant reduction in wear is seen for all composites. The smooth surface does not enable establishment of a transfer film in the case of EP/PTFE/0.2. Thus, the degree of deposit is similar to what is shown in figure 5.15(b). However, for the four composites without PTFE a significant transfer film formation is seen. Figure 5.17 shows the appearance of wear tracks on the steel counterface after sliding against different composites. The composites without PTFE i.e. (b) and (c) give rise to an easily detectable transfer film, whereas the presence of deposits are only weakly indicated in the case of the PTFE containing composite i.e. (a).

Figure 5.18 shows SEM images of the transfer film which is formed by sliding against EP/0.2. The lower bright part of figure 5.18(a) is outside the wear track whereas the dark part is the transfer film. This film is in some areas thin and homogeneous. In these areas it is possible to see the

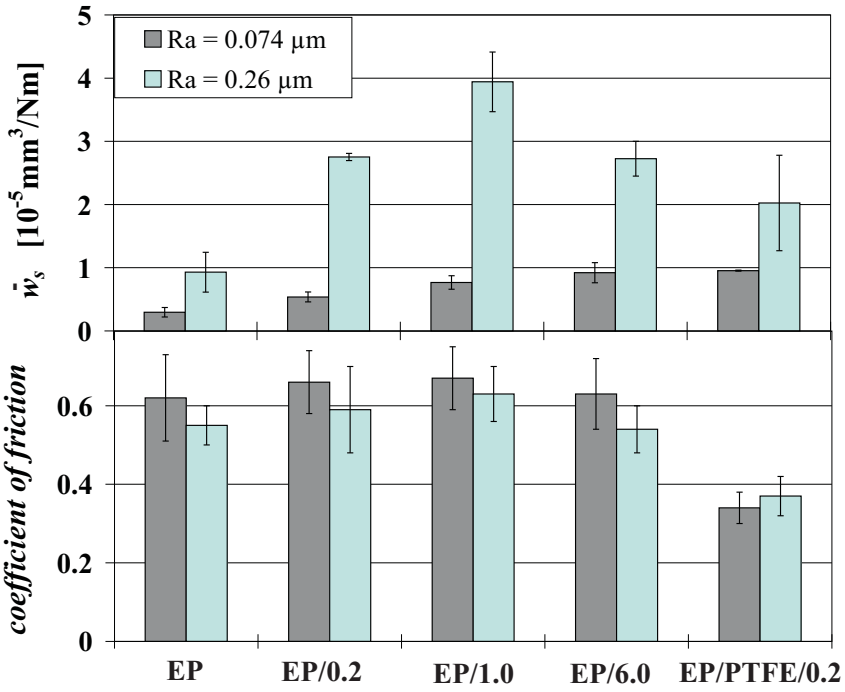

Figure 5.16. Coefficients of friction and specific wear rates ($\dot{w}_s$) measured for selected composites at two different levels of counterface roughness (R_a) i.e. 0.26 μm and 0.074 μm. The applied pv condition is in all cases 0.25 MPa, 6.0 m/s.

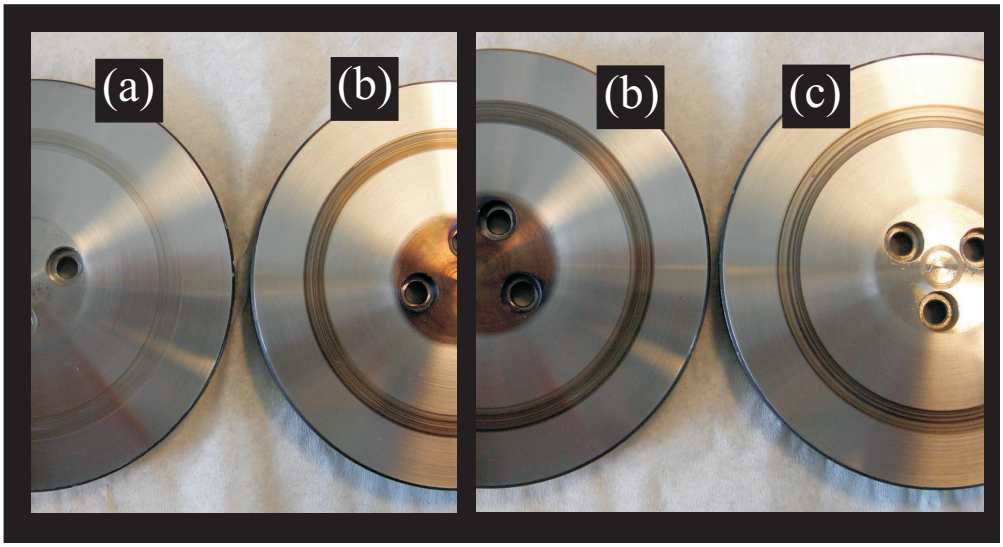

Figure 5.17. The appearance of wear tracks on the steel counterfaces after sliding against (a) EP/PTFE/0.2, (b) EP/0.2 and (c) EP/6.0. Loose debris is removed by compressed air before taking the photos.

structure of the steel counterface through the film. In other areas the film is thicker and more lumpy. An example of the latter is shown at a higher magnification in figure 5.18(b). This thick transfer layer appears to have a high concentration of nano-CuO considering that the tested composite only contains 0.2 vol%. Thus, the proposed accumulation of CuO in the interface, discussed in section 5.3.2, is supported by this image. The reason for this accumulation might be attributted to the following factors. Firstly, the nano-CuO might adhere more strongly to the steel counterface than the polymeric component. Secondly, thermal degradation of polymeric material in the interface will tend to increase the relative content of the more heat resistant CuO. The fact, that EP forms a relatively continuous transfer film is a bit surprising. EP is certainly not know for forming an effective transfer film due to its cross-linked molecular structure. The author suggests that it may be the smooth counterface combined with thermal degradation of EP in sliding contact, which causes film formation.

The increase in μ against the smooth counterface, which is seen for composites without PTFE is probably due to increases in A_r caused by the presence of transfer films. The transfer films are expected to act as a protective spacer between the surfaces, which explains the decrease in wear seen for the four composites without PTFE. Also in this case, addition of nano-CuO to EP increases wear for all composites. Hence, no improvement of transfer film efficiency due to CuO is indicated. The wear reduction for EP/PTFE/0.2 when applying a smoother counterface is possibly due to a shift in mechanism from abrasive toward adhesive wear. The PTFE containing composites are probably better suited to resist adhesive wear, compared to abrasive, due to lower surface energy and hardness relative to the neat EP.

5.3.4 Sliding at high pressure and low velocity

Friction and wear measurements are repeated at the *pv* condition 1.16 MPa, 1.0 m/s in order to examine the effect of shifting to a condition with higher pressure and lower velocity. The counterface roughness is 0.26 μm R_a. It is found that composites without PTFE show a very unsteady wear behavior. Time averaged wear rates are generally high (in the order of 10^{-4} mm^3/Nm) and show severe fluctuation. This fluctuation is observed visually to be associated with formation and breakdown of unstable transfer films. Thus, when the transfer film is absent the wear rate is exceedingly high. Due to lack of reproducibility these measurements are not completed for composites without PTFE. The only exception to the above is EP/10, which shows a steady and relatively low wear rate of 2.2 ($\pm$1) 10^{-5} mm^3/Nm. This result weakly indicates a positive effect of adding nano-CuO when shifting toward higher pressure and lower velocity. The idea that positive effects of nanoparticle addition becomes more pronounced at higher contact pressures has been reported by others

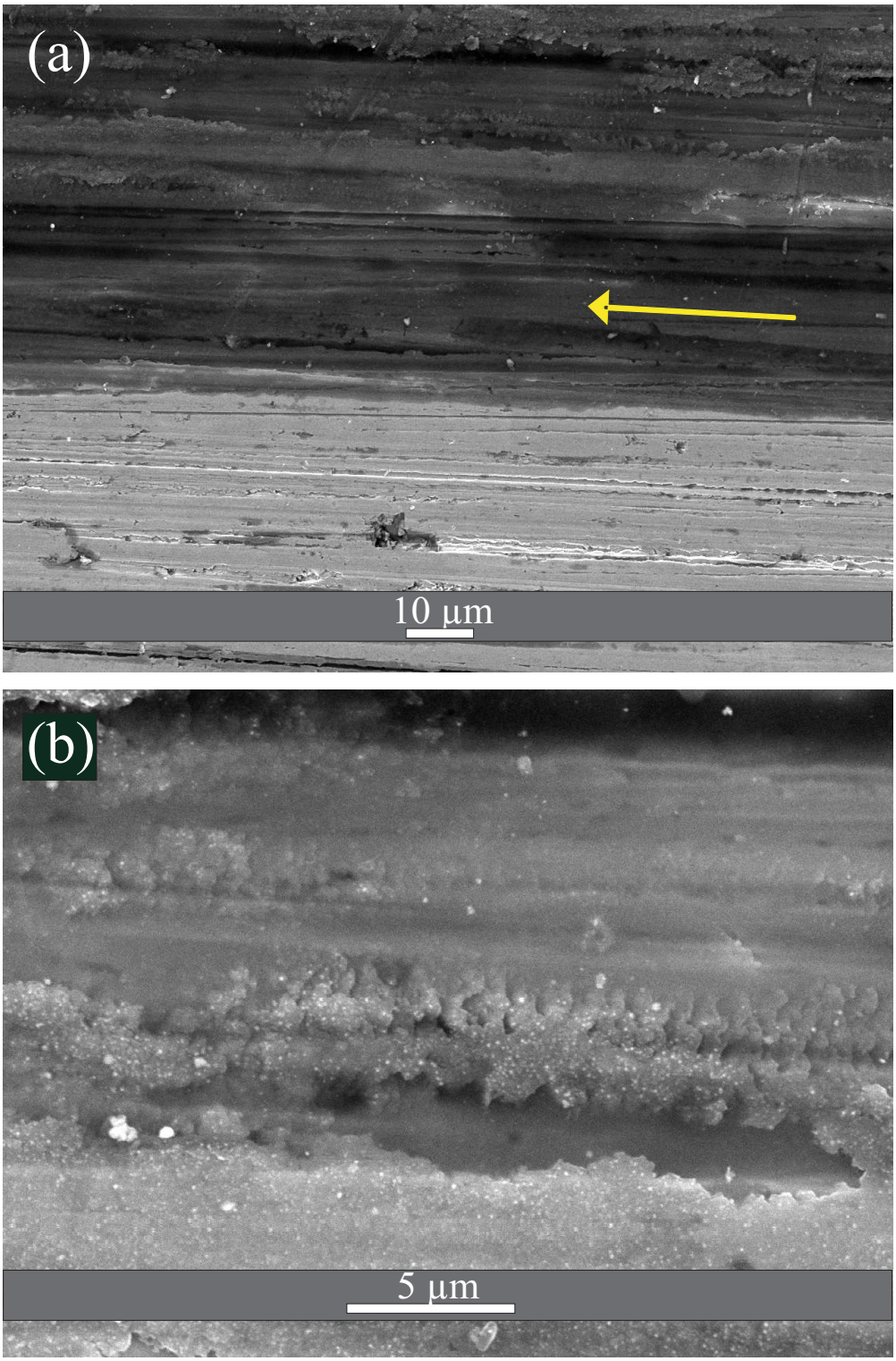

Figure 5.18. SEM images of a transfer film formed on the steel counterface (0.074 μm R_a) after sliding against EP/0.2. (a) Shows the edge of the wear track where the dark upper part is the transfer film and the bright lower part is outside the wear track. The arrow indicates sliding direction. (b) Is a part of the transfer film shown at a higher magnification. The applied pv condition is 0.25 MPa, 6.0 m/s.

[51, 97, 99, 101, 102]. However, this is not explored further in this study.

Figure 5.19 shows friction and wear data for composites with PTFE incorporated. These composites perform well at this condition (1.16 MPa, 1.0 m/s) and the curves for friction and wear, respectively, have similar profiles as the ones shown in figures 5.10 and 5.12. The coefficients of friction are on average reduced by 17% compared to the high velocity condition and the wear rates are on average reduced by 43%. Thus, at this condition PTFE addition leads to a superior friction and wear performance as well as an increased limiting pv factor relative to the neat EP. Furthermore, a positive synergistic effect is seen when PTFE is added together with nano-CuO in a content up to 1.0%. The reason for this is unclear, but it could be related to the tendency of nano-CuO particles to locate themselves in the interface between PTFE and EP, cf. figure 5.8. It might be imagined that the CuO particles act as a compatibilizer, which stabilizes the interface and thereby strengthens the material.

5.4 Fiber reinforced PMCs

The effect of applying two different types of fibrous reinforcement is presented in this section. The two types of reinforcements are a plain glass fiber weave (G) and a carbon/aramid hybrid weave (CA). The performance of these are systematically examined while going from mild to se-

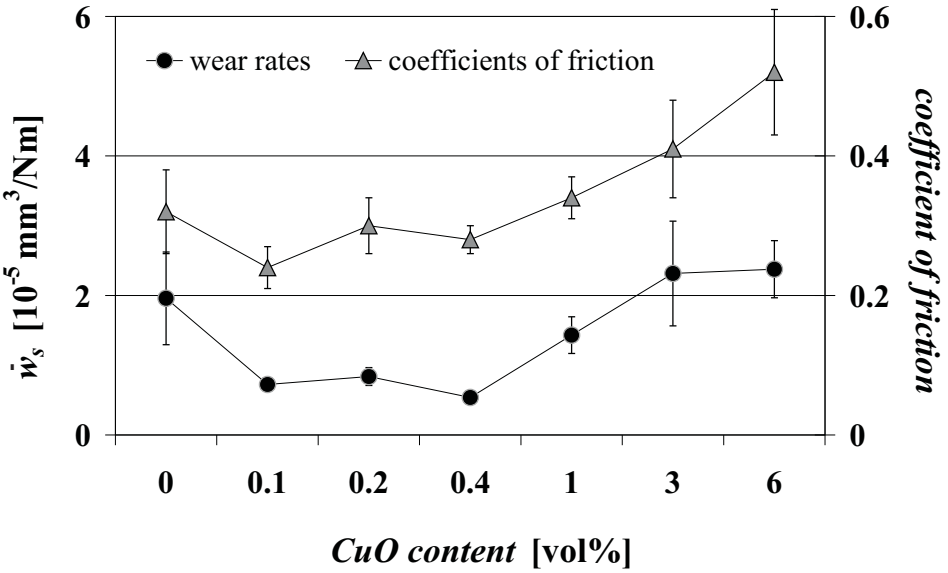

Figure 5.19. Coefficients of friction and specific wear rates ($\dot{w}_s$) measured for EP with PTFE containing different concentrations of nano-CuO. The applied pv condition is in all cases 1.16 MPa, 1.0 m/s. The lines are guides to the eye.

vere sliding conditions. In the case of G/EP, the effect of fiber orientation is also examined. Furthermore, the effect of adding PTFE or nano-CuO together with the carbon/aramid weave is reported.

5.4.1 Comparison of the two types of reinforcements

In order to relate the friction and wear behavior of different composites to each other, it is convenient to compare their values of specific wear rates $\dot{w}_s$ and coefficients of friction μ, since these parameters, from a simplified point of view, should be independent of p and v and therefore represent the general level of performance of the materials in a given system. $\dot{w}_s$ and μ measured for G/EP and CA/EP at different pv conditions are given in table 5.1. Note, that no values are given in table 5.1 for CA/EP at pv factors of 3 MPa m/s or above. This is due to the fact that CA/EP fails under these conditions and is unable to reach a steady state level of both friction and wear. Thus, the limiting pv factor for CA/EP arguably has a value of $pv_{lim} = 3$ MPa m/s, which will be discussed further in section 5.4.5. The average level of μ for G/EP is 0.63 as opposed to 0.41 for CA/EP, which means that a general decrease of approximately 35% is obtained by substituting the glass fiber weave with the given carbon/aramid weave. This difference in the level of μ might be attributed to the following factors. Due to the hardness of glass fibers these are observed by visual inspection after testing to cause a significant roughening of the steel counterface. Furthermore, fragments of glass fibers located in the interfacial zone can act as abrasive particles. Both of these factors might increase the deformation, or ploughing, contribution to μ. The degree of roughening of the counterface seems to depend significantly on the measuring condition and is observed to be most severe at the pv condition: 0.25 MPa, 6.0 m/s. The initial and final roughness of the steel counterface are compared in one case at the mentioned condition. The R_a parameter changes from 0.26 ($\pm$0.03) μm to 0.59 ($\pm$0.05) μm after three hours of sliding. An aditional example of roughening caused by the glass fibers is shown in figure 6 in appendix B. Carbon fibers, on the other hand, might act as a solid lubricant which decreases the interfacial shear force due to the partial graphite structure of these fibers. With respect to abrasiveness the carbon fibers are also in some cases observed to cause some roughening of the steel counterface but to a lesser extent than the glass fibers. The data in table 5.1 shows some variation in μ at different combinations of p and v, but without any indication of clear trends. Thus, it might be concluded that despite a few exceptions, μ is fairly constant and roughly follows Amontons laws of friction, cf. equation 2.4.

The mean of the wear rates $\dot{w}_s$ shown in table 5.1 measured at the six mildest pv conditions is $1.6{\cdot}10^{-5}$ mm^3/Nm for G/EP and $7.3{\cdot}10^{-7}$ mm^3/Nm for CA/EP. Thus, $\dot{w}_s$ is on average a factor of 22 higher for G/EP compared to CA/EP. Furthermore, it is seen that $\dot{w}_s$ generally in-

Table 5.1. Coefficients of friction μ and specific wear rates $\dot{w}_s$ measured for G/EP and CA/EP under different pv conditions. The precision is indicated by standard deviations.

Material	Pressure p [MPa]	Velocity v [m/s]	pv factor [MPa m/s]	Friction μ	Wear $\dot{w}_s$ [10^{-6} mm^3/Nm]
G/EP	0.25	1.0	0.25	0.58 (±0.1)	6.5 (±0.7)
G/EP	0.50	1.0	0.50	0.71 (±0.04)	11 (±0.2)
G/EP	1.0	1.0	1.0	0.46 (±0.06)	11 (±0.1)
G/EP	0.25	3.0	0.75	0.58 (±0.03)	15 (±0.06)
G/EP	0.50	3.0	1.5	0.70 (±0.06)	18 (±0.2)
G/EP	1.0	3.0	3.0	0.70 (±0.03)	28 (±0.07)
G/EP	0.25	6.0	1.5	0.63 (±0.03)	33 (±0.5)
G/EP	0.50	6.0	3.0	0.73 (±0.1)	24 (±0.2)
G/EP	1.0	6.0	6.0	0.56 (±0.05)	34 (±0.1)
CA/EP	0.25	1.0	0.25	0.45 (±0.07)	0.60 (±0.08)
CA/EP	0.50	1.0	0.5	0.43 (±0.05)	0.62 (±0.07)
CA/EP	1.0	1.0	1.0	0.36 (±0.06)	1.0 (±0.2)
CA/EP	0.25	3.0	0.75	0.38 (±0.03)	0.80 (±0.1)
CA/EP	0.50	3.0	1.5	0.44 (±0.05)	0.86 (±0.1)
CA/EP	0.25	6.0	1.5	0.37 (±0.03)	0.49 (±0.03)

creases as a function of p and v. Figures 5.20 and 5.21 show measured depth wear rates $\dot{w}_t$ and steady state interfacial temperatures at different pv conditions for the tested composites. A gradual increase in both parameters are observed as a function of p and v, respectively, as expected from equations (2.15) and (2.17). More specifically, equation (2.15) predicts a linear relationship between $\dot{w}_t$ and the pv factor with a slope equal to $\dot{w}_s$ (or the wear factor). It is clear from table 5.1 that this does not exactly apply since $\dot{w}_s$ is actually not a constant but increases with both p and v. In order to clarify the relationship between $\dot{w}_t$ and pv, these are plotted versus each other in figure 5.22. According to these plots a power law yields a better fit than a linear model.

Three data points at the pv factor 1.5 MPa m/s deviate from the power law trend lines i.e. one data point for G/EP above the trend line and two data points for CA/EP below the trend line. The data point for G/EP above the trend line is measured at the pv condition 0.25 MPa, 6.0 m/s, which as mentioned previously is associated with a particularly high degree of counterface roughening and may therefore explain the deviation. The pv conditions resulting in the two deviating data points for CA/EP are observed visually to facilitate formation of a transfer film to a larger extent than other conditions, which explains the deviation from the trend shown by the other data points.

As mentioned in section 2.3.3, the wear factor k^* is a function of both material properties and system properties and these are both treated as constants. However, considering that the interfacial or counterface temperature varies from 33°C at the lowest pv factor to 218°C at the highest pv factor, cf. figure 5.20 and 5.21, it is obvious that the material prop-

erties will change in this relatively large temperature range. Certainly, the resin properties will change at the glass transition and decomposition temperatures. Thus, this increase in $\dot{w}_t$, beyond what is predicted by equation (2.15), might be related to a gradual deterioration of the resin properties and thereby also in the composite properties with increasing temperatures.

5.4.2 The influence of fiber orientation

From studies on unidirectional fibers it is known that the fiber orientation with respect to sliding direction can have a large impact on the tribological behavior [30]. Since the wear performance measured for G/EP with the N-P fiber orientation is particularly poor, it is chosen to repeat some of the measurements at the P-AP fiber orientation in order to determine if changes in the glass fiber orientation have any impact, cf. figure 5.23. The coefficient of friction measured for the P-AP direction is independent of the pv condition, while the N-P direction shows some variation. Also the specific wear rate $\dot{w}_s$ is roughly the same at the three pv conditions for the P-AP orientation. On the contrary, the N-P direction shows a significant increase in $\dot{w}_s$ when going from a high p - low v condition to a low p - high v condition. As a consequence of this, $\dot{w}_s$ is a factor of 2.6 higher for the N-P direction compared to the P-AP direction at the pv condition 0.25 MPa, 6.0 m/s. The latter might be explained by a difference in abrasiveness between the two directions. G/EP is found to be particularly abrasive at this condition, which might account for the high wear rate. The P-AP

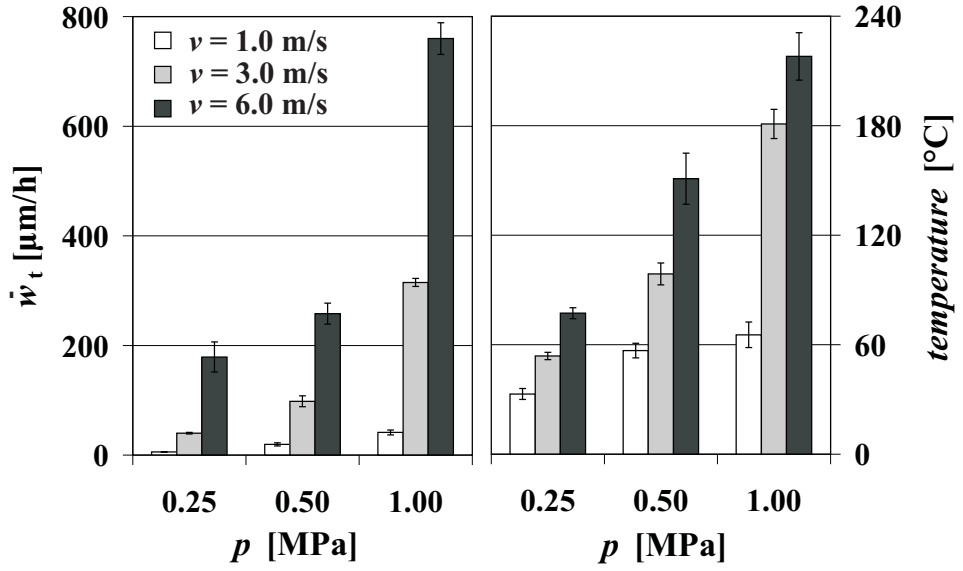

Figure 5.20. Depth wear rates $\dot{w}_t$ and steady state interfacial temperatures at different pv conditions for G/EP.

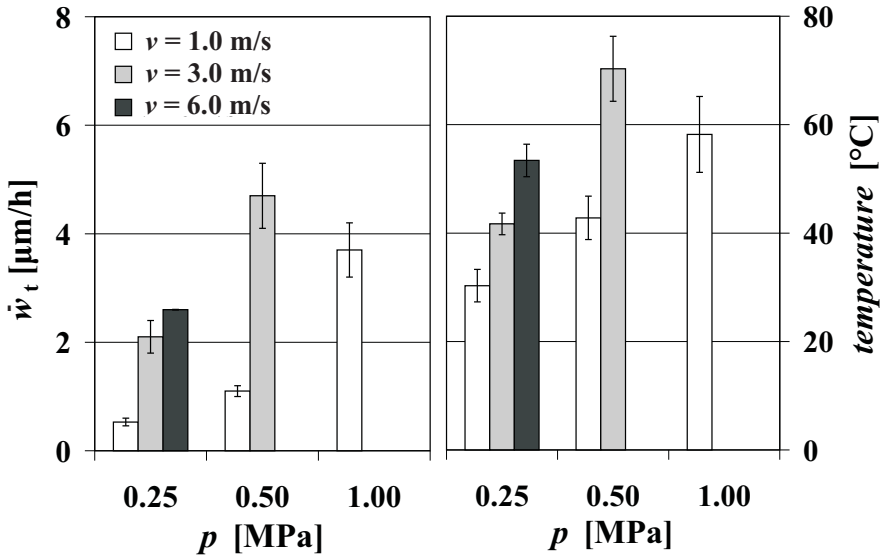

Figure 5.21. Depth wear rates $\dot{w}_t$ and steady state interfacial temperatures at different pv conditions for CA/EP.

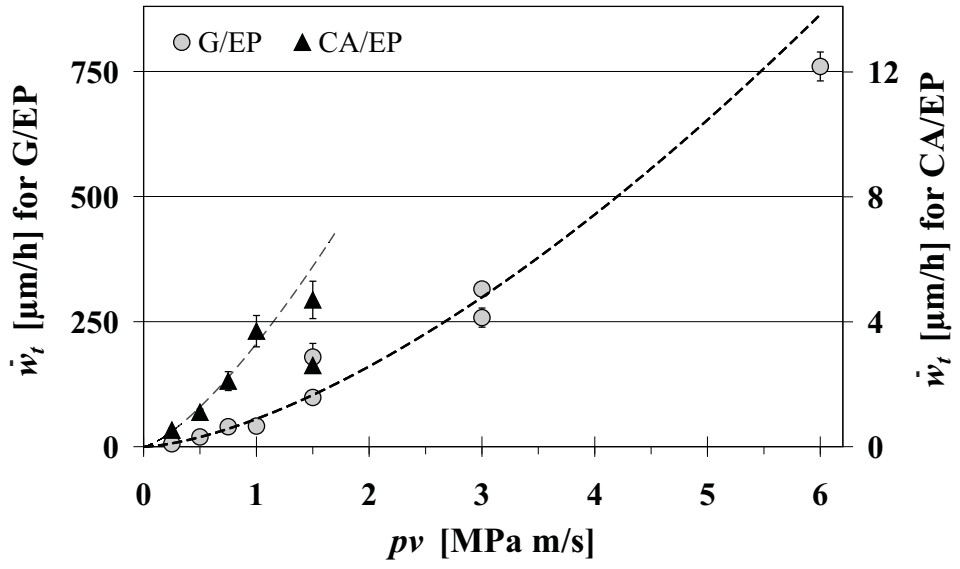

Figure 5.22. Depth wear rates $\dot{w}_t$ for G/EP and CA/EP plotted versus pv factors. The lines are power law trend lines fitted to the experimental data.

orientation is, on the other hand, found by visual inspection to be less abrasive at the same condition and even forms a grayish transfer film. Additionally, the decrease in μ may also contribute to limit temperature induced deterioration of the wear resistance. Cirino et al. examined the influence of fiber orientation for an EP resin reinforced with unidirectional continuous glass fibers [29]. Relative to the wear rate for the neat EP resin, it was found that the parallel and anti-parallel orientation reduced the wear rate by a factor of 2.1 and 1.1, respectively, while the normal direction increased the wear rate by a factor of 2. According to this, it should be beneficial to orient the weave in a way that eliminates the normal fiber orientation, which agrees well with the data presented here.

5.4.3 The effect of incorporating particles

The effect of applying PTFE or nano-CuO together with the carbon/aramid weave is presented below. Furthermore, the differences in tribological behavior between fiber reinforced EP and neat EP is briefly discussed. Figure 5.24 shows friction and wear measured for different composites at

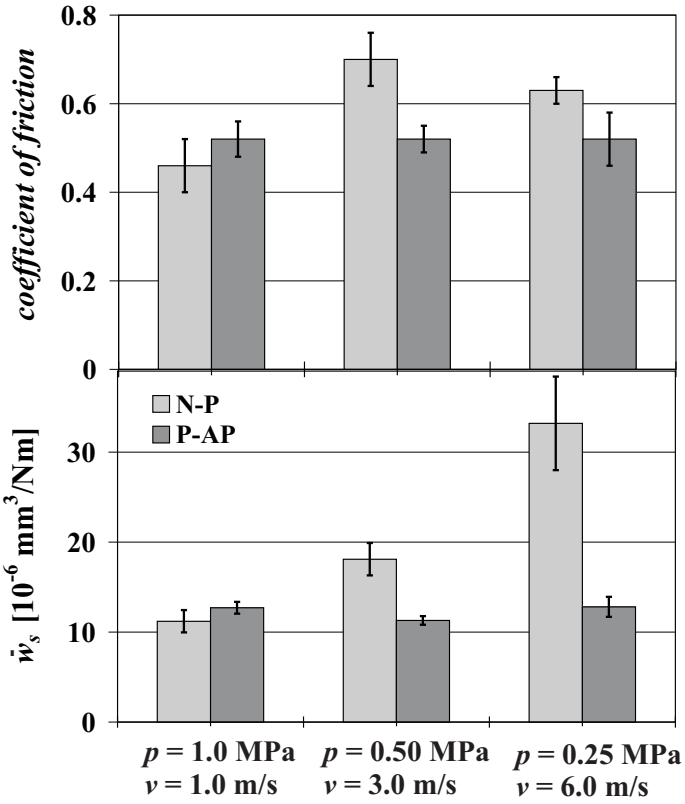

Figure 5.23. Comparison of the coefficient of friction μ and the specific wear rate $\dot{w}_s$ for G/EP when tested with fibers oriented either in the N-P or the P-AP direction. The comparison is made at three different pv conditions.

two *pv* conditions. By looking at the data for the carbon/aramid reinforced composites, it is seen that both friction and wear are largely unaffected by addition of PTFE and CuO nanoparticles, respectively. For composites without fiber reinforcement, addition of PTFE or nano-CuO results in a higher wear rate relative to EP, while friction is decreased by PTFE and slightly increased by nano-CuO. However, the positive effect of PTFE on friction seen for EP/PTFE is not found for CA/EP/PTFE and the negative effect of nano-CuO on wear seen for EP/CuO is not found for CA/EP/CuO. This indicates that the friction and wear behavior are largely controlled by the fibers and not the particles. The latter is in line with results reported for different polymers reinforced with unidirectional continuous fibers. Tough and wear resistant polymers such as PEEK and PA6,6 were clearly superior to EP in the unfilled state but showed roughly comparable wear rates in the fiber reinforced state [79]. The reason why PTFE has no effect on friction for CA/EP/PTFE might be due to the stiffness of the carbon fibers, which possibly act as a stiff micro-scale brush. If a PTFE containing third-body (or transfer film) is formed, it is likely to be disrupted or abraded by these stiff fibers.

Generally, it is seen that the use of CA reinforcement has a large positive impact on the wear behavior, relative to both EP and G/EP, and a more moderate impact on the frictional behavior. The influence of glass fiber reinforcement on the EP resin apparently depends on the applied *pv* condition. It is seen that friction measured for G/EP is slightly higher than for EP at both *pv* conditions. Furthermore, the level of μ is highest at the *pv* condition 0.50 MPa, 3.0 m/s for both composites. The higher hardness of G/EP due to the glass fibers might decrease A_r and thereby result in a decrease in μ, if all other parameters are uninfluenced. However, the abrasiveness of the glass fibers is expected to influence μ oppositely. With respect to wear, it is seen that the glass fibers deteriorate the wear resistance at the *pv* condition 0.25 MPa, 6.0 m/s, while giving rise to a slight improvement relative to EP at the other *pv* condition. This difference is attributed to the following factors. Firstly, the wear rate is relatively high for G/EP at 0.25 MPa, 6.0 m/s due to an especially abrasive behavior at this condition as discussed previously. The change in wear for the neat EP when shifting *pv* condition is due to severe decomposition observed at 0.50 MPa, 3.0 m/s. The latter is caused by a difference in the degree of frictional heating between the two *pv* conditions. This is clearly seen by comparing the frictional behavior for EP shown by curves (b) and (c) in figure 5.1. The measured disk temperatures for EP at 0.25 MPa, 6.0 m/s is on the same level as the temperatures measured for G/EP, which does not show severe decomposition at this condition. However, since the load is probably carried mainly by the more heat-resistant glass fibers, the resin is in this case less likely to be exposed to hot spots (or flash temperatures) leading to decomposition. As a consequence of this, complete failure due to decomposition is likely to occur for EP at milder *pv*

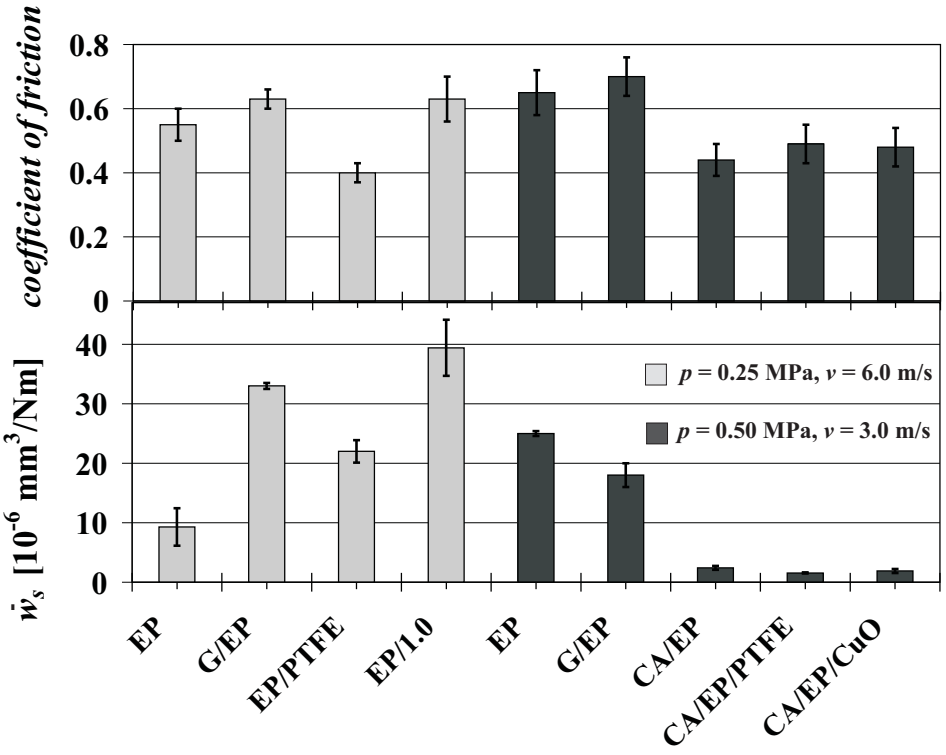

Figure 5.24. Specific wear rates $\dot{w}_s$ and coefficients of friction measured for different composites at two pv conditions. The data presented here for the carbon/aramid reinforced composites is obtained by sliding for a fixed interval of 23 h. The determined rates are averages for this time interval but not necessarily steady state wear rates.

conditions compared to the failure conditions for G/EP.

5.4.4 SEM images of the worn surfaces

In this section SEM images of worn surfaces of the fiber reinforced composites are shown. Generally, the presence of PTFE or nano-CuO particles do not give rise to any clear differences in the appearance of the worn surfaces of the fiber reinforced composites. Therefore, the emphasis is on discussing the difference in wear behavior for different fiber types and relating this to the significant difference in wear rates found for the two types of weave, cf. section 5.4.1. Figure 5.25 shows a worn surface of CA/EP/CuO with carbon fibers in the normal direction. It seems the first wear step is micro-cracking of the resin between the fibers. This results in resin removal, which leaves fiber ends exposed. Such exposed fiber ends, which are observed for both carbon and glass fibers, are brittle and fragile when they are no longer protected by the resin, and are therefore expected to be fractured and removed easily. These images are in agreement with a wear sequence proposed by Friedrich et al. [79], which suggests a repeating process starting with wear and removal of resin, and proceeding to fracture and removal of fiber fragments. In some of the resin-rich areas in figure 5.25(b), fiber ends are not evident which indicates that back-transfer of worn-off material to the composite surface is occurring.

According to the results given in figure 5.12, addition of nano-CuO to the EP resin leads to a major increase in wear rate. Micro-cracking of the resin with nano-CuO incorporated is therefore expected to occur at a higher rate for CA/EP/CuO compared to CA/EP. However, the wear rates are at roughly the same level for these two materials indicating that micro-cracking of the resin is not the rate controlling step.

Figure 5.26 shows glass fibers and aramid fibers, respectively, worn normal to the counterface. In the case of glass fibers, it seems as though the resin is worn out, or eroded, from between the fibers leaving the fiber ends exposed, which is visually similar to what is seen for the carbon fibers. The aramid fibers, on the other hand, are level with the resin. It seems as though the tough aramid fibers inhibit micro-cracking of the resin and thereby prevent exposure of fibers. Figure 5.27 shows glass fibers and aramid fibers, respectively, worn parallel to the counterface. This micrograph is interpreted to show that the glass fibers are initially worn thinner and then ultimately broken into smaller pieces, which are probably easily removed. The aramid fibers are, also in this case, level with the resin and worn in a tough manner seen by fibrillation of the fibers. With respect to carbon fibers parallel to the counterface, these are worn in a manner which visually resembles glass fibers. An example of this is found in figure 12 in appendix B. The wear mechanisms indicated by the SEM images presented here are in general agreement with related studies of similar materials [12, 29, 30].

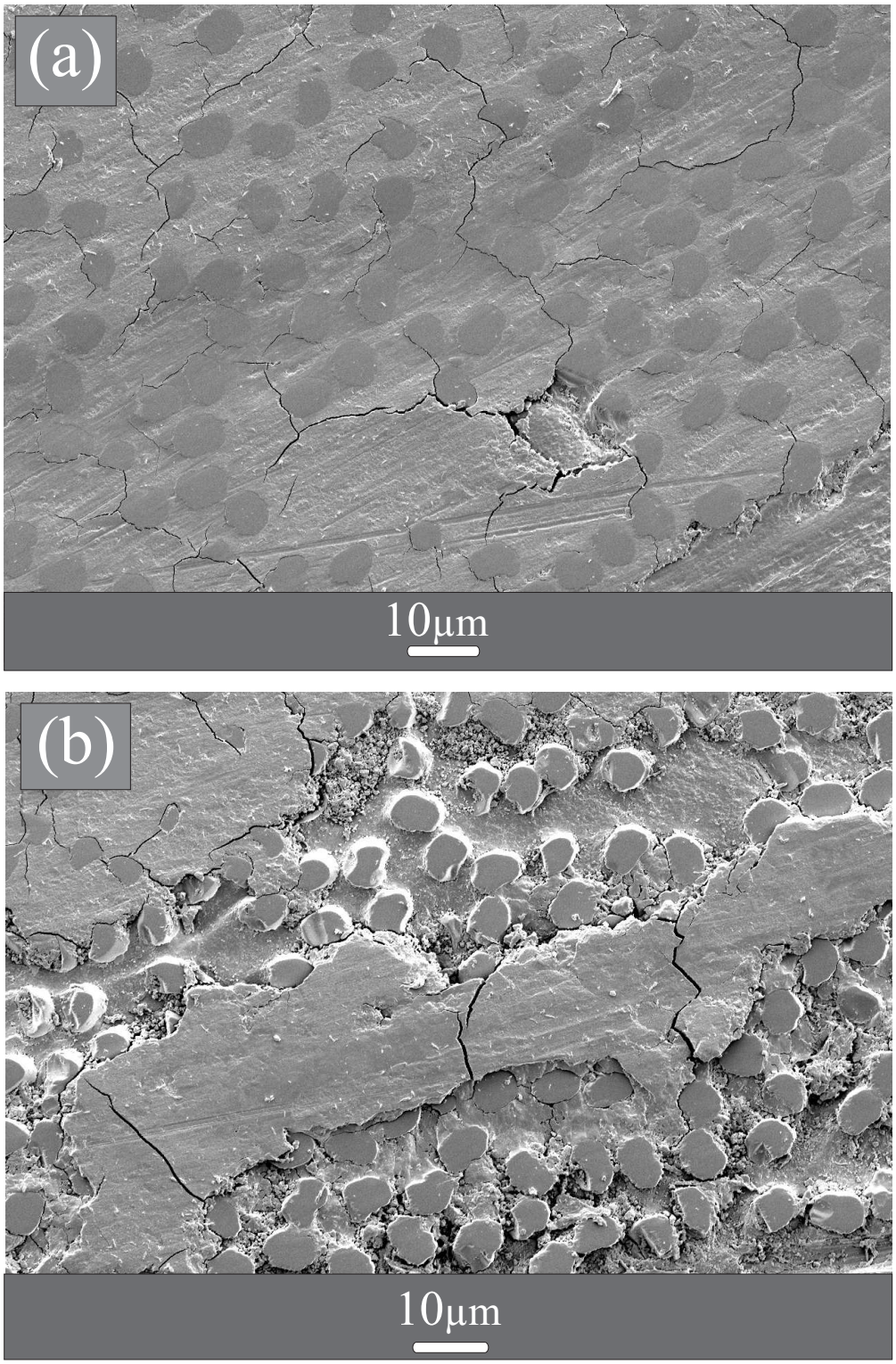

Figure 5.25. SEM images (a) and (b) show the surface of CA/EP/CuO worn at the *pv* condition: 0.50 MPa, 3.0 m/s. Carbon fibers worn normal to the counterface are seen. Both images show micro-cracking of resin but image (b) additionally shows exposed fiber ends.

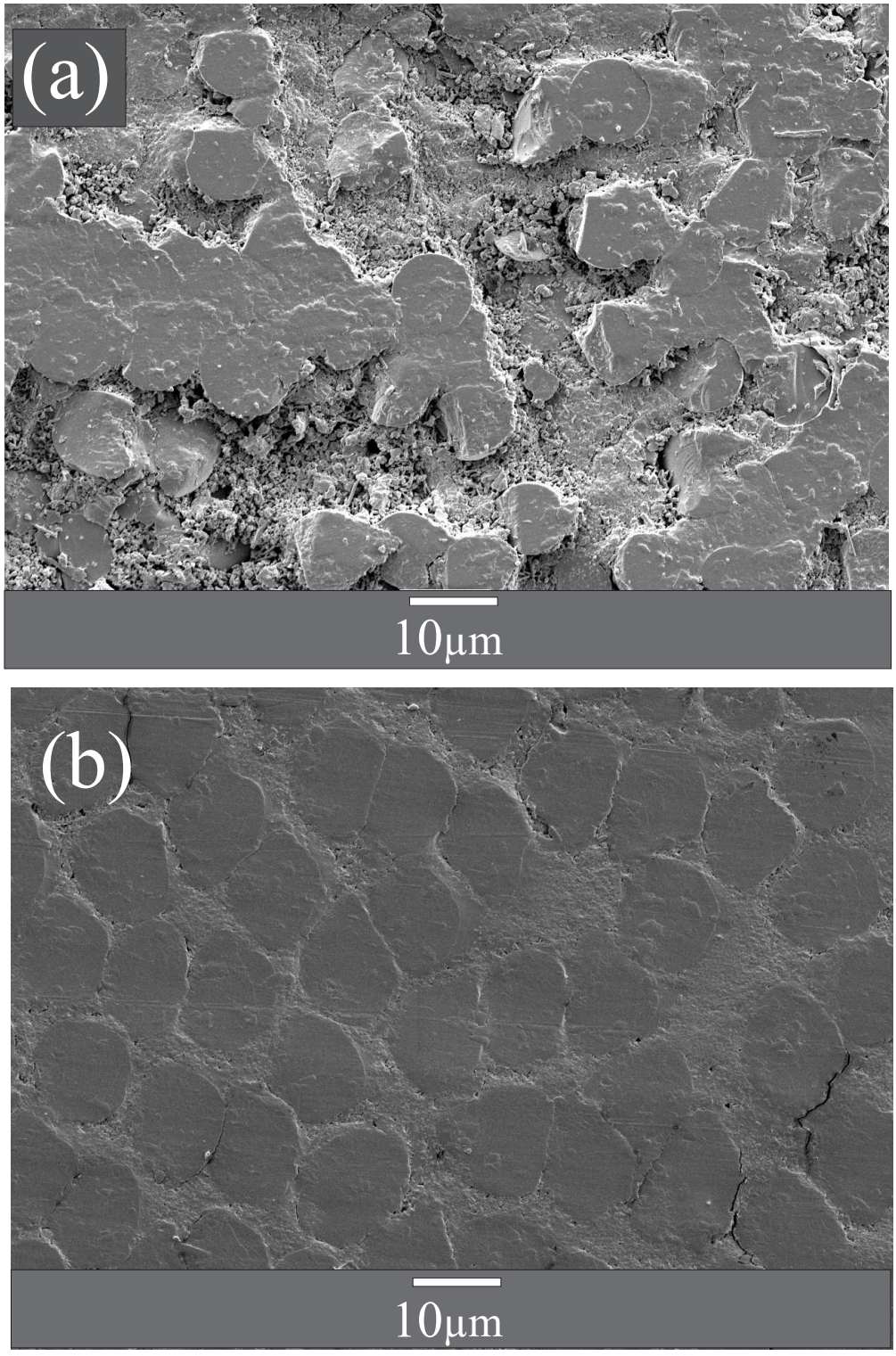

Figure 5.26. SEM image of (a) Glass fibers worn normal to the counterface in the case of G/EP (0.50 MPa, 3.0 m/s) and (b) Aramid fibers worn normal to the counterface in the case of CA/EP (1.0 MPa, 6.0 m/s).

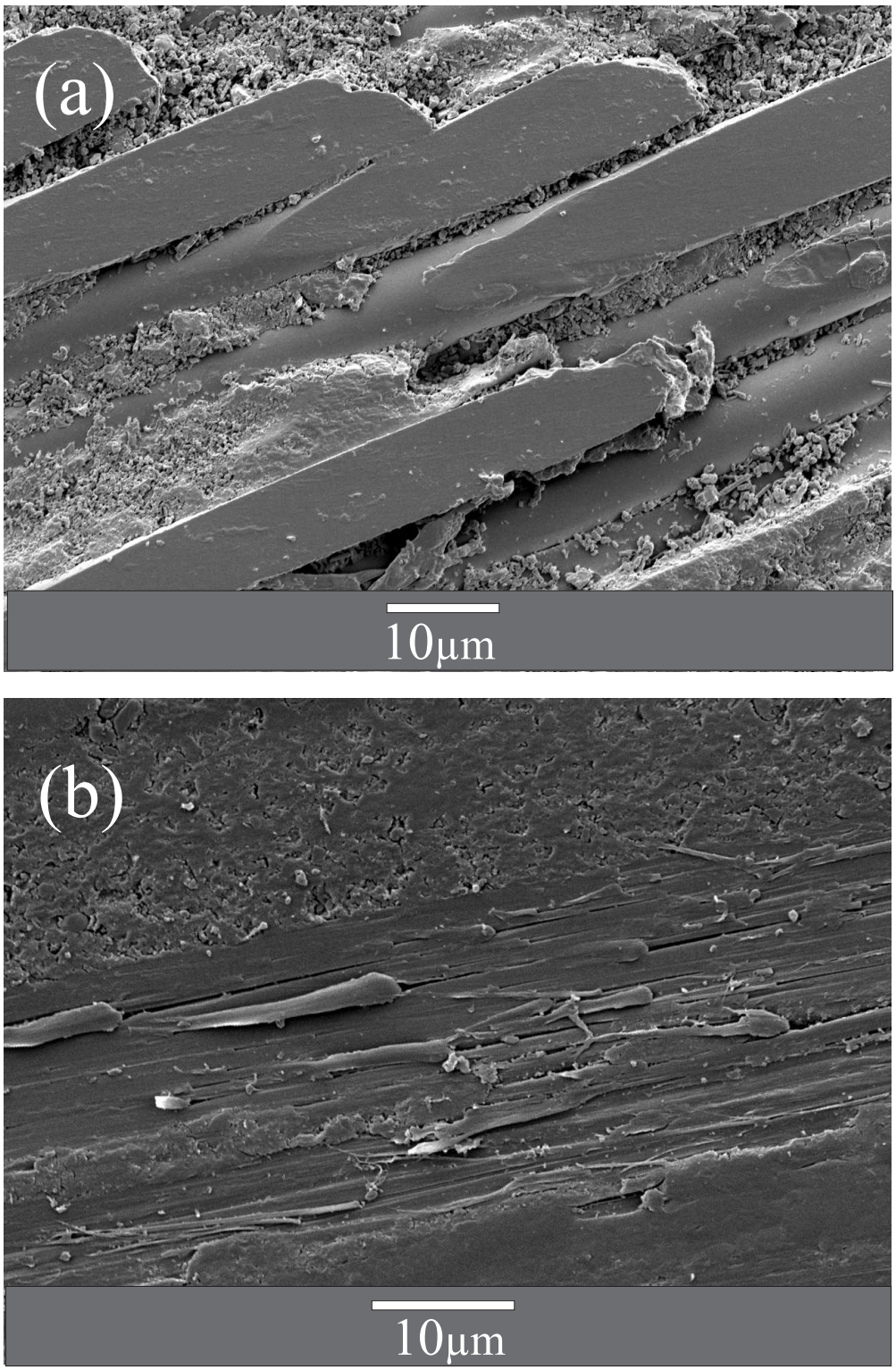

Figure 5.27. SEM image of (a) Glass fibers worn parallel to the counterface in the case of G/EP (0.50 MPa, 3.0 m/s) and (b) An aramid fiber worn parallel to the counterface in the case of CA/EP (0.50 MPa, 3.0 m/s).

Based on the observations discussed above, the significant difference in wear rates between G/EP and CA/EP might be explained as follows. The tough and non-abrasive aramid fibers prevent micro-cracking of the resin. These are therefore not exposed or fractured but instead worn by a fibrillation mechanism, which makes fiber removal more difficult. The carbon fibers are worn in a brittle manner, but they presumably also posses lubricating properties, which lowers friction and thereby also the interfacial temperature. The latter is expected to have a decreasing influence on the wear rate. On the other hand, the glass fibers in G/EP are both brittle and abrasive. During sliding, fractured glass fibers might result in third-body abrasive wear and roughening of the steel counterface. Both of these factors are expected to accelerate the wear rate.

5.4.5 Behavior at severe sliding conditions

This section discusses tribological behaviors observed at the three most severe *pv* conditions: (0.50 MPa, 3.0 m/s), (0.50 MPa, 6.0 m/s) and (1.0 MPa, 6.0 m/s). At these conditions, decomposition of the test-specimens caused by high interfacial temperatures is observed visually after testing. At the highest *pv* factor (6.0 MPa m/s) large-scale cracks, matrix/fiber debonding and depletion of decomposed resin are observed for both kind of weaves. Examples of this are shown in figure 5 in appendix A. Thus, there seems to be a transition from localized small-scale damage at mild *pv* conditions to large-scale damage at more severe *pv* conditions. This large-scale damage, or cracks, can potentially grow from the sliding surface and thereby cause failure of an entire component.

In the case of CA/EP, no steady state levels of friction or wear are obtained at the three most severe *pv* conditions. Figure 5.28 shows examples of frictional behavior for different composites. Firstly, good agreement is seen between measured frictional forces and corresponding temperatures as should be expected. Secondly, G/EP reaches a steady state level (d) while all the composites with carbon/aramid reinforcement (a) to (c) show a gradual increase in frictional force as a function of time and never reach steady state. This difference in behavior for the two types of weave is seen for all measurements conducted at these conditions. The same also applies when the composites are measured in the P-AP orientation. This increase in frictional force seems to continue until the material basically falls apart due to decomposition.

The rate of frictional increase grows at increasingly severe sliding conditions. For G/EP, the response to increasingly severe conditions is instead an increasing fluctuation of the frictional force around a relatively steady average level, cf. curve (a) in figure 5.1. The latter is probably due to decomposition, which generally is observed to some extent for all composites tested at these conditions. The behavior shown in figure 5.28 for the carbon/aramid composites is regarded as complete failure since the material

is not useful as a sliding partner at these conditions i.e. at *pv* factors of 3 and 6 MPa m/s. Based on this the limiting *pv* factor, cf. section 2.3.3, for CA/EP has a value of pv_{lim} = 3 MPa m/s, which is relatively low compared to some values previously reported for similar materials. However, such a comparison can not be made solely based on *pv* factors without also considering the corresponding interfacial temperatures as discussed in section 5.1.

It is believed that the increase in frictional force seen for the carbon/aramid reinforcement is caused by high and increasing interfacial temperatures. At the conditions in question the resin at the surface decomposes to some extent and therefore becomes brittle and fragile. The resin just below the surface is probably above the glass transition temperature and consequently becomes rubbery. When the neat resin (EP) is tested at conditions leading to severe decomposition, it wears at a fast rate and the frictional force fluctuates but does not show a gradual increase as a function of time, cf. curve (b) in figure 5.1. Thus, this phenomenon does not seem to be explained solely by decomposition and softening of the resin. A possible explanation, which considers the combined effect of resin and fibers, is given in the following. This gradual increase in frictional force is probably caused by a corresponding increase in the real area of contact (A_r). When

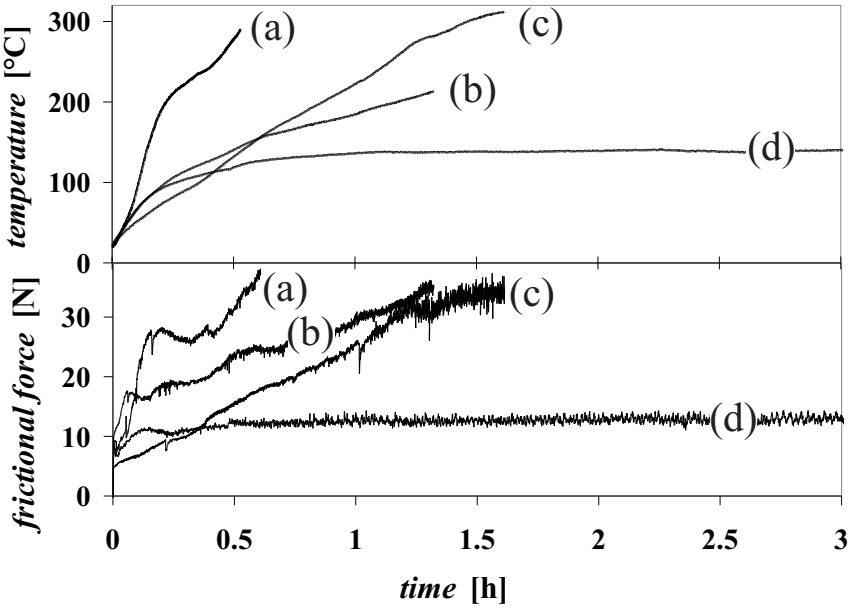

Figure 5.28. Frictional forces and corresponding interfacial temperatures measured as a function of time for different materials. (a) CA/EP/PTFE at the *pv* condition 1.0 MPa, 6.0 m/s, (b) CA/EP at the *pv* condition 1.0 MPa, 3.0 m/s, (c) CA/EP/CuO at the *pv* condition 0.50 MPa, 6.0 m/s and (d) G/EP at the *pv* condition 0.50 MPa, 6.0 m/s.

the resin decomposes and softens, it possibly no longer supports the fibers sufficiently to withstand the local pressures. Figure 5.29(a) shows exposed carbon fibers where the resin is removed due to decomposition. Such exposed carbon fibers are likely to buckle, kink and/or fracture due to high local pressures. Thus, the load carrying capacity is reduced, which may contribute to an increase in A_r. However, the same arguably applies for the glass fibers, which do not show a steady increase in frictional force. Therefore, this phenomenon is presumably closely related to the aramid fibers. Generally, these fibers have poor properties in compression and suffer from rapidly decreasing mechanical properties when temperatures are beyond 200°C [110, 111]. Because of this, the load is probably carried mainly by the carbon fibers especially at elevated temperatures. Consequently, the highest local temperatures are also expected to be in the vicinity of the carbon fibers, which might partly explain why removal of resin due to decomposition seems to occur mainly around these fibers. Figure 5.29(c) shows aramid fibers worn normal to the surface. The fibers are surrounded by resin and appear to be plastically deformed and also show abrasive wear tracks, which might be seen more clearly by comparison with a gently polished surface containing aramid fibers, cf. figure 5.29(b). Thus, it might be imagined that the aramid fibers soften and conform increasingly to the counterface as the temperature rises. This will increase A_r and thereby the frictional force, which in turn will increase the temperature and so forth.

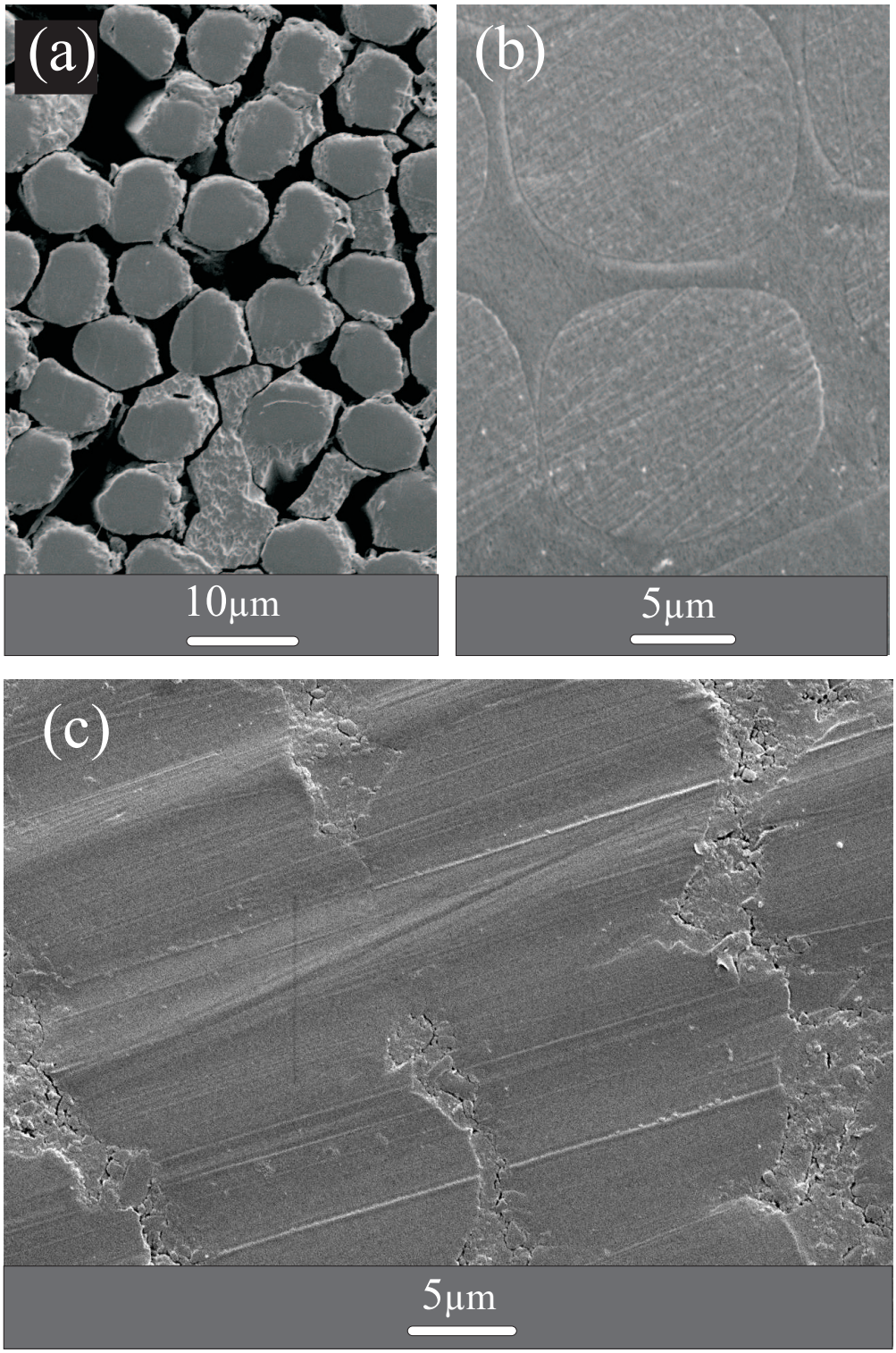

Figure 5.29. SEM images of (a) Carbon fibers worn normal to the surface, (b) A polished surface with aramid fibers in the normal orientation and (c) Aramid fibers worn normal to the surface.

6

Conclusions

In this Ph.D. study, polymer-matrix-composites (PMCs) are produced for tribological studies by using an epoxy resin (EP) as matrix, and reinforcing it by either a glass fiber weave or a carbon/aramid hybrid weave. Furthermore, the effect of incorporating CuO nanoparticles and PTFE microparticles is investigated. The influence of the mentioned components is examined both individually and in combination. The tribological properties of the produced PMCs are measured by using a Pin-On-Disk (POD) apparatus, which is designed and built as a part of this project.

Pin-On-Disk method

A POD apparatus based on a simple design and on a modest budget of about 8000 US dollars is built. This apparatus is successfully applied to collect coefficients of friction (μ), wear rates and counterface temperatures. Reproducible steady state levels of these parameters are generally obtained. In all cases, agreement is seen between the frictional profiles and corresponding temperature profiles, which shows that the measured counterface temperatures are in fact controlled by the frictional process. Furthermore, a linear relationship is found between measured steady state counterface temperatures and the rates of energy dissipation. The slope of the linear trend line is suggested by the author to be an important system specific property to consider when comparing measurements obtained on different Pin-On-Disk apparatuses. The steel disks applied in this study are relatively massive and have a high capacity for heat absorption. Consequently, the counterface temperatures measured in this study at certain pv conditions are relatively high compared to other related studies. This is probably why thermal effects play such a large role in the data presented here even though the applied pv conditions are relatively moderate.

PMCs without fibrous reinforcement

Different amounts of CuO nanoparticles are incorporated into both the neat EP and into EP resin containing PTFE microparticles. The content of CuO is varied in the range of 0 to 10 vol% while the PTFE content is fixed at 7.5 vol%. According to electron microscopy images, both nano-CuO and PTFE particles are relatively well-dispersed in the EP resin. Differential scanning calorimetry and Vickers hardness measurements show

no clear changes in glass transition temperature or hardness as a function of the nano-CuO content. However, both parameters are reduced when PTFE is added. Friction and wear data collected at a low pressure - high velocity (pv) condition shows the following. Without PTFE, the wear rates increase when nano-CuO is added to the neat EP resin at all concentrations. The elevated wear rates are correlated with the appearance of larger-scale cracks on the worn surfaces. This leads to the conclusion that addition of nano-CuO possibly reduces the fracture strength of the resin. Friction is roughly independant of the nano-CuO content. When PTFE is added to the neat EP, wear increases by a factor of 2.5 while friction is reduced by about 35%. Addition of nano-CuO together with PTFE leads to a slight decrease in friction and wear up to a CuO content of 0.4 vol% after which both parameters increase. This increase is attributed to an accumulation of nano-CuO in the interface, which disrupts the friction lowering effect of PTFE. The measurements are repeated for some of the PMCs using a smoother counterface. This gives rise to significantly less wear, which for PMCs without PTFE is attributed to formation of a protective transfer film. Also in this case, addition of nano-CuO to the neat EP increases wear for all tested composites. Friction and wear data is also collected at a high p - low v condition. It is found that PMCs without PTFE generally show exceedingly high and fluctuating wear rates relative to PMCs with PTFE incorporated. The reduction in friction and hence frictional heating due to PTFE make the PMCs useful at more severe sliding conditions since thermal enhancement of wear rates is suppressed. Furthermore, a positive synergistic effect of adding PTFE together with a small amount of nano-CuO is seen.

Fiber reinforced PMCs

The friction and wear behavior of the EP resin reinforced by either a glass fiber (G/EP) or a carbon/aramid hybrid weave (CA/EP) are examined at nine different pv conditions. The following conclusions are drawn. An average decrease in friction of approximately 35% is found by substituting glass fibers with carbon and aramid fibers. Although there are a few exceptions, μ is roughly independent of p and v. The average level of wear rates for G/EP at the six mildest pv conditions is a factor of 22 higher than for CA/EP, which is mainly attributed to the abrasivness of glass fibers opposed to the toughness and lubricating ability of aramid and carbon fibers, respectively.

It is found that the measured depth wear rates ($\dot{w}_t$) for G/EP and CA/EP increase gradually as a function of p and v as expected. However, $\dot{w}_t$ increases more rapidly as a function of these two parameters than predicted by theory. This deviation is believed to be caused mainly by a temperature induced deterioration of material properties with increasingly severe pv conditions. At the three most severe pv conditions

the tested PMCs all show signs of decomposition. The composites with carbon/aramid reinforcement show a gradual increase in friction and interfacial temperature as a function of time, which leads to severe decomposition and ultimately failure. This behavior is probably due to softening and degradation of the resin leading to fracture and softening of carbon and aramid fibers, respectively. The glass fiber reinforced composite does not show this phenomenon but has a relatively steady behavior despite decomposition of the resin and development of large-scale cracks.

For G/EP, it is found beneficial if the fibers in the weave are oriented parallel and anti-parallel (P-AP) with respect to the sliding direction instead of normal and parallel (N-P). The difference between these fiber orientations becomes more pronounced at low p - high v conditions. At the pv condition: 0.25 MPa and 6.0 m/s, the wear rate is reduced by a factor of 2.6 by changing fiber orientation form N-P to P-AP.

Overall conclusions

Addition of PTFE results in the intended effect, that is, a reduction in friction and consequently also in frictional heating, which increases the limiting pv factor. Despite promising particle dispersions, no clear positive effects of adding inorganic nano-scale particles to EP are found in this study. The latter seems to be caused by deteriorated mechanical properties due to the presence of nano-CuO. It could be interesting to verify this by mechanical tests. This is, however, not explored further in this study since the resin is applied in a solvent-based form, which makes it difficult to produce larger specimens for mechanical tests without porosities. Other examples of reduced mechanical properties by nanoparticles are found in the literature. Despite this, improvements in wear resistance are frequently measured, because more effective transfer films are formed due to the nanoparticles. The latter is typically found for thermoplastics, which generally exhibit better film forming abilities than thermoset EP resins as applied here.

Generally, the carbon/aramid reinforcement proves to be superior relative to the glass fiber reinforcement, which is in agreement with other related studies. However, a negative effect of aramid fibers at high counterface temperatures is indicated by the peculiar frictional behavior seen at severe sliding conditions. The positive effect PTFE particles has on friction is not seen when PTFE is incorporated together with the carbon/aramid weave. This is possibly because the stiff carbon fibers act as a stiff micro-scale brush, which disrupts formation of a PTFE containing third-body or transfer film. The negative effect the CuO nanoparticles have on wear of the EP resin is not found when these are incorporated along with the carbon/aramid weave. This indicates that the friction and wear behavior are largely controlled by the fibers.

Bibliography

[1] E. Rabinowicz. *Friction and Wear of Materials - 2nd ed.* John Wiley and Sons, Inc., 1995.

[2] I. M. Hutchings. *Tribology: Friction and Wear of Engineering Materials.* Edward Arnold, 1992.

[3] G. W. Stachowiak and A. W. Batchelor. *Engineering Tribology.* Butterworth and Heinemann, 2001.

[4] S. W. Zhang. State-of-the-art of polymer tribology. *Tribology International*, 31:49–60, 1998.

[5] S. Bahadur and D. Gong. The action of fillers in the modification of the tribological behavior of polymers. *Wear*, 158:41–59, 1992.

[6] J. Bijwe, J. Indumathi, J. J. Rajesh, and M. Fahim. Friction and wear behaviour of polyetherimide composites in various wear modes. *Wear*, 249:715–726, 2001.

[7] Z. Zhang, C. Breidt, L. Chang, K. Haupert, and K. Friedrich. Enhancement of the wear resistance of epoxy: short carbon fibre, graphite, PTFE and nano-TiO_2. *Composites: Part A*, 35:1385–1392, 2004.

[8] M. H. Cho, S. Bahadur, and A. K. Pogosian. Friction and wear studies using Taguchi method on polyphenylene sulfide filled with a complex mixture of MoS_2, Al_2O_3 and other compounds. *Wear*, 258:1825–1835, 2005.

[9] J. A. Williams, J. H. Morris, and A. Ball. The effect of transfer layers on the surface contact and wear of carbon-graphite materials. *Tribology International*, 30:663–676, 1997.

[10] W. Brostow, P. Cassidy, H. Hagg, M. Jaklewitc, and P. E. Montemartini. Fluoropolymer addition to an epoxy: phase inversion and tribological properties. *Polymer*, 42:7971–7977, 2001.

[11] W. Hufenbach, K. Kunce, and J. Bijwe. Sliding wear behavior of PEEK-PTFE blends. *J. Synthetic Lubrication*, 20:227–240, 2003.

[12] K. Friedrich, R. Reinicke, and Z. Zhang. Wear of polymer composites. *Engineering Tribology part J*, 216:415–426, 2002.

[13] K. C. Ho and M. C. Jeng. Tribological characteristics of short glass fibre reinforced polycarbonate composites. *Wear*, 206:60–68, 1997.

[14] J. Bijwe, S. Awtade, and A. Ghosh. Influence of orientation and volume fraction of aramid fabric on abrasive wear performance of polyethersulfone composites. *Wear*, 260:401–411, 2006.

[15] O. Jacobs, R. Jaskulka, C. Yan, and W. Wu. On the effect of counterface material and aqueous environment on the sliding wear of various PEEK compounds. *Tribology Letters*, 18:359–372, 2005.

[16] A. M. Häger and K. Friedrich. Selected thermoplastic bearing materials for use at elevated temperatures. *Wear*, 162:649–655, 1993.

[17] H. H. Shim and O. K. Kwon. Effects of fiber orientation and humidity on friction and wear properties of graphite fiber composites. *Wear*, 157:141–149, 1992.

[18] F.-H. Su, Z.-Z. Zhang, F. Guo, K. Wang, and W.-M. Liu. Study on the friction and wear properties of the composites made of surface modified-Nomex fabrics. *Materials Science and Engineering A*, 416:126–133, 2006.

[19] Q. F. Guan, G. Y. Li, H. Y. Wang, and J. An. Friction-wear characteristics of carbon fiber reinforced friction material. *Journal of Materials Science*, 39:641–643, 2004.

[20] K. Friedrich, K. Váradi, T. Goda, and H Giertzsch. Finite element analysis of a polymer composite subjected to a sliding steel asperity, part II: Parallel and anti-parallel fibre orientations. *Journal of Materials Science*, 37:1575–1583, 2002.

[21] T. Goda, K. Váradi, K. Friedrich, and H. Giertzsch. Finite element analysis of a polymer composite subjected to a sliding steel asperity part I normal fibre orientation. *Journal of Materials Science*, 37:1575–1583, 2002.

[22] C.J. Schwarts and S. Bahadur. The role of filler deformability, filler-polymer bonding, and counterface material on the tribological behaviour of polyphenylene sulfide (PPS). *Wear*, 251:1532–1540, 2001.

[23] Q. Zhao and S. Bahadur. A study of the modification of the friction and wear behavior of polyphenylene sulfide by particulate Ag_2S and PbTe fillers. *Wear*, 217:62–72, 1998.

[24] M. H. Cho, S. Bahadur, and A. K. Pogosian. Observations on the effectiveness of some surface treatments of mineral particles and inorganic compounds from Armenia as the fillers in polyphenylene sulfide for tribological performance. *Tribology International*, 39:249–260, 2006.

[25] G. Zhang, S. Guessasma, H. Liao, C. Coddet, and J.-M. Bordes. Investigation of friction and wear behaviour of SiC-filled PEEK coating using artificial neural network. *Surface and Coatings Technology*, 200:2610–2617, 2006.

[26] S. Bahadur, D Gong, and J. W. Anderegg. Studies of worn surfaces and the transfer film formed in sliding by CuS-filled and carbon fiber-reinforced nylon against a steel surface. *Wear*, 181:227–235, 1995.

[27] S. Bahadur and C. Sunkara. Effect of transfer film structure, composition and bonding on the tribological behavior of polyphenylene sulfide filled with nano particles of TiO_2, ZnO, CuO and SiC. *Wear*, 258:1411–1421, 2005.

[28] S. Kalpakjian and S. R. Schmid. *Manufacturing Engineering and Technology*. Prentice Hall, 2001.

[29] M. Cirino, K. Friedrich, and R. B. Pipes. Evaluation of polymer composites for sliding and abrasive wear applications. *Composites*, 19:383–392, 1988.

[30] T. Tsukizoe and N. Ohmae. Friction and wear performance of unidirectionally oriented glass, carbon and stainless steel fiber-reinforced plastics. In Klaus Friedrich, editor, *Friction and Wear of Polymer Composites - Composite Materials Series volume 1*, pages 205–231. Elsevier, New York, 1986.

[31] K. Friedrich, O. Jacobs, M. Cirino, and G. Marom. Hybrid effects on sliding wear of polymer composites. In P. K. Rohatgi, P. J. Blau, and C. S. Yust, editors, *Tribology of Composite Materials*, pages 277–286. ASM International, Materials Park, Ohio, 1990.

[32] L. Chang, Z. Zhang, C. Breidt, and K. Friedrich. Tribological properties of epoxy nanocomposites I. enhancement of the wear resistance by nano-TiO_2 particles. *Wear*, 258:141–148, 2005.

[33] L. Chang and Z. Zhang. Tribological properties of epoxy nanocomposites part II. a combinative effect of short carbon fibre with nanotio_2. *Wear*, 260:869–878, 2006.

[34] S.-Q. Lai, T.-S. Li, X.-J. Liu, R.-G. Lv, and L. Yue. The tribological properties of PTFE with thermally treated nano-attapulgite. *Tribology International*, 39:541–547, 2006.

[35] Y. Wang, S. Lim, J. L. Luo, and Z. H. Xu. Tribological and corrosion behaviors of Al_2O_3/polymer nanocomposite coatings. *Wear*, 260:976–983, 2006.

[36] Praveen Bhabani, David L. Burris, Jason Action, Gregory W. Sawyer, Gregory C. Toney, Richard W. Siegel, and Linda S. Schadler. Effect of matrix morphology on the wear and friction behavior of alumina nanoparticle/poly(ethylene)terephthalate composites. *Wear*, 258:1437–1443, 2005.

[37] X. Shao, W. Liu, and Q. Xue. The tribological behavior of micrometer and nanometer TiO_2 particle-filled poly(phthalazine ether sulfone ketone) composites. *Journal of Applied Polymer Science*, 92:906–914, 2004.

[38] J.-C. Lin. Compression and wear behavior of composites filled with various nanoparticles. *Composites Part B: engineering*, 38:79–85, 2007.

[39] C. K. Huang. Filling and wear behaviors of micro-molded parts made with nanomaterials. *European Polymer Journal*, 42:2174–2184, 2006.

[40] Y. Chen, S. Zhou, H. Yang, G. Gu, and L. Wu. Preparation and characterization of nanocomposite polyurethane. *Colloid and Interface Science*, 279:370–378, 2004.

[41] S.-Q. Lai, L. Yue, T.-S. Li, and Z.-M. Hu. The friction and wear properties of polytetrafluoroethylene filled with ultrafine diamond. *Wear*, 260:462–468, 2006.

[42] G. W. Sawyer, K. D. Freudenberg, P. Bhimaraj, and L. S. Schadler. A study on the friction and wear behaviour of PTFE filled with alumina nanoparticles. *Wear*, 254:573–580, 2003.

[43] B. Wetzel, P. Rosso, F. Haupert, and K. Friedrich. Epoxy nanocomposites - fracture and toughening mechanisms. *Engineering Fracture Mechanics*, 73:2375–2398, 2006.

[44] B. J. Ash, J. Stone, D. F. Rogers, L. S. Schadler, R. W. Siegel, B. C. Benicewicz, and T. Apple. Investigation into thermal and mechanical behavior of PMMA/alumina nanocomposites. *Materials Research Society Symposium - Proceedings*, 661:2101–2106, 2001.

[45] G. Shi, M. Q. Zhang, M. Z. Rong, B. Wetzel, and K. Friedrich. Sliding wear behavior of epoxy containing nano-Al_2O_3 particles with different pretreatments. *Wear*, 256:1072–1081, 2004.

[46] G. Shi, M. Q. Zhang, M. Z. Rong, B. Wetzel, and K. Friedrich. Friction and wear of low nanometer Si_3N_4 filled epoxy composites. *Wear*, 254:784–796, 2003.

[47] M. Z. Rong, M. Q. Zhang, L. Hong, H. Zeng, B. Wetzel, and K. Friedrich. Microstructure and tribological behavior of polymeric

nanocomposites. *Industrial Lubrication and Tribology*, 53:72–77, 2001.

[48] T. Mahrholz, L. Herbeck, and U. Riedel. New high-performance fibre-reinforced nanocomposites. *JEC - Composites*, 9:71–75, 2004.

[49] B. Wetzel, F. Haupert, K. Friedrich, M. Q. Zhang, and M. Z. Rong. Impact and wear resistance of polymer nanocomposites at low filler content. *Polymer Engineering and Science*, 42:1919–1927, 2002.

[50] C. J. Schwarts and S. Bahadur. Studies on the tribological behavior and transfer film-counterface bond strength for polyphenylene sulfide filled with nanoscale alumina particles. *Wear*, 237:261–273, 2000.

[51] K. Friedrich, Z. Zhang, and A. K. Schlarb. Effects of various fillers on the sliding wear of polymer composites. *Composites Science and Technology*, 65:2329–2343, 2005.

[52] Q. Zhao and S. Bahadur. The mechanism of filler action and the criterion of filler selection for reducing wear. *Wear*, 225:660–668, 1999.

[53] S. Bahadur and V. K. Polinei. Tribological studies of glass fabric-reinforced polyamide composites filled with CuO and PTFE. *Wear*, 200:95–104, 1996.

[54] J. K. Lancaster. Friction and wear. In A. D. Jenkins, editor, *Polymer Science: A Material Science Hand Book*, pages 960–1043. North-Holland, New York, 1972.

[55] A. D. Sarkar. *Friction and Wear*. Academic Press Inc., London, 1980.

[56] J. A. Williams. *Engineering Tribology*. Oxford University Press, 1995.

[57] J. A. Greenwood and J. B. P. Williamson. Contact of nominally flat rough surfaces. *Proceedings of the Royal Society of London*, 295:300–319, 1966.

[58] J. F. Archard. Elastic deformation and the laws of friction. *Proceedings of the Royal Society of London*, 243:190, 1957.

[59] B. J. Briscoe. Interfacial friction of polymer composites. general fundamental principles. In Klaus Friedrich, editor, *Friction and Wear of Polymer Composites - Composite Materials Series volume 1*, pages 26–56. Elsevier, New York, 1986.

[60] S. Bahadur. The development of transfer layers and their role in polymer tribology. *Wear*, 245:92–99, 2000.

[61] W. Wieleba. The statistical correlation of the coefficient of friction and wear rate of PTFE composites with steel counterface roughness and hardness. *Wear*, 252:719–729, 2002.

[62] H. Czichos. Introduction to friction and wear. In Klaus Friedrich, editor, *Friction and Wear of Polymer Composites - Composite Materials Series volume 1*, pages 1–22. Elsevier, New York, 1986.

[63] D. C. Evans and J. K. Lancaster. Wear. In D. Scott, editor, *Treatise on Materials Science and Technology*, pages 85–139. Academic Press, 1979.

[64] J. F. Archard and W. Hirst. The wear of metals under unlubricated conditions. *Proceedings of the Royal Society of London*, 236:397–410, 1956.

[65] A. Mirsa and Finnie I. Some observations on two-body abrasive wear. *Wear*, 68:41–56, 1981.

[66] J. C. Jaeger. *J. and Proc. Roy. Soc. NSW*, 76:203, 1942.

[67] J. K. Lancaster. Transfer lubrication for high temperatures: A review. *Journal of Tribology*, 107:437–443, 1985.

[68] J. Halling. *Principles of tribology*. The MacMillian press LTD, 1975.

[69] H. Schönherr and J. Vancso. The mechanism of PTFE and PE friction deposition: a combined scanning electron and scanning force microscopy study on highly oriented polymeric sliders. *Polymer*, 39:5705–5709, 1998.

[70] M. Palabiyik and S. Bahadur. Mechanical and tribological properties of polyamide 6 and high density polyethylene polyblends with or without compatibilizer. *Wear*, 246:149–158, 2000.

[71] C. Z. Liu, J. Q. Wu, J. Q. Li, J. Tong, and Arnell A. D. Tribological behaviours of PA/UHMWPE blend under dry and lubricating condition. *Wear*, 260:109–115, 2006.

[72] J. Bijwe, S. Sen, and A. Ghosh. Influence of PEEK-PTFE blends on mechanical properties and tribo-performance in various wear modes. *Wear*, 258:1536–1542, 2005.

[73] N. L. McCook, D. L. Burris, G. R. Bourne, J. Steffens, J. R. Hanrahan, and W. G. Sawyer. Wear resistant solid lubricant coating made from PTFE and epoxy. *Tribology Letters*, 18:119–124, 2005.

[74] S. Bahadur, L. Zhang, and J. W. Anderegg. The effect of zinc and copper oxides and other zinc compounds as fillers on the tribological behavior of thermosetting polyester. *Wear*, 203:464–473, 1997.

[75] L. Yu and S. Bahadur. An investigation of the transfer film characteristics and the tribological behaviors of polyphenylene sulfide composites in sliding against tool steel. *Wear*, 214:245–251, 1998.

[76] L. Yu, S. Yang, W. Liu, Q. Xue, and S. Bahadur. Action of transfer film in improving friction and wear behaviors of iron- and copper-filled poly(ether ether ketone) composites. *Journal of Applied Polymer Science*, 76:179–184, 2000.

[77] J. Vande Vort and S. Bahadur. The growth and bonding of transfer film and the role of CuS and PTFE in the tribological behavior of PEEK. *Wear*, 181:212–221, 1995.

[78] K. S. Bhabani and J. Bijwe. Analysis of simultaneous influence of operating variables on abrasive wear of phenolic composites. *Wear*, 253:787–794, 2002.

[79] K. Friedrich and P. Reinicke. Friction and wear of polymer-based composites. *Mechanics of Composite Materials*, 34:503–514, 1998.

[80] K. Friedrich, Z. Lu, and A. M. Häger. Recent advances in polymer composites' tribology. *Wear*, 190:139–144, 1995.

[81] K. Friedrich, Z. Lu, and A. M. Häger. Overview on polymer composites for friction and wear applications. *Theoretical and Applied Fracture Mechanics*, 19:1–11, 1993.

[82] J. Bijwe and U. S. Tewari. Friction and wear studies of polyetheramide composites. *Wear*, 138:61–76, 1990.

[83] R. Reinicke, F. Haupert, and K. Friedrich. On the tribological behaviour of selected, injection moulded thermoplastic composites. *Composites Part A*, 29:763–771, 1998.

[84] A. Bolvari, S. Glenn, R. Janssen, and C. Ellis. Wear and friction of aramid fiber and polytetrafluoroethylene filled composites. *Wear*, 203:697–702, 1997.

[85] O. Jacobs, R. Jaskulka, F. Yang, and W. Wu. Sliding wear of epoxy compounds against different counterparts under dry and aqueous conditions. *Wear*, 256:9–15, 2004.

[86] A. P. Harsha and U. S. Tewari. Tribo performance of polyaryletherketone composites. *Polymer Testing*, 21:697–709, 2001.

[87] J. J. Rajesh, J. Bijwe, and U. S. Tewari. Influence of fillers on abrasive wear of short glass fibre reinforced polyamide composites. *Journal of Materials Science*, 36:351–356, 2001.

[88] J. Bijwe, V. Naidu, N. Bhatnagar, and M. Fahim. Optimum concentration of reinforcement and solid lubricant in polyamide 12 composites for best tribo-performance in two wear modes. *Tribology Letters*, 21:59–66, 2006.

[89] K. Friedrich. Wear of reinforced polymers by different abrasive counterparts. In Klaus Friedrich, editor, *Friction and Wear of Polymer Composites - Composite Materials Series volume 1*, pages 233–285. Elsevier, New York, 1986.

[90] M. N. Gardos and B. D. MacConnell. Development of a high-load-temperature self-lubricating composite, part i-iv. *ASLE Prepre. 81-3A-3 81-3A-6*, 1981.

[91] L.-Y. Zheng, L.-X. Zhao, J.-J. Zhang, and J.-M. Wang. Friction and wear properties of three-dimensionally braided carbon fabric-reinforced nylon composites. *Carbon*, 44:158–193, 2006.

[92] Y. Z. Wan, H. L. Luo, Y. L. Wang, S. Raman, Y. Huang, T. L. Zhang, and H. Liu. Characterization of three-dimensional braided polyethylene fiber-PMMA composites and influence of fiber surface treatment. *Journal of Applied Polymer Science*, 99:949–956, 2006.

[93] B. Suresha and G. Chandramohan. Friction and wear characteristics of carbon-epoxy and glass-epoxy woven roving fiber composites. *Journal of Reinforced Plastics and Composites*, 25:771–782, 2006.

[94] J. Bijwe, J. Indumathi, and A. K. Ghosh. On the abrasive wear behaviour of fabric-reinforced polyetherimide composites. *Wear*, 253:768–777, 2002.

[95] J. Bijwe, S. Awtade, B. K. Satapathy, and A. Ghosh. Influence of concentration of aramid fabric on abrasive wear performance of polyethersulfone composites. *Tribology Letters*, 17:187–194, 2004.

[96] B. S. Tripathy and M. J. Furey. Study of the tribological behavior of unidirectional fiber-reinforced graphite-epoxy composites. In P. K. Rohatgi, editor, *Friction and Wear of Technology for Advanced Composite Materials*, pages 131–141. ASM International, Materials Park, Ohio, 1993.

[97] F.-H. Su, Z.-Z. Zhang, F. Guo, K. Wang, and W.-M. Liu. Effects of solid lubricants on the friction and wear properties of Nomex fabric composites. *Materials Science and Engineering A*, 424:333–339, 2006.

[98] M. García, de M. Rooij, L. Winnubst, W. E. van Zyl, and H. Verweij. Friction and wear studies on nylon-6/SiO_2 nanocomposites. *Journal of Applied Polymer Science*, 92:1855–1862, 2004.

[99] Fei Li, K. Hu, Jian Lin Li, and Bin Yuan Zhao. The friction and wear characteristics of nanometer ZnO filled polytetrafluoroethylene. *Wear*, 249:877–882, 2002.

[100] M. Z. Rong, M. Q. Zhang, G. Shi, Q. L. Ji, B. Wetzel, and K. Friedrich. Graft polymerization onto inorganic nanoparticles and its effect on tribological performance improvement of polymer composites. *Tribology International*, 36:697–707, 2003.

[101] M. Q. Zhang, M. Z. Rong, S. L. Yu, B. Wetzel, and K. Friedrich. Effect of particle surface treatment on the tribological performance of epoxy based nanocomposites. *Wear*, 253:1086–1093, 2002.

[102] Q. L. Ji, M. Q. Zhang, M. Z. Rong, B. Wetzel, and K. Friedrich. Friction and wear of epoxy composites containing surface modified SiC nanoparticles. *Tribology Letters*, 20:115–123, 2005.

[103] Q. Wang, Q. Xue, H. Liu, W. Schen, and J. Xu. The effect of particle size of nanometer ZrO_2 on the tribological behaviour of PEEK. *Wear*, 198:216–219, 1996.

[104] G. Xian, R. Walter, and F. Haupert. Tribological behaviour of polymeric coatings. part i. aramid particle-reinforced epoxy nanocomposite systems. *J. Synthetic Lubrication*, 21:270–285, 2005.

[105] L. Chang, Z. Zhang, H. Zhang, and K. Friedrich. Effect of nanoparticles on the tribological behaviour of short carbon fibre reinforced poly(etherimide) composites. *Tribology International*, 38:966–8, 2005.

[106] Z. Zhang, C. Breidt, L. Chang, and K. Friedrich. Wear of PEEK composites related to their mechanical performances. *Tribology International*, 37:271–277, 2004.

[107] F.-H. Su, Z.-Z. Zhang, and W.-M. Liu. Mechanical and tribological properties of carbon fabric composites filled with several nanoparticulates. *Wear*, 260:861–868, 2006.

[108] S. Ahmed and F. R. Jones. A review of particulate reinforcement theories for polymer composites. *Journal of Materials Science*, 25:4933–4942, 1990.

[109] J. Spanoudakis and R. J. Young. Crack propagation in a glass particle-filled epoxy resin. *Journal of Materials Science*, 19:487–496, 1984.

[110] K. Potter. *An Introduction to Composite Products.* Chapman & Hall, 2-6 Boundary Row, London, UK, 1997.

[111] W. D. Callister. *Materials Science and Engineering an Introduction - sixth edition.* John Wiley and Sons, Inc., 2003.

Appendices

Available online at www.sciencedirect.com
ScienceDirect
Wear 262 (2007) 1013–1020
WEAR
www.elsevier.com/locate/wear

Comparison of friction and wear for an epoxy resin reinforced by a glass or a carbon/aramid hybrid weave

Thomas Ø. Larsen [a], Tom L. Andersen [b], Bent Thorning [c], Andy Horsewell [d], Martin E. Vigild [a,*]

[a] *Danish Polymer Centre, Department of Chemical Engineering, Technical University of Denmark, DK-2800 Kgs. Lyngby, Denmark*
[b] *Risø National Laboratory, Materials Research Department, DK-4000 Roskilde, Denmark*
[c] *Elektro-Isola A/S, Grønlandsvej 197, DK-7100 Vejle, Denmark*
[d] *Department of Manufacturing Engineering and Management, Technical University of Denmark, DK-2800 Kgs. Lyngby, Denmark*

Received 8 March 2006; received in revised form 9 October 2006; accepted 17 October 2006
Available online 28 November 2006

Abstract

Friction and wear properties of an epoxy resin (EP) reinforced by either a glass fiber weave (G/EP) or a carbon/aramid hybrid weave (CA/EP) are reported. The tribological data is collected using a custom-made Pin-On-Disk apparatus which measures wear rates ($\dot{w}$), coefficients of friction (μ) and disk temperatures. The composites are worn by dry-sliding against smooth steel counterfaces under ambient conditions. Tests are performed at nine different combinations of contact pressure (p) and sliding velocity (v) also referred to as pv conditions. The purpose is to systematically compare the performance of the differently reinforced materials while going from mild to rougher sliding conditions. It is found that μ on average is reduced by 35% by substituting the glass fiber weave with the carbon/aramid weave. The coefficient of friction furthermore seems to be roughly independent of p and v. CA/EP shows superior wear behavior at the six mildest pv conditions with the wear rate an average factor of 22 lower than the G/EP rates. At the three roughest pv conditions CA/EP shows complete failure, while G/EP shows a relatively steady tribological behavior despite decomposition and development of larger-scale cracks.

Keywords: Friction; Wear; Fiber reinforced epoxy-matrix composites; Pin-On-Disk; pv conditions

1. Introduction

Polymer matrix composites (PMC) are a class of materials which is used increasingly in applications where friction and wear are important parameters. Examples range from gears, seals and rollers to bearings, brakes and artificial joints. PMCs are often preferred over other materials because of their easy processability, high strength-to-density ratio and chemical resistance. Furthermore, PMCs generally have a low coefficient of friction (μ) even under dry-sliding conditions. This property can be utilized in applications where the addition of lubricants such as oil or grease cannot be tolerated [1–8].

Despite the increasing use of PMCs, the knowledge of their tribological behavior is limited and lacks predictability. Consequently, estimation of tribological properties based on known composite structures and system parameters is often a difficult task. Thus, there is a need for a better understanding of how and why different types of reinforcement and compositions influence the tribological properties at different conditions.

In this study PMCs based on an epoxy resin are tested. Epoxy resins do not generally exhibit good tribological properties due to the cross-linked molecular structure, which inhibits the formation of an efficient transfer film and results in a relatively high degree of brittleness. However, epoxy resins possess other favorable properties such as strong adhesion to many materials, good mechanical and electrical properties, relatively high chemical and thermal resistance [9], and a low price compared to advanced polymers such as polyetheretherketone (PEEK) and polyimide (PI). From this perspective, it is an attractive goal to obtain an epoxy-based composite with excellent tribological properties by incorporating the right kind of components,

* Corresponding author. Present address: Danish Polymer Centre, Department of Chemical Engineering, Technical University of Denmark, Building 423, DK-2800 Kgs. Lyngby, Denmark. Tel.: +45 45252967; fax: +45 45882161.
E-mail address: mev@kt.dtu.dk (M.E. Vigild).

0043-1648/$ – see front matter © 2006 Elsevier B.V. All rights reserved.
doi:10.1016/j.wear.2006.10.004

e.g. fibers or particles. Fibrous reinforcements such as glass, carbon and aramid are widely used to obtain materials with excellent mechanical properties. For certain applications the combination of both good mechanical and tribological properties are required. Others have for unidirectional oriented fiber composites demonstrated the general superiority of continuous carbon and aramid fibers compared to glass fibers when sliding against smooth steel [10,11]. In this study, the friction and wear behavior of two types of bidirectional fibrous reinforcement are examined namely in the form of a plain glass fiber weave and a carbon/aramid hybrid weave. The tribological comparison between different PMCs are often conducted at only one or a few combinations of contact pressure (p) and sliding velocity (v) referred to as pv conditions. Here, tests are performed at nine different pv conditions in order to systematically examine and compare the performance of these two materials as they are exposed to increasingly rougher conditions. The latter is particularly interesting since the applicability of PMCs in applications involving high sliding speeds and/or high environmental temperatures is limited due to their inferior thermo resistant properties compared to metals and ceramics. Thus, expanded knowledge of temperature related failure modes are desirable from the perspective of producing PMCs for extreme applications.

The tribological data are obtained using a custom-made tribotester of the Pin-On-Disk type. Measurements are performed under dry-sliding conditions against smooth steel surfaces at ambient temperature and humidity.

2. Experimental

2.1. Composite and test-pin preparation

The examined glass fiber composite (G/EP) is produced by Elektro-Isola A/S and is commercially available (G-Etronax EP 11). This material is not intended for use in dry-sliding applications but is used as a reference material in this context. The carbon/aramid composite (CA/EP) is produced for the purpose of this study. Both materials are produced using the same production method and the same type of resin, which is a polyfunctional epoxy of the novolac type obtained from Hexion Specialty Chemicals as a 70 wt% solution in methyl ethyl ketone (Epikote 1153-B-70). The reinforcement used in G/EP is a plain glass fiber weave (international style 7637, style number 02022, finish FE130). The reinforcement used in CA/EP is a carbon/aramid hybrid weave obtained from Hexcel Fabrics S.A. The weave (style 73210) is a twill 2 × 2 with carbon fibers (type 3K HR) and aramid fibers (type Ar HM 1270) both oriented in warp as well as weft with the same ratio (61 vol.% aramid/39 vol.% carbon) in both directions.

By using prepreg technology, composite plates are produced in the following way. A certain amount of resin solution is added quantitatively to a square of weave and distributed by applying a roller. The impregnated weaves are subsequently placed in an oven with air circulation (typically 15 min at 120 °C) in order to evaporate the solvent and partially cure the resin. A number of partially cured sheets are then stacked, in order to obtain a laminate thickness of at least 5 mm, and pressed for 3 h applying a pressure of 35 bar and a temperature of 160 °C. Finally, the plates are post-cured for 2 h in an oven at 170 °C. Data characterizing the tested composites are given in Table 1. The composite test-pins for tribological evaluation are obtained by reducing the plate thickness to 5.0 mm by milling, and then using a diamond saw to obtain the final dimensions of height 15 mm and cross-section 7.7 mm × 5.0 mm resulting in an apparent area of contact of 38.5 mm^2. After machining, the pins are dried in an oven for 20 h at 50 °C and subsequently stored in a sealed bag at room temperature.

Table 1
Measured material properties of G/EP and CA/EP

Material	Density (g/cm^3)	Fiber content (vol.%)	T_g (°C)
G/EP	1.83	44	152
CA/EP	1.35	44	133

Here, T_g is glass transition temperature.

2.2. Pin-On-Disk measurements

The applied Pin-On-Disk (POD) apparatus has been described in detail elsewhere [12], but the main principle is sketched in Fig. 1 and summarized in the following: a composite pin is loaded perpendicularly against a rotating disk made of hardened chrome bearing steel (100 Cr6) by applying dead weights (W_N). The test-pin is mounted in a lever-arm via a sample holder. The lever-arm can rotate freely by use of ball bearings but is kept in a fixed position by a load cell which measures the frictional force. Furthermore, a non-contact thermometer estimates the interfacial temperature by collecting infrared radiation from the side of the steel disk. The employed test-procedure is given below:

- The steel counterface is abraded using a piece of emery cloth (grade P400), which gives an initial surface roughness of $R_a = 0.26\,(\pm 0.03)$ μm.
- While mounted in the POD lever-arm, the composite pin is abraded against a piece of emery cloth (grade P400) located on the steel disk in order to obtain conformity between the pin and the counterface.
- Loose debris is removed from the pin and the counterface by blowing with air.

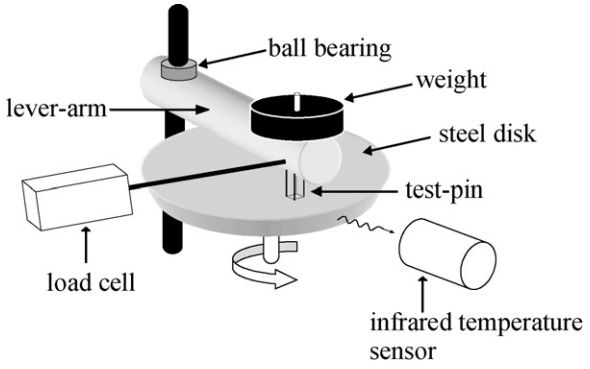

Fig. 1. Sketch of POD apparatus.

- The surfaces of the two sliding partners are cleaned by wiping with paper soaked in acetone followed by blowing with air to evaporate any excess of solvent.
- The weight of the pin plus the sample holder is noted to the nearest 0.1 mg.
- During testing the frictional force and the temperature of the steel disk is recorded by a computer.
- After testing the pin and sample holder is cleaned as previously and weighed again.

It is possible to reinsert the pin and sample holder in the lever-arm and continue the test-run in order to determine how the accumulated weight loss evolves as a function of time. This can reveal whether the accumulated weight loss is simply a linear function of time or showing a more complicated behavior. Wear curves frequently show a running-in period with an initial high wear rate followed by a lower steady state wear rate. This transition from high to lower wear is typically due to modification of the sliding surfaces and development of transfer films.

For G/EP, a linear relationship is found between accumulated weight loss and time without any detectable running-in period in relation to wear. In these cases, the experiments span over 2–24 h depending on the pv condition. The wear rate is determined based on the initial and final weight of the test specimen. CA/EP has a significantly lower wear rate than G/EP and furthermore shows a running-in phenomenon with an initially high wear rate, which decreases and ultimately reaches a steady level. In these cases, the accumulated weight loss is measured as a function of time for periods of 115–200 h. The slope of the approximately linear part of the curve is then used for calculation of the wear rate. The coefficient of friction μ is reported as a time-averaged value based on data points in the steady state regime. As a minimum the composites are measured twice at each pv condition.

The test specimens are placed relative to the sliding direction in such a way that the layers in the laminates are normal to the steel disk and parallel to the sliding direction. This means that some fibers are oriented normal to the steel disk while others are parallel to both the steel disk and the sliding direction. The composites are worn in the weft direction.

2.3. Scanning electron microscopy

Scanning electron microscopy (SEM) is used to study the worn surfaces. The samples are prepared by removing loose debris by compressed air followed by cleaning with acetone and finally coating with a conducting gold layer. The images are obtained by using a microscope of the type JEOL JSM 5900 equipped with a LaB_6 filament. Images are obtained in the secondary electron imaging mode using a conventional E-T detector.

3. Theoretical considerations

During wear experiments it is frequently found that the volume, or mass, of lost material is proportional to the normal load (W_N) and the sliding distance (l), respectively. That this should be the case can also be shown theoretically, for instance, from simple models for abrasive and adhesive wear [13,14], or by assuming that the wear rate is proportional to the rate of energy dissipation in the interface [15]. The specific rate of energy dissipation ($\dot{Q}_d$) is given by Eq. (1) and is simply the rate of energy dissipation per unit apparent contact area:

$$\dot{Q}_d = \mu p v \,(\mathrm{J/m^2\,s}) \tag{1}$$

Here, μ, p and v are coefficient of friction, contact pressure and sliding velocity, respectively. Based on the relations mentioned above, a depth wear rate ($\dot{w}_t$) can be derived:

$$\dot{w}_t = \frac{\Delta h}{t} = k^* p v \,(\mu\mathrm{m/h}) \tag{2}$$

Here, Δh, t and k^* are height reduction of the worn component, time and the wear factor, respectively. Note, that $\dot{w}_t$ is directly proportional to the pv factor as long as k^* is a constant. The latter depends on both material properties and system properties. Thus, if the system properties are fixed, k^* can to some extent be regarded as a material property. The wear factor is also referred to as the specific wear rate ($\dot{w}_s$), which conveniently can be calculated from measured quantities:

$$\dot{w}_s = \frac{\Delta m}{l \rho W_N} \,(\mathrm{mm^3/N\,m}) \tag{3}$$

Here, l, W_N, Δm and ρ are sliding distance, load, mass loss and density of the worn material, respectively.

Eq. (2) does not take temperature increases in the interfacial zone into consideration. However, Eq. (1) shows that the dissipated energy, hence the temperature in the interfacial zone will rise with increasing pv factors. The interfacial temperature furthermore depends on the thermal conductivities of the sliding partners, the ambient temperature and on the real area of contact [13,14]. Generally, Eq. (2) applies inside a certain range of moderate pv factors. However, if either v and/or p exceeds a certain level, a change in wear mechanism might occur due to, e.g. thermal softening and decomposition of the material. The

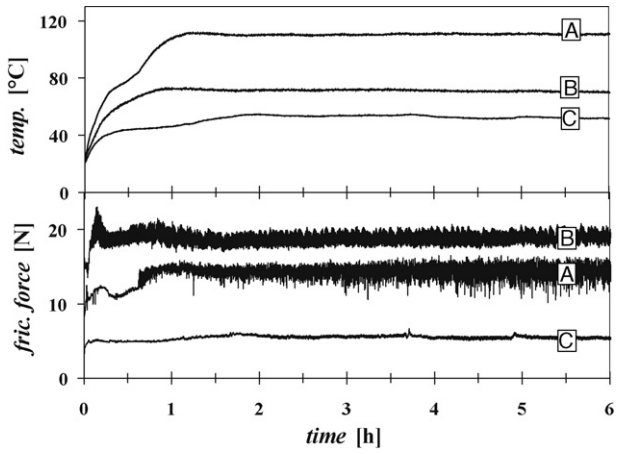

Fig. 2. Three examples of measured temperatures and frictional forces, respectively, as a function of time. The test specimen is in all cases G/EP. (A), (B) and (C) correspond to the pv conditions (0.50 MPa, 3.0 m/s), (1.0 MPa, 1.0 m/s) and (0.25 MPa, 3.0 m/s), respectively.

pv condition where Eq. (2) breaks down and excessive wear can be observed is referred to as the limiting pv factor (pv_{lim}), which can be regarded as a performance parameter for a given PMC at specified sliding conditions. In summary, performance improvement is about decreasing k^* and increasing pv_{lim}.

4. Results and discussion

Examples of measured frictional forces and disk temperatures as a function of time are given in Fig. 2. For all three examples a steady state level is reached for both parameters. Furthermore, measured temperatures and frictional forces mirror one another as should be expected. The latter are observed in all experiments on the POD apparatus.

4.1. Comparison of the tested composites

In order to relate the friction and wear behavior of different composites to each other, it is convenient to compare their values of $\dot{w}_s$ and μ, since these parameters, from a simplified point of view, should be independent of p and v and therefore represent the general level of performance of the materials in a given system. The specific wear rate $\dot{w}_s$ and coefficient of friction μ for the tested composites are given in Table 2 at different pv conditions. Note, that no values are given in Table 2 for CA/EP at factors of $pv = 3$ MPa m/s or above. This is due to the fact that CA/EP fails under these conditions and is unable to reach a steady state level of both friction and wear. Thus, the limiting pv factor for CA/EP arguably has a value of $pv_{lim} = 3$ MPa m/s, which will be discussed further in this section. The average level of μ for G/EP is 0.63 as opposed to 0.41 for CA/EP, which means that a general decrease of approximately 35% is obtained by substituting the glass fiber weave with the given carbon/aramid weave. This difference in the level of μ might be attributed to the following factors. Due to the hardness of glass fibers these are observed by visual inspection after testing to cause a significant roughening of the steel counterface. Furthermore, fragments of glass fibers located in the interfacial zone can act as abrasive particles. Both of these factors might increase the deformation, or plowing, contribution to μ. The degree of roughening of the counterface seems to depend significantly on the measuring condition and is observed to be most severe at this pv condition: 0.25 MPa, 6.0 m/s. The initial and final roughness of the steel counterface are compared in one case at the mentioned condition. The R_a parameter changes from 0.26 (±0.03) to 0.59 (±0.05) μm after 3 h of sliding. Carbon fibers, on the other hand, might act as a solid lubricant which decreases the interfacial shear force due to the partial graphite structure of these fibers. With respect to abrasiveness the carbon fibers are also in some cases observed to cause some roughening of the steel counterface but to a lesser extent than the glass fibers.

According to Amontons laws of friction, μ should be independent of p and v. However, in the case of polymeric materials this is often not the case [16]. The data in Table 2 shows some variation in μ at different combinations of p and v, but without any indication of clear trends. Thus, it might be concluded that despite a few exceptions, μ is fairly constant considering the relatively large range of p, v and interfacial temperatures.

The wear rates $\dot{w}_s$ shown in Table 2 are on average a factor of 22 higher for G/EP compared to CA/EP and $\dot{w}_s$ generally increases as a function of p and v. The latter will be discussed further in Section 4.2.

In order to interpret this significant difference in wear rates of the two PMCs, SEM images are produced of the worn surfaces. Fig. 3 shows glass fibers and aramid fibers, respectively, worn normal to the counterface. In the case of glass fibers, it seems as though the resin is worn out, or eroded, from between the fibers leaving the fiber ends exposed. Since glass fibers are brittle, these exposed ends are expected to be fragmented or broken off relatively easily. The aramid fibers, on the other hand, are level with the resin. It seems as though the tough aramid fibers inhibit micro-cracking of the resin and thereby prevent erosion. Fig. 4 shows glass fibers and aramid fibers, respectively, worn parallel to the counterface. This micrograph is interpreted to show that the glass fibers are initially worn thinner and then ultimately broken into smaller pieces which are probably easily removed. The aramid fibers are, also in this case, level with the

Table 2
Coefficients of friction μ and specific wear rates $\dot{w}_s$ measured for G/EP and CA/EP under different pv conditions

Material	Pressure, p (MPa)	Velocity, v (m/s)	pv condition (MPa m/s)	Friction, μ	Wear, $\dot{w}_s$ (10^{-6} mm^3/N m)
G/EP	0.25	1.0	0.25	0.58 (±0.1)	6.5 (±0.7)
G/EP	0.50	1.0	0.50	0.71 (±0.04)	11 (±0.2)
G/EP	1.0	1.0	1.0	0.46 (±0.06)	11 (±0.1)
G/EP	0.25	3.0	0.75	0.58 (±0.03)	15 (±0.06)
G/EP	0.50	3.0	1.5	0.70 (±0.06)	18 (±0.2)
G/EP	1.0	3.0	3.0	0.70 (±0.03)	28 (±0.07)
G/EP	0.25	6.0	1.5	0.63 (±0.03)	33 (±0.5)
G/EP	0.50	6.0	3.0	0.73 (±0.1)	24 (±0.2)
G/EP	1.0	6.0	6.0	0.56 (±0.05)	34 (±0.1)
CA/EP	0.25	1.0	0.25	0.45 (±0.07)	0.60 (±0.08)
CA/EP	0.50	1.0	0.5	0.43 (±0.05)	0.62 (±0.07)
CA/EP	1.0	1.0	1.0	0.36 (±0.06)	1.0 (±0.2)
CA/EP	0.25	3.0	0.75	0.38 (±0.03)	0.80 (±0.1)
CA/EP	0.50	3.0	1.5	0.44 (±0.05)	0.86 (±0.1)
CA/EP	0.25	6.0	1.5	0.37 (±0.03)	0.49 (±0.03)

The precision is indicated by standard deviations.

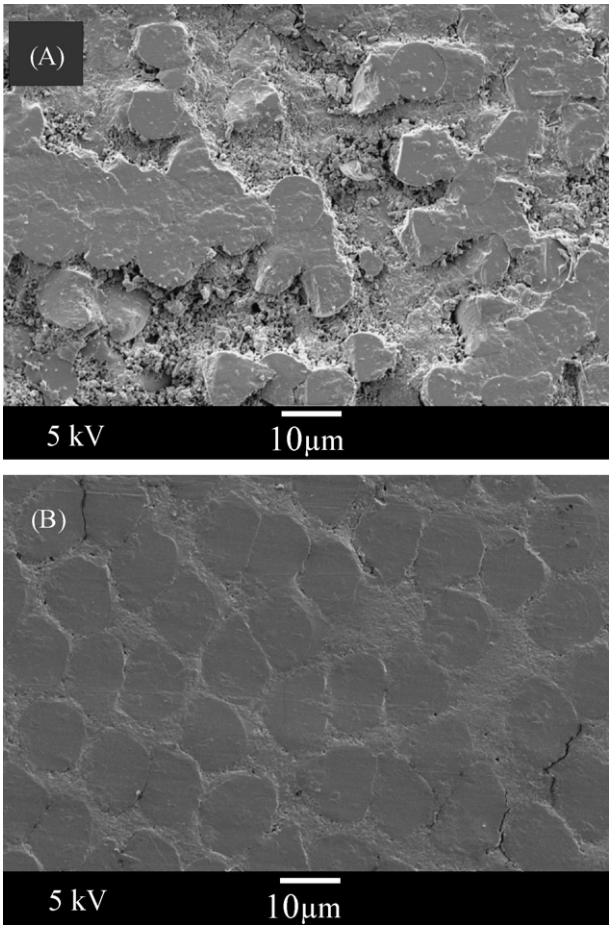

Fig. 3. SEM image of (A) glass fibers worn normal to the counterface in the case of G/EP (0.50 MPa, 3.0 m/s) and (B) aramid fibers worn normal to the counterface in the case of CA/EP (1.0 MPa, 6.0 m/s).

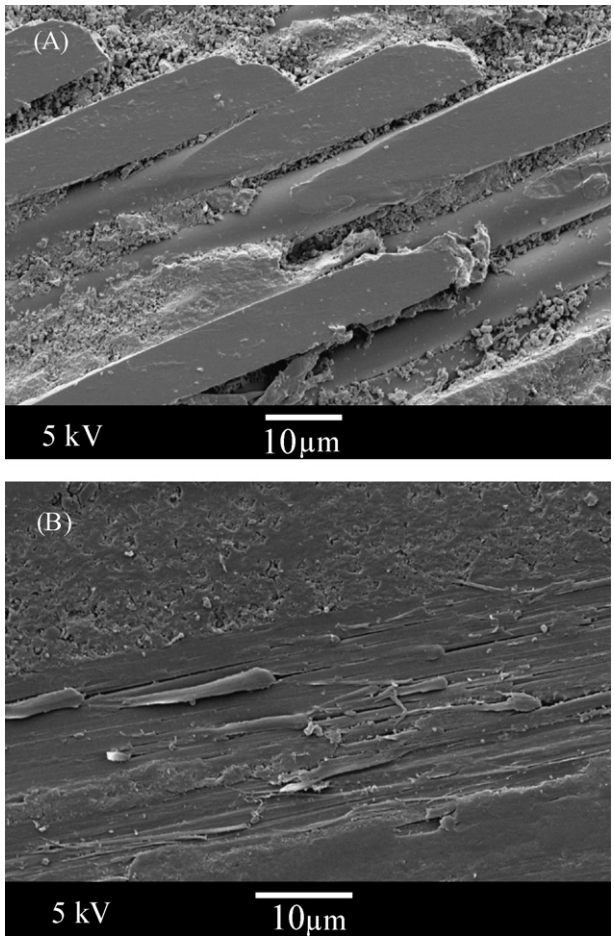

Fig. 4. SEM image of (A) glass fibers worn parallel to the counterface in the case of G/EP (0.50 MPa, 3.0 m/s) and (B) an aramid fiber worn parallel to the counterface in the case of CA/EP (0.50 MPa, 3.0 m/s).

resin and worn in a tough manner seen by fibrillation of the fibers. With respect to carbon fibers, these are worn in a manner which visually resembles glass fibers. In summary, the differences in $\dot{w}_s$ seem to be caused by the following main factors. Glass fibers fail to prevent micro-cracking of the resin which leads to cracking of exposed fiber ends. These broken fiber ends can act as abrasive particles and cause third-body wear. The carbon fibers are not expected to cause these problems to the same extent due to a lower hardness and a proposed friction reducing ability. The aramid fibers seem to effectively prevent micro-cracking of the resin and are due to their toughness hard to remove from the surface.

The wear behavior discussed above is in agreement with the study of Cirino et al. on continuous fiber reinforced epoxy-matrix composites [10]. The data presented in that study is on unidirectional (UD) reinforcement and therefore not directly comparable with the data on bidirectional (BD) reinforcement presented here. However, comparable estimates can be calculated by averaging $\dot{w}_s$ for the relevant fibers and orientations. For example, the estimated value for G/EP is simply the average of $\dot{w}_s$ for the UD glass fiber composite tested in the normal and parallel direction, respectively. This procedure shows a good agreement between the two data sets both in absolute and relative values of $\dot{w}_s$ especially when considering experimental differences. With respect to studies of the wear mechanisms for glass, aramid and carbon fibers there is good consistency between the findings in this paper and other related publications [11,17].

At the three roughest pv conditions, decomposition of the test specimens caused by high interfacial temperatures is observed visually immediately after testing. Fig. 5 shows SEM images of surfaces worn at the highest pv factor (6.0 MPa m/s). In the case of both composites, larger-scale cracks, matrix/fiber debonding and depletion of decomposed resin are observed. Thus, there seems to be a transition from localized small-scale damage at mild pv conditions to larger-scale damage at rough pv conditions. This larger-scale damage, or cracks, can potentially grow from the sliding surface and thereby cause failure of an entire component. In the case of G/EP, steady state wear rates are obtained also at the three roughest pv conditions despite severe decomposition. According to the data presented in Fig. 6, the frictional force fluctuates more at the highest pv factor due to the aforementioned larger-scale damage. However, the frictional force seems to fluctuate around a relatively stable level. In the case of CA/EP, no steady state levels of μ or $\dot{w}_t$ are obtained at the three roughest pv conditions. Fig. 7 shows a gradual increase in frictional force and hence in interfacial temperature

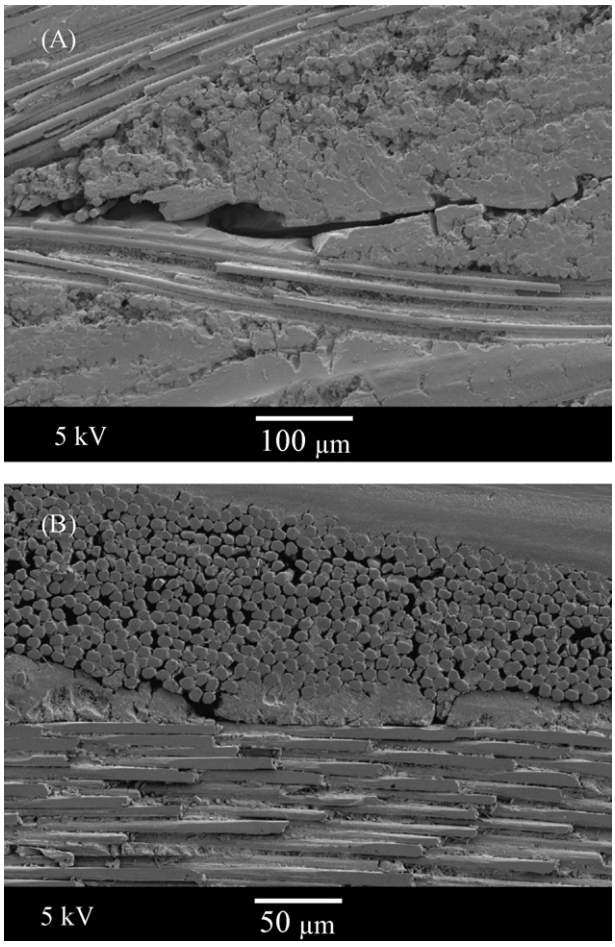

Fig. 5. SEM images of surfaces worn at the highest pv factor (1.0 MPa, 6.0 m/s). (A) G/EP showing glass fibers oriented both normal and parallel to the counterface and (B) CA/EP showing carbon fibers oriented both normal and parallel to the counterface.

which ultimately result in decomposition and complete failure of the specimen. This phenomenon is explained as follows. Stiffness and strength in compression are important tribological parameters in relation to both friction and wear because they influence the magnitude of the real area of contact. In this respect glass fibers are generally superior to carbon and especially aramid fibers. It is believed that this gradual increase in μ is triggered by thermal softening and decomposition of the resin located close to the surface. It seems like this phenomenon initiates at temperatures below the glass transition temperature ($T_g = 133\,^{\circ}C$) of the resin. However, it must be emphasized that the measured disk temperatures surely underestimate the actual flash temperatures at the contacting asperities. When thermal softening sets in, it might cause a self-accelerating cycle where an increase in the real area of contact causes an increase in the frictional force, which again causes an increase in interfacial temperature and so on. Thus, it might be imagined that the zone of rubbery and decomposed resin, respectively, expands from the sliding surface and into the material as the interfacial temperature increases. During this process, the carbon and aramid fibers probably loose their load-bearing capacity as the support from the matrix decreases. Glass fibers in the same

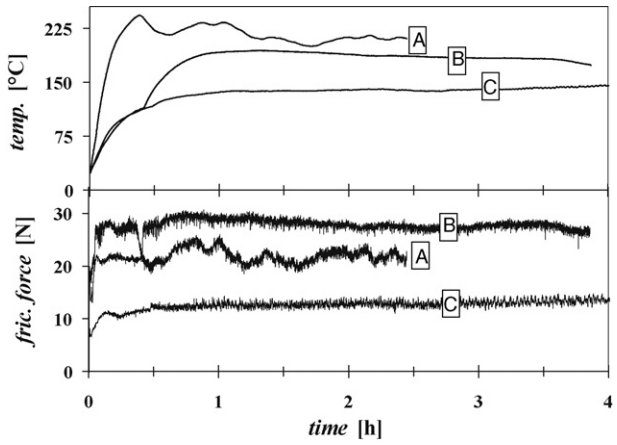

Fig. 6. Three examples of measured temperatures and frictional forces as a function of time for G/EP. (A), (B) and (C) correspond to the pv conditions (1.0 MPa, 6.0 m/s), (1.0 MPa, 3.0 m/s) and (0.50 MPa, 6.0 m/s), respectively.

situation might still be capable of supporting the load due to higher compressive stiffness and strength.

The behavior shown in Fig. 7 is regarded as complete failure since the material is not useful as a sliding partner at these conditions, i.e. at pv factors of 3 and 6 MPa m/s. Based on this the limiting pv factor, cf. Section 3, for CA/EP has a value of $pv_{lim} = 3$ MPa m/s, which is relatively low compared to some values previously reported for similar materials. However, such a comparison cannot be made solely based on pv factors without also considering the corresponding interfacial temperatures. The latter depends, besides from the parameters mentioned in Section 3, on the thermal properties of the applied tribotester, which is controlled by, e.g. geometry/design of components, thermal conductivities of applied materials and application of cooling devices. In Fig. 8 measured steady state temperatures at different pv conditions are plotted as a function of $\dot{Q}_d$ given by Eq. (1). There seems to be a linear relationship between the interfacial temperature and the rate of energy dissipation caused by the frictional process. Furthermore, the linear trend line extrapolates to a value close to the ambient temperature at $\dot{Q}_d = 0$ as expected. The magnitude of the slope ($\beta_f = 59\,^{\circ}C\,m^2\,s/J$) is

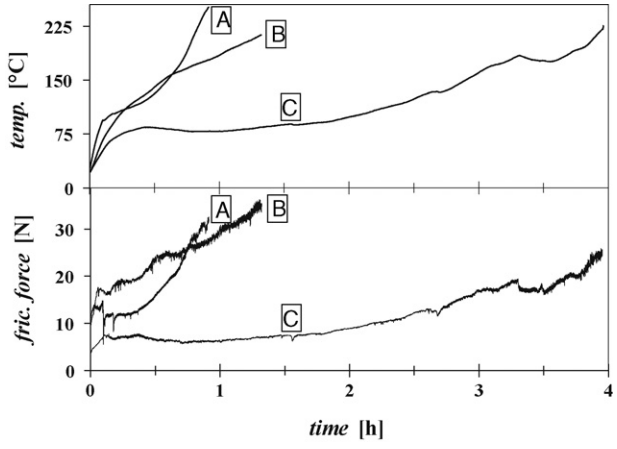

Fig. 7. Three examples of measured temperatures and frictional forces as a function of time for CA/EP. (A), (B) and (C) correspond to the pv conditions (1.0 MPa, 6.0 m/s), (1.0 MPa, 3.0 m/s) and (0.50 MPa, 6.0 m/s), respectively.

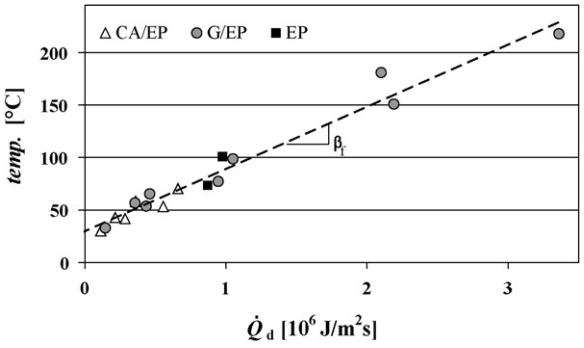

Fig. 8. Measured steady state temperatures at different pv conditions plotted vs. the specific rate of energy dissipation $\dot{Q}_d$. EP is the neat resin. β_f is the slope of the linear trend line.

specific for the applied test system and has a large impact on the observed wear behavior since it links the tribological process to the corresponding interfacial temperature. This linear relationship between the steady state interfacial temperature and the specific rate of energy dissipation (or specific rate of frictional work) is also found by Chang et al. [18]. The magnitude of the slope found on the POD used in that study is approximately a factor of 2 lower than the one presented here. Consequently, the interfacial temperatures measured under a certain set of sliding conditions are also a factor of 2 lower than the ones found in this study. Such a temperature difference can potentially also result in a significantly different outcome of friction and wear tests.

4.2. Correlation between pv factors and wear rates

Figs. 9 and 10 show measured depth wear rates $\dot{w}_t$ and steady state interfacial temperatures at different pv conditions for the tested composites. A gradual increase in both parameters are observed as a function of p and v, respectively, as expected from Eq. (2). More specifically, Eq. (2) predicts a linear relationship between $\dot{w}_t$ and the pv factor with a slope equal to $\dot{w}_s$ (or the wear factor). It is clear from Table 2 that this does not exactly apply since $\dot{w}_s$ is actually not a constant but increases with both p and v. In order to clarify the relationship between $\dot{w}_t$ and pv, these are plotted versus each other in Fig. 11. According to these plots a power law yields a better fit than a linear model. An exception

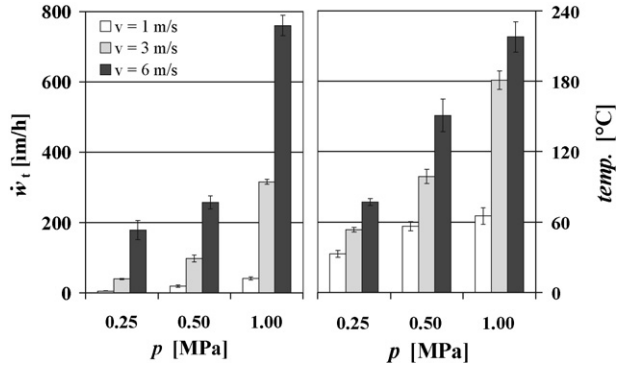

Fig. 9. Depth wear rates $\dot{w}_t$ and steady state interfacial temperatures at different pv conditions for G/EP.

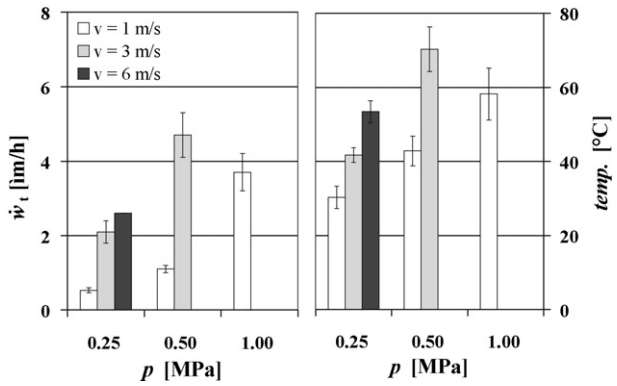

Fig. 10. Depth wear rates $\dot{w}_t$ and steady state interfacial temperatures at different pv conditions for CA/EP.

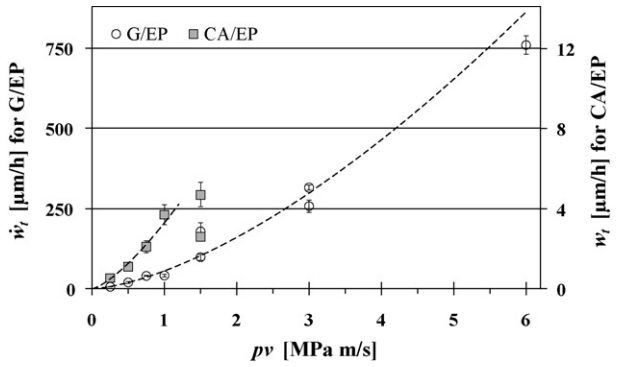

Fig. 11. Depth wear rates $\dot{w}_t$ plotted vs. pv factors for (▒) CA/EP and (○) G/EP. The lines are power law trend lines fitted to the experimental data.

to this trend are the two data points for CA/EP at the pv factor 1.5 MPa m/s. Based on visual inspection, these two conditions seem to facilitate formation of a protective transfer film, relative to other conditions, which explains the deviation from the trend shown by the other data points. As mentioned in Section 3, the wear factor is a function of both material properties and system properties and these are both treated as constants. However, considering that the interfacial temperature varies from 33 °C at the lowest pv factor to 218 °C at the highest pv factor, cf. Figs. 9 and 10, it is obvious that the material properties will change in this relatively large temperature range. Certainly, the resin properties will change at the glass transition and decomposition temperatures. Thus, this increase in $\dot{w}_t$, beyond what is predicted by Eq. (2), might be related to a gradual deterioration of the resin properties and thereby also in the composite properties with increasing interfacial temperatures.

5. Conclusion

An average decrease in the coefficient of friction μ of approximately 35% is found by substituting a glass fiber weave with a carbon/aramid hybrid weave in an epoxy-matrix. This decrease is considered to be due to the lubricating effect of carbon fibers as opposed to the abrasive nature of glass fibers. Although there are a few exceptions, μ is found to be roughly independent of contact pressure p and sliding velocity v.

The average level of wear rates for G/EP is a factor of 22 higher than for CA/EP which is believed to be caused by the following main factors. The aramid fibers seem to inhibit micro-cracking of the resin, which in the case of glass and carbon fibers leads to exposed fiber ends. These exposed, and brittle, fiber ends seem to be fragmented and broken easily relative to the tough aramid fibers, which are worn by a fibrillation mechanism. Furthermore, third-body abrasive wear caused by fragmented glass fibers probably also contributes significantly to the high wear rate found for G/EP.

In the case of CA/EP the specimen fails at a limiting pv factor of 3 MPa m/s, which probably is due to buckling of the aramid and carbon fibers as the supporting resin softens and decomposes. When G/EP is tested at the same conditions, a similar failure is not observed, but decomposition of the resin and development of larger-scale cracks is evident.

A linear relationship is found between the measured steady state interfacial temperatures and the calculated rates of energy dissipation. The slope of the linear trend line is suggested to be an important system specific property to consider when comparing measurements obtained on different Pin-On-Disk apparatuses, since it relates the tribological process to the resulting interfacial temperature.

The depth wear rates plotted versus pv factors seem to follow a power law more closely than a linear model predicted by theory. This is believed to be caused mainly by a gradual deterioration of material properties with increasing interfacial temperatures.

Acknowledgements

The work is financially supported by a grant given in equal parts by the Technical University of Denmark, The Danish Research Training Council and Civilingeniør Frederik Leth Christensens ALMENNYTTIGE FOND. The latter is furthermore gratefully acknowledged by the authors for financing the applied Pin-On-Disk apparatus.

References

[1] K. Friedrich, P. Reinicke, Friction and wear of polymer-based composites, Mech. Compos. Mater. 34 (1998) 503–514.
[2] A.M. Häger, K. Friedrich, Selected thermoplastic bearing materials for use at elevated temperatures, Wear 162 (1993) 649–655.
[3] A.P. Harsha, U.S. Tewari, Tribo performance of polyaryletherketone composites, Polym. Test. 21 (2001) 697–709.
[4] C. Schwarts, S. Bahadur, The role of filler deformability, filler–polymer bonding, and counterface material on the tribological behaviour of polyphenylene sulfide (PPS), Wear 251 (2001) 1532–1540.
[5] H. Unal, A. Mimaroglu, Friction and wear behaviour of unfilled engineering thermoplastics, Mater. Design 24 (2003) 182–187.
[6] S. Bahadur, The development of transfer layers and their role in polymer tribology, Wear 245 (2000) 92–99.
[7] Q. Zhao, S. Bahadur, Investigation of the transition state in the wear of polyphenylene sulfide against steel, Tribol. Lett. 12 (2002) 23–33.
[8] H. Schönherr, J. Vancso, The mechanism of PTFE and PE friction deposition: a combined scanning electron and scanning force microscopy study on highly oriented polymeric sliders, Polymer 39 (1998) 5705–5709.
[9] S. Kalpakjian, S.R. Schmid, Manufacturing Engineering and Technology, Prentice Hall, 2001.
[10] M. Cirino, K. Friedrich, R.B. Pipes, Evaluation of polymer composites for sliding and abrasive wear applications, Composites 19 (1988) 383–392.
[11] T. Tsukizoe, O. Nobuo, Friction and wear performance of unidirectionally oriented glass, carbon and stainless steel fiber-reinforced plastics, in: K. Friedrich (Ed.), Friction and Wear of Polymer Composites—Composite Materials Series, vol. 1, Elsevier, New York, 1986, pp. 205–231.
[12] T.Ø. Larsen, PhD thesis, 2006, submitted for publication.
[13] E. Rabinowicz, Friction and Wear of Materials, 2nd ed., John Wiley and Sons, Inc., 1995.
[14] J.A. Williams, Engineering Tribology, Oxford University Press, 1995.
[15] J. Halling, Principles of Tribology, The MacMillian Press Ltd., 1975.
[16] I.M. Hutchings, Tribology: Friction and Wear of Engineering Materials, Edward Arnold, 1992.
[17] K. Friedrich, R. Reinicke, Z. Zhang, Wear of polymer composites, Eng. Tribol. J 216 (2002) 415–426.
[18] L. Chang, Z. Zhang, C. Breidt, K. Friedrich, Tribological properties of epoxy nanocomposites. I. Enhancement of the wear resistance by nano-TiO_2 particles, Wear 258 (2005) 141–148.

The effect of particle addition and fibrous reinforcement on epoxy-matrix composites for severe sliding conditions

B

Available online at www.sciencedirect.com
ScienceDirect
Wear xxx (2007) xxx–xxx
WEAR
www.elsevier.com/locate/wear

The effect of particle addition and fibrous reinforcement on epoxy-matrix composites for severe sliding conditions

Thomas Ø. Larsen [a], Tom L. Andersen [b], Bent Thorning [c], Martin E. Vigild [a,*]

[a] *Danish Polymer Centre, Department of Chemical Engineering, Technical University of Denmark, Produktionstorvet, Building 423, DK-2800 Kgs. Lyngby, Denmark*
[b] *Risø National Laboratory, Materials Research Department, DK-4000 Roskilde, Denmark*
[c] *Elektro-Isola A/S, Grønlandsvej 197, DK-7100 Vejle, Denmark*

Accepted 6 December 2006

Abstract

This paper reports production and tribological testing of epoxy-matrix composites for dry-sliding conditions. The examined composites are produced using the following components: epoxy resin (EP), glass fiber weave (G), carbon/aramid hybrid weave (CA), PTFE particles and nano-scale CuO particles. Friction, wear and interfacial temperatures are measured on a custom-built pin-on-disk apparatus using a steel disk as counterface. The performance of the two types of reinforcing weaves are compared at nine different combinations of contact pressure (p) and sliding velocity (v) also called pv conditions. The purpose is to systematically compare the performance of the differently reinforced materials while going from mild to severe sliding conditions. It is found that the coefficient of friction (μ) on average is reduced by 35% by substituting the glass fiber weave with the carbon/aramid weave. The latter, shows superior wear behavior at the six mildest pv conditions with the wear rate ($\dot{w}$) an average factor of 22 lower than the rates for glass fiber reinforcement. An effect of fiber orientation with respect to sliding direction is found for the glass fiber reinforcement. The best tribological properties are seen when the fibers are parallel and anti-parallel (P–AP) to the sliding direction compared to normal and parallel (N–P). Experiments with incorporating micro-scale PTFE particles and nano-scale CuO particles, respectively, into the epoxy resin along with the carbon/aramid weave shows no difference in friction but minor improvements in wear. When micro-scale PTFE particles are incorporated into the neat epoxy resin, i.e. without fibers, an increase in $\dot{w}$ and a decrease in μ are measured. When the same is done with nano-CuO a deterioration of both friction and wear properties are seen. At the three roughest pv conditions all tested composites show signs of decomposition. Despite this, glass fiber reinforcement has a relatively steady behavior while carbon/aramid reinforcement gives raise to a gradually increasing frictional force, which ultimately results in complete failure of the test-specimen.

Keywords: Friction; Wear; Epoxy-matrix composites; Fibrous reinforcement; PTFE micro-scale particles; CuO nano-scale particles

1. Introduction

A widely used way of decreasing friction and wear is to use liquid lubricants such as oil to separate sliding surfaces by a film of low shear strength. Liquid lubricants have a limited lifetime due to decomposition and/or contamination and requires changing from time to time [1]. Furthermore, certain disadvantages are associated with this type of lubrication: (1) it typically requires filters, pumps and cooling systems; (2) has a negative impact on the environment partly due to disposal of used lubricants and partly due to leakages and emissions of gases or particles; (3) can contaminate products, e.g. foods and textiles, during manufacturing. Due to these limitations and downsides, there exists an interest in solid lubricants and self-lubricating materials. Polymer matrix composites (PMCs) are obvious candidates as self-lubricating substitutes for oil-lubricated metals. Firstly, polymers generally have a low coefficient of friction (μ) during dry-sliding, which excludes cold-welding and consequently catastrophic sliding failure as seen for metals when lubricating systems fail. Secondly, some polymers are intrinsically solid lubricants, e.g. polytetraflouroethylene (PTFE) [2,3].

Polymers are generally weak materials compared to metals and ceramics which obviously results in some limitations [4]. To

* Corresponding author. Tel.: +45 45252967; fax: +45 45882161.
E-mail addresses: tol@kt.dtu.dk (T.Ø. Larsen), tom.loegstrup.andersen@risoe.dk (T.L. Andersen), b.thorning@elektro-isola.dk (B. Thorning), mev@kt.dtu.dk (M.E. Vigild).

0043-1648/$ – see front matter © 2007 Elsevier B.V. All rights reserved.
doi:10.1016/j.wear.2006.12.078

overcome this drawback different types of reinforcements, e.g. fibers and particles, are often applied which results in structured composite materials with excellent specific properties [5,6]. This is typically to improve mechanical properties but also in many cases for enhanced friction and wear control [7,8]. PMCs are increasingly utilized as sliding partners often against steel counterfaces, and relatively much empirical knowledge exists in this field. However, published data frequently seems to be conflicting and general guidelines are difficult to extract. This causes design and optimization of such tribological systems to be largely controlled by trial and error. Thus, there certainly is a need for more knowledge and understanding, which may lay the foundation for predictive guidelines for structuring self-lubricating PMCs toward enhanced friction and wear control.

One of the limitations in the use of PMCs is their inferior thermo-resistant properties relative to metals and ceramics. During sliding, the mechanical energy is mainly dissipated as heat. This may lead to decomposition and deterioration of mechanical properties, which in turn often decrease the friction and wear performance. This limits the life time and application range of components made from PMCs. This is especially a problem in applications involving high contact pressures (p) and sliding velocities (v), since this results in a high specific rate of energy dissipation ($\dot{Q}_d$), i.e. the rate of dissipated energy per unit apparent contact area:

$$\dot{Q}_d = \mu p v \,(\mathrm{J/m^2\,s}) \quad (1)$$

Here μ, p and v are coefficient of friction, contact pressure and sliding velocity, respectively. It is seen that $\dot{Q}_d$ is directly proportional to μ and to the product of p and v also called the pv condition. Thus, in order to obtain PMCs for heavy duty applications, the thermal properties, e.g. glass transition, heat distortion and decomposition temperatures, must be improved or frictional heating must be reduced by e.g. applying lubricating resins or fillers.

In this study, PMCs are produced using an epoxy resin (EP) as matrix. Epoxy resins do typically exhibit relatively high wear rates and coefficients of friction when dry-sliding against steel counterfaces. This is basically due to the cross-linked molecular structure, which inhibits the formation of an efficient transfer film and results in a relatively high degree of brittleness. However, epoxy resins possess other favorable properties such as strong adhesion to many materials, good mechanical and electrical properties, relatively high chemical and thermal resistance [9], and a low price compared to advanced polymers such as polyetheretherketone (PEEK) and polyimide (PI). From this perspective, it is an attractive goal to obtain an epoxy-based composite for severe sliding conditions by incorporating the right kind of components, e.g. fibers or particles. Two types of fibrous reinforcement are applied in this study: a plain glass fiber weave (G) and a carbon/aramid hybrid weave (CA), which in both cases give raise to bidirectional fiber orientations in the composite. Others have for unidirectional oriented fiber composites demonstrated the general superiority of continuous carbon and aramid fibers compared to glass fibers when sliding against smooth steel [10,11]. The tribological comparison between different PMCs are often made at one or a few pv conditions. However, the tribological properties of PMCs are often highly sensitive to the applied pv condition. In this study, the two types of weave are therefore compared at nine different pv conditions in order to systematically examine and compare the performance of these two materials as they are exposed to increasingly rough sliding conditions.

Additionally, this paper reports preliminary experiments with incorporating micro-scale PTFE particles and nano-scale CuO particles into either the neat epoxy resin or into the resin along with the carbon/aramid weave. It is anticipated that the lubricating effect of the PTFE particles might reduce frictional heating and thereby make the composite useful at more severe pv conditions. The use of inorganic nano-scale particles receives relatively much attention presently [12–16]. These nanocomposites have in some cases shown promising results regarding reduction in μ and/or wear rate ($\dot{w}$). As opposed to micro-scale particles it has been proposed that nano-scale particles can improve mechanical properties of the composite, while avoiding acting as an abrasive against the steel counterface due to their small size [17]. In other cases, the cause of friction and wear improvement seems to be the ability of the particles to promote adhesion of a protective transfer film to the counterface. Furthermore, experimental data indicate that the optimum nanoparticle concentration is typically in the range of 1–5 vol.%, which is a factor of 10 lower than typically found for micro-scale fillers [18]. This low optimum content makes it possible to utilize these particles to potentially improve the resin properties of fiber-reinforced composites.

The tribological data are obtained using a custom-built tribotester of the pin-on-disk type [19]. Measurements are performed under dry-sliding conditions against smooth steel surfaces ($R_a = 0.26 \pm 0.03\,\mu m$) at ambient temperature ($22 \pm 2\,^\circ C$) and humidity (74 ± 5RH).

2. Experimental

2.1. Materials

An overview of the tested composites are given in Table 1. The examined glass fiber composite (G/EP) is produced by Elektro-Isola A/S and is commercially available (G-Etronax EP 11). This material is not intended for use in dry-sliding applications but is used as a reference material in this context. The composites which are reinforced with the carbon/aramid hybrid weave

Table 1
Nomenclature, composition and density of tested materials

Nomenclature	Weave type (vol.%)	Particle type (vol.%)	Density (g/cm^3)
EP	–	–	1.2
EP/PTFE	–	PTFE/7.5	1.3
EP/CuO	–	Nano-CuO/1	1.2
G/EP	Glass fiber/44	–	1.8
CA/EP	Carbon/aramid/44	–	1.3
CA/EP/PTFE	Carbon/aramid/47	PTFE/5	1.4
CA/EP/CuO	Carbon/aramid/45	Nano-CuO/1	1.4

Please cite this article in press as: T.Ø. Larsen et al., The effect of particle addition and fibrous reinforcement on epoxy-matrix composites for severe sliding conditions, Wear (2007), doi:10.1016/j.wear.2006.12.078

are produced for the purpose of this study. All tested materials are produced using the same production method and the same type of resin, which is a polyfunctional epoxy of the novolac type obtained from Hexion Specialty Chemicals (Epikote 1153-B-70). The glass fiber weave (Plain, international style 7637) is delivered by P-D Interglas Technologies AG and the carbon/aramid hybrid weave (twill 2 × 2, style 73210) are obtained from Hexcel Fabrics S.A. and has carbon and aramid fibers both oriented in warp as well as weft with the same ratio (61 vol.% aramid/39 vol.% carbon) in both directions. The incorporated PTFE particles (TF 9207) are purchased as micropowder from Dyneon ™. CuO nano-particles (NanoArc ™U1102DBE) are delivered by Nanophase Technologies Corporation. The particles are recived as coated particles dispersed in a diester solvent mixture.

2.2. Specimen preparation

In the case of CA/EP/PTFE and CA/EP/CuO the particles are mixed with the epoxy solution prior to impregnation of weaves. PTFE micropowder is swelled in xylene (ratio 1:3) while stirring and then mixed mechanically with the epoxy solution. The nano-CuO dispersion is sonicated for 2 h before mixing it mechanically with the epoxy solution. When producing test-specimens without reinforcing weaves, the resin is cured in a mould by heating: 2 days at 45 °C, 1 h at 100 °C, 30 min at 130 °C, 1.5 h at 150 °C and finally 30 h at 170 °C. This slow heating procedure is applied in order to avoid porosity caused by solvent evaporation and to make sure that all residual solvent is removed. Weave-reinforced composites are produced by prepreg technology in the following way. A certain amount of epoxy solution, with or without particles, is added quantitatively to a square of weave and distributed by applying a roller. The impregnated weaves are subsequently placed in an oven with air circulation (typically 15 min at 120 °C) in order to evaporate the solvent and partially cure the resin. A number of partially cured sheets are then stacked, in order to obtain a laminate thickness of at least 5 mm, and pressed for 3 h applying a pressure of 35 bar and a temperature of 160 °C. Finally, the plates are post-cured for 2 h in an oven at 170 °C. The composite test-pins for tribological evaluation are obtained by reducing the plate thickness to 5.0 mm by milling, and then using a diamond saw to obtain the final dimensions of height 15 mm and cross-section 7.7 mm × 5.0 mm resulting in an apparent area of contact of 38.5 mm^2. After machining, the pins are dried in an oven for 20 h at 50 ° C and subsequently stored in a sealed bag at room temperature.

2.3. Pin-on-disk measurements

Photos of the applied custom-built pin-on-disk apparatus (POD) are shown in Fig. 1. The principle is summarized in the following. A composite pin is loaded perpendicularly against a rotating disk made of hardened chrome bearing steel (100 Cr6) by applying dead weights (W_N). The test-pin is mounted in a lever-arm via a sample holder. The lever-arm can rotate freely by use of ball bearings but is kept in a fixed position by a load

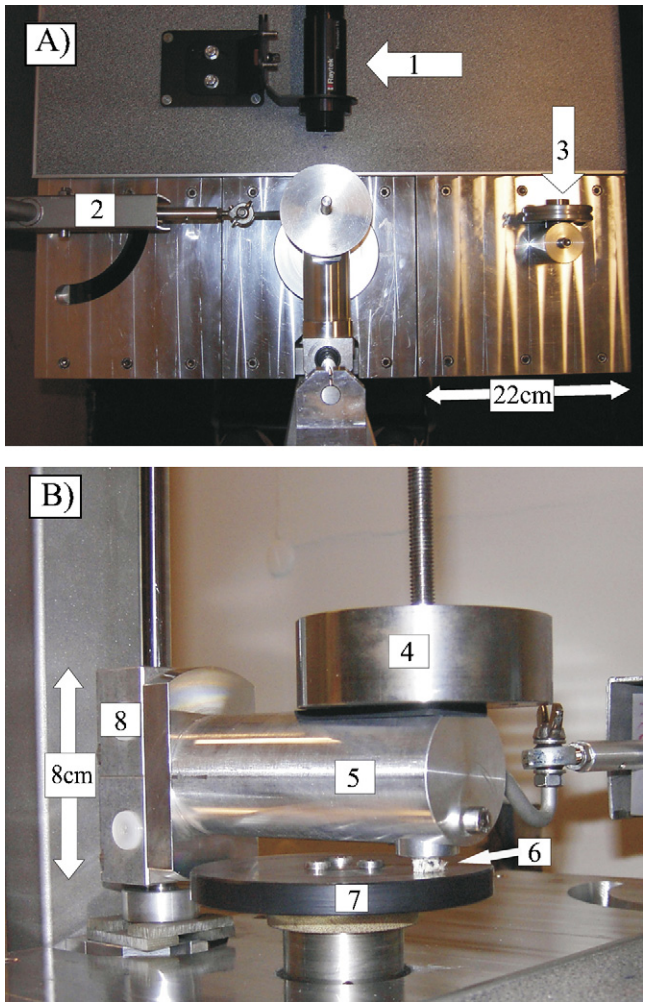

Fig. 1. (A) Top-view of the mechanical parts: 1, infrared temperature sensor; 2, load cell; and 3, pulley for load cell calibration. (B) Side-view of a composite pin loaded against the rotating steel disk: 4, weight; 5, lever-arm; 6, composite pin; 7, steel disk; and 8, alumina housing with ball bearings.

cell which measures the frictional force (F_f). The coefficient of friction (μ) is obtained by using Amontons first law of friction, i.e. $\mu = F_f / W_N$, and is reported as a time-averaged value based on data points in the steady state regime. The wear rate $\dot{w}$ is obtained simply by measuring the weight loss of the test-pin as a function of time. Furthermore, a non-contact thermometer estimates the interfacial temperature by collecting infrared radiation from the side of the steel disk.

The employed test-procedure is as follows: the steel counterface is abraded using a piece of emery cloth (grade P400) in order to obtain a fixed initial counterface roughness. The test-pin is mounted in the POD lever-arm when abrading it against a piece of emery cloth placed on the steel disk in order to obtain alignment of the surfaces. Before and after testing, the two surfaces are cleaned using acetone and compressed air. The initial and final weight of the test-pin plus the sample holder is noted to the nearest 0.1 mg. It is possible to reinsert the pin and sample holder in the lever-arm and continue the test-run in order to determine how the accumulated weight loss evolves as a function of time. This can reveal whether the accumulated weight loss is

Please cite this article in press as: T.Ø. Larsen et al., The effect of particle addition and fibrous reinforcement on epoxy-matrix composites for severe sliding conditions, Wear (2007), doi:10.1016/j.wear.2006.12.078

simply a linear function of time or showing a more complicated behavior due to e.g. modification of sliding surfaces or development of transfer films. Interruption of test-runs for weighing is kept brief and it is verified that this do not have any significant influence on the measured parameters.

Since the tribological behavior depends significantly on both materials and pv conditions, some adjustments in wear measurements are made for different materials and conditions. For G/EP, a linear relationship is found between accumulated weight loss and time without any detectable running-in period. In these cases, the experiments span over 2–24 h depending on the pv condition. The steady state wear rate is determined based on the initial and final weight of the test-specimen. The other tested materials do, at some conditions, show a running-in phenomenon with an initial wear rate, which decreases and ultimately reaches a steady level. In these cases, the accumulated weight loss is measured as a function of time for periods of 3–200 h. The slope of the approximately linear part of the curve is then used for calculation of the steady state wear rate. An exception to the above, is when examining the effect of adding PTFE and nano-CuO particles to the epoxy resin along with the carbon/aramid weave. In this case, the samples are run for a fixed interval of 23 h and the determined rates are averages for this time interval but not necessarily steady state wear rates. As a minimum, all materials are measured twice at each pv condition.

The fiber-reinforced test-specimens are placed in such a way that the weaves in the composites are either normal or parallel to the counterface during sliding, cf. Fig. 2. In the normal direction, the fibers in the weave are oriented normal and parallel (N–P) with respect to sliding direction whereas the fibers are parallel and anti-parallel (P–AP) with the sliding direction when the weave is oriented parallel to the counterface. The measured orientation is N–P unless stated otherwise.

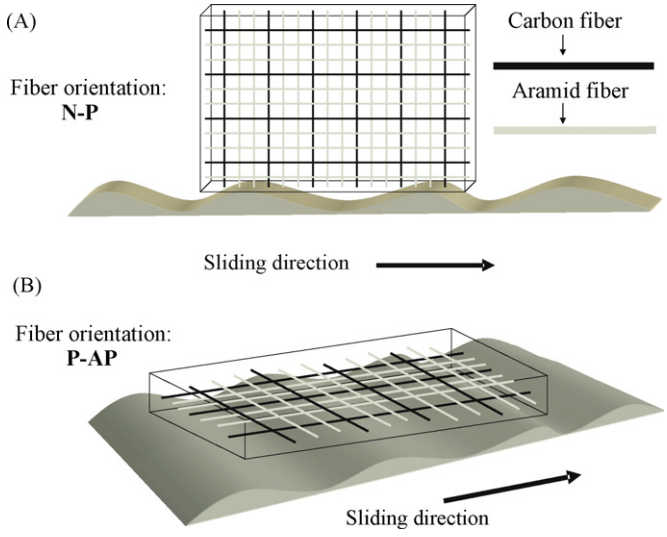

Fig. 2. Illustration of the two orientations of the reinforcing weaves during POD measurements shown here for the carbon/aramid weave. (A) The weave in the resin is normal to the counterface and the fibers are normal and parallel to the sliding direction (N–P). (B) The weave in the resin is parallel with the counterface and the fibers are parallel and anti-parallel to the sliding direction (P–AP).

2.4. Wear equations

Wear rates are reported either as a depth wear rate, $\dot{w}_t$ cf. Eq. (2), or as a specific wear rate, $\dot{w}_s$ cf. Eq. (3):

$$\dot{w}_t = \frac{\Delta h}{t} = k^* pv\,(\mu\text{m/h}) \tag{2}$$

Here Δh, t and k^* are height reduction of the worn composite pin, time and the wear factor, respectively. Note, that $\dot{w}_t$ is directly proportional to the pv factor as long as k^* is a constant. The latter depends on both material properties and system properties. Thus, if the system properties are fixed, k^* can to some extent be regarded as a material property. The wear factor is also equal the specific wear rate $\dot{w}_s$, which is normalized to load and distance, and is therefore more suitable for comparing wear data obtained under different conditions:

$$\dot{w}_s = \frac{\Delta m}{l\rho W_N}(\text{mm}^3/\text{Nm}) \tag{3}$$

Here l, W_N, Δm and ρ are sliding distance, load, mass loss and density of the worn composite, respectively.

2.5. Scanning electron microscopy images

Scanning electron microscopy (SEM) is used to study composite structures and worn surfaces. Samples for documenting composite structures are polished before cleaning. All samples are prepared by removing loose debris by compressed air followed by cleaning with acetone and finally coated. Both gold and carbon is applied as coating. The latter is used when documenting the dispersion state of nano-CuO particles using the backscattered electron detector. Images are obtained by using a microscope of the type JEOL JSM 5900 equipped with a LaB_6 filament.

3. Results and discussion

3.1. Composite structures

SEM images are given in the following to document the micro-structures of some of the tested composites. It is chosen to show particle containing composites as examples, since a good particle distribution is important for the properties and can be difficult to achieve. Fig. 3 shows the micro-structures of (A) EP/PTFE and (B) CA/EP/PTFE. In the case of EP/PTFE, it is seen that the micro-particles are relatively well-distributed in the resin. The image of CA/EP/PTFE shows a zone of resin, marked by the dashed line, containing the PTFE particles. Within this resin zone, the particles are relatively well distributed. However, it is generally seen that the PTFE particles are only located in resin between, and not within, fiber bundles. Thus, the particles are too large to enter the fiber bundles, which thereby act as filters preventing a more homogeneous particle distribution. This filtering effect is a common problem with micro-scale particles especially in relation to injection techniques such as resin transfer molding (RTM) [20]. Fig. 4 shows the micro-structures of (A) EP/CuO and (B) CA/EP/CuO. The CuO particles seem to be

Please cite this article in press as: T.Ø. Larsen et al., The effect of particle addition and fibrous reinforcement on epoxy-matrix composites for severe sliding conditions, Wear (2007), doi:10.1016/j.wear.2006.12.078

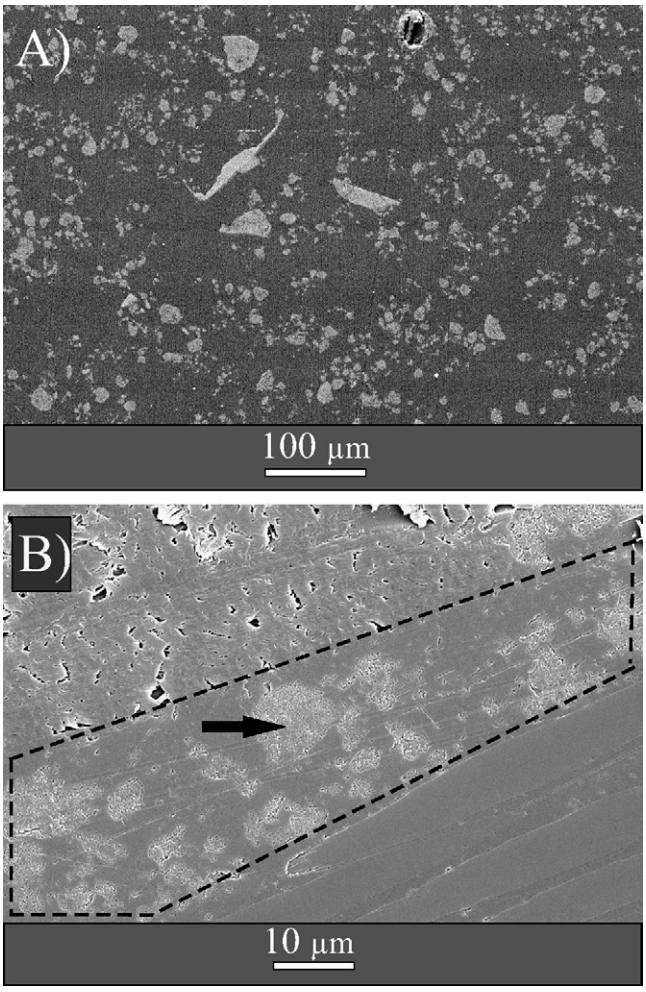

Fig. 3. SEM images showing the composite structures of (A) EP/PTFE and (B) CA/EP/PTFE. The light gray phase is PTFE and a single particle is marked by an arrow. The area given by the dashed line is a zone of resin where the PTFE particles are located. The lower right corner and the upper left corner of (B) show carbon fibers and aramid fibers, respectively, parallel to the surface.

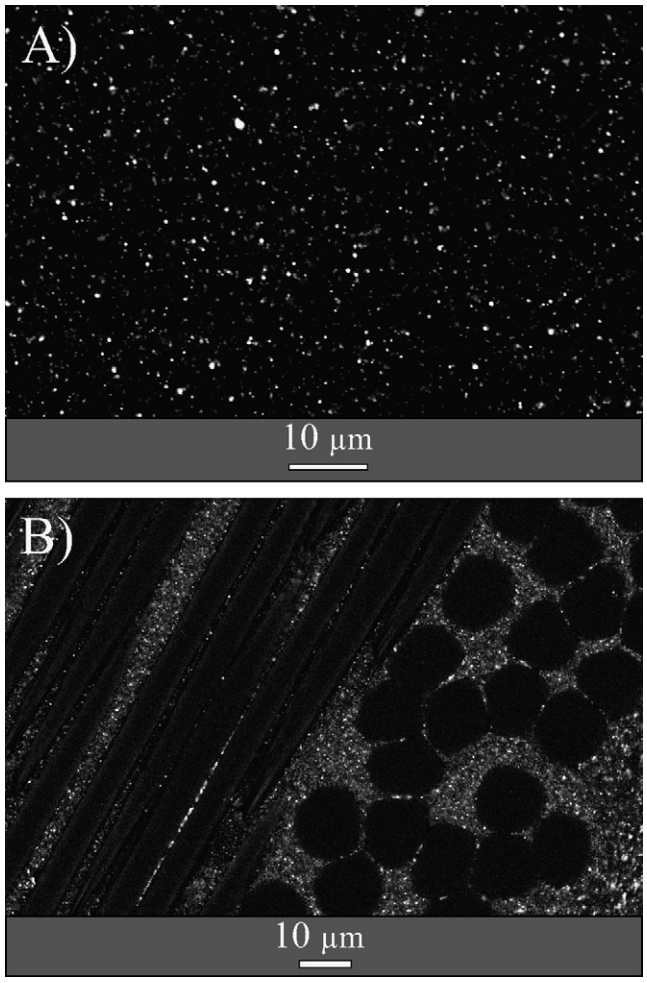

Fig. 4. SEM images showing the composite structures of (A) EP/CuO and (B) CA/EP/CuO. Nano-CuO particles are seen as bright stars. In (B) carbon fibers and aramid fibers, respectively, are seen oriented parallel and normal to the surface.

relatively well-dispersed in the epoxy resin. Based on Fig. 4 A it is not possible to see if the nano-particles are present as primary particles or as small clusters. However, all particles or clusters appear to be sub-micron in size. Image Fig. 4 B shows nano-particles distributed in the resin both between and within fiber bundles. Thus, the problem with particle filtering seen for the micro-scale PTFE particles are avoided by going to nano-size.

3.2. Comparison of the two types of weave

Fig. 5 shows measured values of μ for G/EP and CA/EP at different pv conditions. The average level of μ for G/EP is 0.63 as opposed to 0.41 for CA/EP, which means that a general decrease of approximately 35% is obtained by substituting the glass fiber weave with the carbon/aramid weave. This difference in the level of μ might be attributed to the following factors. Due to the hardness of glass fibers these are observed by visual inspection to cause significant roughening and wear of the steel counterface at some conditions. A severe example of this is seen in Fig. 6. Furthermore, fragments of glass fibers located in the interfacial zone can act as abrasive particles. Both of these factors might increase the deformation, or ploughing, contribution to μ. On the other hand, carbon fibers might act as a solid lubricant which decreases the interfacial shear force due to the partial graphite structure of these fibers. With respect to abrasiveness the carbon fibers are also in some cases observed to roughen the steel counterface but to a lesser extent than the glass fibers. The frictional data do not show any clear variation as a function of p or v despite a few exceptions. Thus, it might be concluded that μ is fairly constant and roughly follows Amontons laws of friction.

Figs. 7 and 8 show measured steady state depth wear rates $\dot{w}_t$ and interfacial temperatures at different pv conditions for G/EP and CA/EP, respectively. In the case of CA/EP, no values are given for the three most severe pv conditions since steady state could not be obtained. This point will be discussed further in Section 3.6. A gradual increase in both $\dot{w}_t$ and temperature is observed as a function of p and v as expected from Eqs. (1) and (2). More specifically, Eq. (2) predicts a linear relationship between $\dot{w}_t$ and the pv factor with a slope equal to the wear factor k^*. Actually, $\dot{w}_t$ generally increases more rapidly as a

Please cite this article in press as: T.Ø. Larsen et al., The effect of particle addition and fibrous reinforcement on epoxy-matrix composites for severe sliding conditions, Wear (2007), doi:10.1016/j.wear.2006.12.078

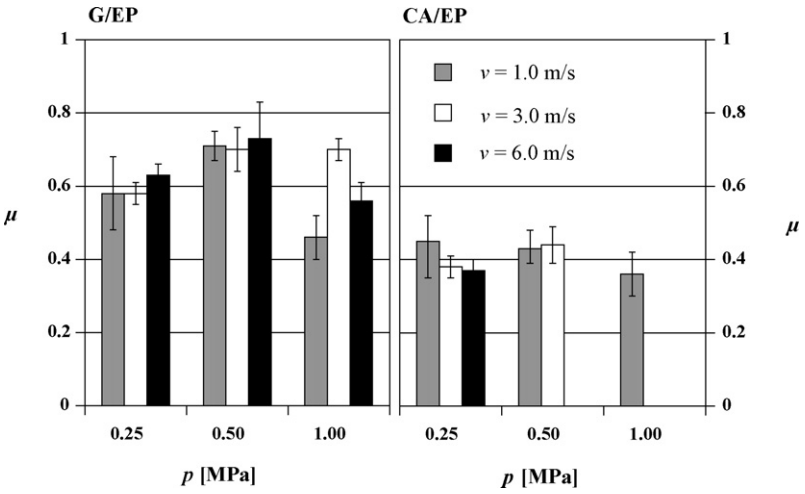

Fig. 5. Coefficients of friction μ measured at different pv conditions for G/EP and CA/EP.

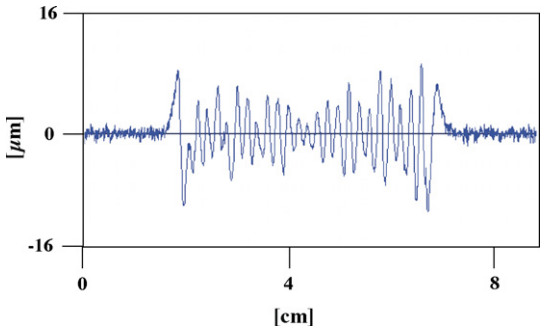

Fig. 6. Profilometer measurement of the roughness profile across the wear track on the disk. The middle part of the profile shows the roughness of the 5 cm wide wear track after being worn against G/EP ($p = 0.25$ MPa, $v = 6.0$ m/s). The initial roughness profile is seen on each side of the wear track.

function of p and v than predicted by this linear model. As previously mentioned, k^* is a function of material properties and system properties and these are both treated as constants. However, considering that the interfacial temperature varies from 33 °C at the lowest pv factor to 218 °C at the highest pv factor, it is obvious that the material properties will change in this relatively large temperature range. Thus, this increase in $\dot{w}_t$, beyond what is predicted by Eq. (2), might be related to a temperature induced deterioration of composite properties with increasing interfacial temperature.

Another important point seen from Figs. 7 and 8 is the striking difference in wear rates between the two materials. The average of the wear rates at the six mildest pv conditions for G/EP and CA/EP, expressed as specific wear rates $\dot{w}_s$, are 1.6×10^{-5} and 7.3×10^{-7} (mm^3/Nm), respectively. Thus, the wear rates are on average a factor of 22 higher for G/EP compared to CA/EP. Reasons for this significant difference are discussed in Section 3.5.

3.3. The influence of fiber orientation

From studies on unidirectional fibers it is known that the fiber orientation with respect to sliding direction can have a large impact on the tribological behavior [11]. Since the wear performance measured for G/EP at the N–P fiber orientation is particularly poor, it is chosen to repeat some of the measurements at the P–AP fiber orientation in order to determine if

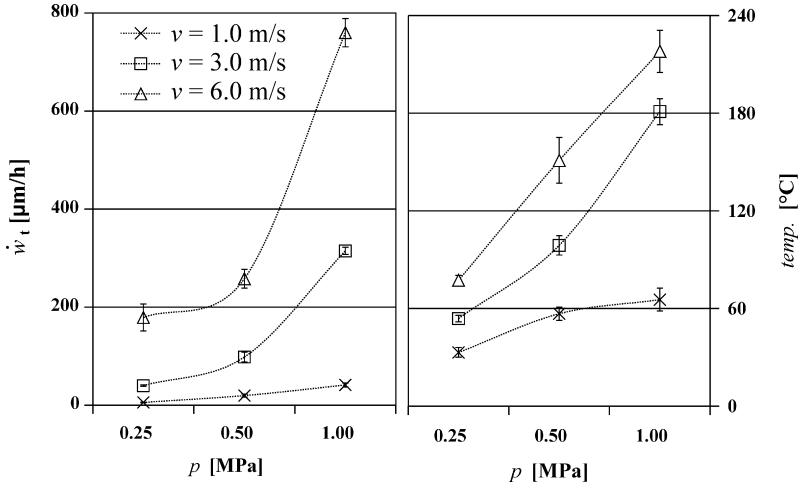

Fig. 7. Steady state depth wear rates $\dot{w}_t$ and interfacial temperatures at different pv conditions for G/EP.

Please cite this article in press as: T.Ø. Larsen et al., The effect of particle addition and fibrous reinforcement on epoxy-matrix composites for severe sliding conditions, Wear (2007), doi:10.1016/j.wear.2006.12.078

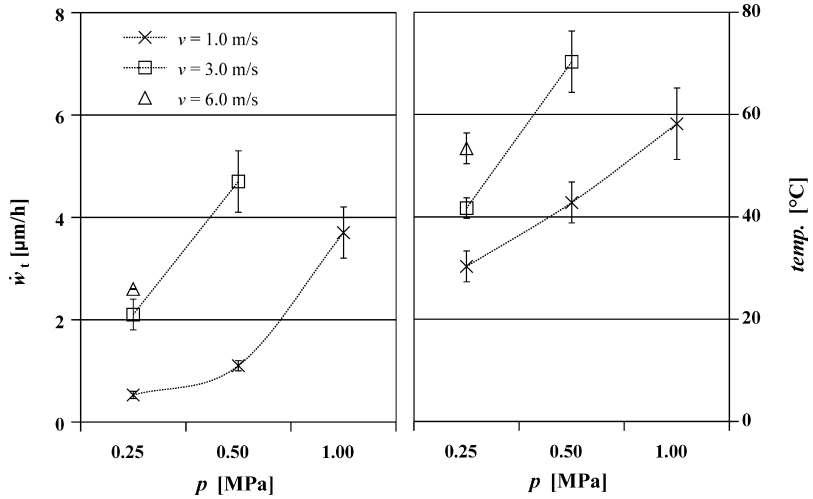

Fig. 8. Steady state depth wear rates $\dot{w}_t$ and interfacial temperatures at different pv conditions for CA/EP.

changes in the glass fiber orientation have any impact, cf. Fig. 9. The coefficient of friction μ measured for the P–AP direction is independent of the pv condition, while the N–P direction shows some variation. Also the specific wear rate $\dot{w}_s$ is roughly the same at the three pv conditions for the P–AP orientation. On the contrary, the N–P direction shows a significant increase in $\dot{w}_s$ when going from a high p–low v condition to a low p–high v condition. As a consequence of this, $\dot{w}_s$ is a factor of 2.6 higher for the N–P direction compared to the P–AP direction at the condition: $p = 0.25$ MPa, $v = 6.0$ m/s. The latter might

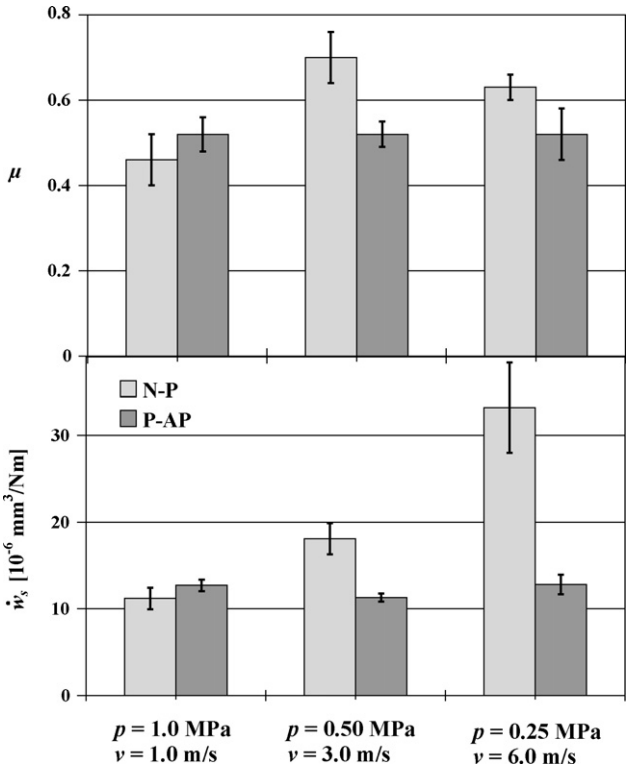

Fig. 9. Comparison of the coefficient of friction μ and the specific wear rate $\dot{w}_s$ for G/EP when tested with fibers oriented either in the N–P or the P–AP direction. The comparison is made at three different pv conditions.

be explained by a difference in abrasiveness between the two directions. G/EP is found to be particularly abrasive at this condition, cf. Fig. 6, which might account for the high wear rate. The P–AP orientation is, on the other hand, found by visual inspection to be less abrasive at the same condition and even forming a grayish transfer film. Additionally, the decrease in μ may also contribute to limit temperature induced deterioration of wear resistance. Cirino et al. examined the influence of fiber orientation for an epoxy resin reinforced with unidirectional continuous glass fibers [10]. Relative to the wear rate for the neat epoxy resin, it was found that the parallel and anti-parallel orientation reduced the wear rate by a factor of 2.1 and 1.1, respectively, while the normal direction increased the wear rate by a factor of 2. According to this, it should be beneficial to orient the weave in a way that eliminates the normal fiber orientation, which agrees well with the data presented here.

3.4. The effect of added particles

The measured effects on friction and wear of adding PTFE and nano-CuO particles are shown in Fig. 10. As a general observation, the use of carbon/aramid reinforcement has a large positive impact on the wear behavior but only a minor impact on the frictional behavior. For materials without fiber reinforcement, it is seen that addition of PTFE and especially nano-CuO leads to an increase in wear rate. This behavior is frequently seen when PTFE is incorporated into a stronger polymer resin. The relatively poor strength and adhesive properties of PTFE most likely result in deterioration of mechanical composite properties. However, PTFE shows the intended effect on the frictional behavior. EP/PTFE has a coefficient of friction approximately 30% lower than EP, which consequently also results in a decrease in measured steady state temperature from 69 ± 3 to $50 \pm 6\,^{\circ}$C. Regarding nano-particles, the influence on mechanical properties is less predictable. Both positive and negative effects of adding nano-particles are found in the literature, and the mechanisms behind reported improvements are

Please cite this article in press as: T.Ø. Larsen et al., The effect of particle addition and fibrous reinforcement on epoxy-matrix composites for severe sliding conditions, Wear (2007), doi:10.1016/j.wear.2006.12.078

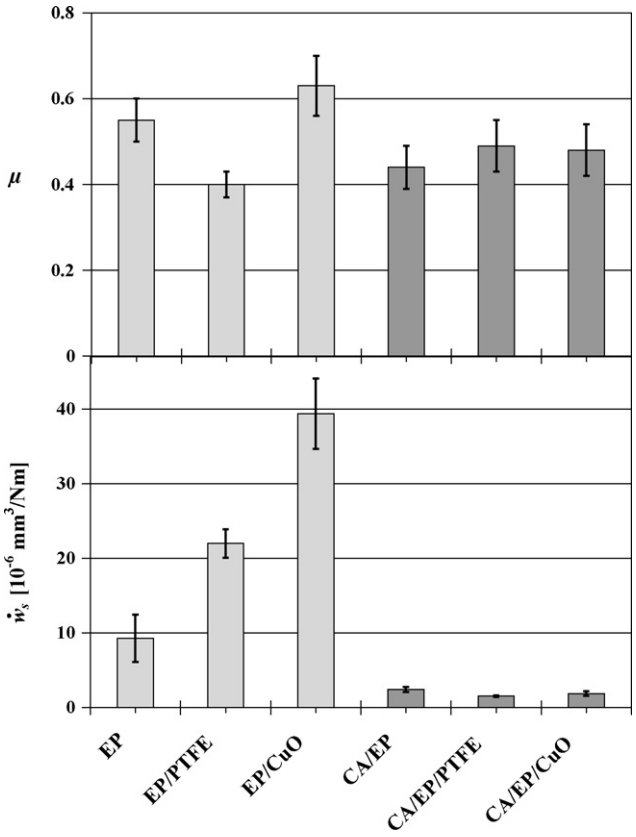

Fig. 10. Specific wear rates $\dot{w}_s$ and coefficients of friction μ measured for different materials. Composites without carbon/aramid reinforcement are measured at the pv condition: 0.25 MPa, 6.0 m/s, whereas composites with carbon/aramid reinforcement are measured at the pv condition: 0.50 MPa, 3.0 m/s.

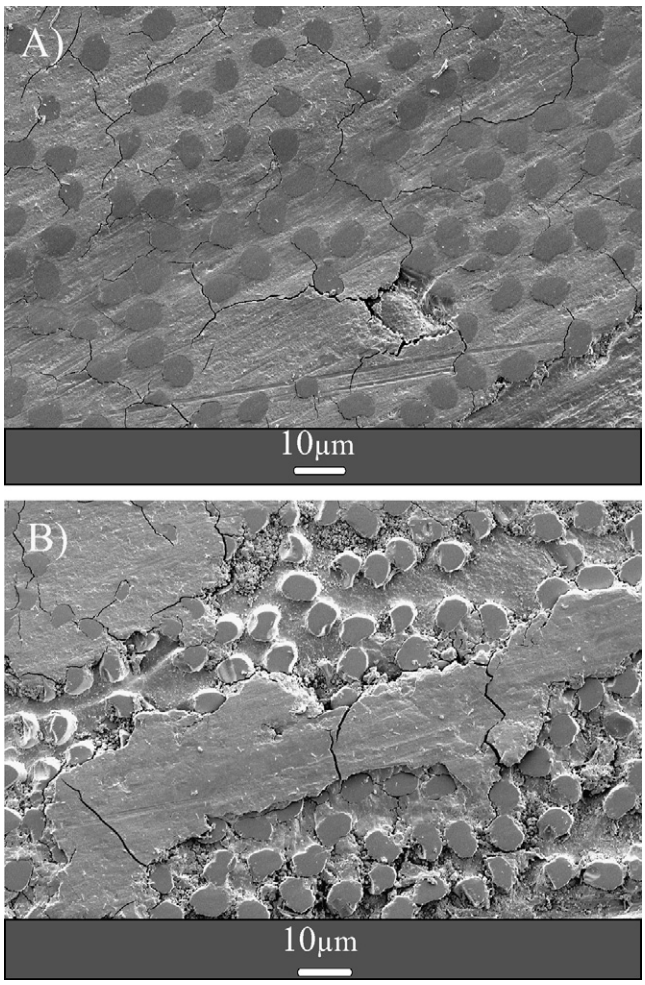

Fig. 11. SEM images (A) and (B) show the surface of CA/EP/CuO worn at the pv condition: 0.50 MPa, 3.0 m/s. Carbon fibers worn normal to the counterface are seen. Both images show micro-cracking of resin but image (B) additionally shows exposed fiber ends.

not entirely understood. In this study, it is hypothesized that the high wear rate for EP/CuO is associated with the large interfacial area between particles and resin, which might result in a strengt reduction of the material and thereby in an elevated wear rate. When PTFE and nano-CuO are added along with the carbon/aramid weave, a minor improvement in wear behavior is seen instead of a negative influence. The coefficient of friction is basically unaffected by addition of these particles. Thus, the negative effect of nano-CuO on wear seen for EP/CuO is not found for CA/EP/CuO, and the positive effect of PTFE on friction seen for EP/PTFE is not found for CA/EP/PTFE. This indicates that the friction and wear behavior are largely controlled by the fibers and not the particles.

The reason why PTFE has no effect on μ in CA/EP/PTFE might be due to the stiffness of the carbon fibers, which on micro-scale possibly act as a stiff brush. If a PTFE containing third-body (or transfer film) is formed, it is likely to be disrupted or abraded by these stiff fibers. The effect of PTFE and nano-CuO reported here is examined at only one concentration of particles. The effect of adding nano-CuO in different concentrations to the neat epoxy resin is currently being investigated. Furthermore, possible synergy effects of adding PTFE particles together with different concentrations of nano-CuO is being examined at two pv conditions and at two levels of counterface roughness.

3.5. SEM images of worn surfaces

In this section SEM images of worn surfaces for the fiber-reinforced composites are shown. Generally, the presence of PTFE or nano-CuO particles do not give raise to any differences in the appearance of the worn surfaces. Therefore, the emphasis is on discussing the difference in wear behavior for different fiber types and relating this to the significant difference in wear rates found for the two types of weave, cf. Section 3.2. Fig. 11 shows a worn surface of CA/EP/CuO with carbon fibers in the normal direction. It seems like the first wear step is micro-cracking of the resin between the fibers. This results in resin removal, which leaves fiber ends exposed. Such exposed fiber ends, which are observed for both carbon and glass fibers, are brittle and fragile when they are no longer protected by the resin. These exposed ends are therefore expected to be fractured and removed easily. Thus, a repeating process might be imagined, which starts with micro-cracking of resin, followed by resin removal and finally proceeding to fracture and removal of fiber fragments. Fiber ends are not seen in some of the resin on the surface, cf. Fig. 11 B. This indicates, that

Please cite this article in press as: T.Ø. Larsen et al., The effect of particle addition and fibrous reinforcement on epoxy-matrix composites for severe sliding conditions, Wear (2007), doi:10.1016/j.wear.2006.12.078

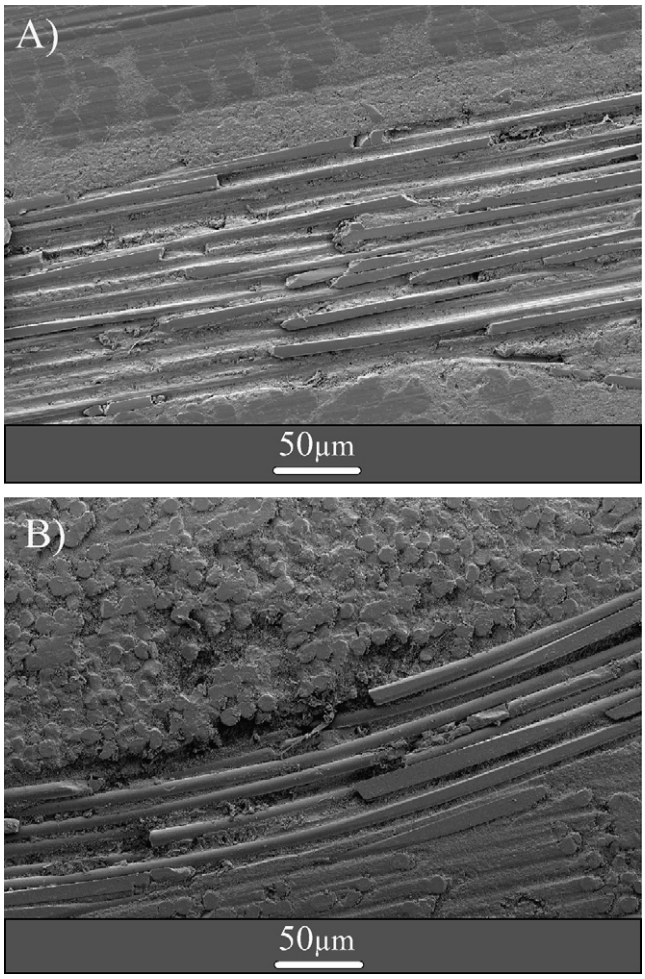

Fig. 12. SEM images of worn surfaces. (A) CA/EP/PTFE with carbon and aramid fibers, respectively, parallel and normal to the counterface. (B) G/EP with glass fibers both normal and parallel to the counterface. The *pv* condition is in both cases: 0.50 MPa, 3.0 m/s.

back-transfer of worn-off material to the composite surface is occurring.

According to the results given in Fig. 10, addition of nano-CuO to the epoxy resin leads to a major increase in wear rate for EP/CuO compared to EP. Micro-cracking of the resin with nano-CuO are therefore expected to occur at a higher rate for CA/EP/CuO compared to CA/EP. However, since the wear rates are at roughly the same level for these two materials, it indicates that micro-cracking of the resin is not the rate controlling step. Fig. 12 A shows a worn surface of CA/EP/PTFE. Aramid fibers oriented normal to the counterface are seen. As opposed to the carbon and glass fibers, the aramid fibers do not show exposed fiber ends. Instead, these are on level with the resin and seem to prevent micro-cracking of the resin due to their toughness. Furthermore, carbon fibers oriented parallel to the counterface are seen. These partially exposed fibers seem to be worn thinner and then ultimately fracture into smaller pieces, which are probably swept away easily. Fig. 12 B shows a worn surface of G/EP. The wear mechanism for glass fibers are visually similar to carbon fibers. The glass fibers also show fiber thinning and exposed fiber ends followed by fiber fracture. The wear mechanisms deduced from the SEM images presented here agrees well with the mechanisms proposed by Friedrich et al. in relation to studies on unidirectional continuous fiber PMCs [21,22].

Based on the observations discussed above, the significant difference in wear rate between G/EP and CA/EP might be explained as follows: the tough and non-abrasive aramid fibers prevent micro-cracking of the resin. These are therefore not exposed or fractured but instead worn by a fibrillation mechanism, which makes fiber removal more difficult. The carbon fibers are worn in a brittle manner, but they presumably also posses lubrication properties, which lower μ, cf. Fig. 5, and thereby also the interfacial temperature. The latter is expected to have a decreasing influence on the wear rate. On the other hand, the glass fibers in G/EP are both brittle and abrasive. During sliding, fractured glass fibers might result in third-body abrasive wear and roughening of the steel counterface, cf. Fig. 6. Both of these factors are expected to accelerate the wear rate.

3.6. Data obtained at severe *pv* conditions

This section discusses tribological behaviors observed at the three most severe *pv* conditions: ($p = 1.0$ MPa, $v = 3.0$ m/s), ($p = 0.50$ MPa, $v = 6.0$ m/s) and ($p = 1.0$ MPa, $v = 6.0$ m/s). Fig. 13 shows examples of frictional behavior for different composites. Firstly, good agreement is seen between measured frictional forces and corresponding temperatures as should be expected. Secondly, G/EP reaches a steady state level (D) while all the composites with carbon/aramid reinforcement (A–C) show a gradual increase in frictional force as a function of time and never reaches steady state. This difference in behavior for the two types of weave is seen for all measurements conducted at these conditions. The same also applies when the composites are measured in the P–AP orientation. This increase in frictional force seems to continue until the material basically falls apart due to decomposition. The rate of frictional increase grows at increasingly severe sliding conditions. For G/EP, the response

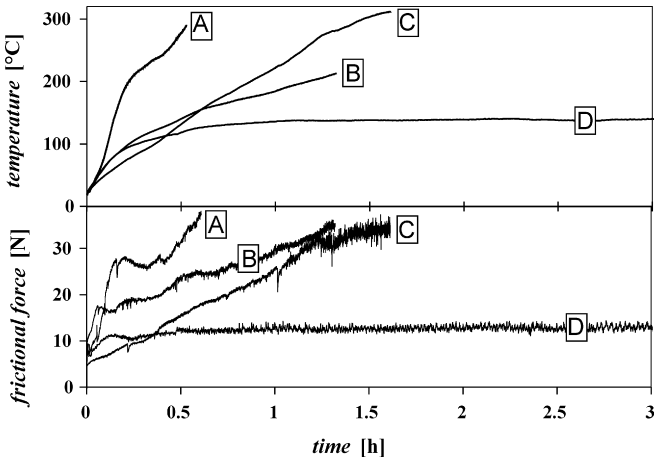

Fig. 13. Frictional forces and corresponding interfacial temperatures measured as a function of time for different materials. (A) CA/EP/PTFE at the condition $p = 1.0$ MPa, $v = 6.0$ m/s, (B) CA/EP at the condition $p = 1.0$ MPa, $v = 3.0$ m/s, (C) CA/EP/CuO at the condition $p = 0.50$ MPa, $v = 6.0$ m/s and (D) G/EP at the condition $p = 0.50$ MPa, $v = 6.0$ m/s.

Please cite this article in press as: T.Ø. Larsen et al., The effect of particle addition and fibrous reinforcement on epoxy-matrix composites for severe sliding conditions, Wear (2007), doi:10.1016/j.wear.2006.12.078

to increasingly severe conditions is instead an increasing fluctuation of the frictional force around a relatively steady level. The latter is probably due to decomposition, which generally is observed to some extent for all composites tested at these conditions.

It is believed that this increase in frictional force seen for the carbon/aramid reinforcement is caused by high and increasing interfacial temperatures. At the conditions in question the resin at the surface decomposes to some extent and therefore becomes brittle and fragile. The resin just below the surface is probably beyond the glass transition temperature and consequently becomes rubbery. When the neat resin (EP) is tested at rough sliding conditions it wears with a fast rate and the frictional force fluctuates but does not show a steady increase as a function of time. Thus, this phenomenon does not seem to be explained solely by decomposition and softening, respectively, of the resin. A possible explanation which considers the combined effect of resin and fibers is given in the following: this gradual increase in frictional force is probably caused by an increase in the real area of contact (A_r). When the resin decomposes and softens, it possibly no longer supports the fibers sufficiently to withstand the local pressures. Fig. 14 A shows exposed carbon fibers where the resin is removed due to decomposition. Such exposed carbon fibers are likely to buckle and/or fracture if the local pressure is high enough. Thus, the load carrying capacity is reduced, which contributes to an increase in A_r. However, the same arguably applies for the glass fibers, which do not show a steady increase in frictional force. Therefore, this phenomenon is presumably

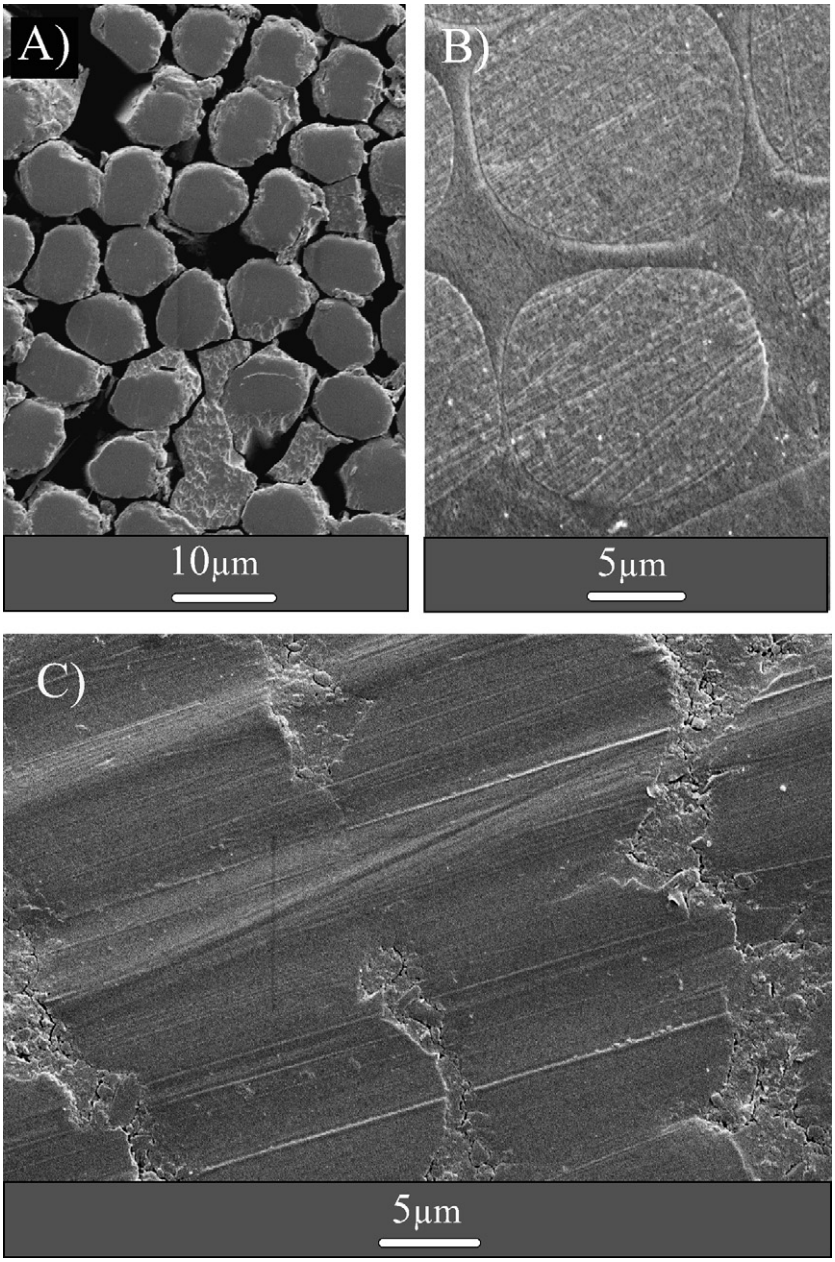

Fig. 14. SEM images of (A) carbon fibers worn normal to the surface, (B) a polished surface with aramid fibers in the normal orientation and (C) aramid fibers worn normal to the surface.

Please cite this article in press as: T.Ø. Larsen et al., The effect of particle addition and fibrous reinforcement on epoxy-matrix composites for severe sliding conditions, Wear (2007), doi:10.1016/j.wear.2006.12.078

close related to the aramid fibers. Generally, these fibers have poor properties in compression and suffers from rapidly decreasing mechanical properties when temperatures are beyond 200 °C [4,23]. Because of this, the load is probably carried mainly by the carbon fibers especially at elevated temperatures. Consequently, the highest local temperatures are also expected to be in the vicinity of the carbon fibers, which might partly explain why removal of resin due to decomposition seems to occur mainly around these fibers. Fig. 14 C shows aramid fibers worn normal to the surface. The fibers are surrounded by resin and appear to be deformed and also show abrasive wear tracks, which might be seen more clearly by comparison with a gently polished surface containing aramid fibers, cf. Fig. 14 B. Thus, it might be imagined that the aramid fibers soften and conform increasingly to the counterface as the temperature raises. This will increase A_r and thereby the frictional force, which in turn will increase the temperature and so on.

4. Conclusions

The friction and wear behavior for an epoxy resin reinforced by either a glass fiber (G/EP) or a carbon/aramid hybrid weave (CA/EP) are examined at nine different pressure–velocity pv conditions. The following conclusions are drawn: an average decrease in the coefficient of friction μ of approximately 35% is found by substituting glass fibers with carbon and aramid fibers. This decrease is considered to be due to the lubricating effect of carbon fibers as opposed to the abrasive nature of glass fibers. Although there are a few exceptions, μ is found to be roughly independant of contact pressure p and sliding velocity v. The average level of wear rates $\dot{w}$ for G/EP, at the six mildest pv conditions, is a factor of 22 higher than for CA/EP. This is believed to be caused by the following main factors: the aramid fibers seem to inhibit micro-cracking of the resin, which in the case of glass and carbon fibers leads to exposed fiber ends. These exposed and brittle fiber ends seem to be fragmented and broken easily relative to the tough aramid fibers, which are worn by a fibrillation mechanism. Furthermore, third-body abrasive wear caused by fragmented glass fibers probably contributes significantly to the high wear rate found for G/EP.

For G/EP, it is found beneficial if the fibers in the weave are oriented parallel and anti-parallel (P–AP) with respect to sliding direction instead of normal and parallel (N–P). The difference between these fiber orientations becomes more pronounced at high v–low p conditions. At the pv condition: 0.25 MPa and 6.0 m/s, the wear rate is reduced by a factor of 2.6 by changing fiber orientation form N–P to P–AP.

Incorporation of micro-scale PTFE particles and nano-scale CuO particles into either the neat epoxy resin or into the resin along with the carbon/aramid weave is reported. According to SEM images, the micro-structures and particle distributions in the produced composites seem promising. However, addition of nano-CuO into the neat resin results in a deterioration in friction and especially wear properties. PTFE particles also cause an increase in $\dot{w}$ but a 30% decrease in μ. When these particles are added along with carbon/aramid reinforcement, a minor improvement in wear and no difference in friction are found. This indicates that the friction and wear properties are largely controlled by the fibers.

It is found that the measured depth wear rates $\dot{w}_t$ for G/EP and CA/EP increases gradually as a function of p and v as expected. However, $\dot{w}_t$ increases more rapidly as a function of these two parameters than predicted by theory. This deviation is believed to be caused mainly by a temperature induced deterioration of material properties with increasingly severe pv conditions. At the three most severe pv conditions the tested composites all show signs of decomposition. The composites with carbon/aramid reinforcement show a steady increase in friction and interfacial temperature as a function of time, which leads to severe decomposition and ultimately failure. This behavior is probably due to softening and decomposition of resin leading to fracture and softening of carbon and aramid fibers, respectively. The glass fiber-reinforced composite does not show this phenomenon but has a relatively steady behavior despite decomposition of resin and development of larger scale cracks.

Acknowledgements

The work is financially supported by a grant given in equal parts by the Technical University of Denmark, The Danish Research Training Council and Civilingeniør Frederik Leth Christensens ALMENNYTTIGE FOND. The latter is furthermore gratefully acknowledged by the authors for financing the applied pin-on-disk apparatus.

References

[1] G.W. Stachowiak, A.W. Batchelor, Engineering Tribology, Butterworth and Heinemann, 2001.
[2] Q. Zhao, S. Bahadur, Investigation of the transition state in the wear of polyphenylene sulfide against steel, Tribol. Lett. 12 (2002) 23–33.
[3] H. Schönherr, J. Vancso, The mechanism of PTFE and PE friction deposition: a combined scanning electron and scanning force microscopy study on highly oriented polymeric sliders, Polymer 39 (1998) 5705–5709.
[4] W.D. Callister, Materials Science, Engineering an Introduction, 6th ed., John Wiley and Sons Inc., 2003.
[5] B. Harris, Engineering Composite Materials, 2nd ed., IOM Communications Ltd., 1999.
[6] I.K. Partridge, Advanced Composites, Elsevier Applied Science, 1989.
[7] K. Friedrich, Z. Lu, A.M. Häger, Recent advances in polymer composites' tribology, Wear 190 (1995) 139–144.
[8] K. Friedrich, Z. Zhang, A.K. Schlarb, Effects of various fillers on the sliding wear of polymer composites, Compos. Sci. Technol. 65 (2005) 2329–2343.
[9] S. Kalpakjian, S.R. Schmid, Manufacturing Engineering and Technology, Prentice Hall, 2001.
[10] M. Cirino, K. Friedrich, R.B. Pipes, Evaluation of polymer composites for sliding and abrasive wear applications, Composites 19 (1988) 383–392.
[11] T. Tsukizoe, O. Nobuo, Friction and wear performance of unidirectionally oriented glass, carbon and stainless steel fiber-reinforced plastics, in: K. Friedrich (Ed.), Friction and Wear of Polymer Composites—Composite Materials Series, vol. 1, Elsevier, New York, 1986, pp. 205–231.
[12] M.H. Cho, S. Bahadur, A.K. Pogosian, Friction and wear studies using Taguchi method on polyphenylene sulfide filled with a complex mixture of MoS_2, Al_2O_3 and other compounds, Wear 258 (2005) 1825–1835.
[13] L. Chang, Z. Zhang, C. Breidt, K. Friedrich, Tribological properties of epoxy nanocomposites I. Enhancement of the wear resistance by nano-TiO_2 particles, Wear 258 (2005) 141–148.

Please cite this article in press as: T.Ø. Larsen et al., The effect of particle addition and fibrous reinforcement on epoxy-matrix composites for severe sliding conditions, Wear (2007), doi:10.1016/j.wear.2006.12.078

[14] G.W. Sawyer, K.D. Freudenberg, P. Bhimaraj, L.S. Schadler, A study on the friction and wear behaviour of PTFE filled with alumina nanoparticles, Wear 254 (2003) 573–580.
[15] C.J. Schwarts, S. Bahadur, Studies on the tribological behavior and transfer film-counterface bond strength for polyphenylene sulfide filled with nanoscale alumina particles, Wear 237 (2000) 261–273.
[16] M.Z. Rong, M. Qiu Zhang, L. Hong, H. Zeng, B. Wetzel, K. Friedrich, Microstructure and tribological behavior of polymeric nanocomposites, Ind. Lubr. Tribol. 53 (2001) 72–77.
[17] G. Shi, M.Q. Zhang, M.Z. Rong, B. Wetzel, K. Friedrich, Friction and wear of low nanometer Si_3N_4 filled epoxy composites, Wear 254 (2003) 784–796.
[18] S. Bahadur, D. Gong, The action of fillers in the modification of the tribological behavior of polymers, Wear 158 (1992) 41–59.
[19] T.Ø. Larsen, Ph.D. thesis, in preparation.
[20] T. Mahrholz, L. Herbeck, U. Riedel, New high-performance fibre-reinforced nanocomposites, JEC-Composites 9 (2004) 71–75.
[21] K. Friedrich, P. Reinicke, Friction and wear of polymer-based composites, Mech. Compos. Mater. 34 (1998) 503–514.
[22] K. Friedrich, R. Reinicke, Z. Zhang, Wear of polymer composites, Eng. Tribol. Part J 216 (2002) 415–426.
[23] K. Potter, An Introduction to Composite Products, Chapman & Hall, 2–6 Boundary Row, London, UK, 1997.

Please cite this article in press as: T.Ø. Larsen et al., The effect of particle addition and fibrous reinforcement on epoxy-matrix composites for severe sliding conditions, Wear (2007), doi:10.1016/j.wear.2006.12.078

Changes in the tribological behavior of an epoxy resin by incorporating CuO nanoparticles and PTFE microparticles

Available online at www.sciencedirect.com
ScienceDirect
Wear xxx (2007) xxx–xxx
WEAR
www.elsevier.com/locate/wear

Changes in the tribological behavior of an epoxy resin by incorporating CuO nanoparticles and PTFE microparticles

Thomas Ø. Larsen [a], Tom L. Andersen [b], Bent Thorning [c], Andy Horsewell [d], Martin E. Vigild [a,*]

[a] *Danish Polymer Centre, Department of Chemical Engineering, NanoDTU, Technical University of Denmark, DK-2800 Kgs. Lyngby, Denmark*
[b] *Risø National Laboratory, Materials Research Department, DK-4000 Roskilde, Denmark*
[c] *Elektro-Isola A/S, Grønlandsvej 197, DK-7100 Vejle, Denmark*
[d] *Department of Manufacturing Engineering and Management, Technical University of Denmark, DK-2800 Kgs. Lyngby, Denmark*

Received 13 December 2006; received in revised form 6 August 2007; accepted 8 October 2007

Abstract

Different amounts of CuO nanoparticles are incorporated into both a neat epoxy resin and into an epoxy resin containing PTFE microparticles. The content of CuO is varied in the range of 0–10 vol.% while the PTFE content is fixed at 7.5 vol.%. The dispersion state of added particles is examined by scanning electron microscopy (SEM) and transmission electron microscopy (TEM), which show a relatively good dispersion of both kinds of particles. Differential scanning calorimetry (DSC) and Vickers hardness measurements show no clear changes in glass transition temperature or hardness as a function of the nano-CuO content. However, both parameters are reduced when PTFE is added. Friction and wear data is collected using a custom-made tribotester of the pin-on-disk type. Measurements are performed under dry-sliding conditions against smooth steel counterfaces. When a pressure–velocity (*pv*) condition of 0.25 MPa, 6.0 m/s is applied the following is found: without PTFE, the coefficient of friction (μ) is roughly independent of the nano-CuO content. When PTFE is added, an average reduction in μ of 35% is found in the CuO range of 0–0.4 vol.%. At higher CuO concentrations the friction lowering effect of PTFE deteriorates. Addition of CuO increases wear relative to the neat epoxy at all concentrations. When nano-CuO is added to epoxy with PTFE incorporated, the wear rate decreases slightly up to a CuO content of 0.4 vol.% after which it increases. The measurements are repeated for some of the composites using a smoother counterface. This gives rise to significantly less wear, which for composites without PTFE is attributed to formation of a protective transfer film. At a *pv* condition of 1.16 MPa, 1.0 m/s the following is found: composites without PTFE generally show an unsteady behavior with high average wear rates whereas composites with PTFE generally show a good friction and wear performance. The best results are seen at a CuO content in the range of 0.1–0.4 vol.%. The latter shows a positive synergistic effect of adding a small amount of nano-CuO together with PTFE into the epoxy resin.

Keywords: Friction; Wear; Epoxy resin; CuO nanoparticles; PTFE microparticles; Nanocomposites

1. Introduction

Control of friction and wear of polymer-matrix-composites (PMCs) is of importance in many applications, e.g. vacuum pumps, seals, bearings and implants. Solid lubricants are often added to the polymer matrix to decrease adhesion to the counterface or to form a transfer film with a low shear strength, which may reduce friction and wear. Different types of reinforcements are applied to improve mechanical properties, which in turn often enhance the wear resistance. Relatively much research has been conducted on the effect of solid lubricants [1–5], reinforcing fibers [6–15] and inorganic micro-scale particles [16–20] for tribological optimization of PMCs.

* Corresponding author. Present address: Danish Polymer Centre, Department of Chemical Engineering, Technical University of Denmark, Building 423, DK-2800 Kgs. Lyngby, Denmark. Tel.: +45 45252967; fax: +45 45882161.
E-mail address: mev@kt.dtu.dk (M.E. Vigild).

0043-1648/$ – see front matter © 2007 Published by Elsevier B.V.
doi:10.1016/j.wear.2007.10.003

Presently, the use of inorganic nano-scale particles receives a lot of attention. Utilization of these nanoparticles seems to be a promising way to improve friction and wear properties. Generally, an optimum concentration of nanoparticles is found in the range of 2–5 vol.% [21], which is approximately a factor of 10 lower than typically found for microparticles. Such a low particle content makes it possible to use nanoparticles to improve the properties of resins used for continuous fiber reinforced composites with a high fiber content. In this respect, it has been shown that nanoparticles can penetrate fiber bundles whereas microparticles are filtered out [22]. Furthermore, the problems with abrasiveness as seen for hard microparticles may be avoided by going to nano-size.

The mechanisms behind optimization by nanoparticles are not entirely understood and cannot be explained by models for larger-scale reinforcement. However, based on existing publications, the overall reasons for tribological improvements can roughly be divided into two categories: (1) improvements are due to better mechanical and thermal properties of the PMC, and (2) improvements are due to an enhanced ability to form a thin, homogeneous and tenacious transfer film on the steel counterface. With respect to mechanical properties, it is reported that nanoparticles frequently increase strength and stiffness while simultaneously increasing strain-to-failure and toughness [23–28]. This is opposite the trend typically found for microparticles where improvement in one property often is obtained at the expense of another [29]. The combination of a high tensile strength (σ_s) and stain-to-failure (ϵ) is expected to enhance the wear resistance according to the Ratner-Lancaster correlation, which implies that wear of polymers is proportional to $1/\sigma_s\epsilon$ [30]. With respect to transfer film formation several papers report that improved wear properties due to nanoparticle addition are correlated with the formation or stabilization of a protective transfer film on the counterface [31–34]. In some cases, such an improvement is reported despite a measured deterioration in flexural strength [35,36]. Thus, improvements in mechanical properties may not always be a requirement for tribological optimization. The stabilization of transfer films is typically attributed to tribo-chemical reactions, which increase the adhesion of the film to the counterface, or to an ability of the particles to smoothen the counterface in a manner which favors adhesion. Furthermore, it is suggested that the cohesive strength of the transfer film is increased because the nanoparticles are capable of blending well with the wear debris [21,36].

In this study, CuO nanoparticles are incorporated into an epoxy resin with volume fractions ranging from 0 to 10 vol.%. Furthermore, possible synergistic effects of adding different amounts of nano-CuO together with PTFE microparticles into the epoxy resin is examined. Epoxy is a widely used resin for PMCs and generally posses good mechanical and thermal properties. However, the brittleness of epoxy resins often leads to relatively poor tribological properties. It is therefore interesting to examine if the tribological properties can be improved by incorporating CuO nanoparticles. The effect of different microparticles, e.g. TiO_2, CuO, CuS, ZnF_2 and CaF_2, are reported by others [37]. The effect on wear depends on the type of particles applied. Since CuO is reported to yield good results on micro-scale [38,39] it seems like a logical choice also to test this compound on nano-scale.

As mentioned above, the positive effect of particles is often through stabilization of transfer films. However, epoxy resins do generally not form effective transfer films due to the cross-linked molecular structure. Therefore, the combined effect of adding PTFE as a solid lubricant as well as nano-CuO is investigated. The underlying hypothesis is that the nanoparticles might stabilize a transfer film created by the incorporated PTFE and thereby decrease friction and wear.

The tribological data are collected using a custom-made tribotester of the pin-on-disk type. Measurements are performed under dry-sliding conditions against smooth steel surfaces at ambient temperature and humidity.

The investigation presented here is a part of a more comprehensive study, which aims at improving the properties of epoxy when used as a resin for fabric reinforced PMCs produced by prepreg technology. The three components, i.e. the epoxy pre-polymer, nano-CuO and PTFE are therefore applied in a solvent dispersed form, which make them potentially applicable for prepreg production. This may differentiate the production method applied here from many of the studies referred to in this introduction.

2. Experimental

2.1. Materials

The applied resin is a polyfunctional epoxy of the novolac type obtained from Hexion Specialty Chemicals as a 70 wt% solution in methyl ethyl ketone (Epikote 1153-B-70). The incorporated PTFE particles (TF 9207) are purchased as micropowder from Dyneon^{TM}. CuO nanoparticles (NanoArc ^{TM} U1102DBE) are delivered by Nanophase Technologies Corporation. The particles are received as coated particles dispersed in a diester solvent mixture. The coating accounts for approximately 20 wt% of the dry-weight of the nano-CuO and enables a relatively stable solvent dispersion. In one case, a test specimen is prepared using non-coated CuO nanoparticles (NanoArc ^{TM} Copper Oxide), which are delivered as powder by Nanophase Technologies as well.

2.2. Specimen preparation and compositions

PTFE and nano-CuO particles are mixed with the resin solution in the following way: first, a PTFE dispersion is prepared by swelling PTFE micro-powder in xylene (ratio 1:3) while stirring. The PTFE dispersion is subsequently added quantitatively to the epoxy solution and stirred mechanically. The as received nano-CuO dispersion is sonicated for 2 h before mixing it quantitatively with the epoxy solution using mechanical stirring for 5 min. Epoxy dispersions with different particle content are transferred to a custom-made mold and cured by heating: 2 days at 45 °C, 1 h at 100 °C, 30 min at 130 °C, 1.5 h at 150 ° C and finally 30 h at 170 °C. This slow and prolonged heating procedure is applied partly to avoid porosity caused by uncontrolled solvent evaporation and partly to make sure that all residual sol-

Please cite this article in press as: T.Ø. Larsen, et al., Changes in the tribological behavior of an epoxy resin by incorporating CuO nanoparticles and PTFE microparticles, Wear (2007), doi:10.1016/j.wear.2007.10.003

Table 1
Composition and nomenclature for tested composites

Nomenclature without PTFE	Nomenclature with 7.5 vol.% PTFE	CuO content (vol.%)
EP	EP/PTFE	0
EP/0.1	EP/PTFE/0.1	0.1
EP/0.2	EP/PTFE/0.2	0.2
EP/0.4	EP/PTFE/0.4	0.4
EP/1.0	EP/PTFE/1.0	1.0
EP/3.0	EP/PTFE/3.0	3.0
EP/6.0	EP/PTFE/6.0	6.0
EP/10	–	10

vent is removed. The dimensions of the composites after curing are 70 mm × 70 mm ×1 mm. These are subsequently divided into smaller slabs with a thickness of 1 mm and a cross-section of 7.7 mm ×5.0 mm. In order to perform pin-on-disk measurements, these small slabs are glued on top of a test-pin with the same cross-sectional area and a height of 15 mm. Thus, friction and wear tests are performed on composite slabs with an apparent area of contact of 38.5 mm^2 and an initial thickness of 1 mm.

For composites where PTFE is incorporated the content is fixed at 7.5 vol.%. The nano-CuO content is varied in the range of 0.1–10 vol.%. Compositions and nomenclature of the produced and tested composites are given in Table 1. As an example of the applied nomenclature, a composite consisting of epoxy, PTFE and 3 vol.% nano-CuO is given the name EP/PTFE/3.0.

2.3. Measurement of hardness and glass transition temperature

Vickers micro-hardness (HV) of the produced composites is measured (LEITZ-Kleinhrtsprfer). A pyramid-shaped diamond indenter is pressed against polished composite surfaces for 30 s using a load of 200 g. Glass transition temperatures are measured using differential scanning calorimetry (DSC, type TA instruments Q1000) with a heating/cooling rate of 10 °C/min.

2.4. Measurement of friction and wear

The applied pin-on-disk (POD) apparatus is described elsewhere [40] but the principle is summarized in the following. A test-pin is loaded perpendicularly against a rotating disk made of hardened chrome bearing steel (100 Cr6) by applying dead weights (W_N). The test-pin is mounted in a lever-arm via a sample holder. The lever-arm can rotate freely by use of ball bearings but is kept in a fixed position by a load cell which measures the frictional force (F_f). The coefficient of friction (μ) is obtained by using Amontons first law of friction, i.e. $\mu = F_f / W_N$, and is reported as a time-averaged value based on data points in the steady state regime. The wear rate ($\dot{w}$) is obtained simply by measuring the weight loss of the test-pin as a function of time. Furthermore, a non-contact thermometer estimates the interfacial temperature by collecting infrared radiation from the side of the steel disk.

The employed test-procedure is as follows: the steel counterface is abraded using a piece of emery cloth (grade P400 or P800) in order to obtain a fixed initial counterface roughness. Two roughness levels are applied in this study: $R_a = 0.26\ (\pm 0.03)\ \mu m$ and $R_a = 0.074\ (\pm 0.003)\ \mu m$. The test-pin is mounted in the POD lever-arm when abrading it against a piece of emery cloth placed on the steel disk in order to obtain alignment of the surfaces. Before testing, the two sliding surfaces are cleaned using compressed air and tissue paper soaked in acetone. During testing, the accumulated weight loss of the test-pin is determined as a function of time by stopping the test-run briefly at certain time intervals and noting the weight loss to the nearest 0.1 mg. Before each weighing the surface of the test-pin is cleaned as mentioned previously. The materials tested in this study generally show a run-in period followed by steady state where the accumulated weight loss is a linear function of time. The slope of the linear part of the curve is then used to calculate the specific wear rate ($\dot{w}_s$) given by the following equation:

$$\dot{w}_s\ (mm^3/Nm) = \frac{\Delta m}{l \rho W_N} \quad (1)$$

Here l, W_N, Δm and ρ are sliding distance, load, mass loss and density of the worn material, respectively. Steady state is typically reached within 30 min. The duration of the test depends on the wear rate of the test specimen and is in the range of 3–6 h. This corresponds to sliding distances in the range of 11–22 and 65–130 km for sliding velocities of 1.0 and 6.0 m/s, respectively. Frictional forces and disk temperatures are collected automatically by a computer during the test-run. All tribological measurements are repeated at least three times.

2.5. Electron microscopy images

Scanning electron microscopy (SEM, type JEOL JSM 5900) is used to study the structure of the produced composites and also wear scars on the worn surfaces and wear tracks on the counterface. When studying composite structures, the surfaces are polished, cleaned and finally coated with a conducting carbon layer. When studying the wear scars, the worn surfaces are cleaned and coated with a conducting gold layer. Cleaning are in both cases done by removing loose debris by compressed air followed by gently wiping with tissue paper soaked in acetone. Loose debris is removed from the steel disk by compressed air prior to studying the wear track. However, cleaning with acetone on the wear track is omitted in order to avoid removing possible transfer layers. Transmission electron microscopy (TEM, type JIOL 2000 FX) is applied to study the dispersion state of nanoparticles in the epoxy resin. This is done by preparing thin foils with a thickness of approximately 50 nm using an ultramicrotome (LEICA EMFCS) equipped with a cryo-chamber.

3. Results and discussion

3.1. Characterization of the produced composites

In order to obtain improvement by incorporating nanoparticles it is typically a demand that the particles are well-dispersed

Please cite this article in press as: T.Ø. Larsen, et al., Changes in the tribological behavior of an epoxy resin by incorporating CuO nanoparticles and PTFE microparticles, Wear (2007), doi:10.1016/j.wear.2007.10.003

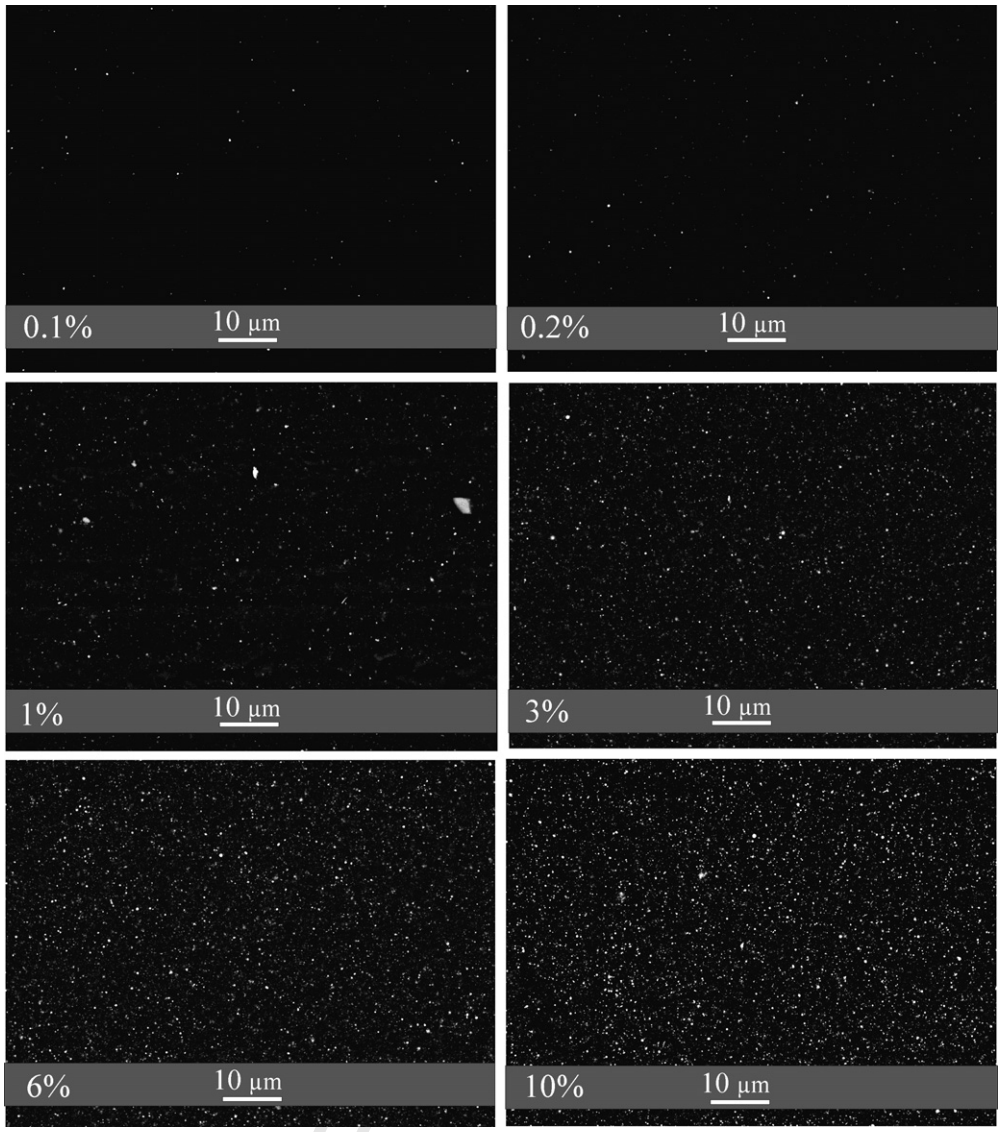

Fig. 1. SEM images of EP containing different amounts (vol.%) of nano-CuO. The images are obtained using a solid-state backscatter electron detector (BSE) resulting in atomic number contrast. This makes the CuO particles appear as bright stars.

in the polymeric matrix. Negative results by nanoparticles are often correlated with an insufficient dispersion, i.e. too many and too large agglomerates [27,41]. This is probably also the reason why negative results typically are obtained at high concentrations of nanoparticles due to increased agglomeration. Fig. 1 shows SEM images of epoxy (EP) filled with different concentrations of CuO. The gradual increase in concentration while going from 0.1 to 10 vol.% is clearly seen from the images. Furthermore, the dispersion seems to be fairly homogeneous at the applied magnification. In order to get a more clear view of the actual size of the particles, TEM images are produced. Fig. 2 shows the dispersion state at a nano-CuO content of 1 and 6 vol.%. A distribution of sizes is seen which ranges from about 30 to 250 nm in diameter. The smallest particles are the primary particles which size-wise agrees with the values given by the manufacture of the particles. An increased tendency to form agglomerates is evident at 6 vol.%. Furthermore, some of the larger particles do not appear to be agglomerates but rather unintentional large particles formed during production. These will probably be very difficult to shear into smaller particles. Compared to other publications, e.g. [23,34,42], the obtained particle distribution seems satisfactory. The images also show that a fairly good dispersion can be obtained by using a simple laboratory mixer when coated nanoparticles are added in a solvent dispersed form.

Fig. 3 shows the micro-structures of (a) EP/PTFE, (b) EP/PTFE/0.2 and (c) EP/PTFE/3.0. Image (a) shows PTFE particles (light gray phase) which are relatively well-distributed in the resin. Image (b) shows PTFE and nano-CuO particles where examples are indicated by a small circle for a nanoparticle and a large circle for a PTFE particle. The image furthermore shows that the nanoparticles apparently have a tendency to locate themselves in the interface between PTFE and EP. Image (c) shows both PTFE and nano-CuO particles which appear to be relatively well-distributed.

Please cite this article in press as: T.Ø. Larsen, et al., Changes in the tribological behavior of an epoxy resin by incorporating CuO nanoparticles and PTFE microparticles, Wear (2007), doi:10.1016/j.wear.2007.10.003

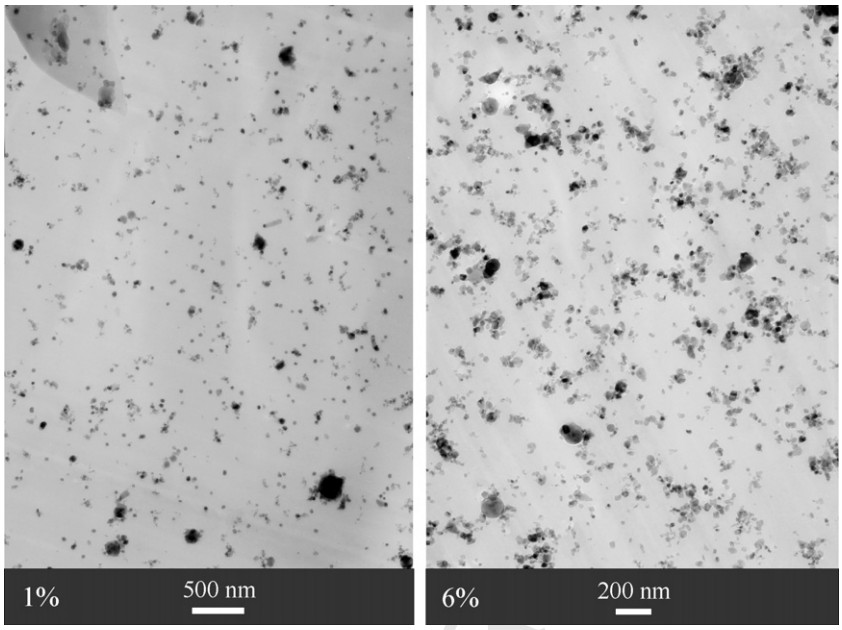

Fig. 2. TEM images of EP containing 1 and 6 vol.% nano-CuO, respectively.

Fig. 4 shows glass transition temperatures (T_g) and Vickers hardness (HV) values measured for EP with different particle content. The T_g values do not show any clear trend as a function of the nano-CuO content. It is expected that a strong interaction over the large interfacial area between nanoparticles and resin might restrict mobility to some extent and thereby cause an increase in T_g. For the PTFE containing composites, the T_g values are generally lower, which may be due to an increased mobility caused by a weak interfacial strength between PTFE and EP. Vickers hardness does not show any clear trend as a function of the nano-CuO content either. However, the hardness is on average reduced by 19% when PTFE is incorporated. Since the hardness of neat PTFE is significantly lower than for EP, a decrease would also be expected based on a rule-of-mixtures estimate.

3.2. Friction and wear at low pressure and high velocity

The tribological data presented in this section is obtained using a contact pressure (p) of 0.25 MPa, a sliding velocity (v)

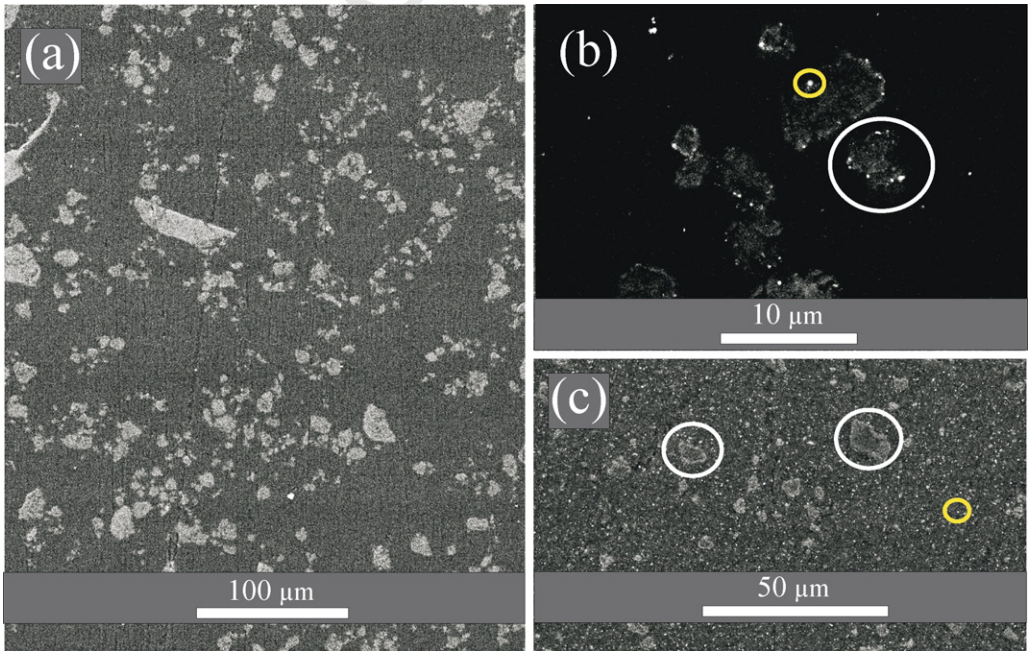

Fig. 3. SEM images showing the structures of (a) EP/PTFE, (b) EP/PTFE/0.2 and (c) EP/PTFE/3.0. Three examples of PTFE particles (large circles) and two examples of a nanoparticle (small circle) are indicated.

Please cite this article in press as: T.Ø. Larsen, et al., Changes in the tribological behavior of an epoxy resin by incorporating CuO nanoparticles and PTFE microparticles, Wear (2007), doi:10.1016/j.wear.2007.10.003

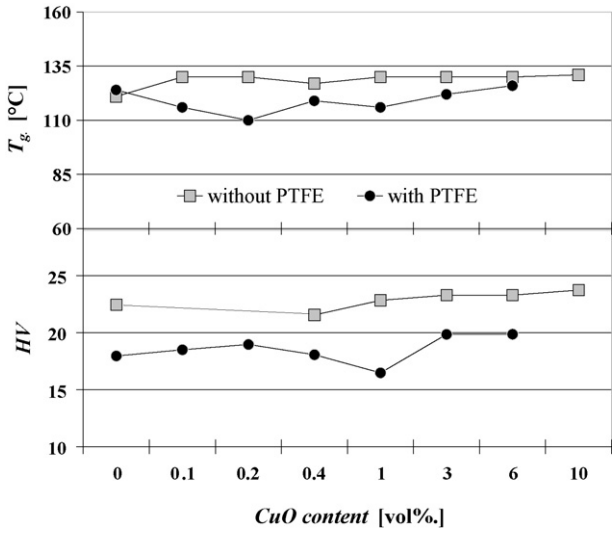

Fig. 4. Glass transition temperature (T_g) and Vickers hardness (HV) measured for EP, with and without PTFE, containing different concentrations of nano-CuO. The lines are guides to the eye.

of 6.0 m/s and a counterface roughness of 0.26 μm R_a. Note that the sliding velocity applied here is highly relative to similar studies, which typically used velocities of 1 m/s or below. Fig. 5 shows measured steady state coefficients of friction (μ) and corresponding disk temperatures. General agreement is seen between friction and temperature as should be expected since the rate of energy dissipation is directly proportional to μ [43]. Without PTFE, μ is roughly independent of the nano-CuO content even though a maximum at EP/1.0 is indicated. When PTFE is added, an average reduction in μ of 35% is found in the CuO

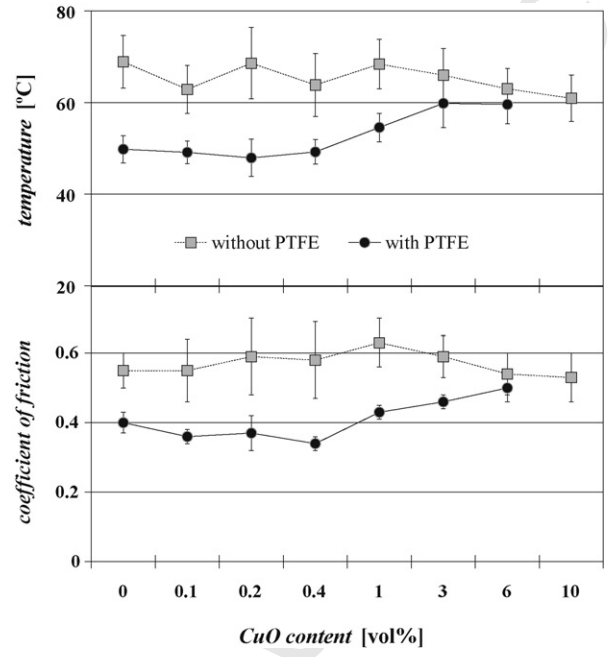

Fig. 5. Coefficients of friction and corresponding disk temperatures measured for EP, with and without PTFE, containing different concentrations of nano-CuO. The applied *pv* condition is 0.25 MPa, 6.0 m/s. The lines are guides to the eye.

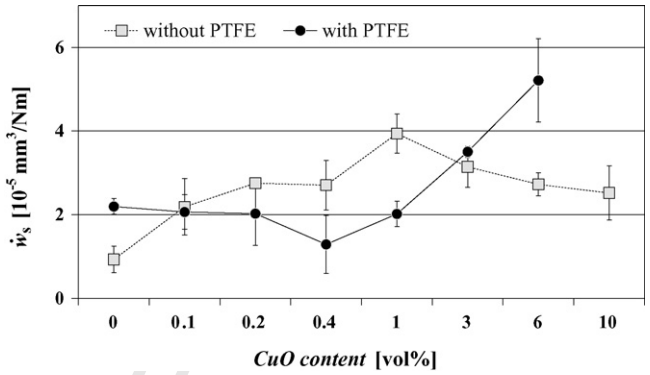

Fig. 6. Specific wear rates ($\dot{w}_s$) measured for EP, with and without PTFE, containing different concentrations of nano-CuO. The applied *pv* condition is 0.25 MPa, 6.0 m/s. The lines are guides to the eye.

range of 0–0.4 vol.%. At higher concentrations of nano-CuO the curves for composites with and without PTFE begin to coincide. This indicates that the friction lowering effect of PTFE deteriorates at a higher CuO content. Furthermore, note that the error bars for composites with PTFE are significantly smaller, which is due to a much more smooth and stable frictional behavior.

In Fig. 6 specific wear rates ($\dot{w}_s$) for EP, with and without PTFE, containing different concentrations of nano-CuO are given. The frictional behavior is to some extent reflected in these wear data. For composites without PTFE, an increase in $\dot{w}_s$ is seen, relative to EP, at all concentrations of nano-CuO. The wear rate increases as a function of the CuO content up to EP/1.0 after which it declines. When PTFE is added to the neat EP, the wear rate increases by a factor of 2.5, which probably is due to weakening of the matrix material caused by PTFE. When CuO is added together with PTFE, the wear rate decreases slightly up to a CuO content of 0.4 vol.% after which it increases significantly.

SEM images of the worn surfaces are produced in order to obtain a better understanding of the wear behavior. Fig. 7 shows images of worn surfaces for (a) the neat EP and (b) EP/3.0. In the case of EP, compressed wear debris and abrasive wear tracks are seen. The more bright regions, e.g. the upper part of the image, contain many small cracks with a length of about 20–30 μm. Image (b) shows the typical behavior found for EP with a CuO content in the range of 0.1–3.0 vol.%. Large cracks of about 100–200 μm are seen perpendicular to the sliding direction. Furthermore, the number and severity of these cracks follow the measured wear rates, i.e. they are mostly observed for EP/1.0 and EP/3.0 with the highest wear rates.

Since hardness (HV), friction (F_f) and temperature is largely unaffected by the CuO content, cf. Figs. 4 and 5, it seems likely that the real area of contact (A_r) also is at the same level at the applied load (W_N) according to $A_r = W_N/HV$. The interfacial shear stress (τ_I) during sliding is presumably also at the same level according to an adhesive model of friction, i.e. $F_f = \tau_I A_r$. Thus, the appearance of these large cracks in Fig. 7(b) is probably caused by a weakening of the material due to incorporation of nano-CuO. This weakening can potentially be due to poor properties of the as-supplied coating on the incorporated nanoparticles. In order to examine this, the composite with the highest wear rate, i.e. EP/1.0 is also produced

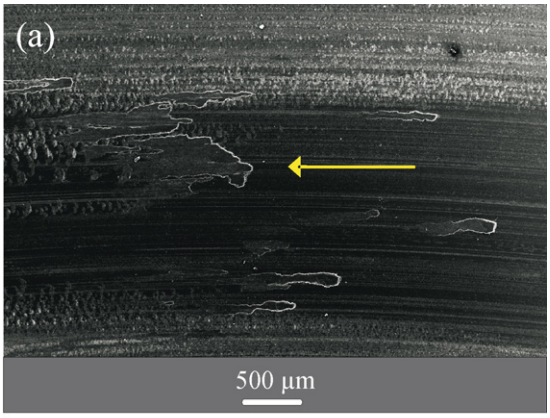

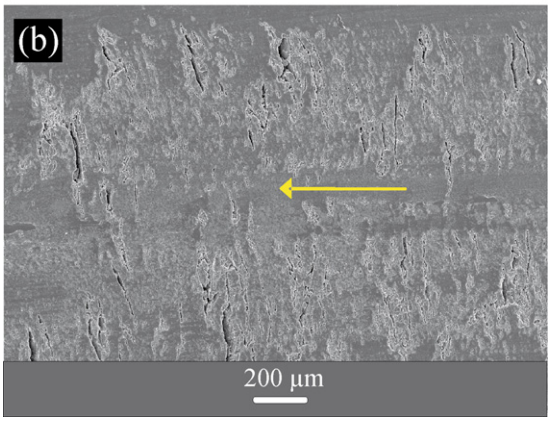

Fig. 7. SEM images showing worn surfaces of (a) the neat EP and (b) EP/3.0. Arrows indicate sliding direction. The applied *pv* condition is in both cases 0.25 MPa, 6.0 m/s.

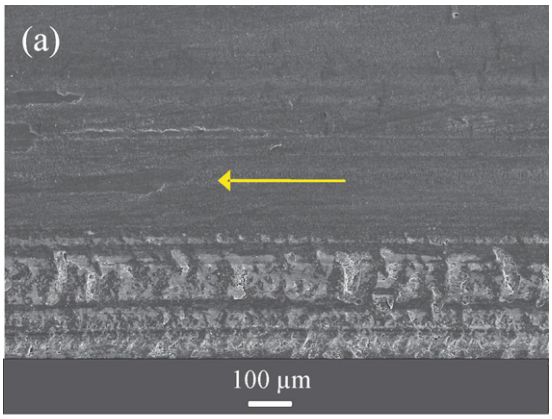

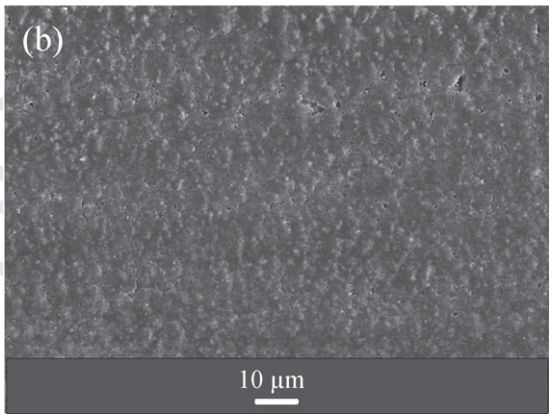

Fig. 8. SEM images showing the worn surface of EP/6.0 at two different magnifications (a) and (b). The arrow indicates sliding direction. The applied *pv* condition is in both cases 0.25 MPa, 6.0 m/s.

using non-coated CuO particles from the same manufacture. The measured values are: $\dot{w}_s = 3.2$ (± 0.6) [10^{-5} mm^3/Nm] and $\mu = 0.55$ (± 0.06) for non-coated particles compared to $\dot{w}_s = 3.9$ (± 0.5) [10^{-5} mm^3/Nm] and $\mu = 0.63$ (± 0.07) for coated particles. Since friction and wear are roughly on the same level it indicates that the coating is not the main reason for the poor wear properties. Bahadur and Sunkara also reported the effect of nano-CuO when added in the range of 0–10 vol.%. The wear rate of the applied polymer (polyphenylene sulfide) decreased because nano-CuO improved transfer film formation. However, the flexural strength was deteriorated in the entire concentration range [35]. In this study, no significant transfer films are observed visually during the measurements presented in Figs. 5 and 6. Generally, only loose debris are formed with no tendency to adhere to the counterface. In short, the high wear rates are believed to be due to weakening of the material by nano-CuO combined with a lack of transfer film formation.

Fig. 8(a) shows a worn surface of EP/6.0. No large cracks are seen on the surface (the same applies for EP/10), which agrees with the lower wear rate relative to EP/1.0 and EP/3.0. Another phenomenon mostly seen at a high CuO content is the accumulation of CuO on the composite surface, which is seen as a light gray track on the lower part of Fig. 8(a). This accumulation is generally seen as isolated tracks or as spots on the worn composite surface. It is confirmed by Energy Dispersive Analysis(EDS) that these tracks or spots contain a large fraction of copper and also in some cases iron. The latter indicates that CuO accumulates to an extent where it becomes capable of causing wear of the steel counterface. This patchy accumulation of copper on the surface could possibly act as a protective coating which decreases wear. On the other hand, accumulation of these hard particles could also increase wear due to abrasive action.

Fig. 8(b) shows the worn surface of EP/6.0 at a higher magnification. The surface appears smooth and only small-scale cracks are seen. Furthermore, it is possible to see nanoparticles distributed in the surface. It is unclear why the wear rate begins to decrease at a high CuO content, but it may indicate a competition between mechanisms, which depend differently on the nano-CuO content. It is not uncommon that incorporation of rigid particles into a polymeric matrix reduces strength and increases toughness. However, the problem with strength reduction is typically diminished by reducing the particle size [44]. Imagine that the strength decreases rapidly at a low particle content and then levels off at higher concentrations. If the toughness simultaneously increases as function of the particle content, e.g. due to enhanced crack deflection, it may explain the observed behavior. Thus, incorporation of particles may increase the number of crack initiation sites due to a week interface while simultaneously increasing toughness by hampering propagation of initiated cracks. Such a behavior has been shown by Spanoudakis and Young for 4.5 μm spherical glass particles in an epoxy resin

Please cite this article in press as: T.Ø. Larsen, et al., Changes in the tribological behavior of an epoxy resin by incorporating CuO nanoparticles and PTFE microparticles, Wear (2007), doi:10.1016/j.wear.2007.10.003

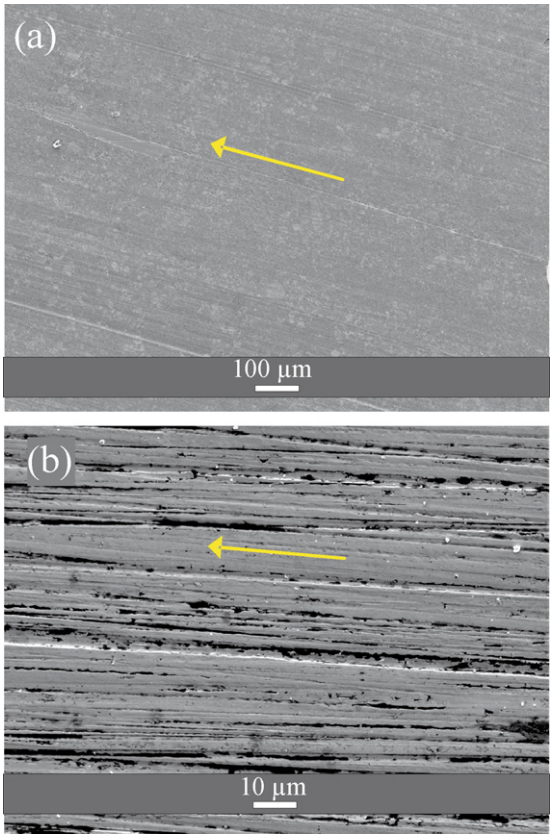

Fig. 9. SEM images of (a) the worn surface of EP/PTFE and (b) the wear track on the steel counterface after sliding against EP/PTFE/0.2. The arrows indicate sliding direction. The applied *pv* condition is 0.25 MPa, 6.0 m/s.

[45]. However, a different behavior is typically seen when going to nano-size.

The worn surface of EP/PTFE shown in Fig. 9(a) appears to be smooth, free from cracks and also shows individual PTFE particles. Similar surfaces are seen for all PTFE containing composites with a nano-CuO content up to 1 vol.%.

The surface for EP/PTFE/6.0 (not shown) appears slightly more rough and the PTFE phase is not easily identified, which agrees with the higher wear rate and coefficient of friction. Fig. 9(b) shows the wear track on the steel counterface after sliding against EP/PTFE/0.2. The appearance of the counterface is similar for all the PTFE containing composites. The dark regions seen in the image are deposits from the composite which is stuck in grooves on the counterface. However, it is not possible to see any indications of an continuous transfer film.

Note that the PTFE particles in Fig. 9(a) seem to be stuck in the surface instead of being pulled out during sliding. Thus, the particles are gradually worn while staying in the surface. It is hypothesized that the formed PTFE containing debris is smeared over the composite surface and thereby decreasing the interfacial shear stress, which lowers μ and results in a more gentle wear mechanism.

Friction and wear begins to increase as a function of the CuO content at EP/PTFE/1.0, which probably is due to the aforementioned interfacial accumulation of hard nanoparticles. This may disrupt the interfacial PTFE containing layer and thereby

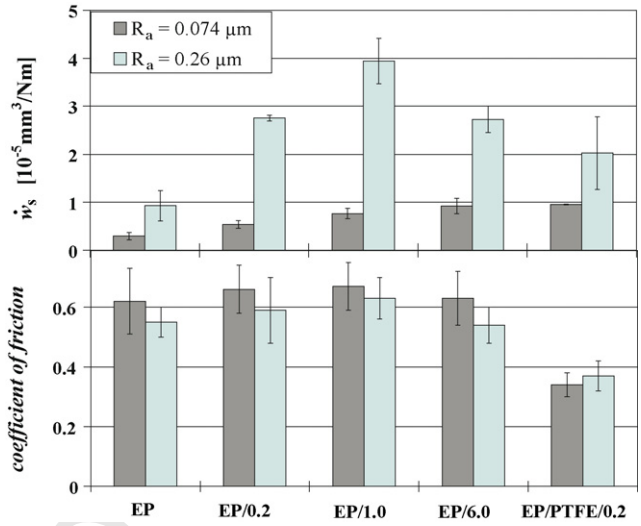

Fig. 10. Coefficients of friction and specific wear rates ($\dot{w}_s$) measured for selected composites at two different levels of counterface roughness (R_a), i.e. 0.26 and 0.07 μm. The applied *pv* condition is in all cases 0.25 MPa, 6.0 m/s.

decrease the lubricating effect. The latter will in turn increase the interfacial shear force and frictional heating, which cause the wear rate to increase simultaneously.

3.3. Friction and wear against a smoother counterface

It is known that the counterface roughness can have a large impact on the formation and stability of polymeric transfer films [46,47]. Schwarts et al. found that addition of alumina nanoparticles to polyphenylene sulfide (PPS) increased wear when sliding against a counterface with a roughness of 0.27 μm R_a while improvements were obtained at other counterface roughnesses. The improvements were attributed to enhanced transfer film coverage [36].

To examine the effect of counterface roughness, some of the tribological tests presented in Section 3.2 are repeated using a smoother counterface with a roughness of 0.074 μm R_a. In Fig. 10 friction and wear data obtained at the two counterface roughnesses are compared. A slight increase in μ is seen when applying the smoothest counterface except for EP/PTFE/0.2. Furthermore, a significant reduction in wear is seen for all composites. The smooth surface does not enable establishment of a transfer film in the case of EP/PTFE/0.2. Thus, the degree of deposit is similar to what is shown in Fig. 9(b). However, for the four composites without PTFE a significant transfer film formation is seen. Fig. 11 shows an example of a transfer film which is formed by sliding against EP/0.2. The lower bright part of Fig. 11(a) is outside the wear track whereas the dark part is the transfer film. This film contains areas where it is thin and homogeneous. In these areas it is possible to see the structure of the steel counterface through the film. In other areas the film is thicker and more lumpy. An example of the latter is shown at a higher magnification in Fig. 11(b). This thick transfer layer appears to have a high concentration of nano-CuO considering that the tested composite only contains 0.2 vol.%. Thus, the proposed accumulation of CuO in the interface, dis-

Please cite this article in press as: T.Ø. Larsen, et al., Changes in the tribological behavior of an epoxy resin by incorporating CuO nanoparticles and PTFE microparticles, Wear (2007), doi:10.1016/j.wear.2007.10.003

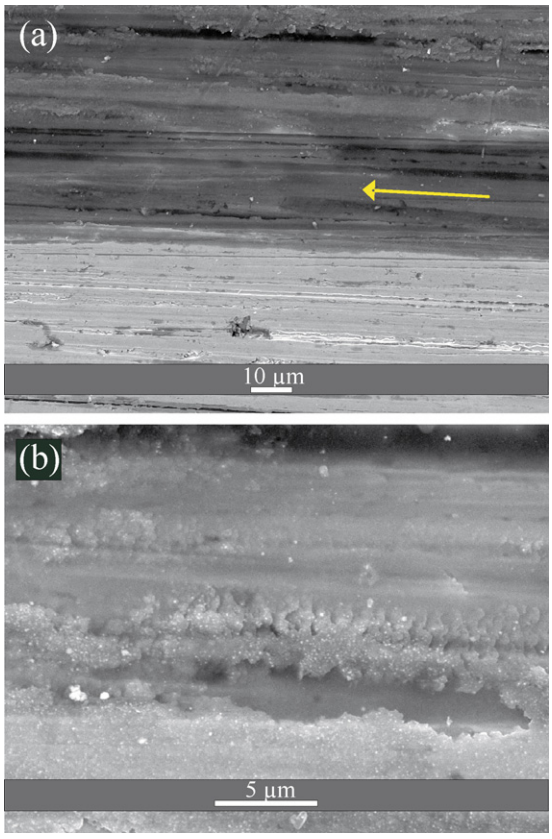

Fig. 11. SEM images of a transfer film formed on the steel counterface (0.074 μm R_a) after sliding against EP/0.2. (a) Edge of the wear track where the dark upper part is the transfer film and the bright lower part is outside the wear track. The arrow indicates sliding direction. (b) A part of the transfer film shown at a higher magnification. The applied *pv* condition is 0.25 MPa, 6.0 m/s.

cussed in Section 3.2, is supported by this image. The reason for this accumulation might be attributed to the following factors. Firstly, the nano-CuO might adhere more strongly to the steel counterface than the polymeric component. Secondly, thermal degradation of polymeric material in the interface will tend to increase the relative content of the more heat resistant CuO. The fact that EP forms a relatively continuous transfer film is a bit surprising. EP is certainly not know for forming an effective transfer film due to its cross-linked molecular structure. The authors suggest that it may be the smooth counterface combined with thermal degradation of EP in sliding contact, which causes film formation. The higher coefficients of friction when sliding against the smooth counterface increase thermal degradation of EP, which is observed visually as a blackening of the surface. The reason why no transfer film is seen for EP/PTFE/0.2 is probably due to the friction reducing effect of PTFE, which decreases frictional heat. This eliminates the thermal degradation of EP, which is hypothesized to be a significant factor for the transfer film formation seen for composites without PTFE.

The increase in μ against the smooth counterface, seen for composites without PTFE, is probably due to increases in contact area A_r caused by the presence of transfer films. The transfer films are expected to act as a protective spacer between the surfaces, which explains the decrease in wear seen for the four composites without PTFE. Also in this case, addition of nano-CuO to EP increases wear for all composites. Hence, no improvement of transfer film efficiency due to CuO is indicated. The wear reduction for EP/PTFE/0.2 when applying a smoother counterface is possibly due to a shift in mechanism from abrasive toward adhesive wear. The PTFE containing composites are probably better suited to resist adhesive wear, compared to abrasive, due to lower surface energy and hardness relative to the neat EP.

3.4. Friction and wear at high pressure and low velocity

Friction and wear measurements are repeated at the *pv* condition 1.16 MPa, 1.0 m/s in order to examine the effect of shifting to a condition with higher pressure and lower velocity. The counterface roughness is 0.26 μm R_a. It is found that composites without PTFE show a very unsteady wear behavior. Time-averaged wear rates are generally high (in the order of 10^{-4} mm^3/Nm) and show severe fluctuation. This fluctuation is observed visually to be caused by formation and breakdown of unstable transfer films. Thus, when the transfer film is absent the wear rate is exceedingly high. Due to lack of reproducibility these measurements are not completed for composites without PTFE. The only exception to the above is EP/10, which shows a steady and relatively low wear rate of 2.2 (±1) [10^{-5} mm^3/Nm]. This result weakly indicates a positive effect of adding nano-CuO when shifting toward higher pressure and lower velocity. The idea that positive effects of nanoparticle addition becomes more pronounced at higher contact pressures has been reported by others [37,42,48–50]. However, this is not explored further in this study.

Fig. 12 shows friction and wear data for composites with PTFE incorporated. These composites perform well at this condition (1.16 MPa, 1.0 m/s) and the curves for friction and wear, respectively, have similar profiles as the ones shown in Figs. 5 and 6. The coefficients of friction are on average reduced by 17% compared to the high velocity condition and the wear rates are on average reduced by 43%. Furthermore, a positive synergistic effect is seen when PTFE is added together with nano-CuO in a content up to 1.0%. The reason for this is unclear

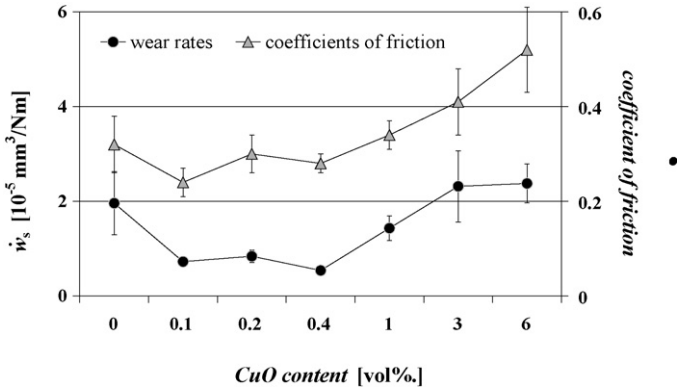

Fig. 12. Coefficients of friction and specific wear rates ($\dot{w}_s$) measured for EP with PTFE containing different concentrations of nano-CuO. The applied *pv* condition is in all cases 1.16 MPa, 1.0 m/s. The lines are guides to the eye.

Please cite this article in press as: T.Ø. Larsen, et al., Changes in the tribological behavior of an epoxy resin by incorporating CuO nanoparticles and PTFE microparticles, Wear (2007), doi:10.1016/j.wear.2007.10.003

but it could be related to the tendency of nano-CuO particles to locate themselves in the interface between PTFE and EP, cf. Fig. 3(b). It might be imagined that the CuO particles act as compatibilizer which stabilizes the interface and thereby strengthens the material.

4. Conclusions

Different amounts of CuO nanoparticles have been incorporated into both a neat epoxy resin and into an epoxy resin containing PTFE microparticles. The content of CuO is varied in the range of 0–10 vol.% while the PTFE content is fixed at 7.5 vol.%. The tribological behavior of these composites is examined and the findings are given below.

According to electron microscopy images, both nano-CuO and PTFE particles are relatively well-dispersed in the epoxy resin. Differential scanning calorimetry and Vickers hardness measurements show no clear changes in glass transition temperature or hardness as a function of the nano-CuO content. However, both parameters are reduced when PTFE is added.

Friction and wear data collected at a low pressure–high velocity condition shows the following: for composites without PTFE the wear rates increase when nano-CuO is added to the neat epoxy resin at all concentrations. The elevated wear rates are correlated with the appearance of larger-scale cracks on the worn surfaces. This leads to the conclusion that addition of nano-CuO possibly reduces the fracture strength of epoxy. The coefficient of friction is roughly at the same level for all concentrations of nano-CuO. When 7.5 vol.% PTFE is added to the neat epoxy resin wear increases by a factor of 2.5 while friction is reduced by 35%. Addition of nano-CuO together with PTFE leads to a slight decrease in friction and wear up to a CuO content of 0.4 vol.% after which both parameters increase. This increase is attributed to an accumulation of nano-CuO in the interface, which disrupts the friction lowering effect of PTFE.

The measurements are repeated for some of the composites using a smoother counterface. This gives raise to significantly less wear, which for composites without PTFE is attributed to formation of a protective transfer film. Also in this case, addition of nano-CuO to the neat epoxy increases wear for all composites.

Friction and wear data is also collected at a high pressure–low velocity condition. It is found that composites without PTFE generally show exceedingly high and fluctuating wear rates. Incorporation of PTFE has a significant positive impact on friction and wear. Furthermore, a positive synergistic effect of adding PTFE together with a small amount of nano-CuO is seen.

Acknowledgments

The work is financially supported by a grant given in equal parts by the Technical University of Denmark, The Danish Research Training Council and Civilingenior Frederik Leth Christensens ALMENNYTTIGE FOND. The latter is furthermore gratefully acknowledged by the authors for financing the applied pin-on-disk apparatus.

References

[1] S. Bahadur, D. Gong, The action of fillers in the modification of the tribological behavior of polymers, Wear 158 (1992) 41–59.
[2] J. Bijwe, J. Indumathi, J.J. Rajesh, M. Fahim, Friction and wear behaviour of polyetherimide composites in various wear modes, Wear 249 (2001) 715–726.
[3] Z. Zhang, C. Breidt, L. Chang, K. Haupert, K. Friedrich, Enhancement of the wear resistance of epoxy: short carbon fibre, graphite, PTFE and nano-TiO_2, Composites Part A 35 (2004) 1385–1392.
[4] M.H. Cho, S. Bahadur, A.K. Pogosian, Friction and wear studies using Taguchi method on polyphenylene sulfide filled with a complex mixture of MoS_2, $Al_2O_3$and other compounds, Wear 258 (2005) 1825–1835.
[5] J.A. Williams, J.H. Morris, A. Ball, The effect of transfer layers on the surface contact and wear of carbon-graphite materials, Tribol. Int. 30 (1997) 663–676.
[6] K. Friedrich, R. Reinicke, Z. Zhang, Wear of polymer composites, Eng. Tribol. Part J 216 (2002) 415–426.
[7] K. Friedrich, Z. Lu, A.M. Hger, Overview on polymer composites for friction and wear applications, Theor. Appl. Fract. Mech. 19 (1993) 1–11.
[8] J. Bijwe, U.S. Tewari, Friction and wear studies of polyetheramide composites, Wear 138 (1990) 61–76.
[9] R. Reinicke, F. Haupert, K. Friedrich, On the tribological behaviour of selected, injection moulded thermoplastic composites, Composites Part A 29 (1998) 763–771.
[10] K.C. Ho, M.C. Jeng, Tribological characteristics of short glass fibre reinforced polycarbonate composites, Wear 206 (1997) 60–68.
[11] A. Bolvari, S. Glenn, R. Janssen, C. Ellis, Wear and friction of aramid fiber and polytetrafluoroethylene filled composites, Wear 203 (1997) 697–702.
[12] K. Friedrich, Wear of reinforced polymers by different abrasive counterparts, in: K. Friedrich (Ed.), Friction and Wear of Polymer Composites—Composite Materials Series, vol. 1, Elsevier, New York, 1986, pp. 233–285.
[13] B.S. Tripathy, M.J. Furey, Study of the tribological behavior of unidirectional fiber-reinforced graphite-epoxy composites, in: P.K. Rohatgi (Ed.), Friction and Wear of Technology for Advanced Composite Materials, ASM International, Materials Park, OH, 1993, pp. 131–1411.
[14] J. Bijwe, J. Indumathi, A.K. Ghosh, On the abrasive wear behaviour of fabric-reinforced polyetherimide composites, Wear 253 (2002) 768–777.
[15] K. Friedrich, Z. Lu, A.M. Hger, Recent advances in polymer composites' tribology, Wear 190 (1995) 139–144.
[16] C. Schwarts, S. Bahadur, The role of filler deformability, filler–polymer bonding, and counterface material on the tribological behaviour of polyphenylene sulfide (PPS), Wear 251 (2001) 1532–1540.
[17] Q. Zhao, S. Bahadur, A study of the modification of the friction and wear behavior of polyphenylene sulfide by particulate Ag_2S and PbTe fillers, Wear 217 (1998) 62–72.
[18] S. Bahadur, L. Zhang, J.W. Anderegg, The effect of zinc and copper oxides and other zinc compounds as fillers on the tribological behavior of thermosetting polyester, Wear 203 (1997) 464–473.
[19] J.V. Vort, S. Bahadur, The growth and bonding of transfer film and the role of CuS and PTFE in the tribological behavior of PEEK, Wear 181 (1995) 212–221.
[20] K.S. Bhabani, J. Bijwe, Analysis of simultaneous influence of operating variables on abrasive wear of phenolic composites, Wear 253 (2002) 787–794.
[21] G.W. Sawyer, K.D. Freudenberg, P. Bhimaraj, L.S. Schadler, A study on the friction and wear behaviour of PTFE filled with alumina nanoparticles, Wear 254 (2003) 573–580.
[22] T.Ø. Larsen, M.E. Vigild, T.L. Andersen, B. Thorning, The effect of particle addition and fibrous reinforcement on epoxy-matrix composites for severe sliding conditions, Nordtrib 2006 Special Issue of Wear, in press. Q2
[23] B. Wetzel, P. Rosso, F. Haupert, K. Friedrich, Epoxy nanocomposites—fracture and toughening mechanisms, Eng. Fract. Mech. (2006) 2375–2398.
[24] B.J. Ash, J. Stone, D.F. Rogers, L.S. Schadler, R.W. Siegel, B.C. Benicewicz, T. Apple, Investigation into thermal and mechanical behavior of PMMA/alumina nanocomposites, in: Proceedings of the

Please cite this article in press as: T.Ø. Larsen, et al., Changes in the tribological behavior of an epoxy resin by incorporating CuO nanoparticles and PTFE microparticles, Wear (2007), doi:10.1016/j.wear.2007.10.003

Materials Research Society Symposium, vol. 661, 2001, pp. 2101–2106.
[25] G. Shi, M.Q. Zhang, M.Z. Rong, B. Wetzel, K. Friedrich, Sliding wear behavior of epoxy containing nano-Al_2O_3 particles with different pretreatments, Wear 256 (2004) 1072–1081.
[26] G. Shi, M.Q. Zhang, M.Z. Rong, B. Wetzel, K. Friedrich, Friction and wear of low nanometer Si_3N_4 filled epoxy composites, Wear 254 (2003) 784–796.
[27] M.Z. Rong, M. Qiu Zhang, L. Hong, H. Zeng, B. Wetzel, K. Friedrich, Microstructure and tribological behavior of polymeric nanocomposites, Ind. Lubr. Tribol. 53 (2001) 72–77.
[28] T. Mahrholz, L. Herbeck, U. Riedel, New high-performance fibre-reinforced nanocomposites, JEC - Composites 9 (2004) 71–75.
[29] B. Wetzel, F. Haupert, K. Friedrich, M.Q. Zhang, M.Z. Rong, Impact and wear resistance of polymer nanocomposites at low filler content, Polym. Eng. Sci. 42 (2002) 1919–1927.
[30] I.M. Hutchings, Tribology: Friction and Wear of Engineering Materials, Edward Arnold, 1992.
[31] Q. Wang, Q. Xue, H. Liu, W. Schen, J. Xu, The effect of particle size of nanometer ZrO_2 on the tribological behaviour of PEEK, Wear 198 (1996) 216–219.
[32] X. Shao, W. Liu, Q. Xue, The tribological behavior of micrometer and nanometer TiO_2 particle-filled poly(phthalazine ether sulfone ketone) composites, J. Appl. Polym. Sci. 92 (2004) 906–914.
[33] M. Garca, M. De Rooij, L. Winnubst, W.E.V. Zyl, H. Verweij, Friction and wear studies on nylon-6/SiO_2 nanocomposites, J. Appl. Polym. Sci. 92 (2004) 1855–1862.
[34] P. Bhabani, D.L. Burris, J. Action, G.W. Sawyer, G.C. Toney, R.W. Siegel, L.S. Schadler, Effect of matrix morphology on the wear and friction behavior of alumina nanoparticle/poly(ethylene)terephthalate composites, Wear 258 (2005) 1437–1443.
[35] S. Bahadur, C. Sunkara, Effect of transfer film structure, composition and bonding on the tribological behavior of polyphenylene sulfide filled with nano particles of TiO_2, ZnO, CuO and SiC, Wear 258 (2005) 1411–1421.
[36] C.J. Schwarts, S. Bahadur, Studies on the tribological behavior and transfer film-counterface bond strength for polyphenylene sulfide filled with nanoscale alumina particles, Wear 237 (2000) 261–273.
[37] K. Friedrich, Z. Zhang, A.K. Schlarb, Effects of various fillers on the sliding wear of polymer composites, Compos. Sci. Technol. 65 (2005) 2329–2343.
[38] Q. Zhao, S. Bahadur, The mechanism of filler action and the criterion of filler selection for reducing wear, Wear 225 (1999) 660–668.
[39] S. Bahadur, V.K. Polinei, Tribological studies of glass fabric-reinforced polyamide composites filled with CuO and PTFE, Wear 200 (1996) 95–104.
[40] T.Ø. Larsen, PhD thesis, in preparation.
[41] M.S. Sreekala, B. Lehmann, K. Friedrich, M.Z. Rong, Nanosilica-reinforced polypropylene composites: microstructural analysis and crystallization behavior, Int. J. Polym. Mater. 55 (2006) 577–594.
[42] Q. Ji, M.Q. Zhang, M.Z. Rong, B. Wetzel, K. Friedrich, Friction and wear of epoxy composites containing surface modified SiC nanoparticles, Tribol. Lett. 20 (2005) 115–123.
[43] J. Halling, Principles of Tribology, The Macmillan Press Ltd., 1975.
[44] S. Ahmed, F.R. Jones, A review of particulate reinforcement theories for polymer composites, J. Mater. Sci. 25 (1990) 4933–4942.
[45] J. Spanoudakis, R.J. Young, Crack propagation in a glass particle-filled epoxy resin, J. Mater. Sci. 19 (1984) 487–496.
[46] S. Bahadur, The development of transfer layers and their role in polymer tribology, Wear 245 (2000) 92–99.
[47] W. Wieleba, The statistical correlation of the coefficient of friction and wear rate of PTFE composites with steel counterface roughness and hardness, Wear 252 (2002) 719–729.
[48] M.Q. Zhang, M.Z. Rong, S.L. Yu, B. Wetzel, K. Friedrich, Effect of particle surface treatment on the tribological performance of epoxy based nanocomposites, Wear 253 (2002) 1086–1093.
[49] F. Li, K. Hu, J.L. Li, B.Y. Zhao, The friction and wear characteristics of nanometer ZnO filled polytetrafluoroethylene, Wear 249 (2002) 877–882.
[50] F.-H. Su, Z.-Z. Zhang, F. Guo, K. Wang, W.-M. Liu, Effects of solid lubricants on the friction and wear properties of nomex fabric composites, Mater. Sci. Eng. A 424 (2006) 333–339.

Please cite this article in press as: T.Ø. Larsen, et al., Changes in the tribological behavior of an epoxy resin by incorporating CuO nanoparticles and PTFE microparticles, Wear (2007), doi:10.1016/j.wear.2007.10.003

Joint author statements

D

Joint author statement

If a thesis contains already published articles made in collaboration with other researchers, a joint author statement about the PhD-student's part of the article shall be made by each of the co-authors, cf. article 14, section 3 of the Ministerial Order No. 114 about the PhD degree

Title of the article: Comparison of friction and wear for an epoxy resin reinforced by a glass or a carbon/aramid hybrid weave

Author(s): Thomas Ø. Larsen, Tom L. Andersen, Bent Thorning, Andy Horsewell and Martin E. vigild

Journal: Accepted for publication in **Wear**

PhD-student: Thomas Ø. Larsen Cpr.nr: 310571-1785

Signature of the PhD-student: Date: 22 December 2006

Co-author: Tom L. Andersen Signature:

Description of each author's contribution to the above-mentioned article:
Thomas Ø. Larsen (First author): Planned and conducted the experimental work, and wrote the article.

Tom L. Andersen (co-author): Supervised the first author, engaging in discussions about the results and suggested improvements of the manuscript.

Bent Thorning (co-author): Participated in discussions about the results and suggested improvements of the manuscript.

Andy Horsewell (co-author): Participated in discussions about the results and suggested improvements of the manuscript.

Martin E. Vigild (co-author): Supervised the first author, engaging in discussions about the results and suggested improvements of the manuscript.

Joint author statements shall be delivered to the **AFI, PhD programme** together with the PhD-thesis.

Joint author statement

If a thesis contains already published articles made in collaboration with other researchers, a joint author statement about the PhD-student's part of the article shall be made by each of the co-authors, cf. article 14, section 3 of the Ministerial Order No. 114 about the PhD degree

Title of the article:	Comparison of friction and wear for an epoxy resin reinforced by a glass or a carbon/aramid hybrid weave
Author(s):	Thomas Ø. Larsen, Tom L. Andersen, Bent Thorning, Andy Horsewell and Martin E. vigild
Journal:	Accepted for publication in **Wear**
PhD-student:	Thomas Ø. Larsen Cpr.nr: 310571-1785
Signature of the PhD-student:	Date: 20 December 2006
Co-author:	Bent Thorning Signature:

Description of each author's contribution to the above-mentioned article:
Thomas Ø. Larsen (First author): Planned and conducted the experimental work, and wrote the article.

Tom L. Andersen (co-author): Supervised the first author, engaging in discussions about the results and suggested improvements of the manuscript.

Bent Thorning (co-author): Participated in discussions about the results and suggested improvements of the manuscript.

Andy Horsewell (co-author): Participated in discussions about the results and suggested improvements of the manuscript.

Martin E. Vigild (co-author): Supervised the first author, engaging in discussions about the results and suggested improvements of the manuscript.

Joint author statements shall be delivered to the **AFI, PhD programme** together with the PhD-thesis.

Joint author statement

If a thesis contains already published articles made in collaboration with other researchers, a joint author statement about the PhD-student's part of the article shall be made by each of the co-authors, cf. article 14, section 3 of the Ministerial Order No. 114 about the PhD degree

Title of the article: Comparison of friction and wear for an epoxy resin reinforced by a glass or a carbon/aramid hybrid weave

Author(s): Thomas Ø. Larsen, Tom L. Andersen, Bent Thorning, Andy Horsewell and Martin E. vigild

Journal: Accepted for publication in **Wear**

PhD-student: Thomas Ø. Larsen Cpr.nr: 310571-1785

Signature of the PhD-student: Thomas Ø. Larsen Date: 4 January 2007

Co-author: Andy Horsewell Signature:

Description of each author's contribution to the above-mentioned article:
Thomas Ø. Larsen (First author): Planned and conducted the experimental work, and wrote the article.

Tom L. Andersen (co-author): Supervised the first author, engaging in discussions about the results and suggested improvements of the manuscript.

Bent Thorning (co-author): Participated in discussions about the results and suggested improvements of the manuscript.

Andy Horsewell (co-author): Participated in discussions about the results and suggested improvements of the manuscript.

Martin E. Vigild (co-author): Supervised the first author, engaging in discussions about the results and suggested improvements of the manuscript.

Joint author statements shall be delivered to the **AFI, PhD programme** together with the PhD-thesis.

Joint author statement

If a thesis contains already published articles made in collaboration with other researchers, a joint author statement about the PhD-student's part of the article shall be made by each of the co-authors, cf. article 14, section 3 of the Ministerial Order No. 114 about the PhD degree

Title of the article: Comparison of friction and wear for an epoxy resin reinforced by a glass or a carbon/aramid hybrid weave

Author(s): Thomas Ø. Larsen, Tom L. Andersen, Bent Thorning, Andy Horsewell and Martin E. vigild

Journal: Accepted for publication in **Wear**

PhD-student: Thomas Ø. Larsen Cpr.nr: 310571-1785

Signature of the PhD-student: Thomas Ø. Larsen Date: 20 December 2006

Co-author: Martin E. Vigild Signature: M E Vigild

Description of each author's contribution to the above-mentioned article:
Thomas Ø. Larsen (First author): Planned and conducted the experimental work, and wrote the article.

Tom L. Andersen (co-author): Supervised the first author, engaging in discussions about the results and suggested improvements of the manuscript.

Bent Thorning (co-author): Participated in discussions about the results and suggested improvements of the manuscript.

Andy Horsewell (co-author): Participated in discussions about the results and suggested improvements of the manuscript.

Martin E. Vigild (co-author): Supervised the first author, engaging in discussions about the results and suggested improvements of the manuscript.

Joint author statements shall be delivered to the **AFI, PhD programme** together with the PhD-thesis.

Joint author statement

If a thesis contains already published articles made in collaboration with other researchers, a joint author statement about the PhD-student's part of the article shall be made by each of the co-authors, cf. article 14, section 3 of the Ministerial Order No. 114 about the PhD degree

Title of the article: The effect of particle addition and fibrous reinforcement on epoxy-matrix composites for severe sliding conditions

Author(s): Thomas Ø. Larsen, Tom L. Andersen, Bent Thorning and Martin E. vigild

Journal: Accepted for publication in a 2007 special issue of **Wear**

PhD-student: Thomas Ø. Larsen Cpr.nr: 310571-1785

Signature of the PhD-student: Thomas Ø. Larsen Date: 22 December 2006

Co-author: Tom L. Andersen Signature:

Description of each author's contribution to the above-mentioned article:
Thomas Ø. Larsen (First author): Planned and conducted the experimental work, and wrote the article.

Tom L. Andersen (co-author): Supervised the first author, engaging in discussions about the results and suggested improvements of the manuscript.

Bent Thorning (co-author): Participated in discussions about the results and suggested improvements of the manuscript.

Martin E. Vigild (co-author): Supervised the first author, engaging in discussions about the results and suggested improvements of the manuscript.

Joint author statements shall be delivered to the **AFI, PhD programme** together with the PhD-thesis.

Joint author statement

If a thesis contains already published articles made in collaboration with other researchers, a joint author statement about the PhD-student's part of the article shall be made by each of the co-authors, cf. article 14, section 3 of the Ministerial Order No. 114 about the PhD degree

Title of the article: The effect of particle addition and fibrous reinforcement on epoxy-matrix composites for severe sliding conditions

Author(s): Thomas Ø. Larsen, Tom L. Andersen, Bent Thorning and Martin E. vigild

Journal: Accepted for publication in a 2007 special issue of **Wear**

PhD-student: Thomas Ø. Larsen Cpr.nr: 310571-1785

Signature of the PhD-student: Thomas Ø. Larsen Date: 20 December 2006

Co-author: Bent Thorning Signature: Bent Thorning

Description of each author's contribution to the above-mentioned article:
Thomas Ø. Larsen (First author): Planned and conducted the experimental work, and wrote the article.

Tom L. Andersen (co-author): Supervised the first author, engaging in discussions about the results and suggested improvements of the manuscript.

Bent Thorning (co-author): Participated in discussions about the results and suggested improvements of the manuscript.

Martin E. Vigild (co-author): Supervised the first author, engaging in discussions about the results and suggested improvements of the manuscript.

Joint author statements shall be delivered to the **AFI, PhD programme** together with the PhD-thesis.

Joint author statement

If a thesis contains already published articles made in collaboration with other researchers, a joint author statement about the PhD-student's part of the article shall be made by each of the co-authors, cf. article 14, section 3 of the Ministerial Order No. 114 about the PhD degree

Title of the article: The effect of particle addition and fibrous reinforcement on epoxy-matrix composites for severe sliding conditions

Author(s): Thomas Ø. Larsen, Tom L. Andersen, Bent Thorning and Martin E. vigild

Journal: Accepted for publication in a 2007 special issue of **Wear**

PhD-student: Thomas Ø. Larsen Cpr.nr: 310571-1785

Signature of the PhD-student: Thomas Ø. Larsen Date: 20 December 2006

Co-author: Martin E. Vigild Signature: M.E. Vigild

Description of each author's contribution to the above-mentioned article:
Thomas Ø. Larsen (First author): Planned and conducted the experimental work, and wrote the article.

Tom L. Andersen (co-author): Supervised the first author, engaging in discussions about the results and suggested improvements of the manuscript.

Bent Thorning (co-author): Participated in discussions about the results and suggested improvements of the manuscript.

Martin E. Vigild (co-author): Supervised the first author, engaging in discussions about the results and suggested improvements of the manuscript.

Joint author statements shall be delivered to the **AFI, PhD programme** together with the PhD-thesis.

Joint author statement

If a thesis contains already published articles made in collaboration with other researchers, a joint author statement about the PhD-student's part of the article shall be made by each of the co-authors, cf. article 14, section 3 of the Ministerial Order No. 114 about the PhD degree

Title of the article: Changes in the tribological behavior of an epoxy resin by incorporating CuO nanoparticles and PTFE microparticles

Author(s): Thomas Ø. Larsen, Tom L. Andersen, Bent Thorning, Andy Horsewell and Martin E. vigild

Journal: Submitted for publication in **Wear**

PhD-student: Thomas Ø. Larsen Cpr.nr: 310571-1785

Signature of the PhD-student: Thomas Ø Larsen Date: 22 December 2006

Co-author: Tom L. Andersen Signature:

Description of each author's contribution to the above-mentioned article:
Thomas Ø. Larsen (First author): Planned and conducted the experimental work, and wrote the article.

Tom L. Andersen (co-author): Supervised the first author, engaging in discussions about the results and suggested improvements of the manuscript.

Bent Thorning (co-author): Participated in discussions about the results and suggested improvements of the manuscript.

Andy Horsewell (co-author): Participated in discussions about the results and suggested improvements of the manuscript.

Martin E. Vigild (co-author): Supervised the first author, engaging in discussions about the results and suggested improvements of the manuscript.

Joint author statements shall be delivered to the **AFI, PhD programme** together with the PhD-thesis.

Joint author statement

If a thesis contains already published articles made in collaboration with other researchers, a joint author statement about the PhD-student's part of the article shall be made by each of the co-authors, cf. article 14, section 3 of the Ministerial Order No. 114 about the PhD degree

Title of the article: Changes in the tribological behavior of an epoxy resin by incorporating CuO nanoparticles and PTFE microparticles

Author(s): Thomas Ø. Larsen, Tom L. Andersen, Bent Thorning, Andy Horsewell and Martin E. vigild

Journal: Submitted for publication in **Wear**

PhD-student: Thomas Ø. Larsen Cpr.nr: 310571-1785

Signature of the PhD-student: Thomas Ø. Larsen Date: 20 December 2006

Co-author: Bent Thorning Signature: Bent Thorning

Description of each author's contribution to the above-mentioned article:
Thomas Ø. Larsen (First author): Planned and conducted the experimental work, and wrote the article.

Tom L. Andersen (co-author): Supervised the first author, engaging in discussions about the results and suggested improvements of the manuscript.

Bent Thorning (co-author): Participated in discussions about the results and suggested improvements of the manuscript.

Andy Horsewell (co-author): Participated in discussions about the results and suggested improvements of the manuscript.

Martin E. Vigild (co-author): Supervised the first author, engaging in discussions about the results and suggested improvements of the manuscript.

Joint author statements shall be delivered to the **AFI, PhD programme** together with the PhD-thesis.

Joint author statement

If a thesis contains already published articles made in collaboration with other researchers, a joint author statement about the PhD-student's part of the article shall be made by each of the co-authors, cf. article 14, section 3 of the Ministerial Order No. 114 about the PhD degree

Title of the article: Changes in the tribological behavior of an epoxy resin by incorporating CuO nanoparticles and PTFE microparticles

Author(s): Thomas Ø. Larsen, Tom L. Andersen, Bent Thorning, Andy Horsewell and Martin E. vigild

Journal: Submitted for publication in **Wear**

PhD-student: Thomas Ø. Larsen Cpr.nr: 310571-1785

Signature of the PhD-student: Date: 4 January 2007

Co-author: Andy Horsewell Signature:

Description of each author's contribution to the above-mentioned article:
Thomas Ø. Larsen (First author): Planned and conducted the experimental work, and wrote the article.

Tom L. Andersen (co-author): Supervised the first author, engaging in discussions about the results and suggested improvements of the manuscript.

Bent Thorning (co-author): Participated in discussions about the results and suggested improvements of the manuscript.

Andy Horsewell (co-author): Participated in discussions about the results and suggested improvements of the manuscript.

Martin E. Vigild (co-author): Supervised the first author, engaging in discussions about the results and suggested improvements of the manuscript.

Joint author statements shall be delivered to the **AFI, PhD programme** together with the PhD-thesis.

Joint author statement

If a thesis contains already published articles made in collaboration with other researchers, a joint author statement about the PhD-student's part of the article shall be made by each of the co-authors, cf. article 14, section 3 of the Ministerial Order No. 114 about the PhD degree

Title of the article: Changes in the tribological behavior of an epoxy resin by incorporating CuO nanoparticles and PTFE microparticles

Author(s): Thomas Ø. Larsen, Tom L. Andersen, Bent Thorning, Andy Horsewell and Martin E. vigild

Journal: Submitted for publication in **Wear**

PhD-student: Thomas Ø. Larsen Cpr.nr: 310571-1785

Signature of the PhD-student: Thomas Ø. Larsen Date: 20 December 2006

Co-author: Martin E. Vigild Signature: M.E. Vigild

Description of each author's contribution to the above-mentioned article:
Thomas Ø. Larsen (First author): Planned and conducted the experimental work, and wrote the article.

Tom L. Andersen (co-author): Supervised the first author, engaging in discussions about the results and suggested improvements of the manuscript.

Bent Thorning (co-author): Participated in discussions about the results and suggested improvements of the manuscript.

Andy Horsewell (co-author): Participated in discussions about the results and suggested improvements of the manuscript.

Martin E. Vigild (co-author): Supervised the first author, engaging in discussions about the results and suggested improvements of the manuscript.

Joint author statements shall be delivered to the **AFI, PhD programme** together with the PhD-thesis.